Physically based modelling of rainfall-runoff processes

F.L.M. Diermanse

Stellingen

1 De parameters van het hydrologische model van de Zwalm (een gemodificeerde versie van TOPMODEL) kunnen in twee groepen opgedeeld worden: Parameters die bepalend zijn voor bergingscapaciteit in het stroomgebied en parameters die bepalend zijn voor de stroomsnelheden. Binnen de twee genoemde groepen zijn de parameters onderling afhankelijk m.b.t de modeluitvoer, terwijl daar tussen de twee groepen onderling geen sprake van is.

2 Vaststellen van parameterwaarden middels calibratie, waarbij meerdere parameterwaarden uit één van de bovenstaande groepen afkomstig zijn, is af te raden aangezien in dat geval meerdere parametercombinaties vrijwel gelijke uitvoer zullen vertonen.

3 De voorgeschiedenis van een neerslaggebeurtenis heeft een grote invloed op de hoogte van de afvoer tijdens een neerslaggebeurtenis. Het gebruik van bestaande neerslag-afvoer modellen waarin deze invloed niet is opgenomen is af te raden.

4 Voor het stroomgebied van de Zwalm (114 km^2) kan worden volstaan met gebiedsgemiddelde (gelumpte) modellering. De eventuele verbeteringen die gerealiseerd kunnen worden middels een opdeling in deelgebieden is klein vergeleken bij de fout die het model ten opzichte van gemeten afvoeren maakt.

5 In kleine stroomgebieden wordt de neerslag van één enkel station nogal eens als representatief gesteld. Voor de Zwalm worden met deze verwaarlozing van ruimtelijke variabiliteit doorgaans grote fouten geïntroduceerd (zelfs een verdubbeling van de voorspelde afvoerpiek is mogelijk). Het is voor een gebied van deze orde van grootte (114 km^2) derhalve aan te raden om meerdere neerslagstations te installeren indien men neerslaggebeurtenissen wenst te simuleren met een neerslag-afvoer model.

6 Voor grotere stroomgebieden speelt de looptijd in de rivier een dusdanige rol dat voor het modelleren van de ruimtelijke heterogeniteit gebiedsgemiddelde waarden niet voldoen. Voor de het stroomgebied van de Moezel (28152 km^2) is dan ook aangetoond dat gelumpte modellen inferieur zijn aan gedistribueerde modellen voor wat betreft de afvoervoorspelling bij het uitstroompunt.

7 Om een goede schatting van de gebiedsneerslag van het stroomgebied van de Moezel te verkrijgen kan, indien men slechts in afvoervoorspellingen bij het uitstroompunt geïnteresseerd is, volstaan worden met het gebruik van tien neerslagstations.

8 Zelfs de meest complexe frequentie-analyse van rivierafvoeren zal voor de bewoners van het rivierengebied niet zoveel vruchten afwerpen als de "natte-vinger-methode" van Hansje Brinker.

9 Het wassen van een auto met zuiver drinkwater is van een vergelijkbare decadentie als het aansteken van een sigaar met een briefje van 100 (gulden of euro).

10 Wanneer in 2001 de geplande zonnecentrale op het dak van de zout/zoet hal bij het Waterloopkundig Laboratorium gerealiseerd wordt, zal de uitstraling van minstens even grote waarde zijn als de instraling.

11 De Nederlandse volksaard in ogenschouw nemende, zal het concept van de "ideeënbus" van Albert Heijn succesvoller zijn indien de term "klachtenbus" gehanteerd zou worden.

12 De veelgehoorde stelling "Toeval bestaat niet!" is onjuist. Aangezien het leven een aaneenschakeling is van een zeer groot aantal gebeurtenissen, zou het wel heel toevallig zijn als er nooit iets toevalligs gebeurt.

13 Statistiek is een handig hulpmiddel, maar tevens een gevaarlijk wapen wanneer het in ondeskundige handen valt.

14 De uitdrukking "Geld als water verdienen" zal door de toenemende waterschaarste aan betekenis verliezen.

15 Het verzoek aan musici om nummers van langer dan 5 minuten in te korten, hetgeen doorgaans door de platenmaatschappij wordt gedaan uit commerciële overwegingen, is net zo onzinnig als het verwijderen van de inleiding en conclusies uit een proefschrift.

Physically based modelling of rainfall-runoff processes

Physically based modelling of rainfall-runoff processes

Proefschrift

ter verkrijging van de graad van doctor
aan de Technische Universiteit Delft,
op gezag van de Rector Magnificus prof. ir. K. F. Wakker,
voorzitter van het College voor Promoties,
in het openbaar te verdedigen op 19 februari 2001 om 13.30 uur

door

Ferdinand Lennaert Machiel DIERMANSE

Wiskundig ingenieur

geboren te 's Gravenhage

Dit proefschrift is goedgekeurd door de promotor:

Prof. dr. ir. C. van den Akker

Samenstelling promotiecommissie:

Rector Magnificus	voorzitter
Prof. dr. ir. C. van den Akker	Technische Universiteit Delft, promotor
Prof. dr. ir. H.H.G. Savenije	Technische Universiteit Delft,
Prof. ir. E. van Beek	Technische Universiteit Delft,
Prof. dr. ir. J.K. Vrijling	Technische Universiteit Delft,
Prof. M. Sivapalan	University of Western Australia
Prof. dr. P.A. Troch	Wageningen Universiteit
Dr. J.C.J. Kwadijk	WL Delft Hydraulics

Published and distributed by: DUP Science
DUP Science is an imprint of
Delft University Press
P.O. BOX 98
2600 MG Delft
The Netherlands
Telephone: +31 15 2785121
Telefax: +31 15 2781661
E-mail: DUP@library.tudelft.nl

ISBN: 90-407-2154-8

Preface

Defensive measures against flood dangers are essential to Dutch society. Without dunes and dikes to protect us, about 67 % of the Netherlands would be flooded (Middelkoop, 1998). Our present system of coastal flood defences mainly originates from the flood disaster of 1953 (TAW, 1995), when the sea temporarily reclaimed parts of Zeeland and Zuid-Holland and took the lives of approximately 2000 people. Since then, the Dutch system of dikes and dunes has been reinforced to protect us against extreme (up to probability of occurrence of 10^{-4} per year) floodings of the sea.

Progress of river dike reinforcement, however, was relatively slow (TAW, 1995). In 1993, nature reminded us that flooding dangers are not restricted to the sea only. In December that year the two major Dutch rivers, the river Rhine and the river Meuse, had to cope with extreme precipitation amounts, mainly fallen in Germany and Belgium, which lead to some severe floodings in the river systems. Particularly the abundant Meuse water brought damage to houses, dikes, carpets, furniture etc. Barely one year later, in January 1995, again these two rivers flooded and the consequences were even worse than in 1993. The authorities even decided to evacuate approximately 200.000 people from the endangered areas, albeit mostly as a safety precaution.

The observed peak discharges of the Rhine at Lobith in 1993 and 1995 are the fourth and second highest observed peak discharges of the 20th century (Diermanse, 1999), whereas for the Meuse river these rankings are second and third respectively (Lorenz and Kwadijk, 1999). The occurrence of these two flood events indicated that probabilities of damaging flood events may be significantly higher than generally has been assumed. The estimation of probabilities of extreme events is a highly delicate matter. The problem is that, by definition, extreme events like the ones in 1993 and 1995 occur seldom, which means there's not enough information available to provide an estimation on occurrence probabilities of satisfactory reliability. Nevertheless, the damaging effects of floods like the ones of 1993 and 1995 automatically increase pressure from society on improvement of existing estimation techniques.

In the Netherlands, flood frequency analysis is performed on a purely statistical basis (Diermanse, 1999; Lorenz and Kwadijk, 1999). A number of extreme value probability distribution functions are fitted through the series of observed peak discharges. The resulting functional description relates peak discharges to corresponding exceedance probabilities. By using statistical methods, one looks for a regularity in observed river discharges without taking into account the fact that they are generated by highly non-linear and inhomogeneous

processes. This seriously undermines the validity of the concept, especially in the case of extremely high discharges for which relatively little information is available. The physical conditions in the river basin during extreme high water events usually differ significantly from less extreme events. Floodings in the upstream area of a river basin, for instance, can significantly reduce the magnitude of the peak discharge in downstream part of the river as demonstrated by Silva and Dijkman [2000] for the river Rhine. Since the less extreme events form the majority of the observed series, the derived distribution function hardly accounts for these changing conditions.

Therefore, the only way to improve flood frequency analysis is to move away from pure statistics towards an approach which, to some extent, takes into account the physics occurring in the river catchment. This has been recognised by the Institute for Inland Water Management and Waste Water Treatment (RIZA), a subdivision of the Dutch Ministry of Transport, Public Works and Water Management (Ministerie van V&W). They started the development of an alternative method to derive exceedance probabilities (Parmet et al., 1999). The first step is the development of a stochastic weather generator by the Royal Dutch Meteorological Institute (KNMI) performed under supervision of RIZA (Brandsma and Buishand, 1998). In the near future, results of this generator will be used in flood frequency analysis by translating predicted future rainfall events into discharges of the river Rhine, through the combined use of a rainfall-runoff model (The HBV-model, Killingtveit and Sælthun [1995]) and a one-dimensional hydrodynamic routing model.

These developments raised the interest of both Delft Hydraulics and the section Hydrology and Ecology of Delft University of Technology, who decided to collaborate in research on mathematical modelling of rainfall-runoff processes in hillslope areas. The collaboration resulted in the set-up of a research project, performed by the author at both institutes. The main result of this research project is the thesis you are currently reading.

Table of contents

1. Introduction

1.1 Design criteria for flood defence structures

In the Netherlands, an extensive system of structures like dams, reservoirs, dikes and dunes has been constructed in order to prevent floodings to occur frequently. Even though it may be possible to prevent floodings from occurring at all, the design of these structures is by no means based on this criterion. Instead, (extreme) flood scenarios are defined for which we expect the structures to be able to fulfil their defensive tasks. The selection of these so called "design floods" is based on their estimated probability of exceedance, where exceedance can either refer to water levels (e.g. in case of design of dikes) or volumes (in case of reservoir design). This means that in the case of exceedance, the structures will not protect us completely against damaging effects, i.e. a certain level of flooding risk is accepted. The main reason for this acceptance is the limit it sets on dimensions of defensive structures, which reduces construction and maintenance costs. Furthermore, in the case of river dikes, it saves valuable river landscapes which otherwise would have been disturbed dramatically.

In the Netherlands, the acceptance level of flood risks varies from location to location. Sea dikes, for example, are designed to lower the probability of occurrence of damaging floods up to 1/10000 per year (TAW, 1995), whereas for a small river like "de Geul" a flood probability of 1/10 per year in the rural parts of the catchment is allowed (Diermanse, 1994).
The design criterion for dikes alongside the non-tidal part of our major rivers (the Meuse and the Rhine-branches) is a flood risk of 1/1250 per year. This criterion was set in 1977 after completion of an extensive economically based analysis on possible losses due to floods on one hand and costs of building structures on the other (Commissie rivierdijken, 1977). Later, in 1993, a similar analysis (Boertien I, 1993) showed that the situation in the Netherlands had not changed since 1977 in such a way that safety standards had to be adjusted.

1.2 Statistically based flood frequency analysis

Recently, the magnitude of the peak discharges with an annual exceedance probability of 1/1250 has been estimated at 3830 m^3/s for the river Meuse at Borgharen (Lorenz and Kwadijk, 1999) and at 16000 m^3/s for the river Rhine at Lobith (Diermanse, 1999). The flood frequency analyses for these two rivers have been performed on a purely statistical basis. This means that extreme-value distribution functions (relating exceedance probabilities to corresponding river discharges) are fitted on a set of observed peak discharges (yearly

maximum floods and floods with peak discharges above a certain threshold value). This type of analysis is widely used throughout the world because it is easy to apply and no other methods have proven to be superior yet. The basic procedure is as follows: First, for every observed peak discharge an initial estimation is made on its exceedance probability, which is based on the length of the period of observation and the number of times a peak discharge has been exceeded during this period. An example of such an estimation method is the one introduced by Gringorten (see Shaw, 1988):

$$P = \frac{r - 0.44}{N + 0.12} \tag{1.1}$$

where P is the exceedance probability of an observed peak discharge, r is its rank number (1 = highest observed peak discharge, 2 = second highest observed peak discharge etc.) and N is the total number of peaks considered. Secondly, an extreme value distribution function is selected to fit the set of peak discharges with corresponding initially estimated exceedance probabilities. Some well-known types of extreme value distributions are the Pearson-III distribution, the Gumbel distribution, and the log-normal distribution. An example of this procedure is displayed in Figure 1.1, where the Pearson-III distribution is fitted to 96 annual peak discharges of the river Rhine at Lobith.

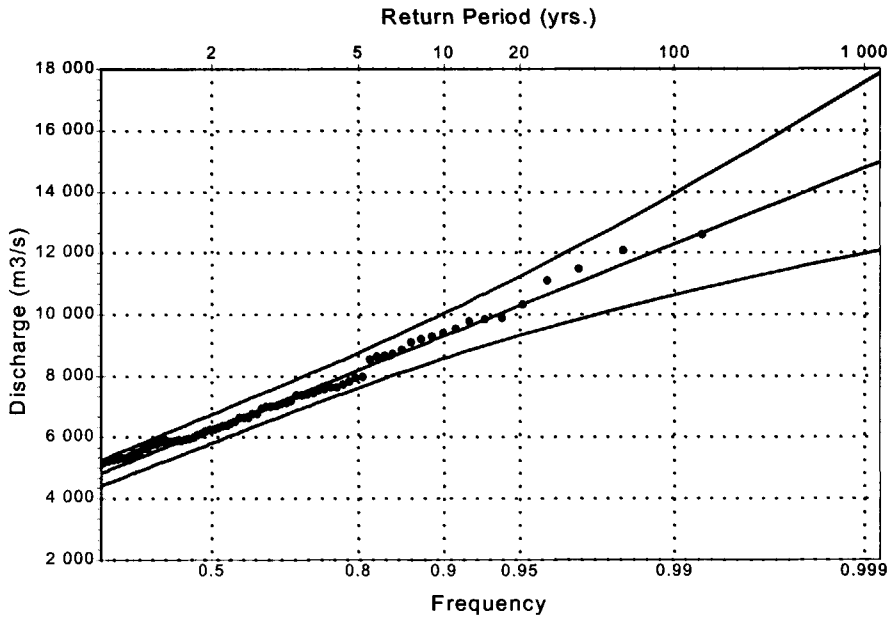

Figure 1.1 The Pearson-III distribution fitted to annual peak discharges of observed discharges in the river Rhine at Lobith during the period 1901-1996. The two outer lines display the 95% confidence interval.

The distribution function relates discharges to estimated return periods[1]. This means for any return period the discharge with this specific return period is known. This is specifically useful when return periods are concerned which exceed the period of observation (as often the case in deriving design floods), since no initial estimates of corresponding discharges are available for these return periods (see equation (1.1)).

1.2.1 Basic theory on extreme value functions

In statistical flood frequency analysis annual maximum floods are considered to be the maximum of a long sequence of random variables. As a consequence, the probability distribution function of a yearly maximum flood is a limiting distribution of the probability distribution of individual discharge measurements. Therefore, theories on statistically based flood frequency analysis originate from general statistical extreme value theories.

In statistical extreme value theories a long series $X_1, X_2,...X_n,...$ of random variables is considered. In his classical paper, Gnedenko [1943] was the first to prove (Smith, 1992) that only three types of extreme value distributions exist, assuming that the variables X_1, $X_2,...X_n,...$ are independent random variables with identical distribution function $F(x)$. With these assumptions, the probability distribution function $F_n(x)$ of the maximum M_n of the series $X_1,X_2,...X_n$ equals:

$$F_n(x) = F^n(x) \tag{1.2}$$

From (1.2) it directly follows that:

$$\lim_{n \to \infty} F_n(x) = 0; \quad \forall x : F(x) < 1 \tag{1.3}$$

which states that if it is possible for a random variable X_i to exceed the value x (i.e. $F(x)<1$), then the maximum of the series $X_1, X_2,...X_n$ almost certainly exceeds the value of x if the series is long enough. Equation (1.3) is rather uninteresting since it hardly contains any information. Therefore, the series maximum, M_n, is rescaled by defining two series of constants, $a_n>0$ and b_n, in such a way, that there exists a distribution function $\Phi(x)$ for which.

$$\lim_{n \to \infty} P\left(\frac{M_n - b_n}{a_n} \le x \right) = \lim_{n \to \infty} F^n(a_n x - b_n) = \Phi(x) \tag{1.4}$$

So, if a combination of $[\Phi(x), a_n, b_n]$ exists for which equation (1.4) holds, the distribution function of the rescaled variable M_n converges to $\Phi(x)$. This converging through rescaling is

[1] A return period is a quantity which is inversely related to the exceedance probability. So, a "return period of 1250" refers to a probability of exceedance of 1/1250 per year.

similar to the convergence of the sum of independent identically distributed stochastic variables to a Gaussian distribution.

If another distribution function $\Phi^*(x)$ is defined in such a way that $\Phi^*(x)=\Phi(Ax+B)$, for any constants A>0 and B, then it can be easily shown that if $[\Phi(x), a_n, b_n]$ is a solution of equation (1.4), then $[\Phi^*(x), a_n^*, b_n^*]$ with $a_n^* = Aa_n$ and $b_n^* = b_n + Ba_n$, is also a solution of equation (1.4). Therefore, two functions Φ and Φ^* are said to be of the same type if $\Phi^*(x)=\Phi(Ax+B)$, for any constants A>0 and B. Gnedenko [1943] proofed that there exist only three types of distribution functions for which equation (1.4) can possibly hold:

$$
\begin{aligned}
&I \quad \Phi_\alpha(x) = \begin{cases} 0 & ;x \le 0 \\ e^{-x^{-\alpha}} & ;x > 0\ ,0 < \alpha < \infty \end{cases} \\
&II \quad \Psi_\alpha(x) = \begin{cases} e^{-(-x)^{\alpha}} & ;x \le 0\ ,0 < \alpha < \infty \\ 1 & ;x > 0 \end{cases} \\
&III \quad \Lambda(x) = e^{-e^{-x}} \qquad ;-\infty < x < \infty
\end{aligned}
\tag{1.5}
$$

The proof of this will be omitted. The interested reader is referred to Smith [1992].

As a result of Gnedenko's theorem, flood frequencies are generally derived by using any distribution function $\Phi^*(x)$ for which:

$$
\Phi^*(Ax+B) = \begin{cases} \Phi_\alpha(x) \\ \Psi_\alpha(x) \\ \Lambda(x) \end{cases}
\tag{1.6}
$$

For certain values of A>0 and B.

1.2.2 Drawbacks of statistically based methods

The statistical method of deriving flood frequencies is known to have some serious drawbacks:

- The historical discharge record is always much too short to determine the probabilities of extreme runoff events. In order to obtain a reliable estimation of, for instance, the 10,000-year flood a discharge record of at least 100,000 years is needed (Klemeš, 1986). The determination of exceedance probabilities of extreme floods is therefore based on dubious extrapolation techniques. The danger of using extrapolation techniques is demonstrated by the fact that extrapolated values of different distribution functions can be found to differ considerably, even if they are all considered to be close approximations of the record of

observed discharge data. (See for an example Commissie Watersnood Maas [1994]). Furthermore, the reliability of extrapolated values is low since confidence intervals increase rapidly with increasing return periods (see Figure 1.1).

- The use of extreme value distributions is based on the assumption that all measured floods are random samples, generated by the same probability distribution. Among other things this means that physical conditions of the river basin did not change during the period of discharge measurements. This stationarity assumption is not likely to hold in real-world catchments.

- Floods can have different causes like snow melt in the spring, long duration (winter) depressions, hurricanes etc., even within the same river catchment. In spite of these differences, the flood frequency distribution is based on all observed peak discharges, since homogeneity is assumed in extreme value theory. Consequently, the derived exceedance probability of, for instance, a flood caused by snow melt can be influenced by the magnitude of a flood caused by a hurricane, which does not make sense.

- The physical conditions in the river catchment during extreme river floods may differ significantly from less extreme events. Since the less extreme events form the majority of the observed series the fitted distribution function cannot be expected to reveal reliable information on extreme floods. A striking real world example of this effect (Klemeš, 1994) is the Santa Anna river basin in California, which is covered for about one third by Lake Elsinor. During an observation period of 80 years, the lake has contributed to river floods a number of times by overflowing. The flooding of the lake generated river discharges which would have been unlikely to occur in case the flooding of the lake would not have been possible. This causes a discontinuity in the series of observed discharges which cannot be properly covered by any of the standard extreme-value distributions.

In general, the drawbacks of the statistical derivation of exceedance probabilities stem from the fact that the basic assumptions of the extreme value theory of Gnedenko [1943] (section 1.2.1) do not hold for peak discharges of real-world rivers. In other words, by fitting extreme value distribution functions, one looks for a regularity in measured river discharges without taking into account the fact that floods are generated by highly non-linear and inhomogeneous processes. It is therefore recognised (Klemeš 1988, Klemeš 1993, Kuchment et al., 1993) that if further progress in flood frequency analysis will ever be made, it can only come from a better understanding of the processes involved in flood generation.

1.3 Physically based flood frequency analysis

1.3.1 Introduction

A physically based approach towards flood frequency analysis implies that information is required on both the meteorological events which can be expected in the future and the hydrological response of river catchments to these events. In modelling terms this means a catchment-runoff model is combined with a meteorological model which generates characteristics of future flood generating events and their probability of occurrence. The schematic view of this type of approach is presented in Figure 1.2. The flood frequency distribution will be either the direct output of the rainfall-runoff model or can be easily extracted from it.

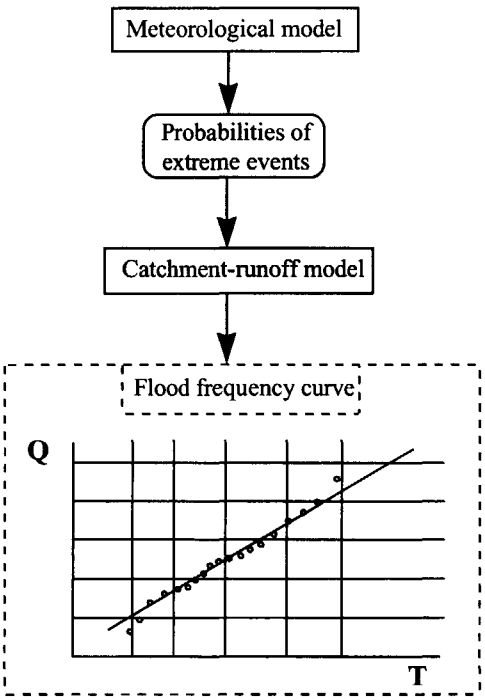

Figure 1.2 Schematic view of a procedure for deriving physically based flood frequency curves

Two different procedures of the physically based approach are recognised: *Analytical methods* (the so called derived distribution approach, Loukas et al [1996]) and *Monte Carlo simulations*. In the first approach, models are built from relatively simple, analytically solvable mathematical equations. As a consequence the flood frequency distribution is

derived without the help of any computer and it will be expressed as a function of all parameters involved in both the catchment-runoff model and the meteorological model. The main advantage of this approach is the direct visibility of the influence of catchment parameters on flood frequencies. This type of flood frequency analysis has been introduced by Eagleson [1972] and extended by Hebson and Wood [1982], Diaz-Granados et al. [1984], Wood and Hebson [1986], Naghettini et al. [1996], Goel et al. [2000] and Iacobellis and Fiorentino [2000]. In the Monte Carlo procedure on the other hand, a long synthetic series of rainfall events is generated by the meteorological model, which is used as input for a catchment-runoff model to derive peak discharges of each event. A distribution function is then fitted through derived discharges in the same way as for the statistical methods of section 1.2. Examples of this type of approach are presented by Beven [1986], Sivapalan et al. [1990] and Loukas et al. [1996].

1.3.2 Modelling occurrence probabilities of future rainfall events

As mentioned in section 1.3.1, the meteorological model has to provide the characteristics of future extreme meteorological events and their probability of occurrence. The predictions are performed on a purely stochastic basis, since deterministic weather forecasts can only be made for a few days ahead. Therefore question marks can be placed when the term "physically-based flood frequency analysis" is used. In spite of these question marks this term will be used here, as it is still possible in theory to overcome some of the drawbacks of the purely statistically based flood frequency analysis, by modelling the runoff processes in a physically based matter.

statistical distribution functions

For the sake of simplicity, characteristics of rainfall events like *intensity*, *duration* and *spatial variation* are usually represented by relatively simple stochastic distribution functions. These distributions can either be used in the Monte Carlo approach to generate long term series of characteristics (intensity, duration, etc.) of rainfall events (Sivapalan et al. 1990) or directly used as input of the catchment-runoff model (Eagleson, 1972) in the analytical approach. Popular distribution functions are the exponential distribution and the gamma distribution (e.g. Eagleson, 1972; Wood and Hebson, 1986; Sivapalan et al, 1990).
In some cases the statistical distribution of rainfall duration is assumed to be independent of the corresponding rainfall intensities (e.g. Eagleson, 1972; Sivapalan et al., 1990). However, this assumption favours the occurrence of long duration events with high rainfall intensities which in some cases may not be appropriate. In order to avoid this possible misconception, intensity-duration-frequency (I.D.F.) curves are more appropriate (Blöschl and Sivapalan, 1997, Goel et al., 2000). These curves represent the bivariate probability distribution function of the both intensity and duration of a storm event.

If spatial variability is considered, it is usually represented by a spatial correlation factor for rainfall intensity (e.g. Sivapalan et al., 1990), since it is impossible to forecast occurrence probabilities of more complex spatial distribution patterns of intensity and duration. The spatial correlation factor reflects the dependence of the area-average rainfall intensity on catchment size which is a dominant factor in flood frequency analysis (Sivapalan et al., 1990; Seo and Smith, 1996). Similar techniques for including spatial variability of rainfall intensities have been developed for I.D.F-curves (Sivapalan and Blöschl, 1998).

Rainfall models based on Weather type classifications

A relatively new and promising approach of long term rainfall predictions is the one based on weather type classifications. Rainfall amounts and corresponding spatial distribution are strongly related to atmospheric circulation patterns. In order to obtain information on rainfall statistics based on circulation patterns, a number of weather types have to be defined and classified. Series of rainfall events and corresponding probabilities can be generated when the following information is available.

1. Probability of occurrence of the defined weather types.
2. Probability distributions of rainfall amounts and spatial variation for every defined weather type.

This information is obtained from analysis of historical data of rainfall events and circulation patterns. An inevitable problem that has to be tackled during this analysis, is to link the coarse scaled available information on circulation patterns to the scale of rainfall patterns that is of interest for the hydrologist.

Reports of river flow simulation based on input of weather type simulation models can be found for instance in Epstein and Ramirez [1994], Kite [1995] and Wilby et al. [1994]. Generally, the hydrological response of a catchment to synthetically generated input is analysed in these studies, without direct emphasis on flood frequency analysis. However, derivation of flood frequency distributions from these studies is just one, relatively easy, extra step. An added advantage is the possibility offered by some of the weather type classification models to asses the impact of climate change on hydrological regimes in catchments (Wilby et al., 1994).

Resampling techniques

The basic idea of resampling techniques is to create a new series of rainfall data by repeatedly selecting data from the original series. In order to maintain the statistical characteristics of the original series the selection of a single data is conditioned (in a probabilistic sense) on the characteristics of its predecessor(s). Examples of such resampling techniques are presented by Kendall and Dracup [1991] and Lall and Sharma [1996]. In the Netherlands, the possibilities of the application of resampling techniques in flood frequency analysis are

currently being explored by the Dutch Ministry of Transport, Public Works and Water Management (Ministerie van V&W), or more in particular the Institute for Inland Water Management and Waste Water Treatment (RIZA) (Parmet et. al., 1999).

1.3.3 Modelling catchment response to rainfall events

The analytical approach

In order to be applicable in physically based flood frequency analysis, a catchment-runoff model has to fit in the framework of the analysis as depicted in Figure 1.2. Furthermore, it should be based on a physically meaningful description of the dominant processes involved in the catchment under consideration. In this respect, a major disadvantage of the analytical approach is the strong limitation it sets on the complexity of process descriptions. The catchment-runoff model has to be constructed from a set of relatively simple mathematical equations in order to be analytically solvable. Furthermore the representation of the configuration of the hydrological system can not be too complex. In practice, the latter generally leads to the use of a fully lumped representation of processes and parameters.

In general, the analytical methods of deriving flood frequencies consist of three major components:

[1] A probability density function for rainfall intensity and duration.
[2] A component in which the amount of net precipitation (the fraction of the precipitation which becomes available for runoff) is derived.
[3] A routing component to represent runoff delay and hydrograph attenuation.

The first component predicts characteristics and occurrence frequencies of future rainfall events, the second component supplies runoff percentages of these events and the third component relates the net precipitation to resulting peak discharges in the river system. In Figure 1.2, components [2] and [3] are essentially covered by the catchment-runoff model.

[2] In his pioneering work on derived flood distributions, Eagleson [1972] modelled infiltration through a constant loss rate. Diaz-Granados et al. [1984] used the Philip's solution for one-dimensional concentration-dependent equation of the diffusion process in unsaturated media and Raines and Valdes [1993] used the Soil Conservation Service (SCS) curve number method. Hebson and Wood [1982] and Wood and Hebson [1986] did not even bother to model the infiltration process. They derived a probability density function for excess (net) precipitation to replace component [1] and [2].
[3] For runoff routing, Eagleson [1972] used the kinematic wave model. In subsequent works the geomorphological unit hydrograph of Rodriguez-Iturbe and Valdés [1979] proved to

be a useful tool in runoff routing (Diaz-Granados et al, 1984; Hebson and Wood, 1982; Sivapalan et al., 1990; Wood and Hebson, 1986).

Catchment-runoff modelling in Monte Carlo simulations

Although the analytical studies have proven to be very useful, two phenomena of concern to runoff generation are usually insufficiently captured by the above mentioned models

I. Spatial heterogeneity of processes and parameters. Different parts of the catchment respond differently to climatic inputs. Runoff, for instance, is known to be predominantly generated on a relatively small, variable, part of the catchment (Betson, 1964; Dunne and Black, 1970b; Hewlett, 1961). The dominant role of this source area, and its increasing size with increasing rainfall amounts, is generally not captured if catchment average representations are used.
II. Interactions between different flood generating processes. During extremely wet meteorological conditions domination of processes can differ significantly from "normal" conditions. Sivapalan et al. [1990], for instance, demonstrate through Monte Carlo simulations that the mixed runoff production mechanisms strongly influence the shape of the flood distribution.

These drawbacks stem from the fact that process descriptions in catchment-runoff models cannot be too complex because they have to be analytically solvable. In theory, the Monte Carlo simulation approach does not suffer from these drawbacks, since it does not require analytically solvable catchment-runoff models. Numerical solution techniques and computational capacities of the current generation of computers allow the mathematical equations of the catchment-runoff models to be as complex as desired. However, since the Monte Carlo approach requires a large number of model runs, the use of extremely complex, time consuming models is generally avoided. Loukas et al. [1996], for instance, combine a simple power relationship to model the infiltration process in combination with a linear reservoir routing technique. Beven [1986] and Sivapalan et al. [1990] apply the TOPMODEL-concept (Beven and Kirkby, 1979) of catchment-runoff modelling to derive flood frequencies. In this concept of catchment-runoff modelling, the (variable) percentage of the catchment which generates direct runoff due to soil saturation is related to topographic and soil characteristics of the catchment under consideration. The spatial variation of these characteristics is represented through fitted distribution functions. This modelling approach is usually labelled "semi-distributed modelling", since it provides a compromise between fully distributed modelling (where the catchment is divided into a number of elements) on the one hand, and models using catchment average values on the other.

Application of fully distributed models in deriving flood frequencies is still not common practice. Only a few attempts are reported. Hess and Inman [1994] used the distributed rainfall-runoff model *DR3M* to asses the effect of flood detention reservoirs on discharges in

two small urban catchments. Simulations were performed for a long rainfall series for a) the situation with detention reservoirs and b) the situation without detention reservoirs. Flood-frequency relations based on the long-term peak discharges were developed for each simulation by fitting the logarithms of the annual peak discharge data to a Pearson type III distribution curve. Kuchment et al. [1993] used a distributed model of forest-steppe zone catchment in Russia. Overland and channel flow was described by one-dimensional kinematic wave equations, whereas infiltration and vertical transfer of soil moisture is described by Richards equation. Currently, the Institute for Inland Water Management and Waste Water Treatment (RIZA), a subdivision of the Dutch Ministry of Transport, Public Works and Water Management is investigating the possibilities of applying a rainfall-runoff model (The HBV-model, Killingtveit and Sælthun [1995]) and a one-dimensional hydrodynamic routing to derive flood frequencies (Parmet et al., 1999).

1.4 The scope of this thesis

In the present chapter, a number of physically based approaches towards flood frequency analysis have been presented. In these approaches catchment-runoff models are combined with meteorological models which generate characteristics of future flood generating events and their probability of occurrence. Although physically based flood frequency analysis is a promising alternative for the classical statistical approach, it is until now hardly aplied in practice. One of the reasons for this is that there is still much research needed on the validity of the concept. Furthermore, it is still unclear whether a physically based approach actually results in estimates of exceedance probabilities of river discharges which are more reliable than estimates which are obtained from purely statistical analyses.

The present research project was started up in 1995 because of the obvious need for further research on the topic of physically based flood frequency analysis. The involved institutes (the section Hydrology and Ecology of Delft University of Technology and Delft Hydraulics) agreed that research mainly had to focus on the hydrological modelling aspects of physically based flood frequency analysis, i.e. the meteorological aspects are only a side issue of the research. Furthermore, since flood frequencies refer to river discharges, the main focus is on catchment-runoff modelling. Naturally, as the interest is on physically based modelling, the internal processes within the catchment are studied and modelled as well, but only in the context of the role they play in runoff generation at the catchment scale. The hydrological systems of interest are the type of catchments which can be found in the basins of the river Rhine and the river Meuse, except for the glacier dominated catchments in the Southern part of the Rhine basin. In general, this means the focus is on hillslope areas, dominated by forestry and agriculture. Climatic conditions are mildly humid.

The central issues that were defined at the beginning of the research were:

- Which rainfall-runoff processes are dominant during extremely wet meteorological conditions?
- Which mathematical equations are suitable to describe these processes?
- Which catchment-runoff models are suitable to be applied in flood frequency analysis?

A literature research was needed to get a perception of the current knowledge on rainfall-runoff processes and models that describe them and to define research issues into more detail. In chapter 2 and chapter 3 the main conclusions of this literature research are described. At the end of chapter 3, a more detailed outline of the thesis is presented.

2. Rainfall-runoff processes

2.1 Introduction

The process of water flowing through rivers is part of the ever continuing process called "the hydrological cycle" (Figure 2.1). Every process within the hydrological cycle has its influence on the amount of water flowing through a river, either directly or indirectly. Careful examination of these processes and assessment of their relative contributions to river floods is a crucial part of physically based flood frequency analysis.

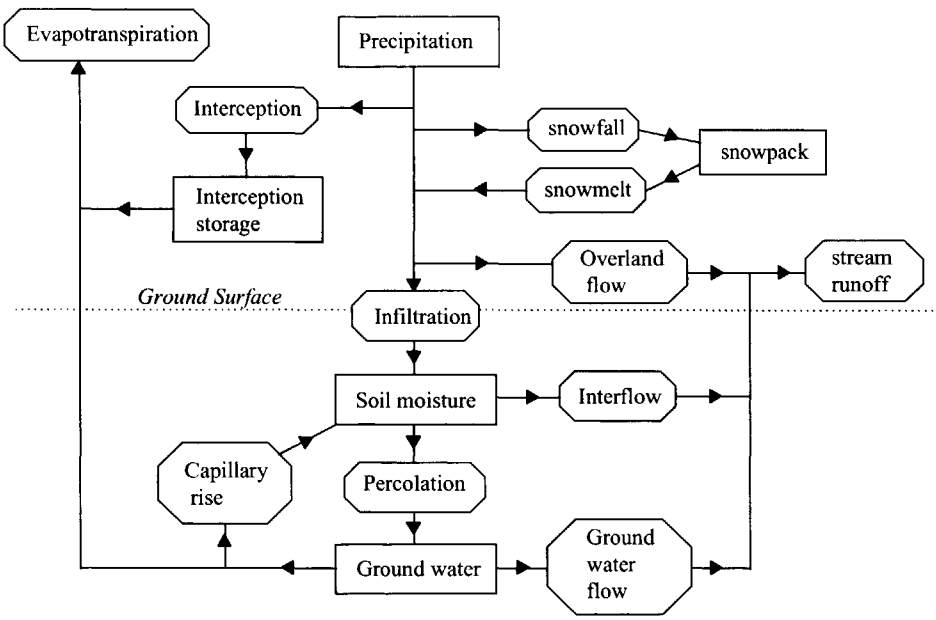

Figure 2.1 Schematic view of the land phase of the hydrological cycle, after Pilgrim, D.H. and Cordery, I., 1993.

Of the various processes shown in Figure 2.1, precipitation is the most dominating control on river discharges. Precipitation, either occurring as rainfall or snowfall, is the key hydrological input of a river catchment. The remaining processes of Figure 2.1 merely decide which percentage of the precipitation is available for runoff and the time which is needed by this runoff water to reach the catchment outlet. If precipitation occurs as snowfall, runoff will be delayed until after this snow has melted. In catchments where snowfall is the main form of

precipitation, high river discharges are likely to occur during the late spring and early summer when the snow pack, which has mounted during the winter months, is melting due to rising temperatures. In this thesis, snowfall-dominated catchments will not be considered, so in this chapter for convenience precipitation is assumed to appear as rainfall only.

The complex interactions between the various runoff processes make the integrated catchment response far from trivial. In order to be able to predict the catchment response, a large amount of catchment-runoff models have been developed, especially in the past three decades. The processes described in these models have been, and still are, extensively monitored in so-called research catchments. These field studies have provided useful information on the occurrence and relative importance of flood generating processes under a variety of physical and climatological conditions. In some cases, results of different field studies seem to contradict each other, which can be put down to the fact that no two catchments are the same and hydrological behaviour can vary significantly between catchments. In catchment-runoff modelling it is therefore crucial to have a concept of the influence of catchment characteristics on the relative dominance of the variety of hydrological processes.

This chapter presents a literature review of a number field studies which were (almost) entirely dedicated to this topic. The main focus is on the processes that dominate during storm events (section 2.2), but also a brief review will be given on the processes that play an indirect role in the generation of peak discharges, by influencing the initial hydrologic conditions of a storm event (section 2.3).

2.2 Storm runoff mechanisms

2.2.1 Introduction

Storm flow (also referred to as direct runoff) is the volume of water entering a stream (or river) during or shortly after a rainfall event minus the amount of base flow water. Generally, it forms the major part of river flow during high water events. Storm flow amounts are often derived through separation of the observed hydrograph as depicted in Figure 2.2. Although attempts have been made to standardise the procedure of hydrograph separation (Hewlett and Hibbert, 1967), it still is a subjective matter, especially since in reality hydrograph shapes are more complex than the one depicted in Figure 2.2.

A major contribution to a better understanding of the characteristics and the relative importance of storm runoff mechanisms has come from the large amount of field studies which have been performed all over the world since the 1960's. The majority of these studies concentrate on the drainage of small (< 1 km^2) watersheds (hillslopes) into small (first order)

streams. This small scale of interest is preferred, because it enables hydrologists to perform measurements on relatively high spatial resolutions, which means a more complete picture of the processes occurring can be obtained.

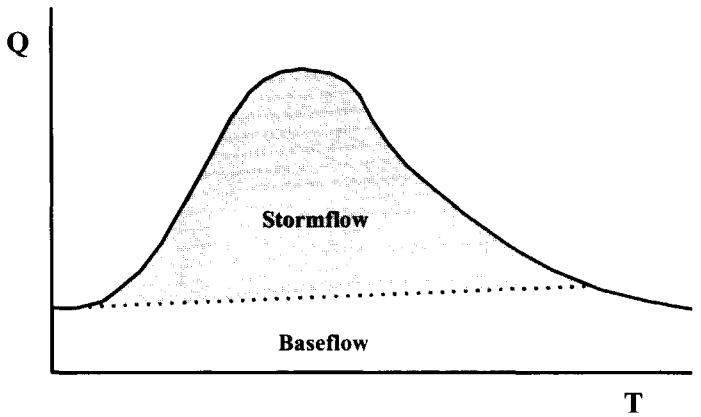

Figure 2.2 Hydrograph separation into base flow and storm flow.

Three types of mechanisms are being recognised to be responsible for the relatively fast transport of rainfall water towards the stream network during storm events (e.g. Dunne, 1983; Pearce et al., 1986; Sklash, 1990):

1. Infiltration excess overland flow (Horton overland flow).
2. Saturation overland flow (Dunne overland flow).
3. Subsurface storm flow (Interflow).

Sometimes a fourth storm flow process (channel interception) is added to this list (e.g. Hewlett and Hibbert, 1967) but it will not be discussed here because of its triviality. In the remainder of this section the three mentioned processes will be discussed separately, and field evidence for their occurrence and relative dominance will be presented.

2.2.2 Infiltration excess overland flow

Infiltration excess overland flow occurs when the infiltration capacity of the topsoil is exceeded by the rainfall intensity. The soil is unable to absorb all rainfall water and after a "ponding time" (the time required for surface depressions to be filled) the excess rainfall will runoff in downslope direction over the ground surface downslope either towards a nearby stream or towards areas where it is able to infiltrate. In general, water is able to flow at significantly higher velocities over land than in the soil. Furthermore overland flow decreases the length of flow paths to the stream network. Overland flow is often thought (modelled) to

occur as sheet flow (e.g. Abbot et al., 1986b), but this is rarely observed in nature (Freeze and Harlan, 1969). When overland flow is generated in nature it flows through small conveyances like micro-channels, rills and gullies, which can be considered as a small scale version of stream flow (Chorley, 1978; Freeze and Harlan, 1969).

Infiltration excess overland flow is often referred to as *Horton overland flow*, after the man who in the 1930's claimed that runoff peaks are generated by this mechanism only (Hall, 1987). His concept of runoff generation, in which infiltrated rainfall water contributes to base flow only, was hardly doubted by anyone until the 1960's, since no results of extensive monitoring studies were available to prove it wrong or to improve conceptualisations of other storm runoff mechanisms (Robinson, 1993). Since the 1960's a large number of field studies, performed all over the world, gave more insight in the validity of this concept. In some basins, often to be found in arid and semi-arid areas, infiltration excess overland flow was indeed evidenced to dominate storm runoff completely (e.g. Pilgrim, 1983). In the majority of the research basins, however, infiltration excess overland flow appeared to be not the only possible storm runoff mechanism. Furthermore, it has been noticed that in a significant number of research catchments all over the world, infiltration excess overland flow hardly occurs, except on unvegetated areas like rocks and roads (Dunne, 1978; Hewlett and Hibbert, 1967).

2.2.3 Saturation overland flow

Saturation overland flow is, like infiltration excess overland flow, a mechanism in which water is transported over the ground surface towards the stream network. However, it has a different cause and consequently it occurs under different conditions. Saturation overland flow occurs on areas where the soil is completely saturated, caused by rising water tables (saturation from below Gerits et al., 1990). Water tables rise at locations where drainage of soil water is exceeded by recharging rainfall water and incoming laterally flowing subsurface water. Rising water tables which cause the topsoil to be saturated can be either perched (ephemeral) water tables or perennial groundwater tables. When the soil is filled to capacity and drainage of soil water is still exceeded by the combination of rainfall water and incoming lateral subsurface flow, part of the rainfall water cannot infiltrate and consequently will runoff over the ground surface in combination with some exfiltrating groundwater.

Anderson and Burt [1990] recognise three locations within a catchment where soil saturation occurs relatively often:

1. *Near-stream areas at the base of a hillslope.* Uphill contributing areas are relatively large for near-stream areas, since flow paths are directed towards the stream network. This gives rise to relatively large supplies of rainfall water, fallen on areas uphill and transported downhill, either over land or through the soil. Conditions at near stream areas

are therefore likely to be relatively wet, which means probabilities of saturation to occur are relatively high. Especially in valley-shaped near stream areas, conditions are favourable for saturation overland flow. The relatively low hydraulic gradients in valley-shaped areas cause the drainage capacity of the subsurface to be relatively small. Field evidence of near-stream areas being saturated relatively often can be found in Betson and Marius [1969], Harr [1977], Mosley [1979] and Rawitz et al. [1970].

2. *Hillslope hollows.* Just as for near stream area's, flow paths are directed towards hillslope hollows, which implies the uphill drainage area is relatively large. Field evidence of hillslope hollows being saturated relatively often can be found in Dunne and Black [1970a,b] and Montgomery and Dietrich [1995].

3. *Locations where a low-conductivity subsurface layer is positioned close to the ground surface.* At these locations the storage capacity of the topsoil is relatively low, which means during a rainfall event, infiltrating rainfall water fills up the topsoil relatively quickly. In some cases the low-conductivity layer separates the saturated topsoil from an unsaturated layer below. In that case the water of the saturated topsoil is often referred to as "perched water table" in order to make a distinction between this water table and the "real water table" (the water table of the continuously saturated zone). Field evidence of undeep low-conductivity layers causing saturation of the topsoil can be found in Betson and Marius [1969], Mosley [1979] and Pierce [1967].

Saturated areas adjacent to streams (point 1. above) are of particular importance in generating storm flow. Rainfall water falling on these areas flows over the ground surface towards the stream network. Since the stream is nearby, travel times are relatively small. As stated above, overland flow water will be guided through micro-channels, rills and gullies, which means these saturated riparian areas can be considered as extended stream systems. Overland flow generated on uphill located saturated areas, on the other hand, can only be important in generating storm flow when these uphill areas and the saturated near-channel areas are connected to each other through saturated flow paths. Without this connection water surface runoff from upslope will re-infiltrate into downslope located soils (Betson and Marius, 1969).

Obviously the (varying) size of the saturated areas is a dominant factor for the generated amount of saturation overland flow. Experiments with artificial storms on a number of watersheds (Corbett et al., 1975; Dunne and Black, 1970a) showed that peak flow hydrographs were almost completely dominated by water coming from the saturated riparian areas. These and other studies caused Dunne [1978] to conclude that saturation overland flow is the dominant peak flow generating process in the majority of watersheds in areas with a humid climate, a statement which still is subject of discussion (see section 2.2.5).

2.2.4 Subsurface storm flow

Introduction

The concept of storm flow generation proposed by Horton (see section 2.2.2), in which infiltrated water does not contribute to storm flow, was based on the idea that the process of water flowing through the subsurface occurs at velocities which are much to low to reach the channel before the hydrograph peak time. The validity of this concept has been rejected, though, by field observations of rainfall events, producing amounts of storm flow which couldn't be accounted for by the observed amounts of overland flow (e.g. Harr, 1977; Mosley, 1979; Rawitz et al., 1970; Whipkey, 1967). Furthermore, results from isotope and tracer studies, in which residence times of rainfall water have been studied, suggest that pre-event water, stored in the soil layer, often accounts for a major proportion of the storm runoff (Harris et al., 1995; Kubota and Sivapalan, 1995; Pearce et al., 1986), which also contradicts the concept of overland flow being the only source of storm runoff. These observations made it clear that in many, especially vegetated, watersheds a considerable part of the storm flow can originate from the subsurface. The term subsurface storm flow (often referred to as interflow or throughflow, although there is no general agreement on the definition of these terms) has been defined to declare the part of the storm runoff which can not be accounted for by overland flow. It has become clear that it is a collective noun for a variety of processes occurring in the subsurface (Hewlett and Hibbert, 1967). In the remainder of this section these processes will be discussed.

Macropore flow

In every soil a large variety of pore sizes can be found. Some of the pores are even too big to retain water through capillary forces, which means they can serve as a relatively fast transport medium for infiltrating rainfall water. Nowadays, it is widely recognised that these relatively large pores (macropores) can influence flow paths, flow rates and flow speeds significantly (McDonnel, 1990; Mikovari et al, 1995; Mosley, 1982; Onodera and Kobayashi, 1995).

As shown by the literature review of macropore size definitions presented by Beven and Germann [1982], definitions of macropores are far from uniform. This overview contains a large variety of the minimum diameters that, according to the referred authors, pores need to have in order to be labelled as a macropore. Two reasons for the non-uniformity of macropore definitions are:

1. The influence of macropores on subsurface water flow varies from soil type to soil type. A relatively large pore with a diameter of, for instance, 3 mm will make more of a difference in fine-textured soils than in core-textured soils.

2. Macropores are often well connected due to a common cause of their existence which means they form channels (preferential pathways). As a consequence, the influence of macropores on subsurface flow rates does not only depend on their size but also on the present structure of the pore network.

There are a number of possible causes for the formation of preferential pathways and these strongly influence the size and structure of the pathways. This has lead to a classification of types of macropores. Some distinguished types of macropores are (Beven and Germann, 1982; Whipkey, 1967):

- *Earthworm holes*: Macropores formed by the movement of earthworms through the soil. Insects may also be responsible for the formation of macropores.

- *Root holes*: Macropores formed by the (sometimes decayed) roots of plants and trees.

- *Cracks and fissures*: Macropores formed by the process of shrinking and swelling of clay soils, due to changes in soil moisture contents.

- *Pipes*: Large-diameter versions of macropores, often formed by the erosive effect of rapid water flow on macropores.

Because of the obvious structure of macropores and their dominant role in subsurface runoff generation, distinction is sometimes made between the macropore system on one hand and the micropore system (soil matrix) on the other hand. Another reason for this distinction is the flow mechanism in macropores, which has been observed to be turbulent (Whipkey, 1967), whereas flow in the matrix system is generally laminar. If the soil matrix directly surrounding a macropore is unsaturated, the capillary forces of the soil matrix will act upon the available macropore water since capillary potentials of the relatively small pores of the soil matrix exceed those of the macropores. In that case water is extracted from the macropore system, that is, if it has been able to enter the macropore system at all. Therefore, the relative role of macropore flow in subsurface flow is likely to increase under increasingly wet conditions.

One of the main consequences of the availability of macropores is the increase in observed infiltration capacities. When the rainfall intensity exceeds the infiltration capacity of the soil matrix, the top layer of the soil will be saturated and ponding will occur at the ground surface. The ponded water will enter the available macropores which enables the ponded water to bypass the soil matrix. This causes a significant increase in infiltration velocities, since the gravity-driven flow in macropores is hardly obstructed by capillary forces. In this way a (major) part of the rainfall water will be transported relatively quickly towards deeper

soil layers where water can be extracted from the macropores by the surrounding soil matrix, provided it is unsaturated. In this way irregularly shaped wetting fronts will be formed, which has been demonstrated by several tracer studies (e.g. Flury et al., 1994; Hornberger et al, 1991). The presence of macropores can obviously increase the infiltration capacity of soils, especially of topsoils in vegetated areas. This is the main reason why infiltration excess overland flow is hardly observed in these type of areas.

Perched water table flow

Especially in vegetated areas, a highly permeable (organic) top layer is often witnessed to overly a significantly less permeable subsoil layer (e.g. clay or bedrock). During rainfall events with rainfall intensities lying in between the permeability values of these two layers, the rainfall water will infiltrate completely into the top layer, but will only partly be able to infiltrate/percolate through the subsoil layer. Therefore, during rainfall events of considerable duration, a perched water table will be formed at the base of the topsoil. This perched water table will be drained downslope over the less permeable layer. The transportation of this perched water table will be relatively quick, since it takes place under saturated conditions in the highly permeable top layer. Furthermore, the downslope transport of the perched water table is often promoted by laterally (downslope) directed preferential flow paths at the topsoil/subsoil interface. Possible causes for the existence and development of these flow paths are:

- Lateral extension of roots over the subsoil, when roots are unable to penetrate the less permeable subsoil (McDonnel, 1990).
- Coverage of (former) bedrock channels by organic layers (Beven and Germann, 1982)
- The erosive effect of the perched water table flow (Jones, 1971).

Diameters of the preferential flow paths at the topsoil/subsoil interface can be relatively large (even up to 1m., Beven and Germann, 1982), so sometimes the term pipe flow is used for this type of flow. Pipe flow can occur at velocities that even exceed overland flow velocities (Anderson and Burt, 1990).

The combined process of vertical flow through macropores in the topsoil towards a less impeding layer over which it will flow downslope towards the stream is found to be the dominant storm runoff process in a considerable amount of study areas (e.g., Peters et al., 1995; Sivapalan, 1993; Whipkey, 1967).

2.2.5 Relation between catchment characteristics and occurrence of storm flow mechanisms

Three processes (infiltration excess overland flow, saturation overland flow and subsurface storm flow) have been identified and evidenced to produce significant amounts of storm flow.

The relative contributions of these processes to storm flow vary heavily between different watersheds due to differing watershed conditions. Furthermore within one watershed the relative contributions have been evidenced to vary significantly from storm event to storm event due to varying soil characteristics and/or rainfall intensities.

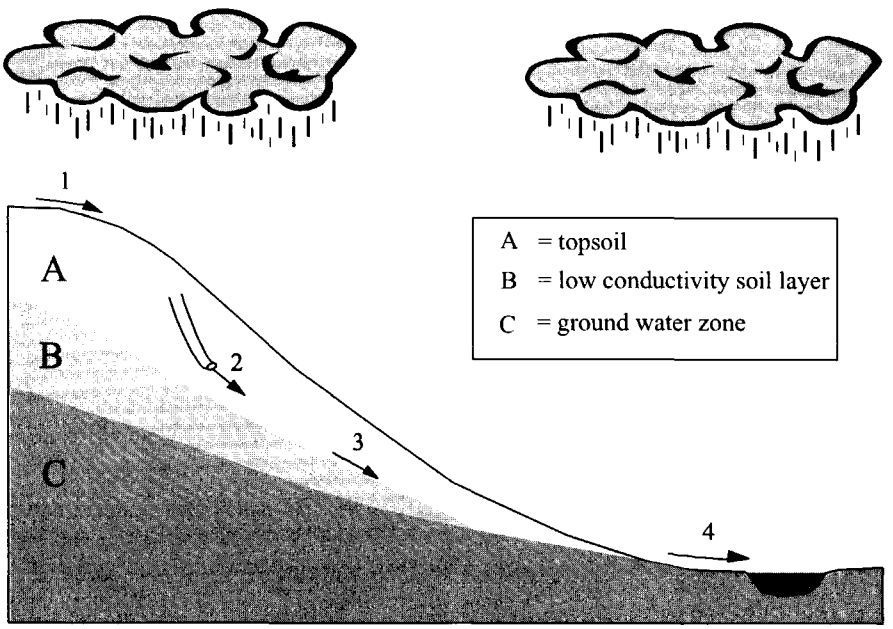

Figure 2.3 Schematisation of a hillslope where four storm flow processes take place: 1. Infiltration excess overland flow on locally impermeable soil 2. bypassing through macropores in the topsoil (=subsurface storm flow), 3. Perched water table flow at the base of the topsoil (=subsurface storm flow) and 4. Saturation overland flow at near-stream saturated areas.

As a consequence, there is no clear, uniformly valid concept of the relative importance of storm flow processes. However, field experiments provided information on the influence of catchment characteristics on the relative contributions of the various processes on storm flow generation. For each storm flow process, a number of factors are known to enhance the occurrence of the process during storm events:

1. *Infiltration excess overland flow*: Impermeable soils, no vegetation, high rainfall intensities.
2. *Saturation overland flow*: Shallow, moderate permeable soils, concave-shaped hills, wide valley bottoms.
3. *Subsurface storm flow*: Steep straight slopes, deep permeable soils, forests, narrow valley bottoms.

The majority of the watersheds consist of a combination of the above factors, which means storm flow will be generated by a combination of the three processes. A problem that arises during identification of storm flow contributions of different runoff processes is that these processes are often difficult, if not impossible, to separate from each other. For instance, rainfall water falling on a bedrock area over which it will flow downslope (infiltration excess overland flow), can infiltrate further downhill into more permeable soils. In the soil it may be transported through the macropore system (subsurface storm flow) towards a valley-shaped saturated hillside bottom where it exfiltrates and flows over land (saturation overland flow) towards the stream network. Since this water reaches the stream over land on saturated soils, it is labelled as saturation overland flow. However, it is clear that the other two storm flow processes also played a significant role in the relatively quick transport of this water towards the channel in a relatively short period of time.

Despite the difficulties in identifying the sources of stream runoff, it is widely recognised that in vegetated watersheds with a humid climate a large proportion of stream runoff originates from a small saturated part of the watershed, mainly to be found adjacent to the stream. This source area is often referred to as or variable source area (Hewlett, 1961) because it expands during rainfall events and shrinks afterwards. Naturally, stream runoff discharges will increase as the source area expands. There are two reasons why these riparian areas are able to generate the majority of storm flow:

1. These areas are often saturated due to the relatively large upslope drainage area and complete soil saturation is the (necessary) condition for saturation overland flow and the best condition for subsurface storm flow to occur.
2. Flow paths towards the stream are relatively short.

A major consequence of the dominating role of saturated areas on runoff amounts is the fact that soil moisture conditions at the beginning of a storm event significantly influence runoff generation during the storm event under consideration. Therefore, the hydrological processes that control the initial moisture conditions also have to be considered in flood generation analysis. In the next section, a brief overview of these processes will be discussed.

2.3 Processes controlling the initial soil moisture condition

2.3.1 Introduction

During storm events, unsaturated soils absorb (part of the) incoming rainfall and prevent it from running off directly towards the stream. The soil can thus be seen as a rainfall reservoir. Runoff amounts of storm events depend strongly on the remaining storage capacity of the soil. This capacity is determined by:

1. The thickness of the soil layer
2. The average porosity of the soil
3. The volumetric water content at the beginning of the rainfall event

The thickness and the average porosity can be considered time-invariant, whereas the volumetric water content at the beginning of the rainfall event varies from event to event. In shallow soils the remaining capacity of the soil will always be small, regardless of initial moisture conditions. These soils will be filled to capacity during the early stages of a rainfall event, allowing the excess rainfall to run off directly. Obviously, the influence of initial moisture condition on runoff production increases with increasing soil thickness. The initial moisture condition is influenced by a number of processes. Although the majority of these processes cannot be labelled as storm flow processes, they can indirectly influence the amount of runoff during storm events by affecting the soil moisture conditions. A short discussion on these processes is presented.

2.3.2 Pre-event rainfall

As mentioned in section 2.1, rainfall is the key input to a river catchment. Therefore rainfall is the dominating control on the soil moisture condition. The rainfall history of several days, weeks or even months (depending on the catchment under consideration) can influence the initial moisture condition of a storm event. Extreme river floods are often reported to have a long history of rainfall amounts which exceed average rainfall amounts (e.g. Engel, 1998; Kunkel, 1994). Consequently, research on extreme rainfall amounts in order to derive flood frequencies, should take into account the concept of the extent of the rainfall history of flood events.

2.3.3 Evaporation

Evaporation is the process of water being converted into water vapour. Evaporation fluxes are mainly controlled by 1) the availability of water in the system, 2) the availability of solar energy, 3) wind force 4) the vapour content of the air and 5) the type of vegetation cover. The part of the rainfall water that evaporates is no longer part of the land phase of the hydrological system and is therefore often considered a loss term in runoff-hydrology. Due to the structural fluctuations in available solar energy throughout the year (relatively high in the summer and relatively low in the winter) evaporation amounts show yearly periodicity. This periodicity is mirrored in soil moisture conditions, i.e. during winter months, soil moisture conditions are usually wetter than in summer. As a consequence, runoff amounts in rainfall dominated catchments are, on average, significantly higher during winter than during summer.

2.3.4 Water uptake through roots

Toplayers of vegetated areas are densely filled with roots that extract water from the so called root zone. The water uptake reduces the soil moisture contents of the root zone and therefore indirectly also reduces the soil moisture content of underlying layers. The amounts of water uptake depend on the type(s) of vegetation as every type of vegetation has its own needs. A change of vegetation cover in a (sub-) catchment can lead to significant changes in soil moisture conditions, and therefore indirectly lead to changes in runoff characteristics.

2.3.5 Groundwater flow

The process of groundwater flow influences the amount of runoff during a storm event in two ways:

1. Groundwater flow generates the base flow in a river on which the storm flow is superimposed.
2. Groundwater flow influences soil moisture conditions.

The influence of groundwater flow can be neglected in areas where the groundwater table remains underneath an impeding layer throughout the year. The dominant storm runoff processes take place above the impeding layer and will not be effected by the groundwater. On the other hand, if the groundwater table does reach into this zone of storm runoff occasionally or permanently, the groundwater table will act as an impeding layer for the infiltrating rainfall water and in this way it will strongly influence storm runoff amounts.

2.4 Conclusions

Extensive filed monitoring studies have contributed greatly to the understanding of the storm runoff mechanisms. In general, three storm flow processes are distinguished: Infiltration excess overland flow, saturation overland flow and subsurface storm flow. Still, though, the understanding of rainfall-runoff processes is still far from complete, due to the fact that several difficulties arise when a complete understanding of processes is demanded:

1. It is often hard to separate the processes taking place, even by intensive measurements.

2. Despite the high spatial and temporal resolutions of measurements of the field studies, it is impossible to measure all processes taking place in a watershed. As natural soil properties show a large degree of heterogeneity, various aspects of occurrence and characteristics of the processes can easily be overseen.

3. Every catchment has it's own unique characteristics which means different catchments can have significantly different hydrologic responses to the same amount of precipitation. This makes it hard, if not impossible, to extrapolate results from measurements from one catchment to another.

4. A single catchment can respond differently to similar rainfall events on different occasions due to differences in antecedent conditions (e.g. soil moisture distribution, swelling/shrinking cracks, change of vegetation).

The contradicting results of some of the field studies indicate there is still a need for a better understanding of rainfall-runoff processes. For this reason it should be taken into account by hydrological modellers that results drawn from models always will contain some uncertainty which is difficult, if not impossible, to quantify.

3. Mathematical modelling of rainfall-runoff processes

3.1 Introduction

A mathematical model is "*..a set of mathematical expressions and logical statements combined in order to simulate the natural system*" (Refsgaard, 1996). In hydrology, mathematical models serve as:

1. Management tool: To assess the impact of human interventions on hydrological systems.
2. Predictive tool: To predict the (near-) future state of hydrological systems.
3. Research tool: To gain and encapsulate knowledge on hydrological processes.

Besides mathematical models also physical models (e.g. small scale laboratory models) are used in hydrology. However, these models are not subject of research here, so in the remainder of this thesis the term "hydrological model" refers to mathematical hydrological models only. Since the mid sixties, progress in computer technology and information from field studies on hydrological processes motivated hydrologists to produce a large number of hydrological models. The need for different types of models stems from the existence of a wide range of applications, related to the variety in:

1. *The time scales of interest* (event based models, models with daily, monthly or yearly time steps)
2. *The spatial scales of interest* (ranging from the laboratory scale to the global scale).
3. *The processes of interest* (e.g. sediment transport, river flow, land/atmosphere interactions)
4. *The physical characteristics of the simulated system* (mountainous/flat catchments, humid/arid conditions)
5. *The objective for which the model is used* (management, predictive or research tool)

As far as these five "issues" are concerned, this thesis concentrates on models build for:

1. The time scale of precipitation events, i.e. from a few hours to a few days
2. The catchment scale
3. All relevant processes involved in flood generation
4. Hilly rural areas under mild humid climatological conditions.

5. Predictions and research.

This chapter presents a brief overview of model concepts in catchment-runoff modelling. Subsequently, the validity and applicability of the different model concepts will be discussed. Finally, a number of relevant research issues on catchment-runoff modelling are presented on which this thesis will focus.

3.2 Modelling concepts

3.2.1 Introduction

Although applied hydrologic engineering is known to exist for at least 5000 years (at 3000 BC King Menes dammed the Nile river, see Biswas 1972), the use of catchment-runoff models has a history of about 150 years. Four major steps in the evolution of catchment-runoff modelling are distinguished:

- *The rational formula of James Mulvany* (1847, see Biswas, 1972), which is considered to be the first serious catchment-runoff model in history. This model is based on the assumption of a constant (time-invariant) percentage of rainfall which runs off. In formula: $Q=C*I*A$, where Q = runoff, C = the runoff factor, I = the rainfall intensity and A = the size of the catchment. Furthermore, a time delay in the transformation from rainfall to catchment runoff was introduced. This delay factor was related to the time of concentration, i.e. the maximum time needed for a drop of net precipitation to reach the catchment outlet.
- *Sherman's Unit Hydrograph method* (Sherman, 1932). In comparison with the rational formula, Sherman's method of the unit hydrograph changes the constant travel time into a distance related travel time. As a consequence the transformation of net precipitation into catchment runoff was controlled by a distribution function called "the unit hydrograph". The unit hydrograph is an empirically based function (at least, in Sherman version) which defines the arrival times at the catchment outlet of all percentiles of one millimetre of net precipitation.
- *The Stanford watershed model* (Crawford and Linsley, 1962). This computer model was the first to take into account the various components of the hydrological cycle. It was presented in 1962 (Crawford and Linsley, 1962) and "completed" (model version IV) in 1966 (Crawford and Linsley, 1966). This model represents storage components of the hydrological cycle (like groundwater, soil moisture, depression storage) as reservoirs and allows interactions between the reservoirs based on the processes involved (e.g. infiltration, interception, evaporation). Both storage components and processes were

modelled on the catchment scale, which has the advantage of relatively small time period needed for one simulation run.

- *The blueprint for a physically based distributed model of Freeze and Harlan, [1969].* These authors recognised an increased need for a representation of the existing spatial variation of processes and parameters within the catchment. They proposed an approach in which a number of submodels, representing the various storage components, are divided into a number of elements. Each element is awarded its own set of parameters and boundary conditions, which results in a representation of the existing spatial variability of the hydrological response within the catchment.

At present, numerical solution techniques and computational capacities of the current generation of computers allow the mathematical equations of rainfall-runoff models to be as complex as desired. However, simple models still prove to be useful in a lot of applications. The rational method of James Mulvany, for instance, is still widely used in urban drainage design (Pilgrim and Cordery, 1992). Different hydrological applications require different model concepts, each with its own advantages. For the sake of clarity, models have been classified (Clarke, 1972; Refsgaard, 1996; Sing, 1995) based on similarities/differences in model concepts.

Models can be either *deterministic* or *stochastic*. In deterministic models, each parameter has one specific value, which means for two equal sets of input the model will generate the same output, provided that initial conditions are the same. In stochastic models on the other hand, some parameter values are randomly generated, so in general two equal sets of input lead to different output. Furthermore models are labelled either as *distributed* or *lumped*. Lumped models use parameters which represent the "average value" of an entire catchment, whereas distributed models take spatial variability into account by dividing the catchment up into a number of elements.

Models can also be classified according to what extent the model takes into account the physics that occur in the catchment. Three categories are recognised (Refsgaard, 1996):

1. *Empirical models*: Models relating input and output series without consideration of the physics involved in the hydrological system of interest.
2. *Lumped conceptual models*: Models using process simulation techniques and parameters which are physically meaningful, but mostly not directly measurable since they are lumped on the catchment scale.
3. *Physically based distributed models*: Models based on physical laws, such as the conservation laws of mass, momentum and energy. The distributed character of these models enable the parameters to be directly measurable and the equations to be solvable by numerical solution techniques.

This classification is of particular interest here, since it shows that introducing physics in flood frequency analysis can be performed to different degrees In the remainder of this section examples of the three types of models are presented to illustrate the essential differences between the concepts.

3.2.2 Empirical models

Hydrological models are labelled "empirical models" if they are based on mathematical equations which do not take into account the physical processes involved in the hydrological system. Parameters of these models are merely based on the analysis of paired time series of input and output. A well-known example of an empirical model is the *unit hydrograph method* (Sherman, 1932). Although techniques exist to relate the shape of the unit hydrograph to physical characteristics of the catchment (e.g. Rodriguez-Iturbe and Valdés, 1979), it is derived through the method of least squares in Sherman's original approach.

The unit hydrograph (UH-) concept is based on the assumption that travel times only depend on distance to the catchment outlet. Ergo, travel times are independent of the intensity and duration of the precipitation event. Consequently, a catchment will always show the same response to 1 mm of net precipitation falling uniformly spread over the entire catchment during a period of 1 hour. The corresponding hydrograph is referred to as the unit hydrograph

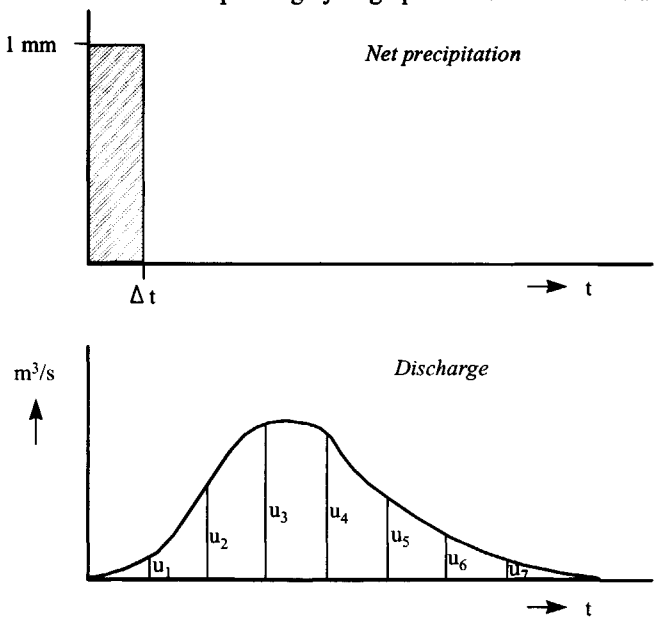

Figure 3.1 The unit hydrograph which theoretically will be observed at the catchment outlet as a consequence of 1 mm net precipitation falling uniformly spread over the entire catchment

during a period of Δt hours. The straight vertical lines are the ordinates of the unit hydrograph.

In general, the unit hydrograph is being referred to as the "*Δt*"-Unit hydrograph (e.g. 1-hour unit hydrograph) since the shape of the unit hydrograph depends on the related time of net precipitation. During a period of length Δt, the precipitation is assumed to fall with constant intensity. In reality, of course, this assumption does not always hold since intensity can vary strongly throughout a rainfall event. A rainfall event is therefore considered to be built up from a number of periods of length Δt. Within one period, the intensity is constant, whereas among the periods the intensity can vary. The length of *Δt* therefore has to be chosen such, that the assumption of constant intensity within one period is valid for the type of rainfall events under consideration. Since a rainfall event consists of a number of periods of unit length, the resulting hydrograph is an accumulation of a number of unit hydrographs. This resulting hydrograph is easily obtainable through application of the following two rules:

1. If the one hour rainfall equals 2 mm, the hydrograph ordinates will be twice as high as would have been in case the one hour rainfall equals 1 mm.
2. If the rainfall intensity in 2 subsequent hours equals 1 mm/hour, the resulting hydrograph equals the sum of two 1-hour unit hydrographs, where one unit hydrograph is shifted one hour in time (see Figure 3.2)

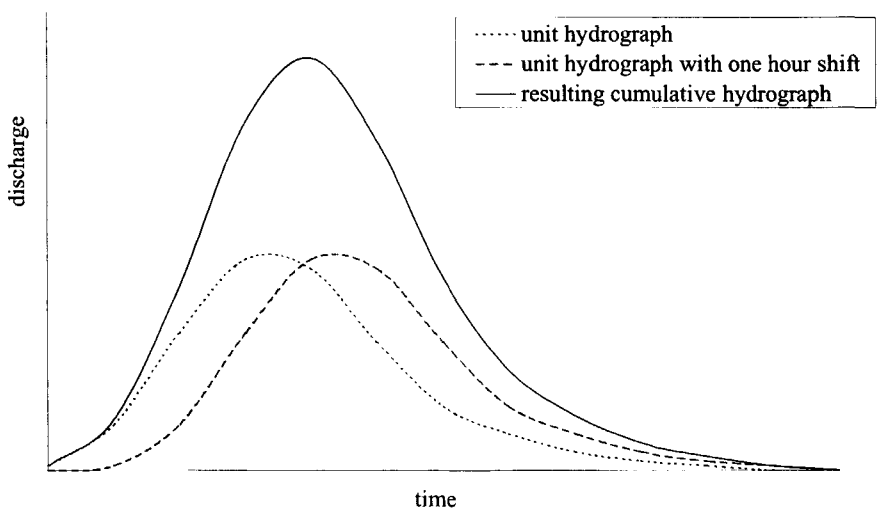

Figure 3.2 Derived discharge as a consequence of two hours of rainfall with an intensity of 1 mm/hr according to the Unit Hydrograph method.

By dividing a precipitation event into a number of periods of length Δt, the UH-method predicts the resulting total runoff hydrograph by simply multiplying the UH-ordinates with observed precipitation intensities and subsequently adding the resulting values. In formula:

$$Q_t = \sum_{k=1}^{K} u_k I_{t-k} \quad ;t = 1..T \tag{3.1}$$

where:

Q_t = Discharge at the catchment outlet at time step t
u_k = Ordinate number k of the unit hydrograph
K = Total number of ordinates of the unit hydrograph
I_t = Rainfall intensity at time step t
T = Number of paired observations (Q_t, I_t)

Before predictions can be made the ordinates of the unit hydrograph have to be derived. This can be done by applying equation (3.1) for T observed paired values of Q_t and I_t ($T \geq K$) and subsequently deriving the set of ordinates $u_1,...,u_K$ that optimally predicts observed values of Q_t according to the least squares criterion:

$$\min_{u_1..u_K} \sum_{t=1}^{T} \left[Q_t - \sum_{k=1}^{K} u_k I_{t-k} \right]^2 \tag{3.2}$$

Clearly, this model can be labelled "empirically based", since the K parameters u_1, u_2, .., u_K are purely based on fitting without taking into account any physical characteristics of the catchment under consideration. However, instead of using the method of least squares, other methods can be used to derive u_1, u_2, .., u_K, some of which are based on physical reasoning involving the use of some catchment characteristics (e.g. Clark, 1945; Naden, 1992; Rodriguez-Iturbe and Valdés, 1979). In that case the Unit Hydrograph concept is being classified as conceptual.

3.2.3 Lumped conceptual methods

Unlike empirical models, conceptual models make use of equations which are based on the physics involved in the hydrological system. These models are usually able to capture to a large extent the dominating rainfall runoff processes in a catchment through application of a set of easy solvable equations. Therefore, conceptual models are considered to be the perfect compromise between the need for simplicity on one hand and the need for a firm physical basis on the other hand. The disadvantage of these type of models, however, is the fact that it is generally impossible to derive parameter values from direct measurements instead of calibration techniques since conceptual models are usually lumped on the catchment scale, (Refsgaard, 1996). Well-known conceptual models are the Stanford watershed model

(Crawford and Linsley, 1962), the HBV model (Bergström, 1995), TOPMODEL (Beven and Kirkby, 1979; Beven et al., 1995) and the Sacramento model (Burnash et al, 1973). A description of the latter will serve as an example of this group of models.

The Sacramento model

Figure 3.3 presents a schematic view of the concept behind the Sacramento model, showing land surface-atmosphere interactions, moisture storages, exchange processes and runoff components. The actual defined model components are shown in Figure 3.4. A flow chart like Figure 3.4 is typical for conceptual catchment-runoff models. Storage components are represented as reservoirs while arrows are used to represent the interactions between these reservoirs. The rate at which the reservoir-interactions take place is strongly related to the current storage of the involved reservoirs either through empirical or simple physically based equations. A global description of the Sacramento model is presented in the remainder of this section.

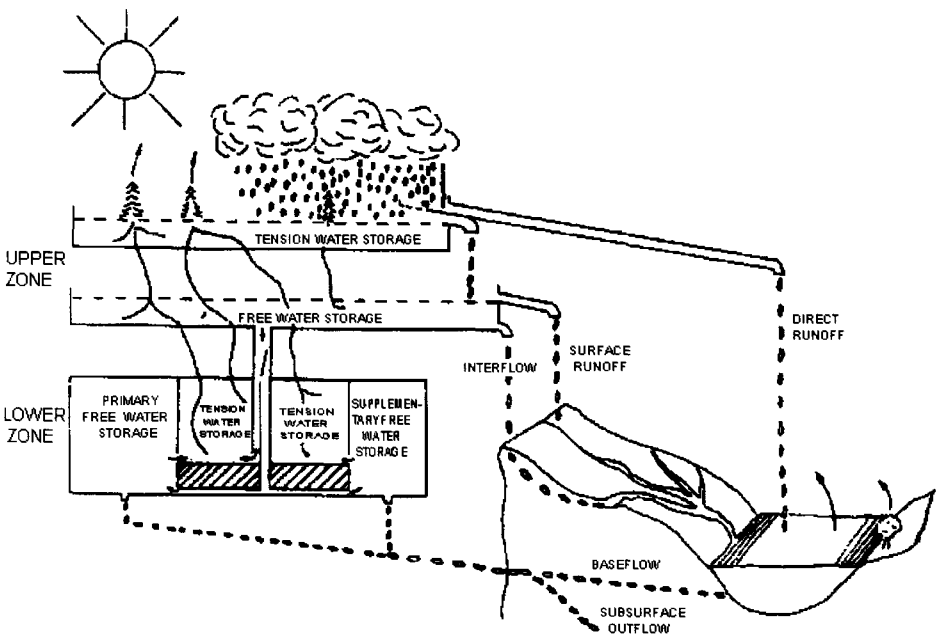

Figure 3.3 Concept of the Sacramento model

Infiltration

A catchment is divided into two parts in order two make a distinction between *pervious areas* and *impervious areas*. If rainfall water falls on the *impervious part* of the catchment, it cannot infiltrate and consequently it runs off directly towards the channel system, except for a small part which evaporates. On the other hand, if rainfall water falls on the *pervious part* of the catchment it is able to infiltrate into the soil. In order to model the various surface and

subsurface processes, the *pervious part* of the catchment is split up into an upper zone (representing the catchment surface system) and a lower zone (representing the catchment ground water reservoir system).

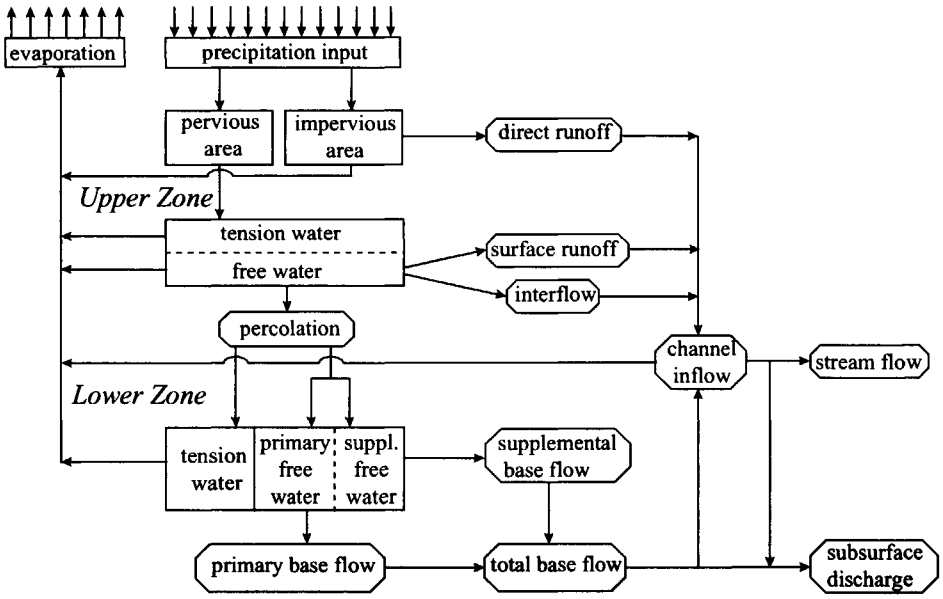

Figure 3.4 Model components of the Sacramento model

The upper zone

The *upper zone* consists of a tension water storage component and a free water storage component. The *tension water* is the part of the precipitation which is needed to meet all interception requirements and to fill up the soil to conditions that are sufficiently wet for percolation to take place. If the tension water storage is filled to capacity, the redundant water becomes available for the free water storage reservoir. The *free water storage* is a temporary storage from which water can either percolate to the lower zone or runoff to the channel system. Two runoff processes are defined: Interflow and surface runoff. Interflow occurs when the maximum percolation rate is exceeded by the incoming precipitation. The interflow rate is directly proportional to the storage content of the upper zone free water reservoir serves. Surface runoff takes place when the precipitation intensity exceeds the sum of the percolation rate and the interflow rate.

The lower zone

The lower zone also contains a reservoir for tension water and a reservoir for free water. The *tension water reservoir* represents the amount of water that is held by the lower zone soil matrix. The soil matrix is filled up through incoming percolation water, unless it is already

filled to capacity (i.e. the field capacity). In that case, all redundant water is directly transferred to the lower zone free water reservoir. However, even before the tension water reservoir is completely filled, the model allows for a part of the percolating water to reach the free water reservoir. The *free water reservoir* of the lower zone is subdivided into a primary and supplementary store, representing the storages leading to a slow and a fast groundwater flow component respectively. The use of two components instead of just one, increases the flexibility to reproduce more complex observed hydrograph recession curves. The available incoming percolating water is divided over these two free water components in a ratio that is proportional two their respective deviation from full capacity. The actual outflow of these components is a percentage of their current water content. Since it represents the fast component of ground water flow, the supplementary free water component has a larger outflow percentage than the primary free water component.
If the two free water components and the tension water zone are all filled to capacity, part of the available percolation is not able to actually percolate and hence will either remain in the free water component of the upper zone or it discharges via the upper zone runoff components.

Evaporation and routing of surface runoff

Water is extracted from a number of model components to represent evaporation. The actual evaporation rate is proportionally related to the atmospheric demand (potential evaporation) and the relative content of the involved model components. A small part of the lower zone free water zone storage, however, is unavailable for evaporation, since even under very dry meteorological conditions the capillary forces of the soil matrix are able to hold some water against tension forces.

Surface runoff from both impervious and fully saturated areas is transported to the channel system, which is not reached instantaneously. In order to represent delay times for surface runoff, a unit hydrograph is used to translate the available runoff into actual inflow of the stream network. This resulting inflow is the main output of the land phase of the Sacramento model and may subsequently be used as input of a separate routing module for the stream network.

3.2.4 Physically based, distributed models

Although conceptual models take into account the dominant processes occurring in the catchment, they are not considered to be suitable as modelling tool for a number of problems related to catchment-runoff modelling. For instance, in order to asses the impact of human activities on the hydrological cycle the parameters of the model need to be physically interpretable. For lumped conceptual models this is extremely difficult (Abbott et al., 1986a) since most of it's parameters need to be determined by calibration procedures.

As a consequence, there is a need for models whose parameter values can be obtained through direct measurements. Since this is hardly possible if parameters are lumped at the catchment scale, a model concept is needed in which a catchment, or any hydrological system, is divided into a number of elements, each with it's own set of parameters. In order to be directly measurable the parameters need to be physically meaningful. Therefore, mathematical equations have to be based on physical laws such as the conservation laws for mass, momentum and energy. The additional advantage of the spatially distributed concept is that it offers possibilities to apply numerical solution techniques. In this way complex mathematical descriptions of physical laws which are not analytically solvable can be tackled.

The development of this type of models started in the late 1960s, motivated by the strong progress in computer technology at that time. Physically based, distributed hydrological response modelling has been inspired by the pioneering work of Freeze and Harlan [1969] who presented a blueprint for this type of models. Since the outcome of this blueprint a number of physically-based hydrological response models that are (partially) based on the blueprint have been developed, such as SHE (Abbott et al., 1986b) IHDM (Beven et al, 1987), THALES (Grayson et al., 1992a.) and BBSIM (Garote and Bras, 1995). This section presents the more or less standard procedures of modelling the various aspects of this type of models.

The modelling framework

In physically based distributed models, the catchment is divided into a number of elements, which are usually subwatersheds or grid cells. Within each element the various relevant processes of the hydrological cycle are simulated. The use of grid cells (or, indeed, subwatersheds) enable the model user to simulate the spatial heterogeneity (in horizontal direction) of processes and parameters. This can be realised through application of different boundary conditions and use of different parameter values on different grids. Furthermore, if spatial variety in the vertical direction is also considered to be relevant, the soil component can be divided into a number of layers.

Each element represents a storage component. Processes are modelled through interactions between neighbouring elements. This is sometimes complicated when elements of different components do not have the same size or when the submodels use different time steps. Therefore, a distributed model contains a complex framework which defines the number of elements and controls mutual interactions between the available elements. Figure 3.5 shows a schematic view of a possible distributed hydrological modelling framework. In this particular scheme, overland flow and groundwater flow are modelled 2-dimensionally (horizontally directed), while subsurface flow (vertical) and channel flow (horizontal) are modelled 1-dimensionally. The modelling of processes in the various components will be discussed separately.

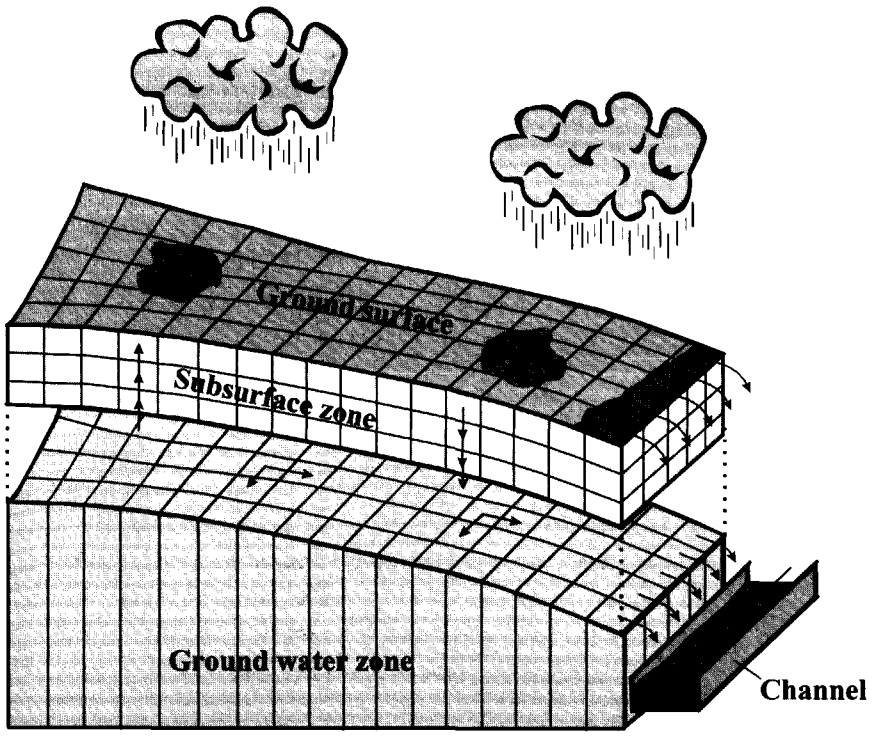

Figure 3.5 Schematic view of a framework of a distributed hydrological model with two-dimensional surface flow, one-dimensional subsurface flow, two-dimensional groundwater flow and one-dimensional channel flow.

Rainfall

Rainfall is modelled as the source term for the overland flow component. Rainfall volumes are added to the overland flow water where it is further routed downslope towards the stream network, that is, if it does not infiltrate directly. Rainfall is modelled in a spatially distributed manner through application of different rainfall intensities to the available grid cells. The spatial distribution of rainfall is usually derived by geostatistical interpolation on measured rainfall intensities in a number of rainfall stations.

Surface runoff

Surface runoff is often divided into two components: Channel flow and overland flow. Channel flow is the flow of water through the stream network and overland flow is the flow of water on the ground surface. Overland flow is often modelled as sheet flow, but in nature this type of flow is rarely observed. When overland flow is generated in nature it flows through small conveyances like micro-channels, rills and gullies, which can be considered as a small scale version of stream flow (Chorley, 1978; Freeze and Harlan, 1969).

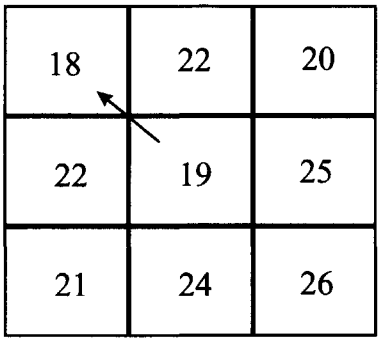

Figure 3.6 Flow direction of the centre cell, based on the lowest surrounding elevation value

If flow is assumed to be directed towards the lowest elevated neighbouring grid cell (see Figure 3.6), both surface runoff and channel flow can be modelled by the one-dimensional hydrodynamic equations of unsteady open channel flow:

$$\frac{\partial h}{\partial t} + h\frac{\partial v}{\partial x} + v\frac{\partial h}{\partial x} = S_{sur} \tag{3.3}$$

$$\frac{\partial v}{\partial t} + v\frac{\partial v}{\partial x} + g\frac{\partial h}{\partial x} + g\left(S_f - S_0\right) = -\frac{v}{h}S_{sur} \tag{3.4}$$

Where:

h	=	Water depth.	[L]
$t.$	=	Time	[T]
v	=	Flow speed.	[LT^{-1}]
x	=	Flow direction co-ordinate.	[L]
S_{sur}	=	Sink/source term	[LT^{-1}]
g	=	Gravity acceleration constant	[$L^1 T^{-2}$]
S_f	=	Friction slope	[-]
S_0	=	Channel bottom slope	[-]

Equations (3.3) and (3.4) are known as the St. Venants equations. These are balance equations for mass and momentum respectively. Sink/source term S_{sur} represents interactions with external components like rainfall intensity, evaporation, infiltration, exfiltration and lateral inflow. S_{sur} is positive when water is added to the surface water component and negative when water is extracted from the surface water component.

Friction slope S_f is usually derived by the Manning formula:

$$S_f = N^2 v^2 R^{-\frac{4}{3}} \tag{3.5}$$

Where:

R = Hydraulic radius of the channel. [L]

N = Manning's roughness coefficient. [$L^{-1/3}T$]

The St. Venants equations need to be solved numerically. Equations (3.3)-(3.5) are discretised on the element scale, provided that the elements are small enough to serve as the basic numerical scale. If this is not the case, the elements need to be split up in a number of even smaller elements.

Depending on the physical system under consideration, some terms of the momentum equation can be neglected, especially in case of overland flow. This leads to popular simplifications of the St. Venants equations such as the kinematic wave model, the diffusion wave model and the dynamic wave model.

Subsurface flow in the soil matrix

The laminar flow of water through porous media is described by the combination of Darcy's law and the mass balance equation. Originally, Darcy's law was stated for flow under saturated conditions, but later it has been extended to Richard's equation, which is valid for all possible soil moisture conditions. If water is assumed to be incompressible, Darcy's law for one dimensional flow states:

$$q_x = -K_x \frac{\partial \varphi}{\partial x} \tag{3.6}$$

Where:

x = Flow direction [L]

q_x = Flow rate in x-direction [LT^{-1}]

K_x = Hydraulic conductivity in x-direction [LT^{-1}]

φ = Hydraulic head [L]

The three dimensional mass balance equation for subsurface flow states:

$$\frac{\partial q_x}{\partial x} + \frac{\partial q_y}{\partial y} + \frac{\partial q_z}{\partial z} - S_{sub} = -\frac{\partial \theta}{\partial t} \tag{3.7}$$

Where:

q_i = Flow rate in direction i, i = x,y,z [LT^{-1}]

x,y = Horizontal co-ordinate directions [L]

z = Vertical co-ordinate direction (positive upwards) [L]

S_{sub}	= Sink/source term	[T^{-1}]
θ	= Soil moisture content per unit volume of the entire medium.	[-]
t	= Time	[T]

Substitution of Darcy's law in the mass balance equation results in:

$$\frac{\partial}{\partial x}\left[K_x \frac{\partial \varphi}{\partial x}\right]+\frac{\partial}{\partial y}\left[K_y \frac{\partial \varphi}{\partial y}\right]+\frac{\partial}{\partial z}\left[K_z \frac{\partial \varphi}{\partial z}\right]+S_{sub}=\frac{\partial \theta}{\partial t} \tag{3.8}$$

Where:

K_i = Hydraulic conductivity in direction i, i = x, y, z [LT^{-1}]

Sink/source term S_{sub} represents water fluxes like root extraction and evaporation[2]. Other exchanging processes like infiltration, exfiltration and percolation towards deeper aquifers result from derived subsurface flow rates at the upper and lower boundary of the subsurface. Hydraulic head φ can be split up in two components:

$$\varphi = z + \psi = z + \frac{p}{\rho g} \tag{3.9}$$

Where:

ψ	=	Pressure head if $\psi \geq 0$ (saturated flow).	[L]
	=	Tension head if $\psi < 0$ (unsaturated flow).	[L]
p	=	Water pressure.	[$ML^{-1}T^{-2}$]
ρ	=	Water density.	[ML^{-3}]
g	=	Gravity acceleration constant.	[LT^{-2}]

For saturated flow, the value of ψ equals the distance to the water table, assuming that the pressure distribution is hydrostatic. For unsaturated flow, ψ and K are functions of the soil moisture content θ. Functions $\psi(\theta)$ and $K(\theta)$ depend on the type of soil through which the water flows. They are empirically based functions, derived by fitting well-known relations like the Brooks-Corey relation or the Van Genuchten relation on field measurements. Since ψ can either represent pressure head or tension head, the model needs to recognise whether subsurface flow occurs under saturated or unsaturated conditions. So, at each time step it has to be determined whether or not the soil moisture content, θ, equals porosity.

If $\psi(\theta)$, $K(\theta)$, S_{sub} and all necessary initial conditions and boundary conditions are known, equation (3.8) can be solved through application of numerical solution techniques. The result

[2] More precisely, S_m is defined as the water volume per unit volume of the entire medium which is extracted from the matrix per unit of time. Consequently, it's dimension is T^{-1}.

is soil moisture content θ as a function of time t and place (x,y,z). The spatial and temporal variation of θ reflects the flow of water through the soil matrix.

Macropore flow

Macropores can be of great influence on subsurface flow rates, especially in topsoils of vegetated areas. Still, there are only a few hydrological response models which contain a separate macropore flow model component (e.g. Bronstert and Plate, 1996; Germann and Beven, 1986). The number of available macropores and their complex structure cannot be measured directly. Furthermore, measurements of the flow process in a single macropore have never been performed, so details of the process itself are still unknown. Therefore, the actual macropore structure can not be modelled in a detailed manner, which means the use of some sort of integrated response function is most effective. Germann and Beven [1986] proposed to use the kinematic wave approximation for one-dimensional vertical macropore flow. In this concept, the conservation law for mass is described as follows:

$$\frac{\partial \theta_m}{\partial t} + \frac{\partial q_m}{\partial z} - S_m = 0 \tag{3.10}$$

Where:

θ_m	=	Volume of macropore water per unit volume of the entire medium.	[-]
t	=	Time.	[T]
q_m	=	Vertical volume flux of macropore water per unit area.	[LT^{-1}]
z	=	Vertical (flow-)direction co-ordinate.	[L]
S_m	=	Sink/source term.	[T^{-1}]

The sink/source term S_m represents interactions between the macropore system and the soil matrix. Water enters a macropore when the matrix system directly surrounding the macropore is completely saturated. If the matrix system is unsaturated the larger available capillary forces of the micropores will extract water from the macropores. The volume flux per unit area q_m is assumed to be related to the macropore water content q_m through a power function:

$$q = b\theta_m{}^a \tag{3.11}$$

where a and b are empirically derived constants. Substitution of equation (3.11) in equation (3.10) and application of the chain rule of differentiation gives:

$$\frac{\partial \theta_m}{\partial t} + ab\theta_m{}^{a-1}\frac{\partial \theta_m}{\partial z} - S_m = 0 \tag{3.12}$$

Equation (3.12) can be used in combination with a flow model for water in the soil matrix (based on equation (3.8)) to model the integrated effect of the available macropores in a soil on subsurface runoff (Bronstert and Plate, 1996).

3.3 Practical difficulties in representing physics in rainfall-runoff models

3.3.1 Introduction

The need for different model concepts stems from the wide variety of problems to be solved in hydrology. Each model concept presented in this chapter has already proven its specific applicability for a number of disciplines in hydrology. As far as this thesis is concerned the interest in hydrological modelling comes from the aim to explore the possibilities of deriving flood frequencies on a physical basis. Therefore, the physically based concept of catchment-runoff modelling as described in section 3.2.4 seems to be the most appropriate and promising approach to concentrate on. In theory these models remain valid even under extremely (unwitnessed) wet hydrological conditions and/or changing catchment characteristics, since they are based on conservation laws of mass, momentum and energy. However, there is a huge difference between theory and practice. A number of practical drawbacks frequently experienced in physically based distributed modelling are:

- The available data set is never detailed enough to fulfil all the needs of distributed models, so usually a number of model components of a distributed model are lumped at much larger scales than the initially intended element scale.
- The scale at which the parameters and physics have been derived are generally some orders of magnitude smaller than the model element scale, so even distributed modelling suffer from the negative effects of lumping.
- The term "physically-based" is rather a subjective one. Models which are labelled as physically based by one hydrologist can be labelled as conceptual by another hydrologist. Darcy's law, for instance is derived on an empirical basis and is therefore labelled empirical by some (e.g. Clarke, 1972), but a physically based derivation of this law is possible (Hassanisadeh and Gray, 1980)
- The large numbers of parameters enable distributed models to "work right for the wrong reasons" (Grayson et al. 1992b; Klemeš, 1986), since it offers enough freedom to the modeller to generate satisfying outputs even when the underlying concepts are known to be unrealistic.
- Every physically based rainfall-runoff model always contains some empirically based components either because they are easier to use or because they are needed to solve the

set of equations derived from conservation laws which generally contains more variables than equations.

- As far as catchment-runoff modelling is concerned, distributed models are often outperformed by simple lumped conceptual models (Storm and Refsgaard, 1996). The physical basis these models promise to give, therefore seems to offer no guarantee for increased reliability.

There are a number of causes for these drawbacks in physically based distributed hydrological modelling. The two main causes (overparameterisation and scale effects) will be discussed in section 3.3.2 and 3.3.3.

3.3.2 Overparameterisation

One of the advantages of physically based hydrological models is that in theory it is possible to derive all parameters and variables of the model by field measurements. In practice, however, this cannot be achieved because a) it is far to expensive and b) the physical reality of some parameters is highly doubtful. Therefore, a number of parameter values have to be determined through calibration. This means the set of parameter values which cannot be measured is chosen such, that the model output approximates the measured output of the modelled system "as good as possible". When too many parameters are determined this way, serious problems arise. First of all the determination of an "optimal" parameter set becomes extremely time consuming and complex. Second, and most important, the best fit of model outputs to measured outputs often can be generated by a number of significantly different sets of parameter values. Mein and Brown [1978] for instance, applied a number of optimisation runs on a rainfall-runoff model and found significantly different optimal parameter sets for different optimisation runs. Differences in optimal parameter sets either came from differences in chosen initial parameter values or from differences in the number of calibrated parameters (varying in number from 3 to 13). Similar results were obtained by Uhlenbrook et al. [1999], who performed a Monte Carlo simulation to analyse parameter uncertainty in the HBV-model. They found 38 parameter sets to perform "very good", in terms of the Nash-Sutcliffe efficiency (Nash and Sutcliffe, 1970), on a 10 year record of measurements. However, when a synthetic 1/100 year precipitation event was simulated by using the 38 different parameter sets, the computed peak runoff values ranged from 40 to 58 mm/day. Another striking effect of calibration was demonstrated by Grayson et al. [1992b] who used a physically based model to simulate runoff generation at the Wagga Wagga catchment in New South Wales, Australia. Runoff in this catchment is mainly produced by saturation overland flow while infiltration excess overland flow doesn't occur. During one simulation run of a rainfall event the infiltration rate at the entire catchment was kept at a value which enabled infiltration excess overland flow to occur. Furthermore, the infiltrated water was considered as a loss which meant that infiltration excess overland flow was the only runoff process during this simulation. Although this concept is in complete contradiction with observations

in the catchment, calibration of a number of parameters enabled this model to generate output which was as good as the output from models based on the more realistic concept of saturation overland flow.

These examples show that models can be based on unrealistic concepts and still provide satisfying outcomes. This is no problem as long as one is interested in the model outcome only and measurements show that the model consistently provides good approximations. Physically-based hydrological models, however, are designed for situations where internal components of the model have to be realistic (e.g. in solute transport modelling) and/or for situations for which hardly or no output measurements exist (e.g. modelling land use change effects or extreme hydrological events).

There are two ways to reduce the negative effects of overparameterisation:

1. Decrease the number of parameters which have to be calibrated, i.e. increase the number of direct measurements of parameters in the field.
2. Calibrate the necessary parameter values on a large number of measured intern state variables like ground water depths, soil moisture contents and discharges at other locations than the catchment outlet. When the model is able to reproduce the measured values of a number intern state variables, the reliability of the model increases significantly compared to the case when only the measured discharge at the catchment outlet is reproduced.

Both approaches require an increased amount of measurements. In case this is not possible, it will be inevitable for the model to suffer from the negative effects of overparameterisation.

3.3.3 Scale effects

Natural hydrological systems contain a high degree of heterogeneity and variability of processes and characteristics. One of the consequences is the need for different descriptions of hydrological processes at different temporal and spatial scales. Concepts of processes are often based on small-scale laboratory experiments and they cannot simply be extrapolated to a larger, numerical grid scale without harming their physical realism (Beven, 1989). A good example of a process description suffering from this phenomenon is Darcy's law, which is derived at the laboratory scale and has been applied at much larger numerical grid scales of, for example, 250 m. ×250 m. (horizontal) by 0.05 m. (vertical) as in the SHE model of the upper Wye catchment (Bathurst, 1986). For this numerical grid scale an effective hydraulic conductivity value K_{eff} has to be derived, which represents the behaviour of the Darcian flow process at this scale. For one-dimensional flow, this means K_{eff} can be determined from the following equation (which is analogous to Darcy's law, equation (3.6)):

$$K_{eff,x} = -\frac{q_x \Delta x}{\Delta h_x} \tag{3.13}$$

where:

q_x	=	Total flux in x-direction in the grid.	[LT^{-1}]
Δx	=	Length of the grid in x-direction	[L]
Δh_x	=	Hydraulic head difference over distance Δx	[L]

Values of q_x, and Δh_x can be estimated from field experiments (Δx, of course, is known) through pumping tests for instance. Often, though, K_{eff} is determined by averaging the hydraulic conductivity values, measured from a number of soil samples within the soil type of interest. For randomly distributed local conductivity values it has been be proven that K_{eff} equals the harmonic mean of the local values for one-dimensional flow and the geometric mean for two- and three-dimensional flow (Wen and Gómez-Hernández, 1996). However, in reality, large scale effective conductivity values are often observed to exceed the geometric mean of local conductivity values significantly. Examples of effective parameters exceeding the geometric mean of measured point values by even a thousand times are known (Sánchez-Villa et al., 1995). Furthermore, in a number of field experiments (e.g. Flury et al., 1994; Hornberger et al., 1991), a description of subsurface flow by Darcy's law proved to be invalid at the plot scale. Flow patterns, revealed by dye-tracing, differed strongly from patterns that follow from a Darcian flow description and the value of K_{eff} was found to depend significantly on the boundary conditions and initial wetness conditions.

Computer simulations have shown that the drawbacks of applying Darcy's law at larger scales can be accounted for by the heterogeneity of point scale values of hydraulic conductivity (Binley et al., 1989; Mantoglou and Gelhar, 1987; Sánchez-Villa et al., 1995), or, more specifically, the structure (spatial correlation) of high conductivity values. In chapter 2 it was already mentioned that macropores, pores of relatively low water-flow resistance, are often very well connected due to a common cause of their existence which means that they can form channels (preferential pathways). However, the influence of flow paths is not just restricted to the scale of macropores (up to a few meters) since connectivity between high permeable soils has also been observed in aquifers at the scale of several kilometres (Sánchez-Villa et al., 1996). Due to this far from random structure, water can be transported relatively quick through channel-like flow paths, which significantly increases the effective conductivity of the entire soil. Effective hydraulic conductivity's generally increase with increasing system domain, which is explained by Blöschl and Sivapalan [1995] as follows: "*.. for a higher dimension, flow is more likely to enter a low resistance path which tend to increase the effective conductivity*". In order to compensate this effect on the model output, higher conductivity values have to be awarded to the grids than originally estimated by the measurements in soil samples. In other words: Measured laboratory-scale conductivity values are generally invalid at the model grid scale.

Darcy's law has been used as an example in this section, but models of other hydrological processes also suffer from scale problems that still need to be tackled. Scale problems can be found in all aspects and disciplines related to hydrology and it is widely recognised that a better understanding of relations of hydrological responses at the range of scales of interest is a crucial step in overcoming unsolved hydrological problems. For an extensive overview of scale problems in hydrology, the interested reader is referred to Blöschl and Sivapalan [1995].

3.4 Discussion and further outline of the thesis

In this chapter a number of approaches of catchment-runoff modelling were presented. Models were classified based on to which extent the model takes into account the physics that occur in the catchment. Three groups of models have been recognised: Empirical models, lumped conceptual models and physically based distributed models. Empirical models simply relate input (precipitation) and output (discharge) series without describing the physical processes occurring in the catchment. Physically based distributed models on the other hand are based on physical laws, such as the conservation laws for mass, momentum and energy. Conceptual models form some sort of compromise between the other two concepts through the application of simplified process descriptions, which are often lumped on the catchment scale.

As far as application in a physically based flood frequency analysis is concerned, the use of physically based distributed models seems to be the most promising, that is, at first sight. In theory, these models remain valid even under extremely wet (unwitnessed) hydrological conditions and/or changing catchment characteristics, since they are based on conservation laws of mass, momentum and energy. In practice, however, they are often witnessed to "work right for the wrong reasons". In other words: physically based models often provide satisfying outputs for calibrated events, even though they are based on concepts which are known to be unrealistic, which means they may not be useful for uncalibrated situations such as extreme flood events. Furthermore, distributed models are often outperformed by simple lumped conceptual models, as far as reproduction of catchment runoff is concerned.

Hydrological models are, like all models, simplified representations of the real world. It is therefore unrealistic to expect them to provide output which is exactly the same as the observed output of the modelled hydrological system. However, by labelling a model as "physically based" an expectancy is created for these models to behave consistently with the physics of the natural systems they represent. Especially in the case of a detailed distributed representation of a hydrological system this expectancy is not likely to be fulfilled. Lack of detailed information and exact process knowledge cause the simulation of the hydrological response at the element scale of a distributed model to be a "mission impossible". For many purposes it may therefore be sensible to use conceptual models. In a way, these models are higher order abstractions of more detailed distributed modelling concepts (Woolhiser, 1996). To a large extent this will take away the false expectancies of fully distributed models. Even in cases where effects of spatial variability are of strong influence on catchment runoff, fully lumped conceptual models can be appropriate. These models can incorporate relevant information on the available spatial variability of catchment characteristics, through application of distribution functions or statistical quantities such as variance or correlation

length. In a wide range of applications this way of representing has proved to be useful for all sorts of processes and parameters.

Still, though, some aspects of spatial variability need to be described in a deterministic manner, i.e. "exact" parameter values have to be awarded to specific field locations. Seyfried and Wilcox [1995] provide field evidence that different concepts of modelling spatial heterogeneity are warranted at different scales for the majority of hydrological entities. Three different concepts are recognised by these authors: [a] homogeneous representation [b] stochastic representation and [c] deterministic representation. From field observations they came to a definition of the *deterministic length scale*, i.e. the scale (or range of scales) at which the entity of interest has to be modelled in a deterministic manner. At smaller scales it can be considered homogeneous, whereas at larger scales a stochastic description suffices.

Consequently, hydrological models can benefit from a concept of representing spatial variability which is based on a notion of the nature of heterogeneity of dominating parameters and processes. The main focus of this thesis are the various aspects that are relevant to the formation of such a concept. More specific, it deals with the representation of spatial variability in models build for catchment-runoff simulation during storm events. Therefore, the following two issues are considered relevant:

1. Which processes and parameters are dominant under (extremely) wet conditions and should therefore be represented on a physically meaningful way in a catchment-runoff model?
2. What model complexity is required to represent the spatial heterogeneity of these parameters and processes?

Chapters 4 and 5 concentrate on the first issue, whereas chapters 6 and 7 focus on the second issue. In chapter 4, a univariate sensitivity analysis as well as a bivariate sensitivity analysis are applied to a well known rainfall-runoff modelling concept to investigate relative importance and mutual dependence of occurring runoff generating processes and related catchment characteristics. In chapter 5, regression analysis and transfer function models are used to find the relation between the catchment-average precipitation and the resulting magnitude of the discharge in the river. The main goal is to find out which information should be generated by a rainfall generator, if one was to be set up in order to predict probabilities of future flood events. In chapters 6 and 7 the relation between the performance of catchment-runoff models and the scale of their elements is investigated. This provides insight in the scales at which effects of spatial heterogeneity really matter and the scales at which these effects can be neglected. The 28152 km^2 Mosel basin (covering parts of France, Germany and Luxembourg) and the 114 km^2 Zwalm catchment in Belgium serve as pilot area throughout this thesis.

4. Sensitivity of runoff generation to catchment characteristics

4.1 Introduction

Even the most comprehensive rainfall-runoff models are simplifications of the real-world systems they represent. Especially the enormous spatial variability present in nature can only be covered to a modest extent in rainfall-runoff models due to limited availability of data and process time. It is therefore essential to incorporate into a model the sources of variability which seriously control the processes of interest.

Seyfried and Wilcox [1995] provided field evidence that these controlling sources of variability are strongly dependent on the considered spatial scale and, consequently, that different concepts of modelling spatial heterogeneity are required at different scales for hydrological processes and parameters. Based on field observations in five different subwatersheds of the Reynolds Creek watershed these authors came to a definition of the *deterministic length scale*, i.e. the scale (or range of scales) at which the process or parameter of interest has to be modelled in a deterministic manner. At smaller scales the entity can be considered homogeneous, whereas at larger scales a stochastic description suffices. Besides spatial scale, also the temporal scale of interest is also of great influence on the nature of spatial heterogeneity. For instance, in small flat catchments, annual precipitation shows no spatial heterogeneity of any significance, whereas convective storm events may generate serious spatial differences in rainfall intensities. Finally, the nature of heterogeneity depends on the type of output that is required. Inter-storm runoff, for instance, is dominated by other processes than the runoff of a storm event.

For each case where hydrological models are required, it is therefore vital to identify the sources of variability which seriously control the processes of interest. The nature of this variability is related to:

[1] The spatial heterogeneity of the individual processes and catchment characteristics.
[2] The relative importance of the occurring runoff generating processes and related catchment characteristics.
[3] The interdependence of processes and characteristics with regard to the integrated catchment response.

The present thesis is largely devoted to the identification of the nature of spatial heterogeneity. In part III (chapters 6 and 7) the spatial heterogeneity of individual processes and catchment characteristics (point [1] above) is the main focus. In the present chapter, the relative importance and interdependence of processes and catchment characteristics (point [2] and [3] above) are investigated. Results of this chapter are used to select the processes and system characteristics for which the heterogeneity research in chapters 6 and 7 is performed.

First, a rainfall-runoff model is developed for a pilot study catchment. Then, a sensitivity analysis is performed on the model parameters to quantify and visualise the relative importance and interdependence of the characteristics and processes they represent. In a sensitivity analysis, model runs are performed for different sets of parameters values. Values are taken from a range, which has to be defined for each parameter individually. This type of analysis is generally performed for calibration purposes, either to find out for which sub-set of parameters calibration should be performed or to find out directly which parameter set generates optimal simulation results. Three approaches of the sensitivity analysis are distinguished:

I. Univariate sensitivity analysis (e.g. Gyasi-Agyei et al., 1996; Troch et al. 1993). A default value is awarded to each of the parameters and during the analysis only one parameter at a time is allowed to differ from its default value. This approach is particularly useful for the assessment of the individual role of a parameter in runoff generation. It is usually applied when most parameter values are considered to be known.
II. Bivariate sensitivity analysis (e.g. Killingtveit, Å, Sælthun, N. R., 1995). A default value is awarded to each of the parameters and during the analysis only two parameters at a time are allowed to differ from their default value. This approach is particularly useful in analysing interdependence among parameters.
III. Multivariate sensitivity analysis (e.g. Duan et al., 1992; Hornberger et al., 1985; Seibert, 1997). The entire parameter space is explored in order to find an "optimal" set of parameters.

Taking in mind the current objectives (i.e. to investigate relative importance and interdependence of parameters and processes) both a univariate sensitivity analysis and a bivariate sensitivity analysis are applied to a rainfall-runoff model. The 114 km^2 Zwalm catchment (Belgium) serves as pilot study area. The rainfall-runoff model is an adapted version of the TOPMODEL-concept of Beven and Kirkby, [1979]. The choice of this concept is motivated by (a) its applicability on the type of catchments of interest (humid conditions, mild slopes, dominance of the saturation excess runoff mechanism) and (b) the availability of parameter values since the TOPMODEL concept has been applied on the Zwalm catchment before (Troch et al. 1993).

4.2 Description of the pilot study: The Zwalm catchment

The data which served as basis of the sensitivity analysis was collected from the 114 km^2 Zwalm catchment during the period 1991-1993. The Zwalm catchment is located in East Flanders, Belgium. Its topography is characterised by rolling hills and mild slopes with a maximum elevation difference of 150 m. The average yearly rainfall is 775 mm, which falls almost uniformly spread over the year. Storm runoff water is mainly generated on saturated parts of the catchment (Troch et al., 1993). A 39.1 m. × 30.9 m. digital elevation model of the catchment is available, alongside data from the following 10 measurement stations (Figure 4.1):

1. *Elst*: Meteorological station (temperature, precipitation, wind speed, radiation).
2. *Neder*: Water level gauge (limnigraph, continuous measurements).
3. *Mater*: Water level gauge (limnigraph, continuous measurements).
4. *Francis*: Water level gauge (limnigraph, continuous measurements).
5. *Velzeke*: Rainfall station (tipping bucket, resolution: 10 minutes).
6. *Blasius*: Rainfall station (tipping bucket, resolution: 10 minutes).
7. *Beren*: Rainfall station (tipping bucket, resolution: 10 minutes).
8. *Schor*: Rainfall station (tipping bucket, resolution: 10 minutes).
9. *Mf_Opbrakel*: Discharge measurement station (flume).
10. *Mf_Velzeke*: Discharge measurement station (flume).

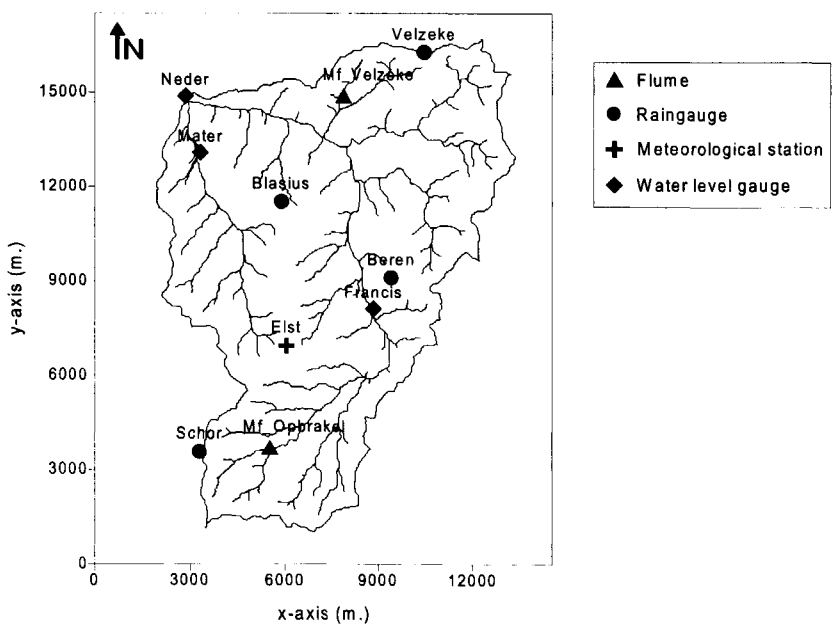

Figure 4.1 The Zwalm catchment with 10 measurement stations.

4.3 Description of the rainfall-runoff model

A rainfall-runoff model is set up for the Zwalm catchment in order to simulate the hydrological behaviour of the catchment during a storm event. The model consists of three major components: A hillslope-runoff model, a stream routing model and an initial state model to derive soil moisture conditions at the beginning of a storm event (Figure 4.2).

The initial state model first derives the area-average ground water table depths, based on the observed base flow at the catchment outlet. Subsequently, the soil moisture content at each location in the catchment is related to this area-average ground water table depth and to local topographic- and soil characteristics. This results in a spatial distribution of soil moisture deficit values, which serves as the initial state condition of the hillslope-runoff model. The hillslope-runoff model computes the percentage of rainfall that becomes available for runoff, and simulates the downslope directed flow of water alongside natural flow paths towards the stream network. The output of the hillslope-runoff model serves as input (incoming lateral flow) to the stream routing model where it is further routed towards the catchment outlet.

In sections 4.3.2 - 4.3.4 a more detailed description of the model components and equations is presented. First, in section 4.3.1, the necessary topographic analysis are described.

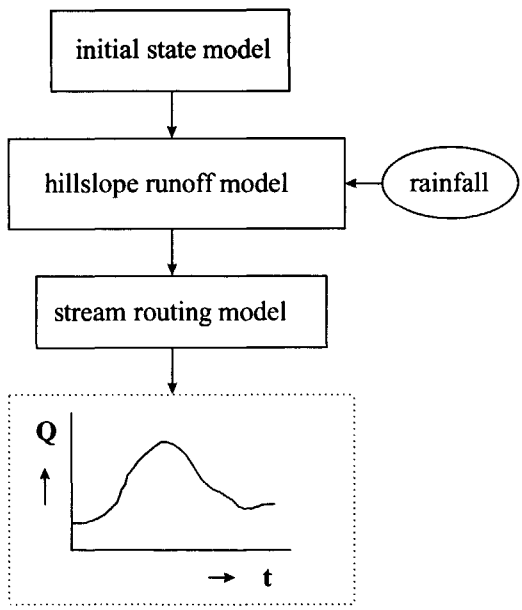

Figure 4.2 Flowchart of the hydrological model of the Zwalm catchment.

4.3.1 Topographic analysis

A digital elevation model (DEM) of a rectangular area of 255 km^2, in which the Zwalm catchment is embedded (Figure 4.3), has been used to derive topographic characteristics of the Zwalm catchment like (sub-) catchment boundaries, flow paths and slope values. The resolution of the DEM is 39.1 m. × 30.9 m, i.e. the area is divided into cells of 39.1 m. by 30.9 m. for which the (average) elevation is known. The following procedure has been applied:

1. The flow direction of available runoff water is derived for each cell of the DEM. Flow is assumed to be directed towards the lowest elevated neighbouring cell (see Figure 4.4)

2. All pits that exist in the DEM, but not in reality, are removed. These unnatural endings of flow paths occur in the DEM due to the fact that an area of, in this case, 39.1 m. by 30.9 m is modelled as an area with a single elevation value, instead of an area with its own internal elevation differences. In case of Figure 4.4, for instance, there may be a stream flowing from the centre cell towards the upper-left cell, which in the current situation is modelled through the perception of all available water flowing towards the lowest elevated neighbouring cell. However, if this stream were to flow through a steep hillslope area, the elevation of the upper-left cell might have been well over 20 m, instead of the current value of 18 m. In that case the elevation of the centre cell is lower than the elevation of its eight surrounding cells. In the DEM this cell will be the endpoint of all flow paths passing through this cell, whereas in reality these flow paths will continue their way towards the upper left cell via the stream. A major consequence for a routing model based on the DEM is that a small lake, which doesn't exist in reality, can arise in the model during a period of heavy rainfall. To prevent this from happening, unnatural pits are removed from the DEM, by slightly changing some elevation values.

3. For every cell in the DEM, the number of upstream contributing cells are determined as shown in Figure 4.5 for cell x. The upstream contributing cells are those cells that drain (directly or indirectly) into the cell of interest, including the cell of interest itself.

4. The location of the stream network is obtained by marking all cells with an upstream area of more than N cells, where N is a user defined number.

5. The river cell at the position of the catchment outlet (or nearest to the position of the catchment outlet) is marked as the outlet cell and the area covered by its contributing cells is considered as the catchment.

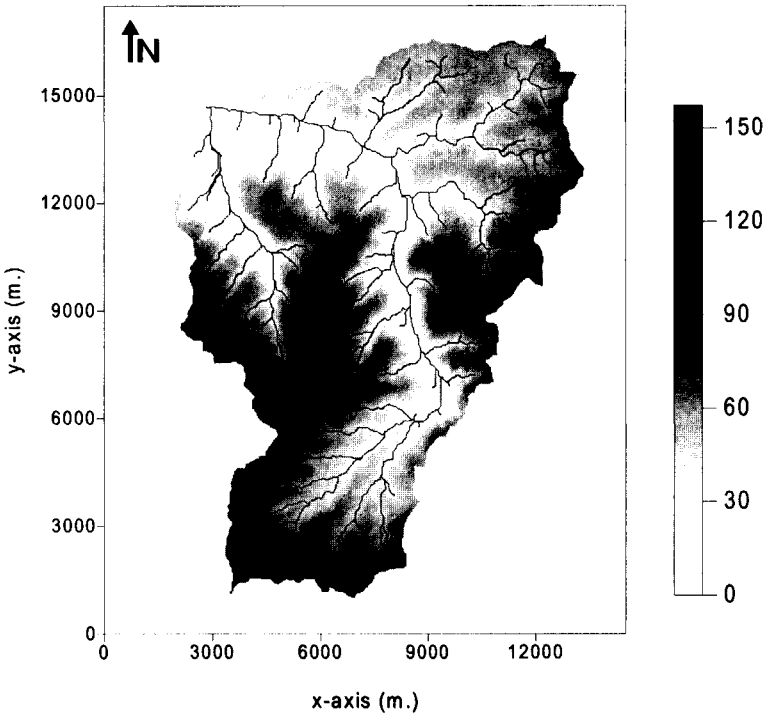

Figure 4.3 Digital elevation model of the Zwalm catchment

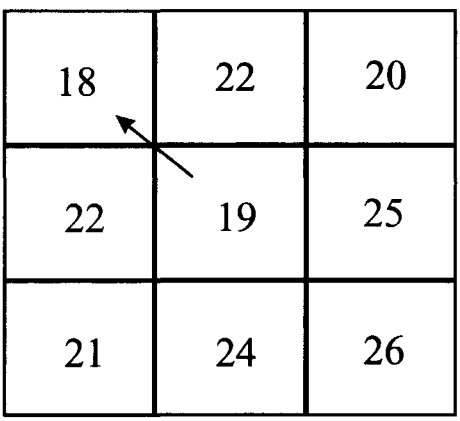

Figure 4.4 Flow direction of the centre cell, based on the lowest surrounding elevation value

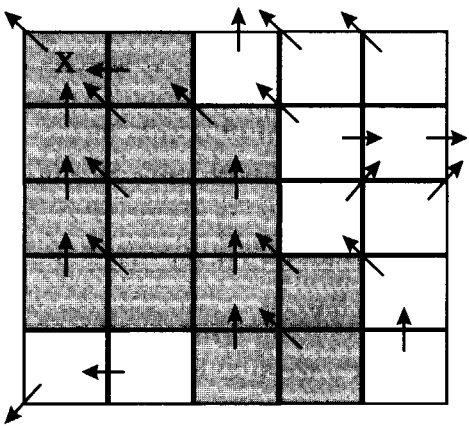

Figure 4.5 Flow directions and upstream contributing area (shaded) of cell x

After applying this five-step procedure, (sub-)catchment boundaries, flow paths and stream-cell locations are known. Furthermore, slope values can easily be obtained since the combined knowledge of elevation values and length of flow paths is now available.

4.3.2 Derivation of initial soil moisture conditions

The method of Sivapalan et al. [1987], combined with the characteristic soil moisture relationship of van Genuchten [1980], is used to estimate the spatial distribution of the initial soil moisture content. Sivapalan et. al [1987] derived soil moisture conditions, through application of a modified version of the TOPMODEL concept (Beven and Kirkby, 1979) for steady-state rainfall-runoff modelling. TOPMODEL is, like any other hydrological model, based on a number of assumptions. The first assumption of TOPMODEL is the exponential decline of the saturated hydraulic conductivity, K_s, of the topsoil.

$$K_s(y) = K_0 \exp(-fy) \tag{4.1}$$

where y is the depth into the soil profile, K_0 is the hydraulic conductivity at y=0 and f is the exponential decline parameter. Field evidence for this assumption is given by Beven [1982]. As a result the downslope transmissivity, T_0, of the soil profile equals:

$$T_0 = \int_0^D K_s(y)dy = K_0 \int_0^D e^{-fy} dy = \frac{K_0}{f}\left[1 - e^{-fD}\right] \tag{4.2}$$

where D represents the lower boundary of the model, often taken to be equal to the depth of the top of an impeding layer underlying the topsoil. Usually, the values of f and D are such, that the value e^{-fD} can be neglected, which means:

$$T_0 = \frac{K_0}{f} \tag{4.3}$$

As a result of this assumption, the downslope transmissivity, T, of the saturated part of the soil (Figure 4.6) equals:

$$T = \int_z^D K_s(y)dy = K_0 \int_z^D e^{-fy} dy = \frac{K_0}{f}\left[e^{-fz} - e^{-fD}\right] = \frac{K_0}{f} e^{-fz} = T_0 e^{-fz} \tag{4.4}$$

where z is the depth to the ground water table. In TOPMODEL, the water table is assumed to be parallel to the ground surface. According to Darcy's law, this means the downslope drainage rate equals:

$$q = T_0 \tan\beta e^{-fz} = \frac{K_0}{f} \tan\beta e^{-fz} \tag{4.5}$$

where $tan\beta$ is the slope of the ground surface.

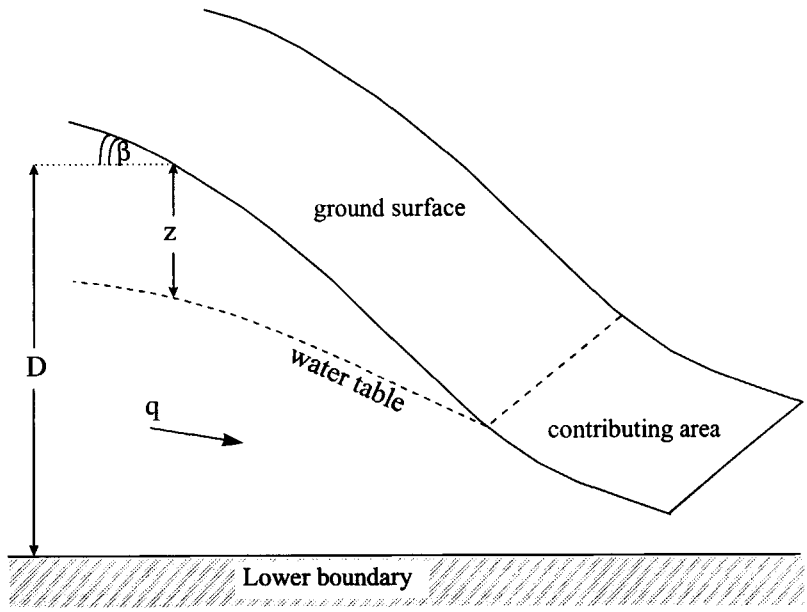

Figure 4.6 Schematical view of a hillslope. (after: Sivapalan et al., 1987)

Furthermore, a steady-state situation is assumed to occur prior to a storm event, which means at each location i, the recharge rate equals the drainage rate:

$$a_i R = T_i \tan\beta_i e^{-f z_i} \Rightarrow z_i = -\frac{1}{f}\ln\left[\frac{a_i R}{T_i \tan\beta_i}\right] \tag{4.6}$$

where R is the rainfall/recharge rate, a_i is the area of hillslope per unit contour length that drains through location i (=A/B in Figure 4.7), $tan\beta_i$ is the slope of the ground surface at location i and T_i is the transmissivity of the soil profile at location i.
The average ground water depth, z_{av}, equals:

$$z_{av} = \frac{1}{A}\int_A z_i\, dA = -\frac{1}{A}\int_A \frac{1}{f}\ln\left[\frac{a_i R}{T_i \tan\beta_i}\right] dA = -\frac{1}{A}\int_A \frac{1}{f}\ln\left[\frac{a_i}{\tan\beta_i}\right] dA$$
$$+\frac{1}{A}\int_A \frac{1}{f}\ln[T_i]\, dA - \frac{1}{A}\int_A \frac{1}{f}\ln[R]\, dA = \frac{1}{f}\{\ln[T_e] - \lambda - R\} \tag{4.7}$$

where A = the surface area of the catchment. T_e and λ are catchment average values of T_i and $ln[a_i/tan(\beta_i)]$ respectively:

$$\ln T_e = \frac{1}{A}\int_A \ln T_i \, dA \qquad ; \lambda = \frac{1}{A}\int_A \ln\left[\frac{a_i}{\tan\beta_i}\right] dA \tag{4.8}$$

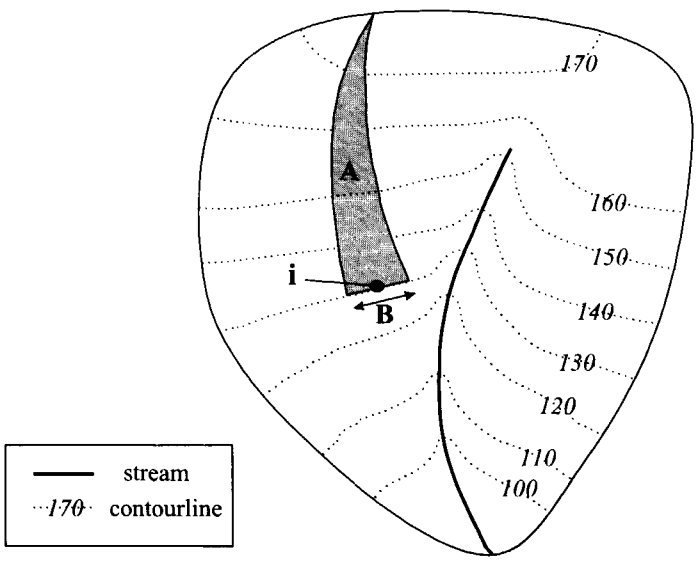

Figure 4.7 Contributing area A for contour length B. A/B is the contributing area per unit contour length at location *i*.

Substituting R by combining equations (4.6) and (4.7) gives:

$$z_i = z_{av} - \frac{1}{f}\left\{\ln\left(\frac{a_i T_e}{T_i \tan\beta_i}\right) - \lambda\right\} \tag{4.9}$$

This equation relates the ground water depth, z_i, at each location in the catchment to the catchment average ground water table depth, z_{av}. The latter can be related to the discharge, $Q(0)$, at the catchment outlet by assuming steady-state conditions. This assumption implies that $Q(0)$ equals the total uphill contributions in the catchment:

$$Q(0) = \int_{2L} q_i \, dL \tag{4.10}$$

where L is the total stream length in the catchment. Substituting equations (4.5) and (4.9) into equation (4.10) gives:

$$Q(0) = \int_{2L} q_i \, dL = \int_{2L} T_i \tan\beta_i \exp(-fz_i) \, dL =$$

$$= \int_{2L} T_i \tan\beta_i \exp\left(-f\left\{z_{av} - \frac{1}{f}\left[\ln\left(\frac{a_i T_e}{T_i \tan\beta_i}\right) - \lambda\right]\right\}\right) dL$$

$$= \int_{2L} T_i \tan\beta_i \exp(-fz_{av} - \lambda)\left(\frac{a_i T_e}{T_i \tan\beta_i}\right) dL = T_e \exp(-fz_{av} - \lambda) \int_{2L} a_i \, dL$$

$$= AT_e \exp(-fz_{av} - \lambda) \tag{4.11}$$

Now, z_{av}, can be written as a function of the observed base flow at the beginning of an event, $Q(0)$, and topographic and soil characteristics (λ, A, T_e, and f):

$$z_{av} = -\frac{1}{f}\ln\left[\frac{Q(0)}{AT_e \exp(-\lambda)}\right] \tag{4.12}$$

With equations (4.9) and (4.12) the water table depth at each location in the catchment can be derived if the outflow, $Q(0)$, at the beginning of the event is known. Subsequently, the initial soil moisture deficit, S_i, is related to the water table depth through:

$$S_i = (\theta_s - \theta_r)\left\{z_i - h_c - \frac{1}{f}[(1 + (\alpha z_i)^{-n})^{-\frac{1}{n}} - (1 + (\alpha h_c)^{-n})^{-\frac{1}{n}}]\right\} \tag{4.13}$$

Where θ_s is the saturated soil moisture content, θ_r is the residual soil moisture content, h_c is the capillary fringe and α and n are empirically based soil parameters. Equation (4.13) is a modification of the Van Genuchten equation (Van Genuchten, 1980), assuming hydraulic equilibrium in the soil (Troch et al., 1993). The initial soil moisture deficit, which can be considered as the remaining capacity in the soil for storage of infiltrating rainfall water, serves as input for the hillslope-runoff model.

4.3.3 Hillslope-runoff modelling

Rainfall input

In the hillslope-runoff model, the volume of rain which falls down in one time step initially is added to the overland flow component. Subsequently, the model decides whether this water either infiltrates or runs off. If a soil profile is saturated ($S_i = 0$), all rainfall water runs off downslope over the surface (=saturation excess overland flow). If the soil is not entirely saturated ($S_i > 0$), all rainfall water infiltrates, unless the rainfall intensity exceeds the infiltration capacity, K_i. In that case, part of the water infiltrates (at a rate equal to K_i) and part of the water runs off downslope over the surface (=infiltration excess overland flow).

Since there is more than one rainfall station available, the input of rainfall intensities is modelled in a spatially distributed manner. A well known geostatistical interpolation technique, the inverse square distance method, has been applied to derive rainfall intensities for the individual elements of the digital elevation model. In order to estimate the rainfall intensity at a location *i*, a weight factor $w_j(i)$, j = 1..M, is assigned to the *M* available rainfall stations. This weight is inversely proportional to the square of the distance of rainfall station *j* to location *i*. According to the inverse square distance method the estimated rainfall intensity, $P_e(i)$ at location *i* equals:

$$P_e(i) = \frac{\sum_{j=1}^{M} w_j(i) P_O(j)}{\sum_{j=1}^{M} w_j(i)} \quad ; w_j(i) = 1/d^2(i,j) \tag{4.14}$$

where $P_0(j)$ is the observed rainfall intensity at station *j* and $d(i,j)$ is the distance from location *i* to station *j*. In this way a map of spatially distributed rainfall intensities in the Zwalm catchment is obtained. During a simulation run of an event, this procedure is repeated every 10 minutes (which is the temporal resolution of the rainfall stations) to capture both spatial and temporal variation of rainfall intensities.

Routing

The hillslope-runoff model routs soil water and surface water downslope along natural flow paths, derived from elevation data. The rate of soil water per unit depth, q_i, flowing downslope from location *i* is described by:

$$q_i = T_0 \tan\beta_i \exp\left(-\frac{S_i}{m}\right) = \frac{K_i}{f} \tan\beta_i \exp\left(-\frac{S_i}{m}\right) \tag{4.15}$$

where *m* is an empirically based decline constant. S_i, $\tan\beta_i$, K_i and *f* are the same as previously defined for the initial soil moisture model. Equation (4.15) is taken from Beven et al [1995].

Overland flow routing (both saturation excess overland flow and infiltration excess overland flow) is realised with the Manning equation:

$$v = \frac{h^{2/3} (\tan\beta_i)^{1/2}}{N} \tag{4.16}$$

where *v* is the flow velocity, *h* is the overland flow height and *N* is Manning's roughness coefficient.

4.3.4 Stream flow routing

For stream flow routing, the flow velocity, c, of all the water in the stream network is assumed to be a power function of the discharge Q at the outlet of the catchment:

$$c = \varepsilon Q^{\delta} \tag{4.17}$$

where ε and δ are constants. Although equation (4.17) is a simple routing equation, it enables the model to simulate the dynamic behaviour of the stream network of relatively small catchments like the Zwalm catchment (Beven and Kirkby, 1979).

4.3.5 Parameter values

Table 4.1 contains parameter values of the catchment-runoff model. These values were taken from a number sources. Topographic parameters a_i and β_i (not depicted in Table 4.1, since they are both modelled in a spatially variable manner) have been derived from the 39.1 m. × 30.9 m. digital elevation model of the Zwalm catchment. Soil parameters f, K_0, h_c, θ_s, θ_r, α, n were taken from Troch et al. [1993] who reported a number of field and laboratory studies of characteristics of the different soil types of the Zwalm catchment. Parameter m was based on hydrograph recession analysis. For parameter N, values found by others in literature for similar soil and vegetation types are used (Engman, 1986; Shen and Julien, 1993). Finally, ε and δ were determined through calibration.

Parameter	Description	value	dimension
K_0	Hydraulic conductivity near the ground surface	0.0012	[m/s]
f	Exponential decline parameter of hydraulic conductivity with increasing depth	2.3	[m^{-1}]
h_c	Length of the capillary fringe	0.6	[m]
n	Parameter of the Van Genuchten equation	1.141	[-]
α	Parameter of the Van Genuchten equation	0.0019	[m^{-1}]
N	Manning's roughness coefficient	0.2	[$m^{-1/3}s$]
θ_s	Saturated soil moisture content	0.42	[-]
θ_r	Residual soil moisture content	0.16	[-]
m	Exponential parameter for the ground water reservoir	0.016	[m^{-1}]
ε	Stream flow velocity parameter	0.5	[m^{-2}]
δ	Stream flow velocity parameter	0.15	[-]

Table 4.1 Default, catchment average, parameter values of the rainfall-runoff model.

Worth noticing is the high value of K_0. This value is taken from the range of values that was obtained by Troch et al. [1993], who derived conductivity values through analysis of recession flow data. These authors noticed that derived K-values were approximately 100 times larger than values measured in soil samples in the laboratory. The reason for this

striking discrepancy lies in the difference in scale between a river catchment and laboratory soil samples. At the catchment scale, flow through preferential flow paths like macropores seriously increases subsurface flow rates. In the model, this phenomenon can only be compensated for by an increase in the value of K_0.

4.3.6 Simulation results

Figure 4.8 and Figure 4.9 display observed and computed hydrographs of two storm events in the Zwalm catchment. The event of 02-06-1992 has been used to calibrate the values of the stream routing parameters ε and δ. Both figures show there are some discrepancies between observed and computed values. However, it is hard to find out whether these discrepancies stem from incorrect modelling concepts, since a significant proportion of the modelling error can be put down to lack of information on the rainfall input. During the event of 02-06-1992, for instance, two rainfall stations were out of order, so information from only three stations is available. Even in a small area like the Zwalm catchment, different stations sometimes show significant mutual differences in observed rainfall intensities, especially during intense storm events. The impact of these spatial differences on the model output can be quite substantial, as can be seen from Figure 4.10. This figure shows computed hydrographs resulting from three different simulations, where catchment average rainfall in each simulation was set equal to the observed values in one of the three available rainfall stations.

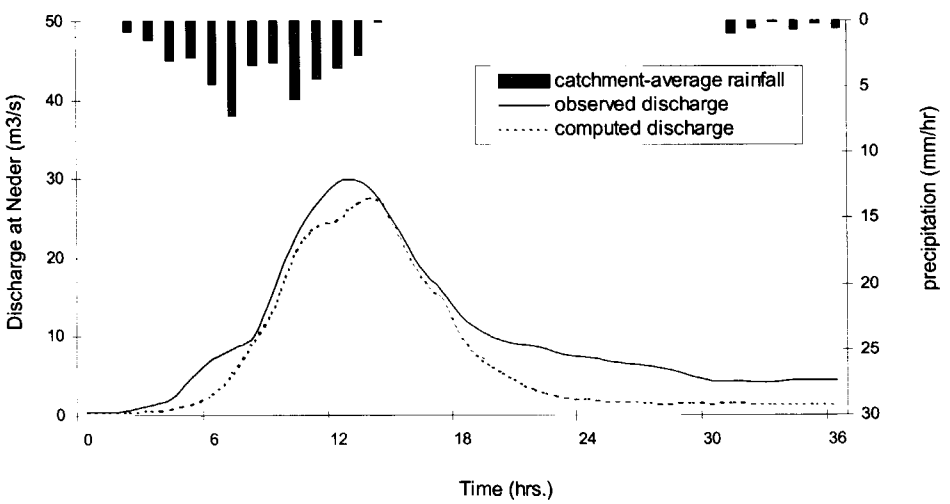

Figure 4.8 Observed and computed discharge of the event of 02-06-1992

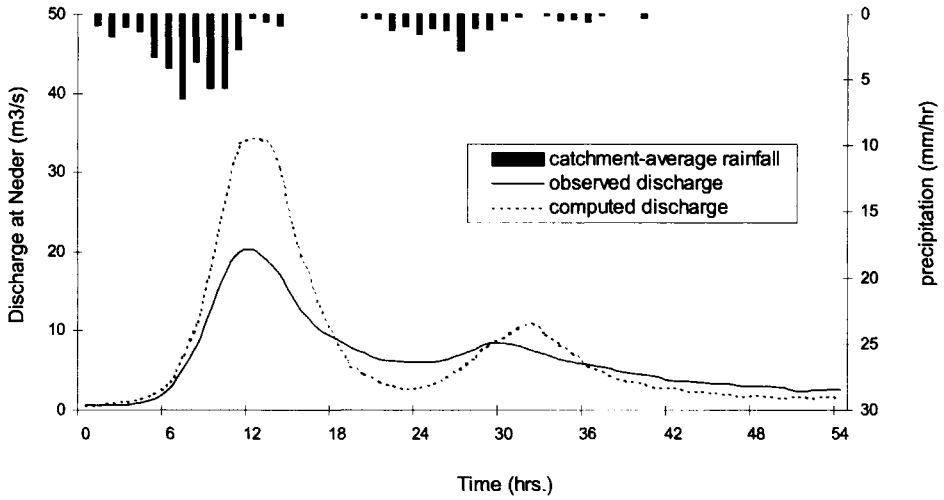

Figure 4.9 Observed and computed discharge of the event of 13-11-1993

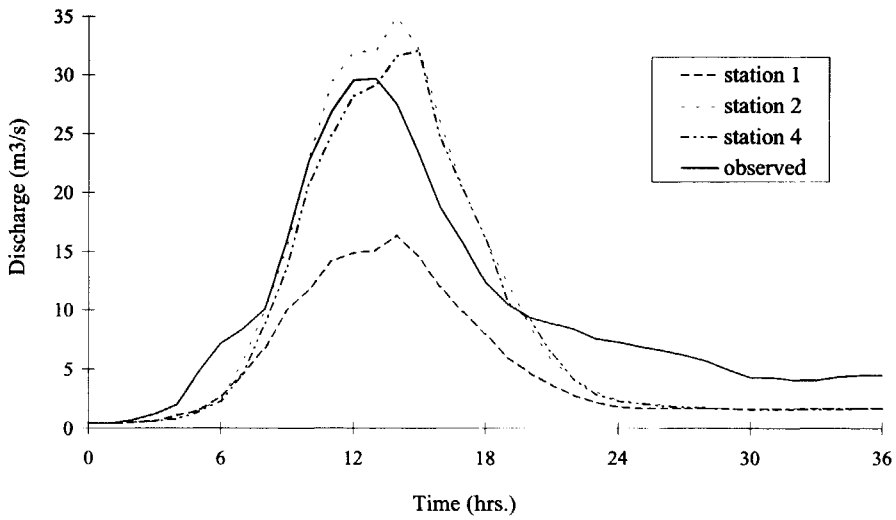

Figure 4.10 Computed hydrographs, resulting from the use of different rainfall inputs. For each simulation the catchment-average rainfall was set equal to the observed rainfall of one rainfall station; Event of 02-06-1992

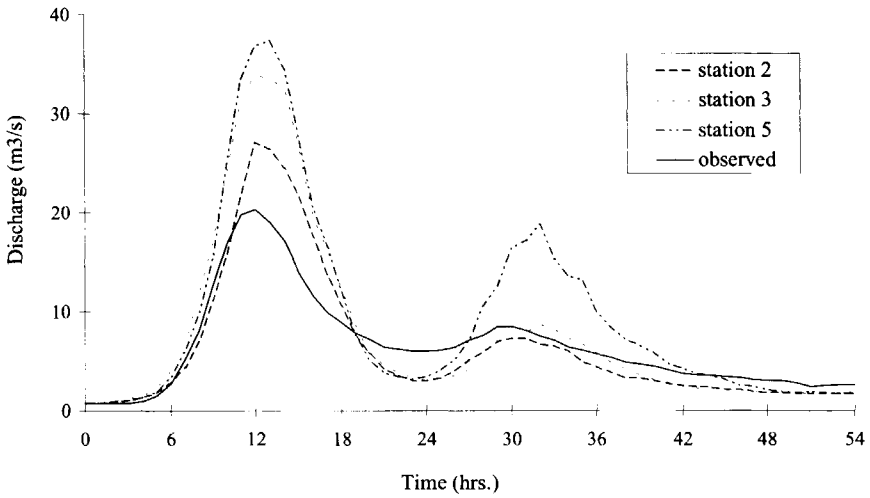

Figure 4.11 Computed hydrographs, resulting from the use of different rainfall inputs. For each simulation the catchment-average rainfall was set equal to the observed rainfall of one rainfall station; Event of 13-11-1993

Figure 4.11 presents a similar picture for the event of 13-11-1993. The two figures show that differences between the three computed hydrographs are in the same order of magnitude as differences between the observed and computed hydrographs in Figure 4.8 and Figure 4.9. Unfortunately, this phenomenon is not restricted to these particular events only. It is therefore hard to filter out modelling errors by comparison of computed and observed hydrographs, unless differences between computed and observed hydrographs show structural characteristics. Table 4.2 shows that for peak values these structural differences do not exist.

Event	observed peak discharge (m^3/s)	computed peak discharge (m^3/s)	error percentage
12-11-1991	24.2	13.6	-44
06-02-1992	29.7	27.3	-8
22-01-1993	27.3	15.4	-44
24-07-1993	29.2	15.9	-46
13-11-1993	27.8	24.0	-14
12-12-1993	18.8	38.2	103
19-12-1993	20.3	34.3	69

Table 4.2 Comparison of observed and computed peak discharges for 7 events

4.4 Univariate sensitivity analysis

4.4.1 Introduction and methodology

A sensitivity analysis is a popular tool to assess the influence of the individual parameters on the output of the model. This type of analysis is generally performed for calibration purposes, either to find out for which sub-set of parameters calibration should be performed or to find out directly which parameter set generates optimal simulation results

The term "univariate sensitivity analysis" refers to the concept of varying the value of one parameter while the other parameters are set equal to their respective default values (see Table 4.1 for default values of the 11 parameters). This type of analysis has been applied to 11 parameters (f, K_0, h_c, n, α, N, θ_s, θ_r, m, ε en δ) of the catchment-runoff model of the Zwalm. Parameters a_i and β_i have not been subjected to the sensitivity analysis since they are modelled in a spatially distributed manner. Furthermore, since these two parameters have been derived from a detailed DEM they are considered to be well-defined.

Before a sensitivity analysis can be performed, a range of optional values needs to be defined for each of the parameters individually. The individual ranges for parameters in a sensitivity analysis are usually based on experience on either [1] calibrated parameter values for a number of modelled catchments (e.g. Uhlenbrook et al., 1999) or [2] observed parameter values in nature (e.g. Hornberger et al, 1985). In theory, these two approaches lead to a more realistic impression of the model sensitivity, since distinction can be made between parameters that are well-defined and parameters that are not. In practice, however difficulties arise which are hard, if not impossible, to overcome:

[1] If ranges are based on calibration experiences, chances are high that wide ranges are awarded to parameters, to which the model is relatively insensitive. These parameters can virtually take on any value, without generating unrealistic results, so the optimal value in calibration terms is likely to vary strongly from case to case. The relatively large ranges will lead to misleading results in a sensitivity analysis, since the sensitivity of the model to this group of parameters will be consistently overestimated.

[2] If ranges are based on measured values in nature, one is confronted with the discrepancy between the scale of measurement and the scale of modelling. In case of the Zwalm catchment this can be illustrated by the scale-sensitivity of parameter K_0 (hydraulic conductivity). The default value of this parameter in the catchment-runoff model is taken to be approximately 100 times larger than values measured in soil samples in the

laboratory (see section 4.3.5). This high K_0-value is used in order to compensate for the effects of preferential flow paths, since unrealistic results would be obtained if measured values were to be used. The currently used value of K_0 is obtained from Troch et al. [1993] who presented a number of K_0-values that lead to realistic results for a ground water model based on Boussinesq's equation. These value don't fit in the range of K_0-values, obtained from direct measurements in the laboratory, which means for this parameter, the range of optional values cannot be obtained without using calibration techniques.

Because of these difficulties, both methods are not considered to be useful here. Instead, for each parameter, the range is taken to be a constant percentage of its default value. Percentages where chosen small enough to hold realistic values for each parameter and large enough to be able to fulfil the initial purpose of the sensitivity analysis (i.e. to asses the individual role of each parameter and to explore interdependence among the parameters). During the analysis, the value of the parameter of interest ranges from 40 % to 160 % of its default value. A uniform sampling routine with a step size of 20 % of the default value is used (except for θ_s which is varied between 70 %-130% of its default value with a step size of 10%, in order to keep its value realistic), which means 7 model runs have been performed for each of the parameters. Subsequently, resulting output hydrographs are compared with the hydrograph that results from a run with default parameter values (see Table 4.1). Deviations are quantified in order to compare the influence of the various parameters on the model output. For this purpose the mean square error (MSE) is used:

$$MSE = \frac{1}{T}\sum_{t=1}^{T}\left[c_t - d_t\right]^2 \tag{4.18}$$

where T is the number of time steps used in one simulation, c_t is the computed discharge at time t of the current simulation and d_t is the computed discharge at time t of a run with default parameters.

4.4.2 Analysis of results

The sensitivity analysis has been applied to the event of 02-06-1992. The various plots of computed MSE-values as a function of the value of the parameter of interest are shown (Figure 4.12- Figure 4.21 with exception of Figure 4.15) and results are analysed/explained based on the model equations. Furthermore, computed hydrographs are presented in Figures A1-A8 of Appendix A. The initial purpose of the analysis is to identify the essential features of a well-known concept (TOPMODEL) for catchment-runoff modelling. Therefore, a thorough analysis of the model equations has been performed in order to explain the observed sensitivity of the model to its parameters. Results are separately discussed for each of the parameters.

Parameter f

Parameter f is the decline parameter in equation (4.1), which is based on the assumption of an exponential decline of hydraulic conductivity with increasing depth into the soil profile. The Mean square error values for different values of this parameter are presented in Figure 4.12. In comparison with other parameters the model is rather sensitive to changes in the value of f. This can be explained from the dominant role of this parameter in the estimation of the area-average groundwater table depth, z_{av}, at the beginning of the event.

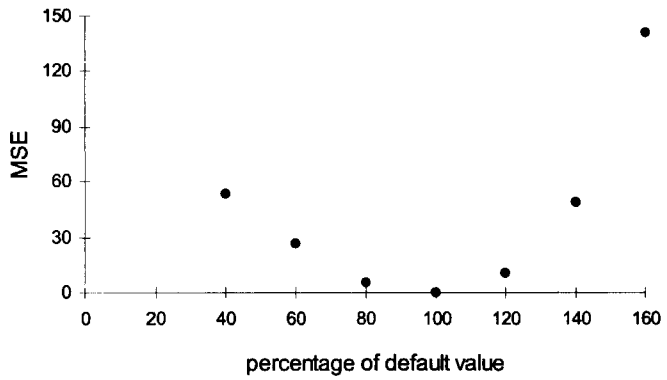

Figure 4.12: Deviation of resulting hydrographs of the sensitivity analysis of parameter f from the hydrograph which has been derived with the default value of f (corresponding to 100 %, see Table 4.1). The deviation is quantified by the Mean Square Error (MSE, equation (4.18)).

The relation between parameter f and the average initial ground water depth z_{av} is captured in equation (4.12), both directly and indirectly, since the value of the area average transmissivity T_e is also related to the value of f:

$$\ln T_e = \int_A \ln T_0 dA \quad ; T_0 = K_0 / f \tag{4.19}$$

If we assume K_0 an f to be spatially invariant, we get:

$$T_e = K_0 / f \tag{4.20}$$

From substitution of equation (4.20) in equation (4.12) we obtain:

$$z_{av}(f) = -\frac{\ln(f) + c_{bf}}{f} \quad ; c_{bf} = \ln\left[\frac{Q(0)}{AK_0 \exp(-\lambda)}\right] \tag{4.21}$$

The derivative of function z_{av} equals:

$$\frac{dz_{av}}{df} = \frac{\ln(f) + c_{bf} - 1}{f^2} \tag{4.22}$$

Now, suppose the function dz_{av}/df is non-negative for some value(s) of f, then:

$$\frac{\ln(f)+c_{bf}-1}{f^2} \geq 0 \;\Rightarrow\; \frac{1}{f}\left\{\frac{\ln(f)+c_{bf}}{f}-\frac{1}{f}\right\} \geq 0$$

$$\Rightarrow\; \frac{1}{f}\left\{-z_{av}-\frac{1}{f}\right\} \geq 0 \;\Rightarrow\; z_{av} \leq -\frac{1}{f} \qquad (4.23)$$

Parameter f is positive by definition, so a non-negative value of dz_{av}/df will only occur in the case of a positive value of the area average initial ground water depth. This is unrealistic, since an area-average ground water table which is situated above the ground surface can only occur in wetlands. Consequently, the value of dz_{av}/df will always be negative at the beginning of a storm event, which means the value of the initial ground water table depth, z_{av}, decreases with increasing value of f. This is in accord with the physical basis of these two parameters: A relatively high value of f implies a relatively low transmissivity, T, of the soil layer (equation (4.20)). In order to generate the observed discharge, $Q(0)$, in case of low transmissivity of the soil, the area-average ground water table has to be situated near the ground surface.[3] An area-average initial ground water table which is situated close to the ground surface promotes the occurrence of saturated soil profiles and, accordingly, generation of the dominant storm runoff mechanism in the Zwalm catchment (saturation overland flow). An increase in the value of f will therefore lead to an increase in storm runoff production which is confirmed by Figure A1 (Appendix A), where computed hydrographs for various values of f are presented.

Besides its influence on the initial ground water depth, parameter f also acts upon groundwater flow rates during storm events, since the transmissivity of the soil layer decreases with increasing values of f (equation (4.3)). This means the previously described effect of an increase in storm runoff production with increasing f is damped. However, as far as intense storm events are concerned this damping effect is only marginal and therefore of negligible importance in this sensitivity analysis.

Parameter K0.

Parameter K_0 represents the saturated hydraulic conductivity of the soil near the ground surface. Furthermore, in combination with parameter f it also represents the hydraulic conductivity at any depth in the soil layer, through equation (4.1). Just like parameter f,

[3] It has to be pointed out that this way of reasoning in order to explain the results of the sensitivity analysis of the hydrological model is based on the assumption of a constant value of the observed base flow $Q(0)$. In reality, of course, a change in parameter f (or actually, a change in the soil characteristics which are represented by parameter f) can also change the value of $Q(0)$.

parameter K_0 is a significant control on initial ground water table depths. Accordingly, the model output is also relatively sensitive to changes in the value of K_0. The mean square error values for different values of this parameter are presented in Figure 4.13.

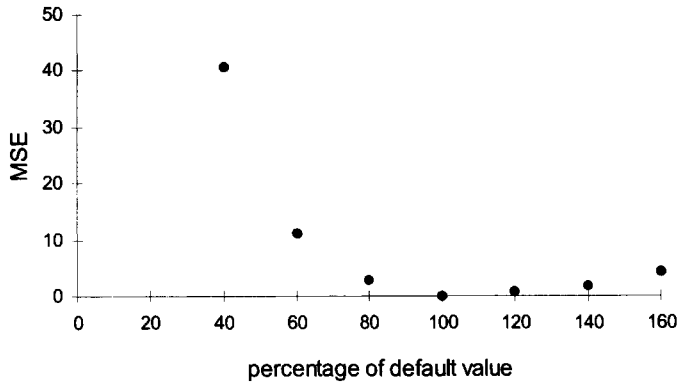

Figure 4.13 Deviation of resulting hydrographs of the sensitivity analysis of parameter K_0 from the hydrograph which has been derived with the default value of K_0 (corresponding to 100 %, see Table 4.1). The deviation is quantified by the Mean Square Error (MSE, equation (4.18)).

Rewriting of equation (4.21) gives:

$$z_{av} = \frac{\ln(K_0) - c_{bk}}{f} \quad ; c_{bk} = \ln\left[\frac{fQ(0)}{A\exp(-\lambda)}\right] \tag{4.24}$$

Since $f>0$, it can be concluded directly from equation (4.24) that z_{av} increases with increasing value of K_0, which means runoff production decreases with increasing value of K_0. This is consistent with the findings from the sensitivity analysis for parameter f: The value of parameter K_0 is proportional to the value of transmissivity T_0, whereas f is inversely proportional to K_0 (see equation (4.20)). As a consequence, the explanation why an increase in f leads to an increase in storm runoff production can also be used to explain why an increase in the value of K_0 leads to a decrease in storm runoff production. To which extent an increase in K_0 values alters runoff hydrographs is shown in Figure A2 (Appendix A), where computed hydrographs for various values of K_0 are presented.

Figure 4.13 and Figure A2 show that effects of a decrease in the value of K_0 are by far more substantial than effects of an increase in the value of K_0. This striking "skewness" can be explained from a closer look at equation (4.24). The derivative of this equation, dz_{av}/dK_0, equals:

$$\frac{dz_{av}}{dK_0}(K_0) = \frac{1}{K_0 f} \tag{4.25}$$

Obviously, the change in the value of the initial ground water depth z_{av} caused by a change in K_0 is inversely proportional to the value of K_0. Even though there is no one to one relationship between initial ground water table depth on one hand and runoff production on the other hand, equation (4.25) largely explains the skewness of Figure 4.13.

Parameter h_c

Parameter h_c represents the length of the capillary fringe, i.e. the length of the saturated zone directly above the ground water table, where soil water is still held by capillary forces against gravitational forces. Consequently, the soil is considered to be completely saturated at location i if the ground water table is situated at a depth $z_i \leq h_c$, (see equation (4.13)). The value of h_c is a significant control on the percentage of saturated soil profiles in the catchment and therefore indirectly of strong influence on the production of saturation overland flow. This influence is reflected in the derived values of the Mean square error as depicted in Figure 4.14.

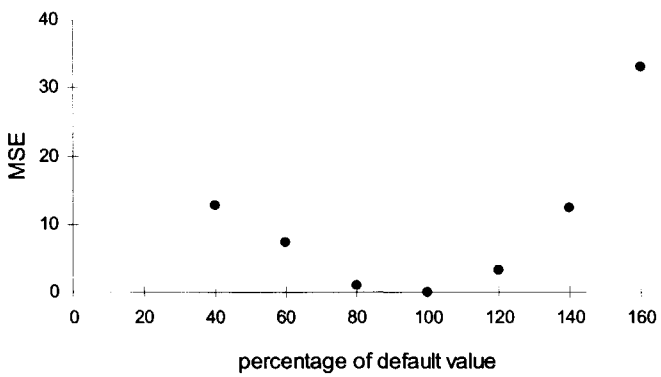

Figure 4.14 Deviation of resulting hydrographs of the sensitivity analysis of parameter h_c from the hydrograph which has been derived with the default value of h_c (corresponding to 100 %, see Table 4.1). The deviation is quantified by the Mean Square Error (MSE, equation (4.18)).

Whether or not a soil profile at location i is saturated depends on the value of z_i which can be derived from equation (4.9). If we assume the transmissivity in the soil to be spatially invariant, equation (4.9) changes into:

$$z_i = z_{av} - \frac{1}{f}\left\{\ln\left(\frac{a_i}{\tan(\beta_i)}\right) - \lambda\right\} \tag{4.26}$$

This means a soil profile is completely saturated when:

$$z_i \le h_c \Rightarrow z_{av} - \frac{1}{f}\left\{\ln\left(\frac{a_i}{\tan(\beta_i)}\right) - \lambda\right\} \le h_c \Rightarrow \ln\left[\frac{a_i}{\tan(\beta_i)}\right] \ge f(z_{av} - h_c) + \lambda \qquad (4.27)$$

The left hand side of this inequality is the topographic index $ln[a/tan(\beta)]$ as defined by Beven and Kirkby [1979]. Figure 4.15 depicts the distribution function, $F(ln[a/tan(\beta)])$, of occurring topographic index values in the Zwalm catchment.

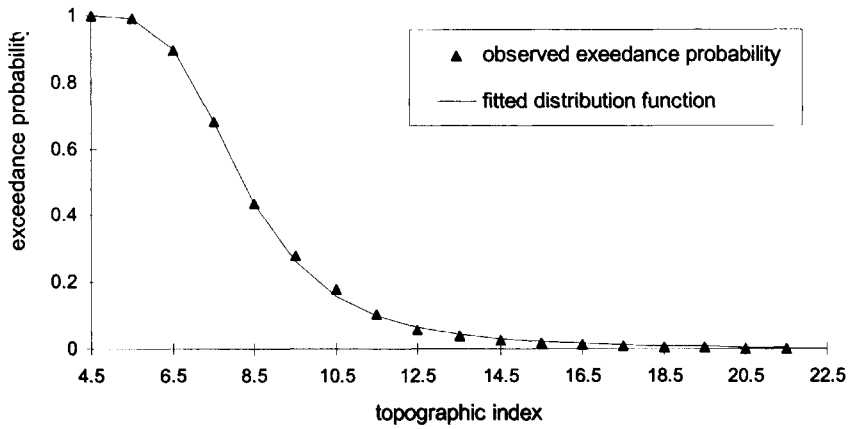

Figure 4.15 Distribution of topographic index values (ln[a/tan(β)]) in the Zwalm catchment

As can be seen in Figure 4.15, the observed exceedance probabilities of topographic index values in the Zwalm catchment can be fitted remarkably well by the following distribution function:

$$G(x) = \frac{(x - c_1)^{c_2}}{c_3 + (x - c_1)^{c_2}} \quad ; x \ge 4.5, c_1 = 4.5, c_2 = 3.5, c_3 = 100 \qquad (4.28)$$

This distribution function is not valid for topographic index values smaller than location parameter c_1 (=4.5), but this is no problem since the percentage of locations in the Zwalm catchment with topographic index values smaller than c_1 is negligible (see Figure 4.15). The fraction of soil profiles in the catchment that are fully saturated, p_s, is equal to the value $G(T_\alpha)$, where T_α is the value of the topographic index for which equality holds in (4.27):

$$p_s = G(T_\alpha) \quad ; T_\alpha = f(z_{av} - h_c) + \lambda \qquad (4.29)$$

From equation (4.29) it follows directly that an increase of Δh_c in the value of h_c will lead to a decrease in the value of T_α of approximately $f\Delta h_c$. Accordingly this results in an approximate increase of $-f\Delta h_c g(T_\alpha)$ in the fraction of saturated soil profiles, where g is the derivative of G.

The value of g is negative for realistic values of T_α (see Figure 4.15), since g can only be equal to zero in case the catchment consists of 0 % saturated soil profiles or 100 % saturated soil profiles, two situations which can not be expected to occur. Consequently, an increase of Δh_c in the value of h_c will lead to an increase in the fraction of saturated soil profiles, which is in accord with the physical meaning of h_c. This increase can be quantified by:

$$p_s(h_c + \Delta h_c) - p_s(h_c) \approx -f\Delta h_c g(T_\alpha) = -f\Delta h_c \frac{c_3 c_2 (T_\alpha - c_1)^{c_2 - 1}}{\left[c_3 + (T_\alpha - c_1)^{c_2}\right]^2} \quad ; T_\alpha \geq c_1 \qquad (4.30)$$

In order to explain the slight skewness in Figure 4.14 we need to examine the function $g(T_\alpha)$. For the current event, $T_\alpha \approx 10.5$, if default parameter values (see Table 4.1) are used. Figure 4.16 shows $g(T_\alpha)$ is a decreasing function for this value of T_α.

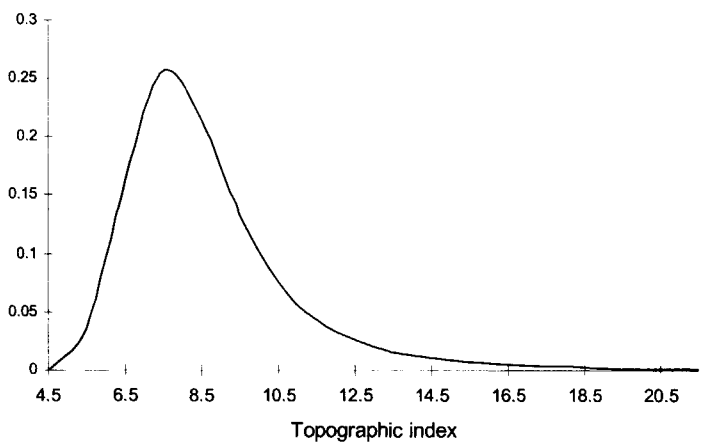

Figure 4.16 Density function g of topographic index values in the Zwalm catchment.

This means an increase in the value of T_α will sort less effect on the initial ground water table than an equally large decrease in the value of T_α. Accordingly (see equation (4.29)), an increase in the value of h_c will sort more effect on the initial ground water table than an equally large decrease in the value of h_c. Moreover, an increase in the value of h_c causes more significant changes in the model output than an equally large decrease in the value of h_c, which can also be seen in both Figure 4.14 and Figure A3 (Appendix A).

Parameters n and α

Parameters n and α are both empirically based parameters of the Van Genuchten equation (Van Genuchten, 1980). Equation (4.13) is a modified version of the Van Genuchten equation, in which hydraulic equilibrium in the soil has been assumed. This equation relates

the initial soil moisture deficit to the depth of the ground water table. The soil moisture deficit can be considered as the remaining capacity in the soil for storage of infiltrating rainfall water. In spite of the relevance of this capacity, the model output turned out to be completely insensitive to changes in the values of these two parameters.

A closer look at equation (4.13) reveals why the choice of a value of parameters n and α is of negligible relevance to the model output. The value of the ground water table depth z_i varies strongly within the catchment, but will never exceed 10 m. Since α is equal to 0.0019 (Table 4.1), αz_i is always less than 0.02. As a consequence, the following approximation is valid:

$$\left(1+(\alpha z_i)^{-n}\right)^{-1/n} \approx \left((\alpha z_i)^{-n}\right)^{-1/n} = \alpha z_i \quad ;|\alpha z_i| \leq 0.02 \tag{4.31}$$

This approximation changes equation (4.13) into:

$$S_i = (\theta_s - \theta_r)\left(1-\frac{\alpha}{f}\right)(z_i - h_c) \tag{4.32}$$

Furthermore, since $|\alpha/f| << 1$, equation (4.32) can be closely approximated by:

$$S_i = (\theta_s - \theta_r)(z_i - h_c) \tag{4.33}$$

This means n and α can both be eliminated from the modified Van Genuchten equation, which explains why the model output is insensitive to these two parameters.

Parameter N

Parameter N is Manning's roughness coefficient, which is one of the controls on the velocity of the available runoff water towards the stream network. High values of N correspond to low velocities. Consequently, in Figure A4 of Appendix A (which contains computed hydrographs of the sensitivity analysis of N) low values of N result in slightly steeper rising limbs of resulting hydrographs. Differences are, however, marginal, which is also reflected in Figure 4.17, where mean square error values for different values of parameter N are presented. Comparison of Figure 4.17 on one hand with Figure 4.12 - Figure 4.14 on the other hand shows the model is by far less sensitive to changes in the value of N than to changes in the value of parameters f, K_0 or h_c. The relatively low sensitivity of the model output to values of parameter N is partly due to the fact that most saturated soil profiles, where the major part of runoff is produced, are situated near the river network.

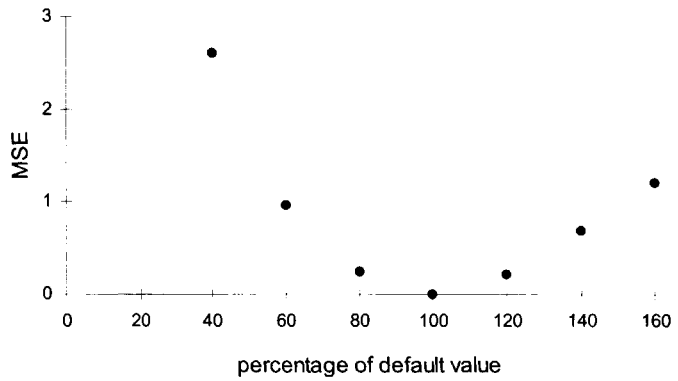

Figure 4.17 Deviation of resulting hydrographs of the sensitivity analysis of parameter N from the hydrograph which has been derived with the default value of N (corresponding to 100 %, see Table 4.1). The deviation is quantified by the Mean Square Error (MSE, equation (4.18)).

This means travel distances are on average relatively short which reduces possible effects of changes in the value of parameter N. Furthermore, high values of N initially lead to low flow velocities and, consequently, to low drainage rates. This means the overland flow height will increase relatively fast under influence of rainfall input. According to Manning's equation, an increase of overland flow heights promotes an increase in flow velocities. So on one hand an increase of N causes a direct decrease in flow velocities, while on the other hand it causes an indirect increase of flow velocities. These two opposite effects are another limiting factor to the influence of variations in N-values on output hydrographs.

Parameter m

Parameter m is the exponential decay parameter of base flow (equation (4.15)) as defined by Beven and Kirkby [1979]. Analogue to parameters n and α, the model turned out to be almost insensitive to changes in values of parameter m. This stems from the fact that during storm flow events, contributions of base flow are only marginal.

Parameter θ_s

Parameter θ_s represents the porosity of the soil. It is therefore a measure of the maximum amount of water the soil can contain. In the model, parameter θ_s is contained in the modified Van Genuchten equation (equation (4.13)), which means it is one of the parameters which relates the soil moisture deficit, S_i, to the depth, z_i, of the ground water table. If θ_s is relatively small, the remaining capacity of unsaturated soil profiles will also be relatively small. In that case, soil profiles will be filled up to complete saturation more easily during rainfall events, which favours the production of saturation excess runoff production. This is confirmed by

Figure A5 (Appendix A) which shows high values of θ_s result in hydrographs with higher peaks and higher volumes of total runoff production, albeit that differences are only marginal.

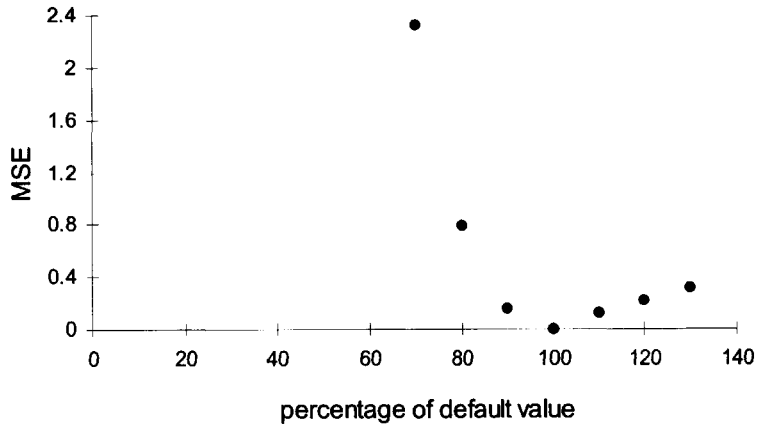

Figure 4.18 Deviation of resulting hydrographs of the sensitivity analysis of parameter θ_s from the hydrograph which has been derived with the default value of θ_s (corresponding to 100 %, see Table 4.1). The deviation is quantified by the Mean Square Error (MSE, equation (4.18)).

Figure 4.18 clearly shows the model is more sensitive to a decrease in the value of θ_s than to an equally large increase in the value of θ_s. This can be explained from the combination of equations (4.26) and (4.33):

$$S_i = (\theta_s - \theta_r)(z_i - h_c) = (\theta_s - \theta_r)\left(z_{av} - \frac{1}{f}\left[\ln\left(\frac{a_i}{\tan(\beta_i)}\right) - \lambda\right] - h_c\right) \tag{4.34}$$

Suppose the net supply of water to the soil profile at location i (i.e. infiltration plus incoming lateral flow from upslope areas minus downslope directed drainage) during a rainfall event equals P_i, then the soil will be saturated if $P_i \geq S_i$, i.e. if:

$$(\theta_s - \theta_r)\left(z_{av} - \frac{1}{f}\left[\ln\left(\frac{a_i}{\tan(\beta_i)}\right) - \lambda\right] - h_c\right) \leq P_i \tag{4.35}$$

Consequently, a soil profile will be saturated at some time during the rainfall event if the topographic index of this profile meets the following requirement:

$$\ln\left(\frac{a_i}{\tan(\beta_i)}\right) \geq f(z_{av} - h_c) - \frac{fP_i}{(\theta_s - \theta_r)} + \lambda \tag{4.36}$$

The fraction, p_s, of soil profiles which will be saturated during the rainfall event can be derived by combining equation (4.36) and distribution function, $G(x)$, of topographic index values (equation (4.28)). Since θ_s is positioned in the denominator of equation (4.36), p_s is more sensitive to a decrease in the value of θ_s than to an equally large increase in the value of θ_s. This explains the skewness in Figure 4.18.

Parameter θ_r

Parameter θ_r is the residual moisture content of the soil layer, i.e. the amount of water held by the soil under extremely dry ("oven dryness") conditions. The difference between θ_s and θ_r is a measure of the total capacity per unit depth of the soil layer for storage of rainfall water. As far as the output of the catchment-runoff model is concerned, θ_s and θ_r can be replaced by one parameter $\theta_d = \theta_s - \theta_r$ without effecting the model output at all (see equation (4.13)). Consequently, the sensitivity of the model to variations in θ_r is strongly related to the sensitivity of the model to variations in θ_s. An increase in the value of θ_r will sort exactly the same effect on the model output as an equally large decrease in the value of θ_s.

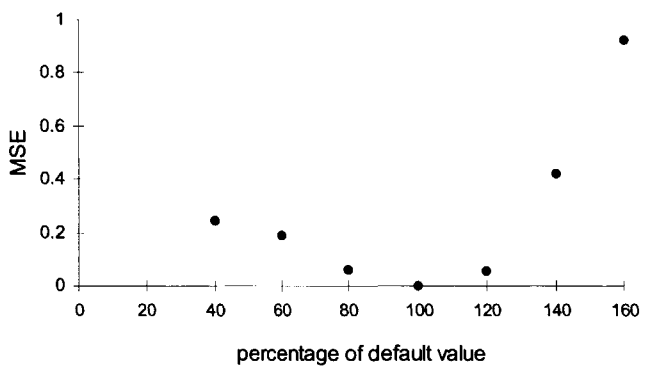

Figure 4.19 Deviation of resulting hydrographs of the sensitivity analysis of parameter θ_r from the hydrograph which has been derived with the default value of θ_r (corresponding to 100 %, see Table 4.1). The deviation is quantified by the Mean Square Error (MSE, equation (4.18)).

Accordingly, Figure 4.19 shows that, as opposed to parameter θ_s, the model is more sensitive to an increase in the value of θ_r than to an equally large decrease in the value of θ_r.

Parameter ε

Parameter ε is one of the parameters of the power function which relates the velocity in the stream network to the discharge at the catchment outlet (equation (4.17)). The velocity in the stream network is proportionally related to the value of ε, so an increase of 20 % in the value of ε results in an increase of 20% in the flow velocity. Figure A7 (Appendix A) shows that an increase in the value of ε results in steeper rising limbs of the hydrograph and an increase in

the peak runoff value. The increase of the peak discharge is due to the fact that peak runoff discharges of subcatchments increasingly coincide when velocities in the river network increase.

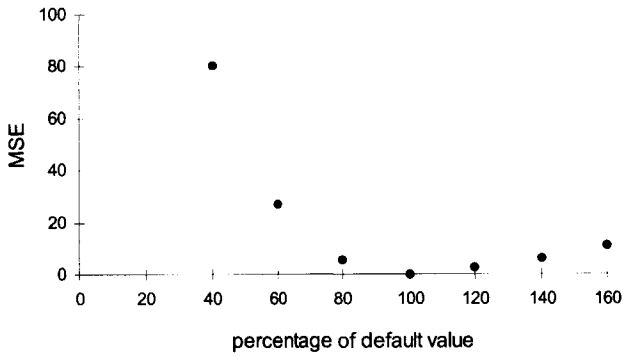

Figure 4.20 Deviation of resulting hydrographs of the sensitivity analysis of parameter ε from the hydrograph which has been derived with the default value of ε (corresponding to 100 %, see Table 4.1). The deviation is quantified by the Mean Square Error (MSE, equation (4.18)).

Both Figure 4.20 and Figure A7 show the model is more sensitive to an decrease in the value of ε than to an equally large increase. This is due to the fact that travel times in the stream network are inversely proportional to the stream velocity and consequently also inversely proportional to ε. An increase in stream flow velocity results in an increased spreading of arrival times of subcatchment peak discharges, which means the resulting hydrograph shape will be wider with a lower peak value. Especially this widening effect makes the model quit sensitive to a decrease in parameter ε.

Parameter δ.

Parameter δ is the second parameter of the power function which relates discharge at the catchment outlet and the velocity in the river network (equation (4.17)). Analogue to parameter ε, an increase in the value of parameter δ promotes steepening of hydrographs (see Figure A8). However, comparison of Figure 4.21 and Figure 4.20 makes clear that for parameter δ this effect is less distinct.

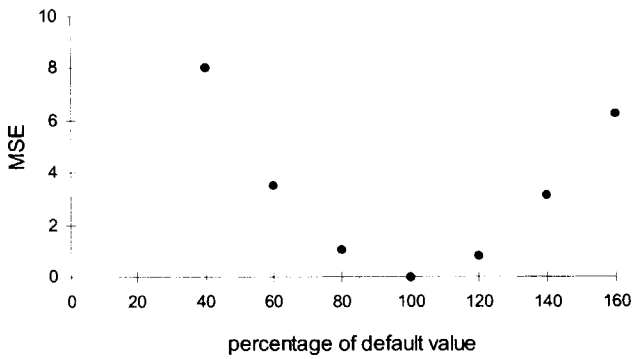

Figure 4.21 Deviation of resulting hydrographs of the sensitivity analysis of parameter δ from the hydrograph which has been derived with the default value of δ (corresponding to 100 %, see Table 4.1). The deviation is quantified by the Mean Square Error (MSE, equation (4.18)).

4.4.3 Conclusions

A univariate sensitivity analysis has been applied to the catchment-runoff model (section 4.3) of the 114 km^2 Zwalm catchment. In terms of sensitivity of the model to changes in values of parameters, the 11 parameters can be divided into three sub-sets:

I Highly sensitive: f, h_c, K_0, ε
II Moderately sensitive: N, θ_s, θ_r, δ
III Insensitive: n, α, m

Naturally, this subdivision is influenced by the choice of the ranges of optional parameter values, which contains some inevitable subjectivity. Still, it is clear that the controlling parameters on the percentage of initially saturated areas, f, h_c and K_0, are dominant factors in runoff generation. This is in accord with Troch et al. [1993] who stated that storm runoff water is mainly generated on saturated parts of the catchment.

The relatively high sensitivity of the model to changes in parameter ε stems from the fact that a change of 20 % can cause a "horizontal shift" of one hour in the computed hydrograph, since travel distances in the river network can go up to 21 km. This horizontal shift causes relatively large errors in terms of the MSE-criterion as defined in equation (4.18). If only differences in generated peak values would have been considered, the model would be significantly less sensitive to parameter ε in comparison with parameters f, h_c and K_0.

The negligible sensitivity of the model to parameters n and α stems from the fact that the modified Van Genuchten equation (4.13) can be closely approximated by an equation in which n and α do not occur (equation (4.33)). This reduces the number of parameters from 11 to 9, which can be useful in preventing the negative side effects of overparameterisation. In case of parameter m such an approximation could not be derived.

In terms of approximation of observed output, equally satisfying model simulations were realised by using a number of different parameter sets. This clearly reveals the possible dangers of overparameterisation. If, based on the results of this sensitivity analysis, calibration of parameters is performed by choosing an optimal set of parameters, it is not clear which set should be chosen, even though we only examined a small part of the entire parameter space. Consequently, calibration of parameters, based on observed discharges, should only be applied to a small subset of parameters. In the following section, this issue will be analysed into further detail.

4.5 Bivariate sensitivity analysis

4.5.1 Introduction

The results of the univariate sensitivity analysis of parameters θ_s and θ_r showed that a change in the value of one parameter can sometimes be compensated for by a change in the value of another parameter, if both parameters are involved in similar aspects of the model. In case of parameters θ_s and θ_r, the only signal in terms of runoff production comes from the difference, $\theta_d=\theta_s-\theta_r$, between the two parameter values (see equation (4.13)). As a consequence, these two parameters cannot be calibrated simultaneously, if calibration is based on observed runoff rates only. In this particular example, problems of parameter identification can be reduced by eliminating parameters θ_s and θ_r in equation (4.13) through transformation: θ_d $=\theta_s-\theta_r$. For other parameter combinations, however, a similar transformation cannot be directly derived from the model equations. This means parameter pairs cannot be replaced by one single parameter, without effecting the output of the model. Still, though, resemblance in resulting hydrographs from different parameter sets indicate that for some combinations strong interdependence may exist.

In order to find out to which extent interdependence among parameters exists, a bivariate sensitivity analysis has been performed. The term "bivariate sensitivity analysis" refers to the concept of varying the value of two parameters while the other parameters are set equal to their respective default values (see Table 4.1 for default values of the 11 parameters of the catchment-runoff model of the Zwalm). This analysis is useful in finding out whether processes/parameters either amplify or attenuate each others influence on runoff production. Furthermore, it may reveal whether or not the model contains some redundant parameters.

4.5.2 Methodology

The bivariate sensitivity analysis has been performed for 8 model parameters (as opposed to 11 in the univariate sensitivity analysis; Parameter n, α and m have been left out of this analysis since the model showed no sensitivity at all towards these parameters). This means 28 possible pairs of parameters have been examined (½×8×7 combinations). For each of the 28 pairs the parameter values have been varied from 40% up to 160 % of their respective default value (see Table 4.1 for the default values of all parameters) while the other model parameters remain constant. A step size of 15% has been used, so each parameter has been awarded 9 different values, which means 81 (9×9) model runs have been performed for every parameter pair.

Again, as in section 4.4, the sensitivity of the model to parameter variation is quantified by the "Mean Square Error"(MSE) of the 81 output hydrographs in relation with the hydrograph, obtained from a model run with default parameter values:

$$MSE = \frac{1}{T}\sum_{t=1}^{T}\left[c_t - d_t\right]^2 \tag{4.37}$$

where T is the number of time steps used in a simulation, c_t is the computed discharge of the current simulation at time t and d_t is the computed discharge of a run with default parameters at time t.

Subsequently, a two-dimensional contour plot is set up, based on interpolation of the 81 derived MSE-values. Figure 4.23, for example, shows the contour plot of the bivariate sensitivity analysis of parameters θ_s and θ_r. The two axis of the plot correspond with the two parameters under consideration. For the sake of clarity, two transformations have been applied prior to the set up of the contour plots.

1. In stead of the MSE-value, the contour plots show the MSE*-value, where:

   $$MSE^* = \ln(1 + MSE) \tag{4.38}$$

   This new measure has been introduced because the range of occurring MSE-values in one contour plot in some cases is too large to produce a clear picture. With original MSE-values, the distance between contour lines becomes too small in some parts of the plot (e.g. in the upper left corner of Figure 4.23) and simultaneously too large in other parts of the plot (e.g. the bottom right corner of Figure 4.23). The structure of the lines then becomes unclear and the plot would provide hardly any useful information.
2. Instead of actual parameter values, the axis show rescaled parameter values, which are related to the real parameter values in the following manner:

   $$p_{val} = p_{def} + p^*_{val} \times \Delta p \quad \Leftrightarrow \quad p^*_{val} = \frac{p_{val} - p_{def}}{\Delta p} \tag{4.39}$$

   where p^*_{val} is the rescaled value of the actual parameter value p_{val}, p_{def} is the default parameter value (corresponding to $p^*_{val}=0$) and Δp is the step size of the parameter value in the sensitivity analysis (i.e. 15% of the default value). A schematic view of this transformation is presented in Figure 4.22. This transformation is performed because the values of two different parameters sometimes differ several orders of magnitude. When true parameter values are used, this can lead to interpolation errors that are unacceptably large in relation to the parameter value with the smallest order of magnitude. In that case the actual underlying structure of the contour lines is completely changed, which means the plots would not be useful.

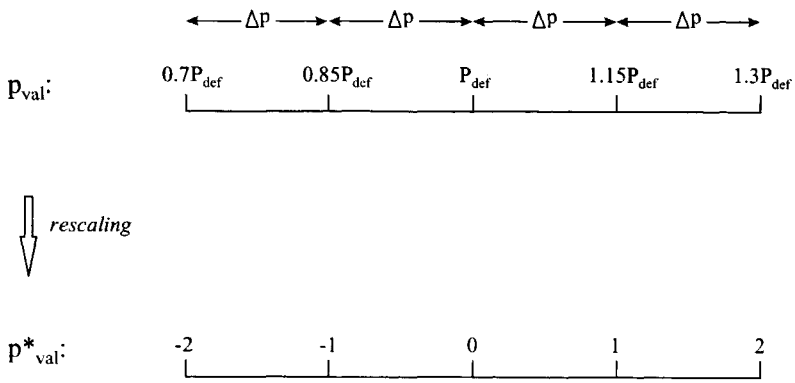

Figure 4.22 Schematic view of the rescaling of parameter values, according to (4.39). Here, Δp is taken to be $0.15p_{def}$.

The 81 dots in the contour plot (see Figure 4.23) correspond to the 81 model runs that have been performed for each parameter pair. The dot with co-ordinates (0,0) corresponds to the model run with default parameters, since (0,0) means p^*_{val}=0 in equation (4.39) for both parameters. Consequently, the MSE* value at (0,0) will be equal to 0 for all parameter pairs.

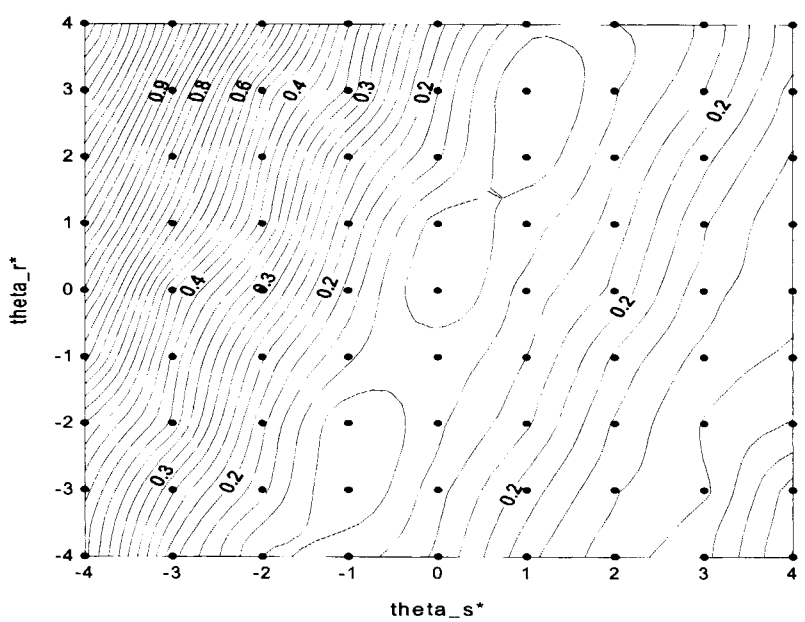

Figure 4.23 Contour plot of *MSE**-values of transformed parameter pairs (θ_s*, θ_r*)

4.5.3 Examples of resulting contour plots; 1. Known parameter relations.

The main purpose of the contour plots is to visualise the mutual relationship between two parameters. In section 4.5.5, the results of the 28 possible pairs of parameters will be presented. First, in section 4.5.3 and 4.5.4 a number of examples will be given to clarify the use of the contour plots in obtaining information on interdependence between the various parameters. In this section, plots are generated for combinations of parameters, of which the interdependence is already known in advance. Results are used to recognise patterns in contour plots, which is useful later on when contour plots of parameter combinations with unknown interdependence are examined.

Parameters θ_s and θ_r

In this first example, results are presented for the parameter combination θ_s (moisture content of the soil at full saturation) and θ_r (residual soil moisture content) as defined in equation (4.13). In section 4.4 it already has been pointed out that the effect of changes in these two parameters are strongly related to each other, since these two parameters can be replaced by one single parameter $\theta_d = \theta_s - \theta_r$, without effecting the model output. As a consequence, the value of MSE* is constant on a line $\theta_s - \theta_r$=constant, which means the contour plot is expected to contain straight contour lines only.

Figure 4.23 does indeed reveal the existence of the relationship between θ_s and θ_r. The only deviation from the expected outcome is the fact that contour lines are not perfectly straight. This is caused by interpolation errors, which is especially visible in areas of the plot where MSE*-values vary relatively slowly (e.g. the bottom right part of Figure 4.23). In the top left half of the plot the contour lines appear to be near perfectly straight, except for the extreme upper left part of the plot, where contour lines appear to be circular. This circular shape is due to the fact that the interpolation procedure of MSE*-values in the extreme upper left part of the plot are dominated by the value in the upper left corner. For this particular parameter pair, the prescribed variation of parameter values from 40 % to 160 % of the default values was not possible because in that case θ_s would be smaller than θ_r for a number of model runs, which is physically unrealistic and moreover impossible to simulate with the model. Therefore, the values of these two parameters have been varied from 70 % to 130 % of the default values with a step size of 7.5 %. The latter results in a step size of $\Delta\theta_s$=0.0315 for θ_s and a step size of $\Delta\theta_r$=0.012 for θ_r. This explains why the contour lines in Figure 4.23 have a gradient of $\Delta\theta_s/\Delta\theta_r \approx 2.6$.

Examples of well-related fictional parameters

The strong relation of values of parameters θ_s and θ_r on one hand, and resulting MSE-values on the other hand, can be described as:

$$MSE(\theta_s, \theta_r) = g_1(\theta_s - \theta_r) \tag{4.40}$$

where $g_1(..)$ is a function of one parameter. Besides relation (4.40), three other forms of interdependence are discussed:

[a] MSE(p1,p2) = g_2(p1+p2)
[b] MSE(p1,p2) = g_3(p1×p2)
[c] MSE(p1,p2) = g_4(p1/p2)

where *p1* and *p2* are the two parameters for which a bivariate sensitivity analysis is being performed, and g_2, g_3, and g_4 are all functions of one parameter. For each of the options [a]-[c] two fictional parameters have been defined. Furthermore, fictional MSE-values have been generated and assigned to the parameter values in such a way that the stated relation ([a]-[c]) holds. Subsequently, a contour plot is produced in the manner as described before. The resulting plots are presented in Figure 4.24 - Figure 4.26. Due to interpolation errors, these three figures show lines which are not perfectly smooth, just as in Figure 4.23,. However, the general picture of the underlying relationship is clearly revealed by the contour plots, i.e. Straight lines for option [a], curved lines for option [b] and diverging lines for option [c]. These three plots are shown here because resulting plots of a bivariate sensitivity analysis often contain patterns, similar to the ones presented in Figure 4.24 t/m Figure 4.26. Recognition of these similarities, provides information on the concept of the interdependence of the two parameters under consideration.

As a concluding remark to this section, it has to be emphasised that contour plots only reveal the global picture of how two parameters are related in terms of producing model output, instead of the exact relationship itself. For instance, the MSE* value at the co-ordinates (2,2) in Figure 4.25 is not equal to the MSE*-value of (4,1), even though Figure 4.25 is based on relationship [b], and 2×2=4×1. This is because the co-ordinates differ from the actual parameter values, since they are indirect representations of the actual parameter values through transformation (4.39). Still, though, the contour plots are a useful tool in obtaining a concept of mutual interdependence between two parameters, as will be demonstrated in section 4.5.4.

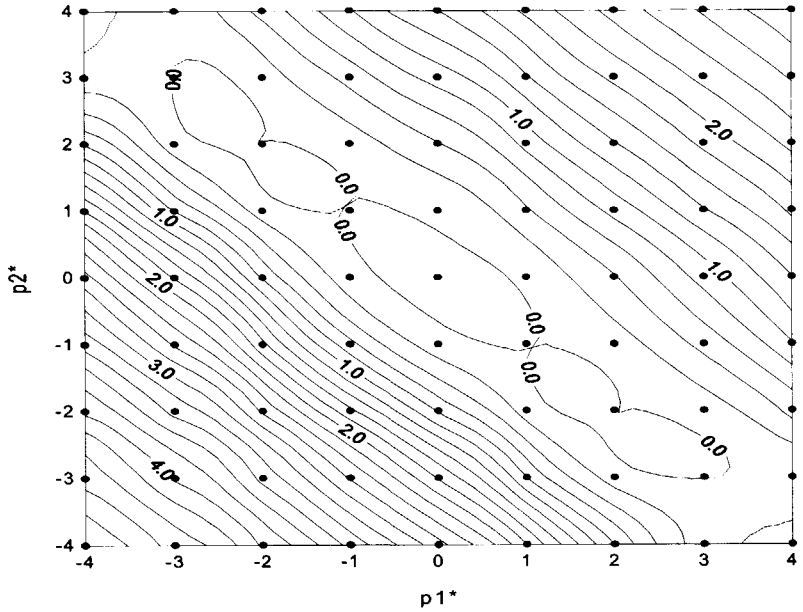

Figure 4.24 Contour plot of *MSE**-values of two fictional parameters p1 and p2 for which MSE*(p1,p2)=g_2(p1+p2)

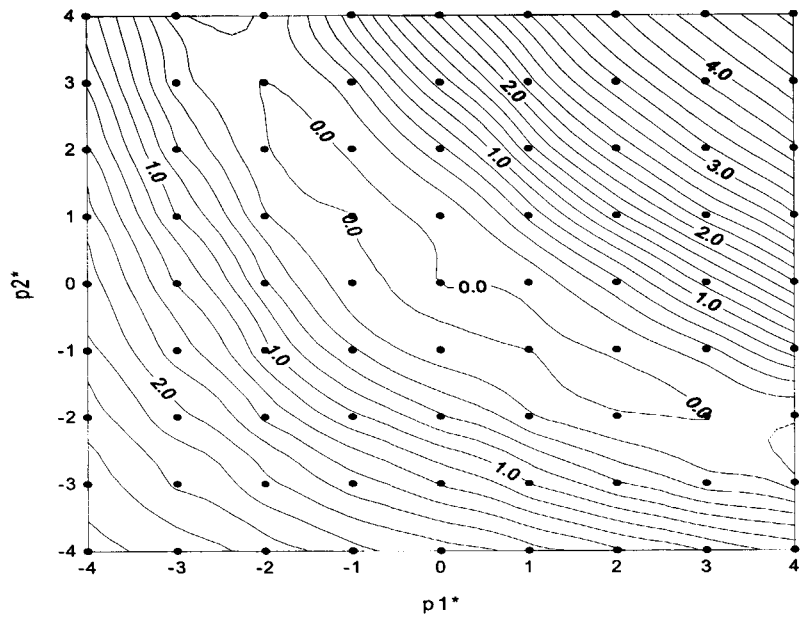

Figure 4.25 Contour plot of *MSE**-values of two fictional parameters p1 and p2, for which MSE*(p1,p2)=g_3(p1×p2)

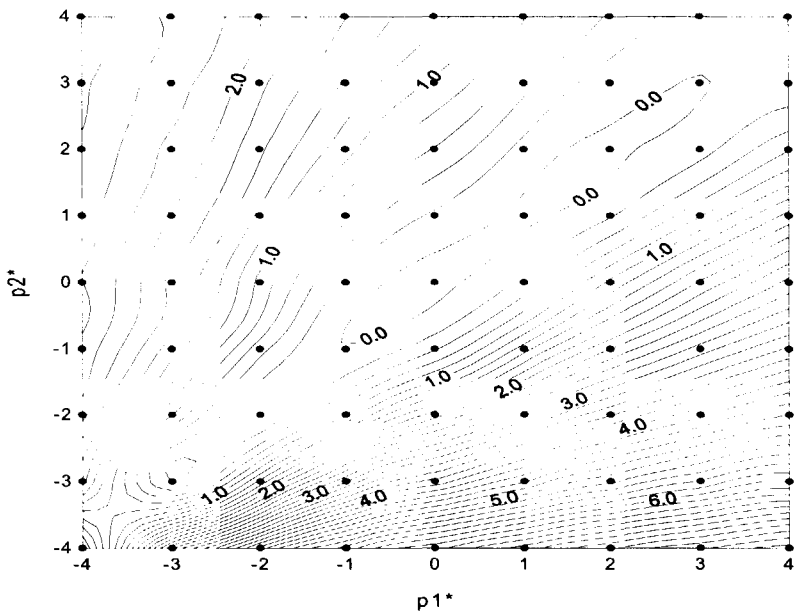

Figure 4.26 Contour plot of *MSE**-values of two fictional parameters p1 and p2, for which MSE*(p1,p2)=g_4(p1/p2)

4.5.4 Examples of resulting contour plots; 2. Unknown parameter relations.

In this section some examples will be given of the derivation of (unknown) relationships between parameters based on a contour plot which is produced in the manner as described in section 4.5.2.

Example of strong interdependence: Parameters f and h_c

A good example of a contour plot which reveals strong interdependence between two parameters is the one resulting from the bivariate sensitivity analysis of parameters f and h_c (Figure 4.27). This Figure strongly resembles Figure 4.25, so at first sight it seems that parameters f and h_c are related as follows:

$$MSE(f,h_c) = g_5(f \times h_c) \tag{4.41}$$

where $g_5(..)$ is a function of one parameter. In case this relation holds exactly, the contour lines connect pairs of parameters which generate exactly the same model output. It cannot be seen from Figure 4.27 whether or not this is the case, since two different parameter sets can generate equal MSE-values, even when the corresponding hydrographs are different. In other words: the shape of the contour lines can be misleading, as will be demonstrated later on (the bivariate sensitivity analysis of parameters h_c and ε). In this case, however, the shapes of the

resulting hydrographs provide further evidence for the existence of a strong relation between parameters f and h_c. Figures A9 and A10 (Appendix A), for example, show resulting hydrographs for two different contour lines in Figure 4.27, both connecting parameter combinations with a resulting MSE*-value of approximately 2. The results of the lower left contour line with MSE*≈2.0 in Figure 4.27 (connecting (1,-4), (-1,-1) and (-2,2)) is displayed in Figure A9, while Figure A10 shows resulting hydrographs for the upper right contour line with MSE*≈2.0 in Figure 4.27 (connecting (4,-3), (1,0), and (0,2)). The hydrographs of Figure A9 differ significantly from the hydrographs of Figure A10 (mainly in height of the peak discharge), while differences between the hydrographs within a single figure are small. So, it looks as if contour lines do connect parameter combinations which generate similar output hydrographs. Further examination of other contour lines and hydrographs (not to be shown here) confirmed the validity of this hypothesis.

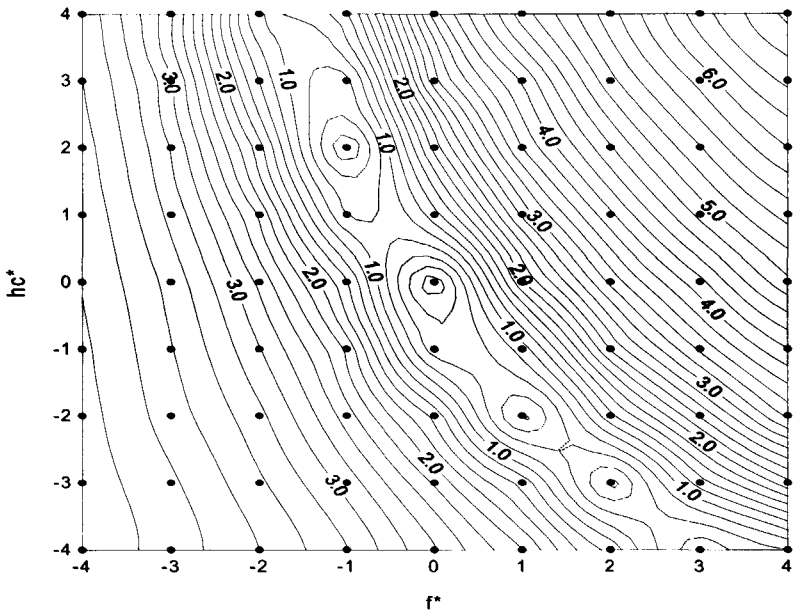

Figure 4.27 Contour plot of *MSE**-values of transformed parameter pairs (f^*, h_c^*)

Although examination of computed hydrographs is warranted, it is unlikely that contour lines in Figure 4.27 connect parameter combinations, which do not generate similar output hydrographs, because of the characteristic structure of the contour lines. It is therefore interesting to find out whether this structure can be explained from the model equations, presented in section 4.3. In section 4.4 it was demonstrated that the model is relatively sensitive to changes in the value of both parameters f and h_c. This sensitivity stems from the strong influence of these parameters on the initial soil moisture conditions, through equations (4.9), (4.12) and (4.13). If transmissivity is assumed to be uniform in the entire catchment, it

has been demonstrated (see equation (4.27)) that the soil profile at location i is saturated at the beginning of the event if:

$$\ln\left[\frac{a_i}{\tan\beta_i}\right] \geq f(z_{av} - h_c) + \lambda \tag{4.42}$$

where z_{av} is the catchment-average value of the ground water table depth, f is the exponential decline parameter of hydraulic conductivity with increasing depth, h_c is the length of the capillary fringe, λ is the catchment average value of the topographic index $\ln[a_i/tan\beta_i]$, a_i is the upslope contributing area per unit contour length and $tan\beta_i$ is the slope of the ground surface. The fraction of soils in the catchment that are saturated at the beginning of the event is equal to $G(T_\alpha)$, where G is the distribution function as described in (4.28) and T_α is the value of the topographic index $ln[a_i/tan(\beta_i)]$ for which equality holds in (4.42). From the combination of equations (4.12), (4.20) and (4.42) it follows that a soil profile is saturated at the beginning of an event if:

$$\ln\left[\frac{a_i}{\tan(\beta_i)}\right] \geq f\left(-\frac{1}{f}\ln\left[\frac{fQ(0)}{AK_0\exp(-\lambda)}\right] - h_c\right) + \lambda$$

$$\Rightarrow \ln\left[\frac{a_i}{\tan(\beta_i)}\right] \geq -\ln\left[\frac{fQ(0)}{AK_0\exp(-\lambda)}\right] - fh_c + \lambda$$

$$\Rightarrow \ln\left[\frac{a_i}{\tan(\beta_i)}\right] \geq -\ln[f] - fh_c - \ln\left[\frac{Q(0)}{AK_0\exp(-\lambda)}\right] + \lambda$$

$$\Rightarrow \ln[f] + fh_c \geq -\ln\left[\frac{a_i}{\tan(\beta_i)}\right] - \ln\left[\frac{Q(0)}{AK_0\exp(-\lambda)}\right] + \lambda \tag{4.43}$$

Equation (4.43) reflects the influence of parameters f and h_c on the percentage of saturated soils. Consequently, if f and h_c would only have been involved in deriving initial soil moisture conditions, the following relationship would hold for the model output:

$$MSE(f, h_c) = g_6(\ln[f] + fh_c) \tag{4.44}$$

where $g_6(..)$ is a function of one parameter. However, since the transmissivity of the soil layer is related to parameter f (equation (4.3)), parameter f is also a control on subsurface flow rates during the storm event. Therefore, relation (4.44) does not hold exactly. Still though, the influence of parameter f on the model output mainly depends on its role in deriving initial soil

moisture conditions, so (4.44) can be expected to give an approximate description of the true relation between f, h_c and MSE. In order to validate this hypothesis, a contour plot has been produced (Figure 4.28) for two fictional parameters f' en h_c' and corresponding fictional model results, for which the following relationship holds:

$$MSE^*(f', h_c') = g_7([f'] + f' h_c') \tag{4.45}$$

where $g_7(..)$ is a function of one parameter.

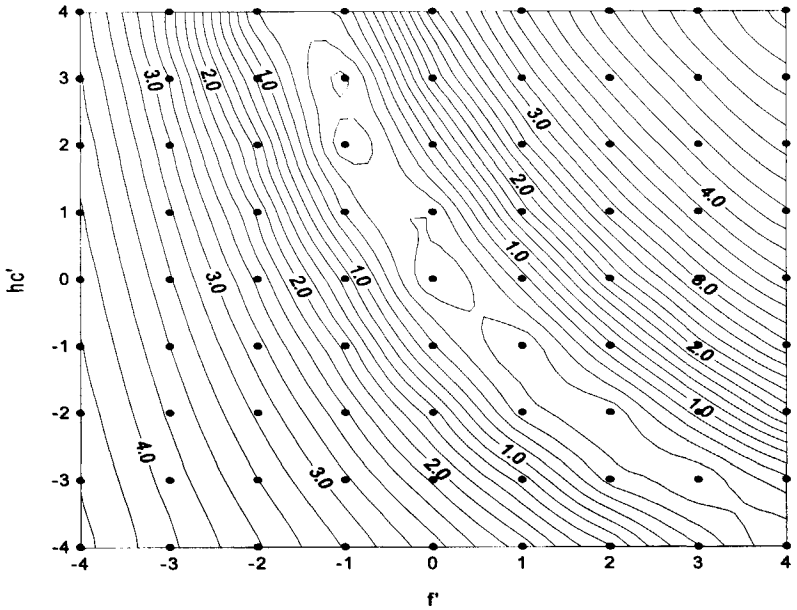

Figure 4.28 Contour plot of MSE^*-values of fictional parameters f' en h_c' for which: $MSE(f', h_c') = g_7(ln[f'] + f' h_c')$

In case (4.44) would hold exactly for the model output, Figure 4.27 en Figure 4.28 would be identical[4]. It can be seen that Figure 4.28 is a close approximation of Figure 4.27, except for small values of f and f'. This is due to the fact that in deriving relationship (4.44), the influence of parameter f on flow rates of soil water during storm events is neglected, while this influence increases with decreasing f.

Another consequence of the double role of parameter f in the model is the fact that hydrographs corresponding to co-ordinates that are connected by one contour line in Figure 4.27 are not exactly the same, even though they are alike. Small differences can be observed between the hydrographs in Figure A9 (or, indeed, Figure A10). So, it is clear that parameters

[4] In this case, "identical" means identical in shape, i.e. if two different parameter sets are connected by a contour line in one figure, then these two parameter are also connected by a contour line in the other figure. However the MSE*-values corresponding to these two contour lines can differ.

f and h_c, unlike parameters θ_s and θ_r, can not be replaced by one single parameter, without effecting the model output. However, if these parameters are replaced by parameter $d_{fh} = ln(f)+fh_c$, the resulting output will be a close approximation of the original output.

Example of weak interdependence: Parameters f en ε

Figure 4.29 shows the resulting contour plot of the bivariate sensitivity analysis of parameter pair (f, ε). The ellipse-like shaped contours indicate there is hardly any combined effect of these two parameters on the model output.

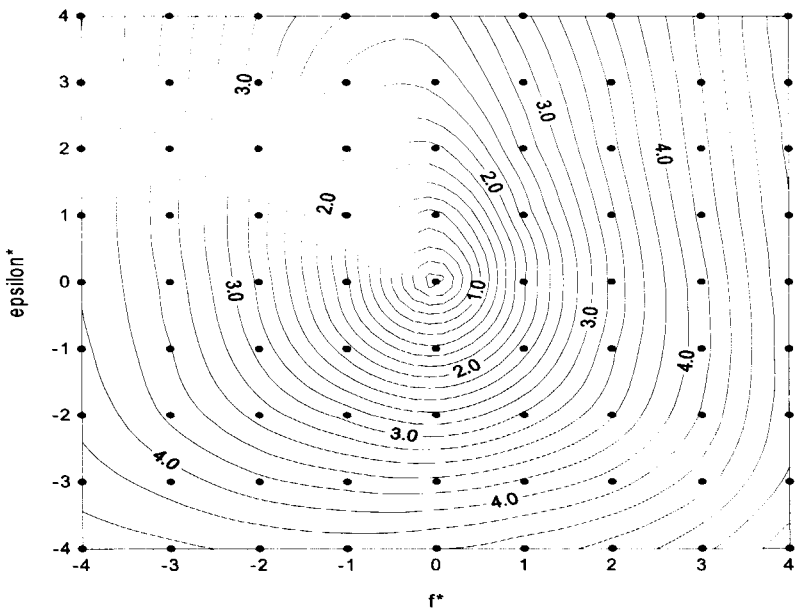

Figure 4.29 Contour plot of *MSE**-values of transformed parameter pairs (f*, ε*).

If we assume the contour lines are exactly ellipse-shaped (with the axis of the ellipse parallel to the axis of the plot) the following relation holds:

$$MSE^*(h_c^*, \varepsilon^*) = (c_1 h_c^*)^2 + (c_2 \varepsilon^*)^2 \qquad (4.46)$$

where c_1 and c_2 correspond to the lengths of the axis's of the ellipse and f and ε are transformations of the actual parameter values of f and ε according to (4.39). In case equation (4.46) holds, the effect of a change in the value of f* on the value of *MSE** is independent of the value of ε*, which means parameters f and ε would be mutually independent with respect to the resulting model output. However since equation (4.46) does not hold exactly, the mutual dependency of the two parameters appears to be weak instead of not present at all.

Additional proof of the weak interdependence of these two parameters is provided by Figure A11 (Appendix A). This figure depicts resulting hydrographs for different parameter pairs (f, ε), connected by the same contour line (MSE*≈3.0) in Figure 4.29. As opposed to the sensitivity analysis for parameter pairs (f, h_c) and (θ_s, θ_r), where strong interdependence was witnessed, no two hydrographs in Figure A11 are alike.
Therefore, parameters f and ε cannot be replaced by one parameter, without seriously effecting the model results.

Example of an unclear contour plot: Parameters N and ε

Unfortunately, not every contour plot reveals as much information as the ones, previously shown. A good example is presented in Figure 4.30, where the contour plot of parameters N and ε is shown.

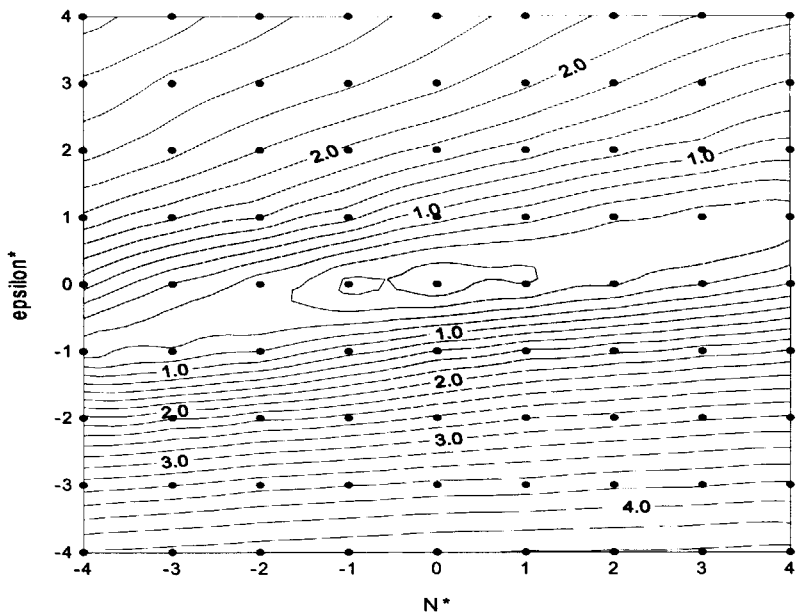

Figure 4.30 Contour plot of *MSE**-values of transformed parameter pairs (N^*, ε^*)

In the bottom half of the plot, contour lines are almost horizontal, indicating the sensitivity of the model to parameter N is negligible to the sensitivity of the model to parameter ε. Therefore, it is unclear whether the plot either contains a line structure as in Figure 4.23, or is made up of flat ellipse-shaped contours, with parts of the contours falling outside the boundary of the Figure. In case of a line structure, the plot would indicate strong interdependence between parameters N and ε, whereas ellipses indicate weak (no) interdependence.

In cases like this, the desired information needs to be obtained from examination of computed hydrographs. Figure A12 (Appendix A) depicts hydrographs of 4 different parameter combinations (N, ε) of which the corresponding dots are connected by the same contour line in Figure 4.30 (MSE*≈1.8 in the top half of the plot). Differences between the hydrographs are marginal, in spite of the fact that parameter ε (a parameter to which the model is quite sensitive, see section 4.4) is involved. So, although it cannot be seen directly from the contour plot, in this case the contour lines do connect points of similar output. This indicates there is some interdependence between parameters N and ε, which could have been expected, since they are both flow velocity parameters.

4.5.5 Results

The resulting hydrographs and MSE-values of each of the 28 possible parameter pairs have been subjected to the type of analysis as described in sections 4.5.3 and 4.5.4. Contour plots of MSE*-values have been set up and hydrographs with equal MSE*-values have been compared. As far as redundancy of parameters is concerned, only parameters θ_s and θ_r can be replaced by one parameter ($\theta_d = \theta_s - \theta_r$) without effecting the model output. However, for a substantial number of parameter pairs the bivariate sensitivity analysis revealed significant interdependence, implying that as long as parameter values vary within acceptable ranges, a close approximation of the original output can be realised through substitution of the two parameters by one single parameter. Table 4.3 contains all 28 parameter pairs and reveals whether or not relevant interdependence has been detected.

Combination		Interdependence?	Combination		Interdependence?
f	K_0	+	h_c	θ_s	+
f	h_c	+	h_c	θ_r	+
f	N	-	h_c	ε	-
f	θ_s	+	h_c	δ	-
f	θ_r	+	N	θ_s	-
f	ε	-	N	θ_r	-
f	δ	-	N	ε	+
K_0	h_c	+	N	δ	+
K_0	N	-	θ_s	θ_r	+
K_0	θ_s	+	θ_s	ε	-
K_0	θ_r	+	θ_s	δ	-
K_0	ε	-	θ_r	ε	-
K_0	δ	-	θ_r	δ	-
h_c	N	-	ε	δ	+

Table 4.3 Indication of the existence of a relevant interdependence for each of the 28 parameter pairs that have been subjected to the bivariate sensitivity analysis. A "+" means interdependence has been observed, while a "-" means there no interdependence has been observed.

Initially, for two parameter pairs ((f, N) and (θ_r, ε)) neither the contour plots nor the computed hydrographs contained sufficient information in order to conclude whether or not relevant interdependence between the parameters exists. Therefore, two extra runs of the bivariate sensitivity analysis were performed, during which the range of values of parameters f and ε were decreased, while the ranges of N and θ_r remained the same.

The results of Table 4.3 indicate that, as far as interdependence is concerned, the 8 parameters can be divided in two groups. The first group consists of parameters f, h_c, K_0, θ_s and θ_r and the second group consists of parameters N, δ and ε. Between two parameters of the same group relevant interdependence does exist, while this is not the case for two parameters, taken from the opposite groups. The reason why this strict subdivision is possible is the fact that the first group consists of parameters that are (mainly) involved in relating the initial soil moisture conditions to the observed base flow at time t=0, while the second group consists of parameters that are only involved in controlling flow velocities during storm events. The only exception are parameters f and K_0 that control both initial moisture conditions (equations (4.9), (4.12) and (4.13)) and flow velocities during storm events (equation (4.15)), but their impact on flow velocities is only marginal compared to their impact on initial moisture conditions.

The possibility of a subdivision of parameters into these two subgroups confirms that catchment-runoff modelling during storm events essentially comes down to the derivation of:

[I] The percentage of rainfall which becomes available for runoff.
[II] The time needed for the available runoff water to reach the catchment outlet.

The effects on the model output, caused by a change in the value of one parameter can be largely compensated for by a change in another parameter, as long as these two parameters are either both involved in [I] or both involved in [II]. Consequently, simultaneous calibration of two parameter that belong to the same group is a delicate matter and should be advised against if these parameters are used for purposes which require physically meaningful parameters.

4.6 Conclusions

An adapted version of TOPMODEL (Beven and Kirkby, 1979) has been set up to simulate the hydrological response of the 114 km^2 Zwalm catchment during storm events. The TOPMODEL-concept is known for its applicability on catchments such as the Zwalm (humid conditions, mild slopes, dominance of the saturation excess runoff mechanism). Still, though, some discrepancies between observed and simulated discharges could not be avoided, partly due to insufficient information on the rainfall input.

All basic model parameters (described in Table 4.1) have been subjected to a sensitivity analysis. Due to the moderate complexity of the model, results of the sensitivity analysis could easily be explained from a closer look at the model equations. However, the moderate complexity does not prevent the model to be exposed to dangers of overparameterisation. In terms of approximation of observed output, equally satisfying model simulations were realised by using a number of different parameter sets.

Four parameters were identified to which the model is most sensitive. Three of them, f, h_c and K_0, are controls on the percentage of saturated soils, while the fourth one, ε, is the dominant control on flow velocities in the river network. Three parameters were identified to which the model is almost insensitive. Two of them, n and α, could be eliminated from the model through derivation of a close approximation (equation (4.33)) of the modified Van Genuchten (equation (4.13)). A further reduction of the available number of parameters can be obtained through elimination of parameters θ_s and θ_r in equation (4.13) through transformation: $\theta_d = \theta_s - \theta_r$. This means the model only needs 8 instead of the original 11 parameters. From this, a further reduction of the number of parameter is not possible without affecting the model output.

However, a bivariate sensitivity analysis revealed significant interdependence among a number of parameters, implying that as long as parameter values vary within acceptable ranges, a close approximation of the original output can be realised through substitution of the two parameters by one single parameter. As far as interdependence is concerned, the 8 parameters that have been subjected to the bivariate sensitivity analysis can be divided in two groups. The first group consists of parameters f, h_c, K_0, θ_s and θ_r and the second group consists of parameters N, δ and ε. Between two parameters of the same group, relevant interdependence does exist, while this is not the case for two parameters, taken from the opposite groups. The reason why this strict subdivision is possible stems from the fact that the first group consists of parameters which are (mainly) involved in relating the initial soil moisture conditions to the observed base flow at t=0, while the second group consist of parameters that are only involved in controlling flow velocities during storm events. The

effects on the model output, caused by a change in the value of one parameter can be largely compensated for by a change in another parameter, as long as these two parameters are both from the same group. Consequently, simultaneous calibration of two parameters that belong to the same group is a delicate matter and should be advised against if calibration is only based on the observed runoff at the catchment outlet.

5. The rainfall runoff behaviour of a river basin

5.1 Introduction

Flood events can last from a few hours (e.g. see Gozzini et. al., 1998) up to even a number of months (e. g. see Melcher and Parrett, 1993) depending on the catchment and/or type of meteorological event under consideration. In small catchments like the Zwalm (see chapter 4) the majority of the high peak discharges are generated by relatively short duration storm events. Typically, these events show a few hours of intense rainfall, causing a steep rise of the hydrograph. Within a few hours, discharge at the catchment outlet of the Zwalm can rise from 1 m^3/s to 25 m^3/s. The actual start of such a storm event usually can be clearly identified, due to its high rainfall intensities. Still, this does not mean that meteorological inputs of the catchment prior to the storm event are of negligible influence on the magnitude of the peak discharge. In the previous chapter it was shown that the hydrological conditions at the beginning of a storm event can be a rather strong control on runoff percentages during the storm event. Therefore, in order to obtain reliable predictions of peak runoff rates, the hydrological state of the catchment at the beginning of the storm event should be known to a certain extent.

This type of information may be obtained through direct measurements of state variables such as ground water tables, soil moisture contents, discharges, etc. However, in physically based flood frequency analysis (see Figure 5.1) real-time measurements of the initial state cannot be performed, since hypothetical future meteorological events are involved. Therefore, in order to take into account the influence of the pre-event period on the magnitude of the peak discharge, the initial state condition in the catchment needs to be added as an additional stochastic input of an event (besides the precipitation amount of the event itself). An example of a flood frequency analysis which takes into account the effects of the initial conditions is presented by Sivapalan et al. [1990]. These authors introduced a stochastic component which describes the probability of exceedence of initial base flow rates. Subsequently, spatially distributed initial state conditions were related to this base flow according to the method of Sivapalan et al. [1987], which has been discussed extensively in chapter 4 of this thesis. Sivapalan et al. [1990] arbitrarily assumed that the probability of the initial base flow has a gamma distribution. Furthermore, it was assumed to be independent of both the season of occurrence and the rainfall amount of the storm event under consideration. The authors recognised that these assumptions are not expected to hold in real-world catchments.

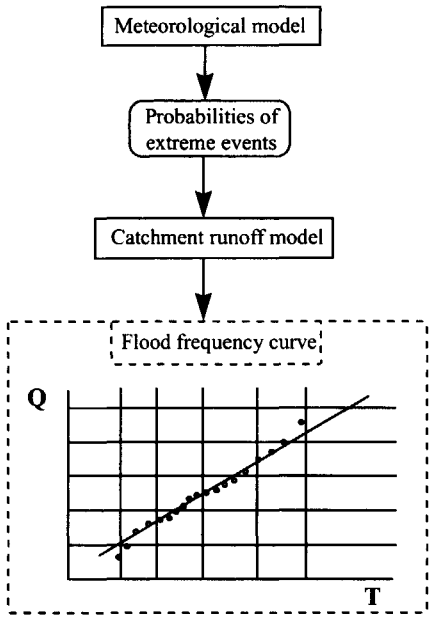

Figure 5.1 Schematic view of a procedure for deriving physically based flood frequency curves

Consequently, physically based flood frequency analysis stand to benefit from a conceptualisation of the dependence of the catchment response during an event on the hydrological and meteorological characteristics of the pre-event period. This also implies that a concept of the "memory" of the system is required, i.e. an idea of the number of days, *b*, for which the hydrological state of the catchment at day *t-b* is of negligible influence on the observed (peak) discharge at day *t*. In small, steep, rainfall dominated catchments with impervious soils the value of *b* is probably equal to 1 or 2, since during storm events most rainfall runs off on the same day. In large river basins on the other hand, the extent of the pre-event period may even go up to a couple of months. The great Mississippi summer flood of 1993, for instance, is suggested to have its origin in November 1992 (Kunkel, 1994; Melcher and Parrett, 1993), which is about seven months before the major floodings of June 1993.

In order to obtain a conceptual relation between the characteristics of flood events and pre-event periods, the catchment response behaviour to meteorological inputs has to be analysed. Naturally, the response behaviour is strongly dependent on the physical and climatological conditions of the catchment under consideration. Therefore, the purpose of this study is not to obtain some sort of universally valid answer. Instead, it serves to illustrate the applicability of the methodology that has been developed. The pilot study area in this chapter is the Mosel river basin, which is the largest tributary to the river Rhine. Statistical analyses are performed on a series of observations that have been performed in the period from 1971 to 1995. The

Mosel basin is simply treated as a black box of which only the output series (discharge) and the input series (precipitation) are considered. Through application of regression analysis and transfer function models the response behaviour of the basin is thoroughly analysed. Subsequently, the predictability of the discharge at the basin outlet is related to the amount of information used on the precipitation pattern in the preceding period.

5.2 Description of the pilot study: The Mosel basin

The Mosel river is the largest tributary of the river Rhine. The area of the basin is 28152 km^2, spread over France, Germany, Luxembourg and Belgium (Figure 5.2). The length of the river is 520 km, stretching from its source on the Col de Bussang in the French Vosges mountains to its outlet in Koblenz (Busch et al., 1996). Elevations in the basin range from 59 m. (Koblenz) to 1365 m. (Vosges mountains). Its largest tributaries are the rivers Meurthe, Sauer and Saar.

5.2.1 Data availability

Figure 5.3 shows location in the Mosel basin where rainfall measurements have been performed. The data set concerns the period of 1960-1997, but only a few series cover this whole period. Therefore, only data from the period of 1971-1995 was used in the analysis. The location of the gauge at Cochem was considered to be the basin outlet in the analysis, so the size of the basin under consideration is 27030 km^2 instead of 28152 km^2. All available series are of daily resolution.

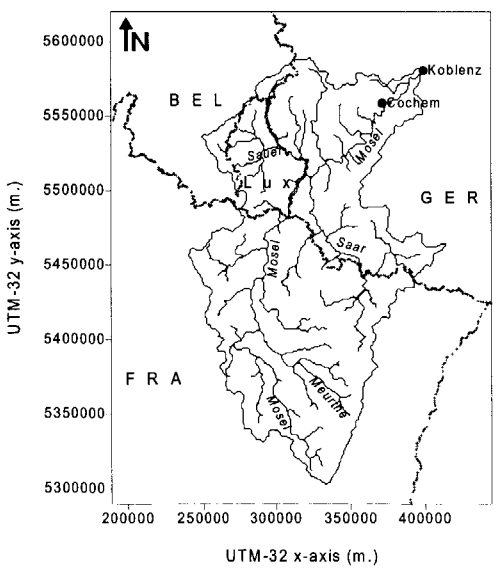

Figure 5.2 The Mosel river basin

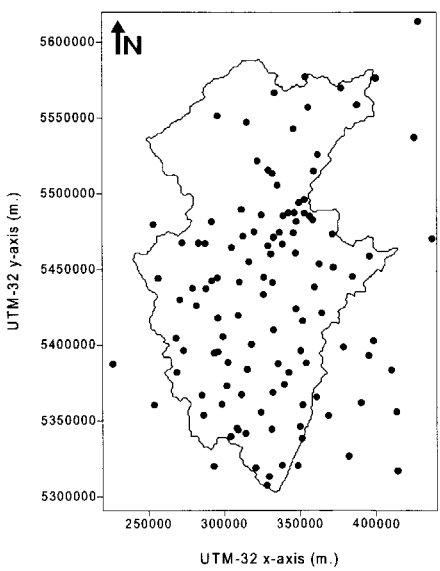

Figure 5.3 The Mosel river basin with 103 rainfall stations.

5.2.2 Derivation of the area-average precipitation

For each day in the period 1971-1995 (9130 days in total), the area-average precipitation has been derived from observed values in the 103 available rainfall stations. Because of the large amount of days and stations involved, a relatively simple geostatistical method has been applied to save computation time: The method of Thiessen polygons. This means that the precipitation in each location in the basin is assumed to be equal to the observed precipitation in the nearest rainfall station. As a consequence, the basin is divided up into a number of polygons, that form sets of locations for which one particular rainfall station is nearest by. Subsequently, the area-average precipitation, P_{av}, is derived as follows:

$$P_{av} = \sum_{i=1}^{M} w_i P_O(i) \quad ; w_i = {}^{O_i}\!/_{O_\Sigma} \tag{5.1}$$

where:

$P_O(i)$ = the observed depth of precipitation in rainfall station i, i=1..M.

O_i = the surface area of the polygon of station i, i=1..M.

O_Σ = the surface area of the entire basin.

During the period of 1971-1995 some of the rainfall stations were out of order for one or more periods of time. To take this into account in deriving the areal precipitation, factor w_i of station i is set equal to 0 for the entire period that this station is out of order, while the other w-factors are increased in such a way, that the sum of w-factors remain equal to 1:

$$w_i' = \begin{cases} 0 & ; i \in \Phi \\ \left(\dfrac{1}{1 - \sum_{j \in \Phi} w_j} \right) w_i & ; i \notin \Phi \end{cases} \tag{5.2}$$

where Φ is the set of malfunctioning rainfall stations, and w_i' is the factor that is used in equation (5.1) instead of w_i. Since the percentage of malfunctioning rainfall stations is always marginal (17% at maximum during 1971-1995) the error that is introduced in the basin-average precipitation depth through application of (5.2) is small.

5.2.3 Average yearly hydrological pattern in the Mosel basin

Figure 5.4 shows monthly average values of discharge at Cochem and area-average precipitation, based on the series of measurements of 1971-1995. A simple mass balance evaluation shows the yearly averages for precipitation, evaporation and discharge are

approximately 900 mm/y, 500 mm/y and 400 mm/y, respectively. Figure 5.4 shows monthly average discharges vary strongly throughout the year. The maximum average monthly discharge (in January), is on average five times the magnitude of the minimum average monthly discharge (August and September). Since precipitation is almost uniformly distributed over the year (see Figure 5.4) the yearly fluctuations in available solar energy are responsible for this strong variation of monthly discharges.

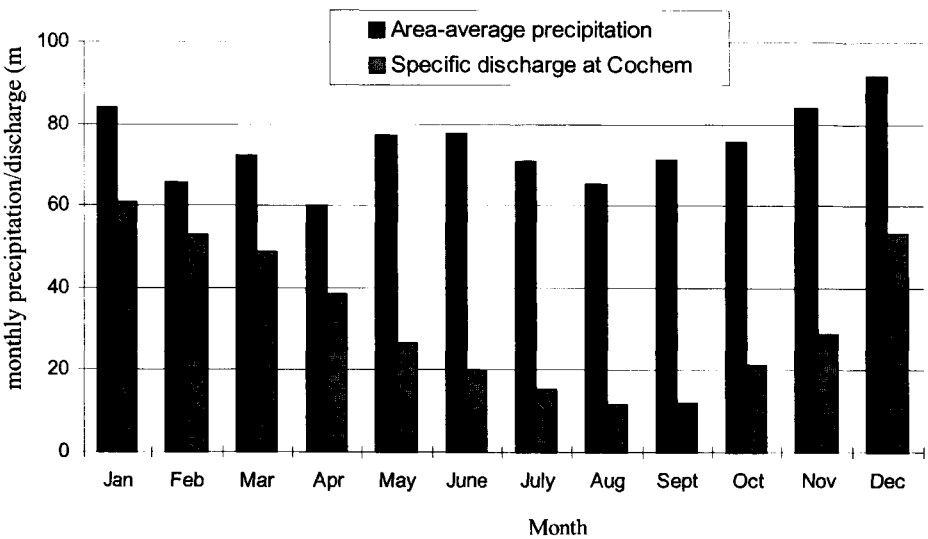

Figure 5.4 Average monthly precipitation in the Mosel basin and average monthly specific discharge in the river Mosel basin at Cochem, based on observations during the period of 1971-1995.

Precipitation in the Mosel basin occurs predominantly as rainfall. During incidental events, runoff may be delayed when precipitation occurs as snowfall, but at the monthly time scale this does not play a significant role. In snowfall-dominated catchments, runoff amounts are generally maximum around April, whereas for the Mosel, the total runoff in April is on average only 63% of the total runoff in January.

5.3 Statistical analysis of precipitation-discharge relations

5.3.1 Introduction

This section describes the statistically based derivation of precipitation-runoff relations. In particular, the analysis concentrates on the relation between the magnitude of the daily averaged discharge at Cochem and the individual precipitation amounts in the Mosel basin of the preceding days. To a large extent, the analyses of this section are similar to a unit hydrograph analysis. However, a unit hydrograph is only concerned with arrival times of a drop of *net* precipitation (i.e. precipitation which does not infiltrate into the soil), whereas in this case the *total* precipitation is considered. This choice is motivated by the fact infiltrating rainfall water can be of significant influence on near-future discharge since it fills up the available pore space in the soils so that near-future runoff percentages increase. In other words it strongly influences the "memory" of the system, which is the main subject of interest in this chapter. If only net precipitation is considered, this influence will not be revealed.

Two statistical techniques have been applied to assess the contribution of daily precipitation amounts to the resulting discharge at the basin outlet: correlation analysis and transfer function modelling. The basic theory on these techniques is described in Appendices B and C respectively. First, in section 5.3.2, the series of precipitation and discharge are both normalised in order to improve the predictions of both techniques.

5.3.2 Improvement of predictions through normalisation of the observed series

Correlation analyses serve to quantify the extent of mutual dependence between different physical quantities. In some cases, however, correlation is detected "for the wrong reasons". For instance, if we consider the series of monthly discharges and monthly area-average precipitation in the Mosel basin with a time-lag of exactly five years between the two series, a correlation coefficient is found that significant differs from zero, even though it is obvious that this month's discharge is not influenced by the precipitation that was observed five years before. The reason for the correlation that is found, is the annual periodicity in precipitation and discharge. During winter months the average daily values of both precipitation and discharge are above their yearly averages. As a consequence, there is a good chance that both discharge in December in year J and precipitation in December in year J-5 are above yearly averages, which adds to the result that R differs significantly from zero.

In this section it is shown how this seasonal variation of hydrological characteristics can also have a negative effect on the predictive value of the statistical models. Subsequently, it is

demonstrated how this effect can be filtered out through normalisation of the observed series of precipitation and discharge.

Univariate correlation between precipitation and discharge at various time scales

Based on 25 years of observations the correlation between total annual discharge at Cochem and total area-average precipitation in the Mosel basin equals 0.935 (R^2=0.874). The 25 paired observations of yearly precipitation and runoff are shown in Figure 5.5.

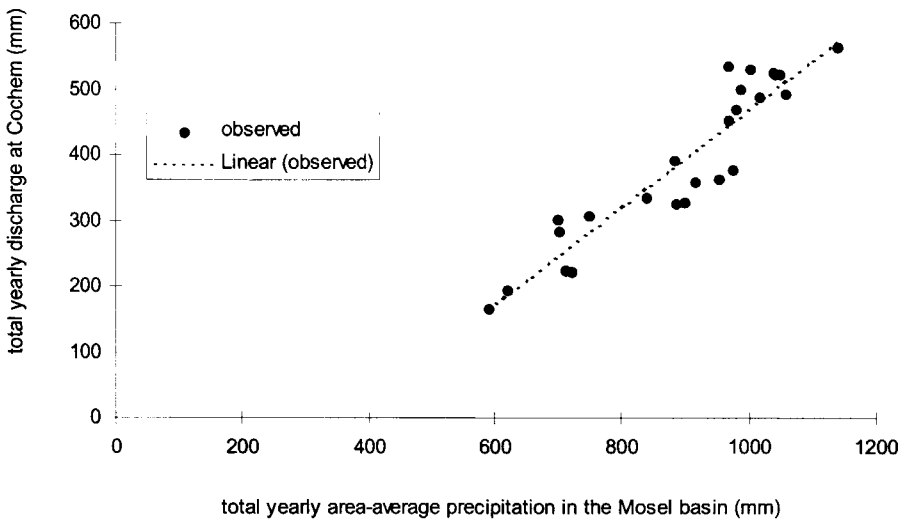

Figure 5.5 Paired observations of yearly precipitation and runoff from 1971-1995

From this Figure it can be seen that a linear fit is possible. The high value of R indicates that precipitation is the most dominant controlling factor on runoff generation. Although this seems evident, it is not always the case. Wilcox et al. [1991], for example, performed the same type of analysis for five small watersheds in Idaho. In three cases, values of $R^2 \leq 0.15$ were found. These authors observed that for these five watersheds, the correlation decreased with aridity. In perennial streams under humid conditions, correlations between annual precipitation and runoff are not expected to be that low.

If we move from the annual time scale to the monthly time scale, the correlation decreases from 0.935 to 0.603. Furthermore, if we move to the daily time scale, the correlation drops to 0.165. In general, there is a decrease in correlation with decreasing time-scale, as is shown in Figure 5.6.

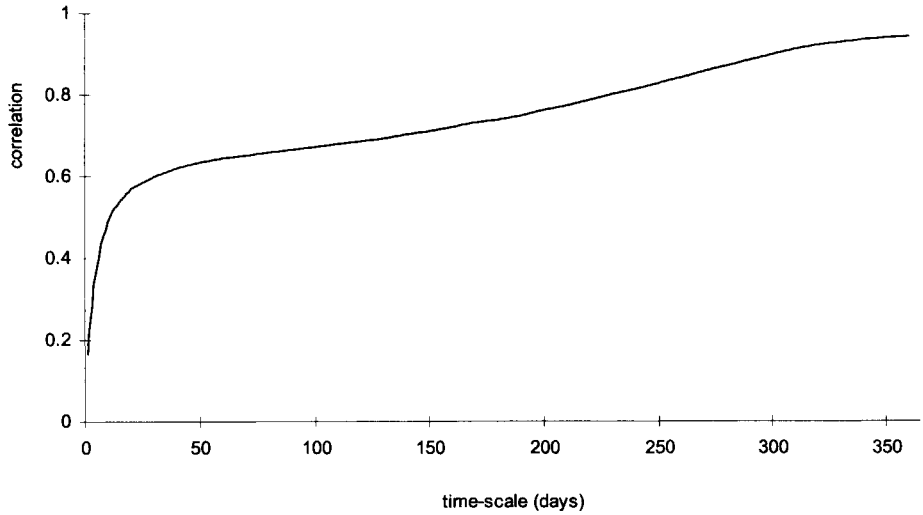

Figure 5.6 Relation between time scale T and correlation R between precipitation and discharge. Paired observations of precipitation and discharge are taken from the same period (i.e. no lag-time has been introduced); Mosel basin 1971-1995.

The increasing value of the correlation coefficient, R, with increasing time scale has three main causes:

1. *Residence times.* A percentage of the precipitation that is recorded in an arbitrary period of interest, reaches the catchment outlet after the period has ended. This causes a decrease in the derived correlation coefficient of precipitation and runoff. For instance, during a relatively dry month, base flow amounts can still be considerable if the preceding month was rather wet. Furthermore, at the end of a wet month the soils are likely to be close to saturation, which means runoff percentages at the beginning of a dry month are relatively high. When the time scale of interest increases, the percentage of precipitation that reaches the catchment outlet after the period under consideration, decreases. Consequently, its negative influence on the correlation coefficient decreases.

2. *The non-uniform, non-homogeneous hydrological response in a catchment.* If we consider a day of average precipitation in the Mosel basin, being approximately 2.5 mm/day, this precipitation can:
   - fall well-spread over the basin or be concentrated in a small part of the basin.
   - fall as rainfall or as snow.
   - fall during a short period or well-spread over the day.
   - .....

As a consequence, all kinds of hydrological responses to this 2.5 mm/day of precipitation can be expected, especially when taking into consideration that other factors such as available potential evaporation are of significant influence to the hydrological response as well. This contributes to the unpredictability of discharge based on precipitation amounts only, which means it causes a decrease in the correlation between daily precipitation and daily discharge. During a period of one year a certain mixture of the described scenarios is likely to occur. Therefore, on the annual basis, the variety of optional hydrological responses to an amount of daily precipitation is "averaged out" to a considerable extent. In general, the non-uniform and non-homogeneous catchment response behaviour is of increasing importance when the time-scale decreases.

3. *Seasonal variations of hydrological processes.* In section 5.2.3 the annual hydrological pattern in the Mosel basin has been described. It was shown that precipitation is almost uniformly distributed over the year, whereas monthly discharges vary strongly throughout the year. Runoff rates are on average significantly higher during winter months than in summer, as during winter the influence of evaporation and interception is relatively small. This structural variation in runoff percentages is in contradiction with the use of a single regression equation for different seasons. Consequently, the seasonal variations have a decreasing effect on the derived correlation, especially if the correlation is derived at the seasonal time scale. At the annual time-scale, the effects of seasonal variations on the derived correlation are strongly reduced, since the hydrological response of a catchment at the annual time-scale is an integrated response of all four seasons.

Each of the three above mentioned aspects are considered in the remainder of this chapter. The residence times (point 1. above) are the main focus of the statistical analysis of this chapter. Their influence can be estimated from [i] the coefficients of the multiple regression equation or [ii] the impulse response weights of the transfer function. The effect of the non-linear behaviour of catchment response (point 2. above) can be evaluated from the prediction errors of both the multiple regression model and the transfer function.

The misleading effect of annual patterns on derived correlation's (point 3. above) will first be dealt with. Two options are available:

(i) Dividing the year into a number of periods during which both series (discharge and precipitation) are approximately stationary (in a statistical sense).

(ii) Normalisation of both series.

Both approaches are executed in the remainder of the chapter. First, option (ii) is considered.

Normalisation of the observed series

For each day in the year, the average and standard deviation of both daily discharge and daily precipitation have been derived from the observed series of the period of 1971-1995. Since

this period consists of "only" 25 years, the derived series are suffering from serious small scale fluctuations. This can be seen, for instance, in Figure 5.7, where mean daily average discharge values are shown for the river Mosel at Cochem.

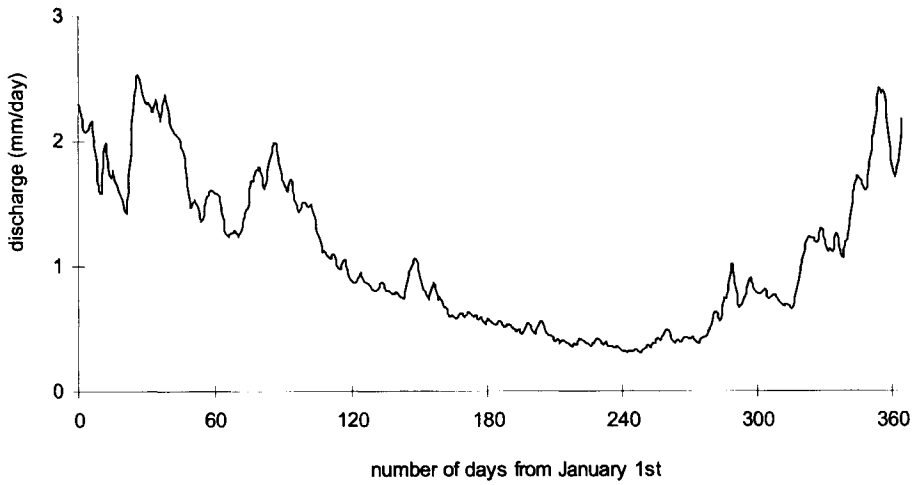

Figure 5.7 Mean daily discharge for the Mosel at Cochem during the period of 1971-1995

The fluctuations of Figure 5.7 are filtered out through a smoothing procedure, which uses Fourier sums. The original series of daily average discharges, μ_i, i=1..365, are transformed into a series of smoothed discharges μ^*_i, i=1..365, through:

$$\mu_i^* = \frac{1}{2} A_0 + \sum_{k=1}^{K} \left\{ A_k \cos\left(\frac{2\pi k}{P} i\right) + B_k \sin\left(\frac{2\pi k}{P} i\right) \right\} \tag{5.3}$$

where P equals the number of days in a year, and A_k and B_k are equal to:

$$A_k = \frac{2}{P} \sum_{i=1}^{P} \mu_i \cos\left(\frac{2\pi k}{P} i\right) \quad ; B_k = \frac{2}{P} \sum_{i=1}^{P} \mu_i \sin\left(\frac{2\pi k}{P} i\right) \tag{5.4}$$

Equation (5.3) states that a sum of $2K$ periodical functions is fitted through the discharge series D_i. Since D_i already contains an obvious periodical structure, the value of K does not have to be very large to obtain a satisfying fit. Figure 5.8 shows the fit of the series of average daily discharge for a value of K=2.

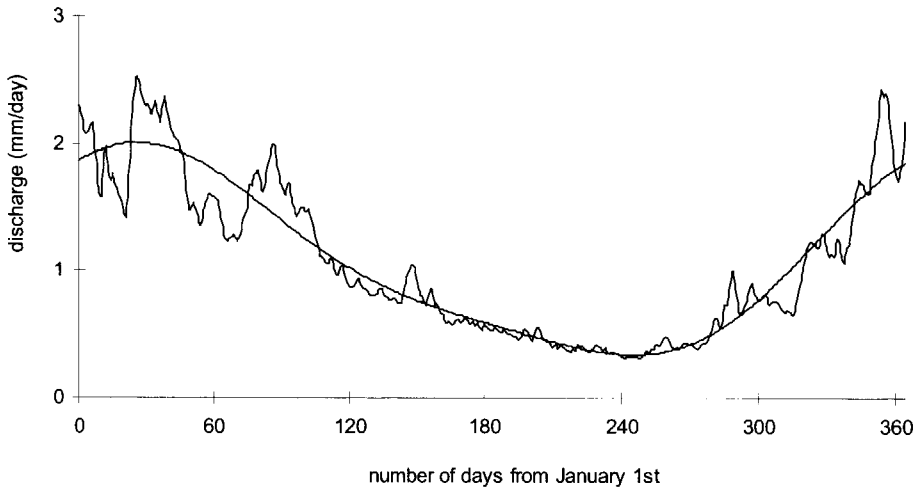

Figure 5.8 Smoothing of the mean daily discharge for the Mosel at Cochem through Fourier sums.

This smoothing procedure has been applied to the derived standard deviation of daily discharge as well. Subsequently the normalisation is performed. Define:

$D_{j,i}$ = Discharge on day i of year j; j=1971..1995; i=1, 2,.., 365
μ_i^* = Average discharge of day i; i=1, 2,..., 365
σ_i^* = Standard deviation of discharge on day i; i=1, 2,.., 365

Then, for each day the normalised discharge, $D_{j,i}^n$ is derived from the observed discharge, $D_{j,i}$, as follows:

$$D_{j,i}^n = \frac{D_{j,i} - \mu_i^*}{\sigma_i^*} \tag{5.5}$$

This procedure has also been applied to the series of daily precipitation's. The resulting series are labelled "normalised", since for each day in the year the expected value and the standard deviation are equal to 0 and 1 respectively.

Changes in derived correlation's after normalisation

The correlation between the normalised series of precipitation and discharge has been derived at a number of time-scales, varying from one day to a whole year[5]. Results are shown in Figure 5.9, in combination with derived results of the original series.

5 So, the two series have been normalised on the daily time scale and subsequently the derived normalised values have been accumulated for a variety of time scales. If the sequence of these two procedures would have

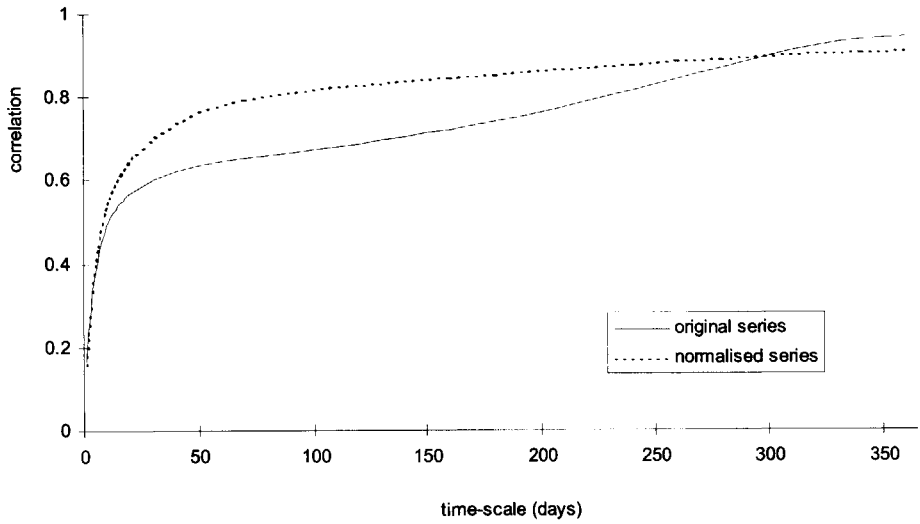

Figure 5.9 Relation between time scale T and correlation R of the original series of precipitation and discharge and the normalised series of precipitation and discharge. Paired observations of precipitation and discharge are taken from the same period (i.e. no lag-time has been introduced).

Differences between the results for the normalised series on one hand and the original series on the other hand are discussed for a number of time scales:

- *Daily time-scale*: At the daily time scale, the difference between the resulting correlation for the normalised series and the original series is very small. The decreasing effect of seasonal variations in the hydrological pattern on the correlation is not noticeable at this small time scale, since the correlation is already relatively low due to the influence of both the residence times of precipitation and the non-linear characteristics of catchment response.

- *From daily to seasonal scale*: In this range of time scales, the difference between resulting correlations for the normalised series and the original series increases with increasing time-scale. The difference is largest at 95 days, which is approximately equal to the number of days in one season. This means that the effect of seasonal variations in the hydrological pattern on the correlation coefficient is most noticeable at the seasonal scale.

- *From seasonal to yearly time scale*: As stated before, the seasonal variations do not effect the derived correlation at the yearly time scale since the hydrological response of a

been the other way around (i.e. accumulation for a number of time scales and subsequently normalisation for each of the investigated times scales) results wouls be somewhat different.

catchment at this time-scale is an integrated response of all seasons. Therefore, as the time scale increases from seasonal to yearly time scale the difference between resulting correlation for the normalised series and the original series decreases.

- *Yearly time scale*: At the yearly time scale, the derived correlation for the original series is even higher than for the normalised series. This is due to the slight loss of information, caused by the normalisation process. The total normalised precipitation for one year still provides information about whether the actual precipitation was below or above average, but the exact amount of precipitation cannot be derived from it.

At time scales of interest in the remainder of this chapter (i.e. up to approximately 40 days) prediction results are significantly improved after normalisation. Therefore, from now on only the normalised series are used, unless mentioned otherwise.

5.3.3 Multiple regression analysis

In this section the following multiple regression equation is considered:

$$D_t = \lambda_{-1} + \lambda_0 P_t + \lambda_1 P_{t-1} + .. + \lambda_c P_{t-c} = \lambda_{-1} + \sum_{i=0}^{c} \lambda_i P_{t-i} \tag{5.6}$$

where:

D_t = (normalised) daily discharge on day t.
P_t = (normalised) daily precipitation on day t.
$\lambda_{-1}..\lambda_c$ = regression coefficients.

Equation (5.6) is a linear description of the relation between the discharge on day t and the precipitation of c+1 preceding days. The choice of the value of c depends on the "memory" of the catchment under consideration. For small, steep, rainfall dominated catchments with impervious soils, for instance, the value of c can be taken small (0 or 1) to obtain satisfying predictions since most rainfall runs off on the same day. For the Mosel river, a somewhat larger value of c is recommended, since the travel time for a drop of net precipitation to reach the outlet can easily exceed one day. The choice of the value of c may be based on the results of Figure 5.10.

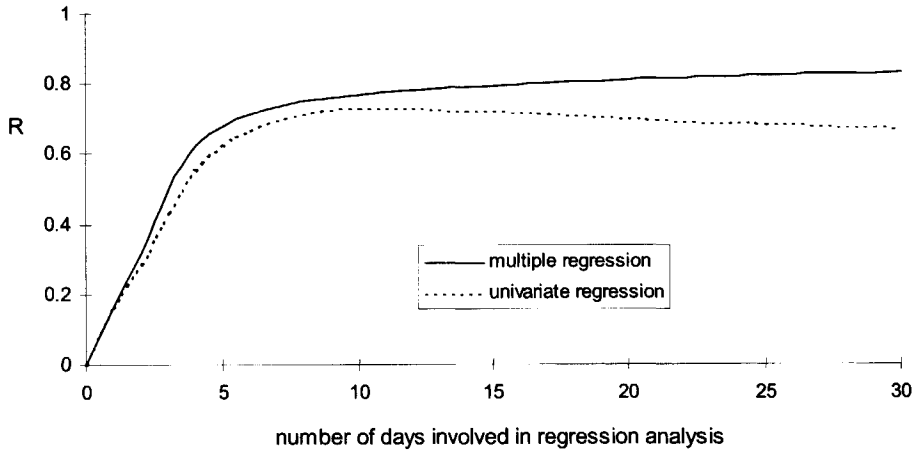

Figure 5.10 Correlation coefficient R as a function of the number of days involved in the regression analysis. In the multiple regression equation this number is equal to the number of independent variables (c+1) used in regression equation (5.6). In the univariate analysis the independent variable is equal to the accumulated precipitation of the period under consideration.

The full line in Figure 5.10 shows the correlation coefficient R as a function of the number of independent variables in equation (5.6). By definition this is a non-decreasing function since the addition of an extra independent variable can never lead to a worse linear fit. With respect to discharge predictions it is possible to assess the benefit of using an additional independent variables in equation (5.6) through analysis of the gradient of the increasing function R(c). As a result, three different intervals can be distinguished:

1. Steep gradient, if $0 \leq c < 5$.
2. Moderate gradient, if $5 \leq c < 10$.
3. Near-zero gradient, if $c \geq 10$.

So, if the regression equation is used for prediction purposes, each value of $c \geq 10$ will lead to almost equally satisfying prediction results.

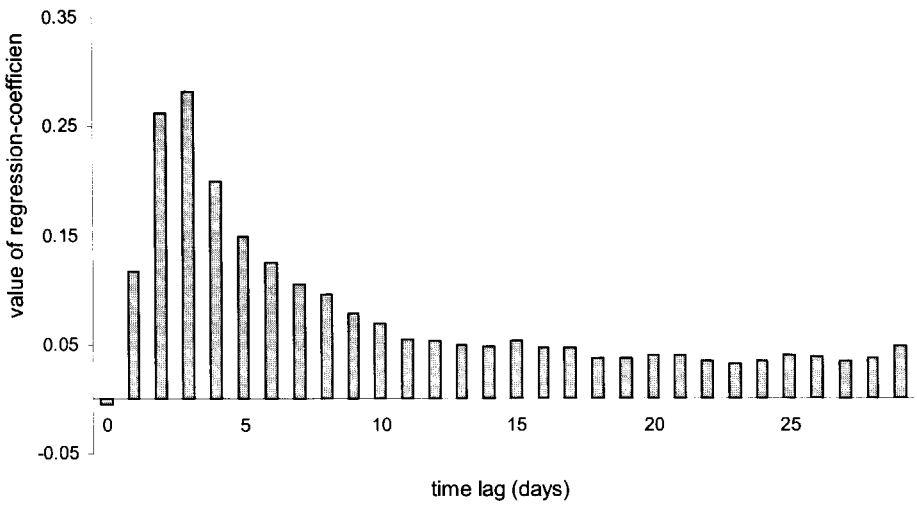

Figure 5.11 Regression coefficients ($\lambda_0,..,\lambda_c$ in equation (5.6)) if c is taken to be 29.

Figure 5.11 shows the coefficients ($\lambda_0,..,\lambda_c$ in equation (5.6)) of the multiple regression equation if 30 independent variables are used (i.e. c=29 in equation (5.6)). The value of λ_0 turns out to be approximately equal to zero, which means the travel distances in the Mosel basin are too large to notice a significant influence of today's rainfall on today's discharge at the basin outlet. The highest values of λ_i are found for i=2 and i=3, which shows the time to peak for the Mosel basin is somewhere between two and three days. For values of $i \geq 10$, λ_i stays more or less constant. This indicates that almost all direct runoff reaches the basin outlet within 10 days. For time lags of more then 10 days, precipitation only influences the discharge in two ways: Either directly through base flow contributions or indirectly through filling up of the soil which increases runoff percentages of subsequent precipitation.

Figure 5.12 depicts individual F-values (see Appendix B) corresponding to the 30 independent variables. These F-values are quantifications of the significance of the individual contribution of an independent variable to the goodness of fit of the regression equation. In other words, it quantifies to which extent the errors of the predictions increase if the individual variable of interest is left out of the regression equation. Again, this figure shows highest contributions of P_i for i=2 and i=3, while F-values are small for i≥10.

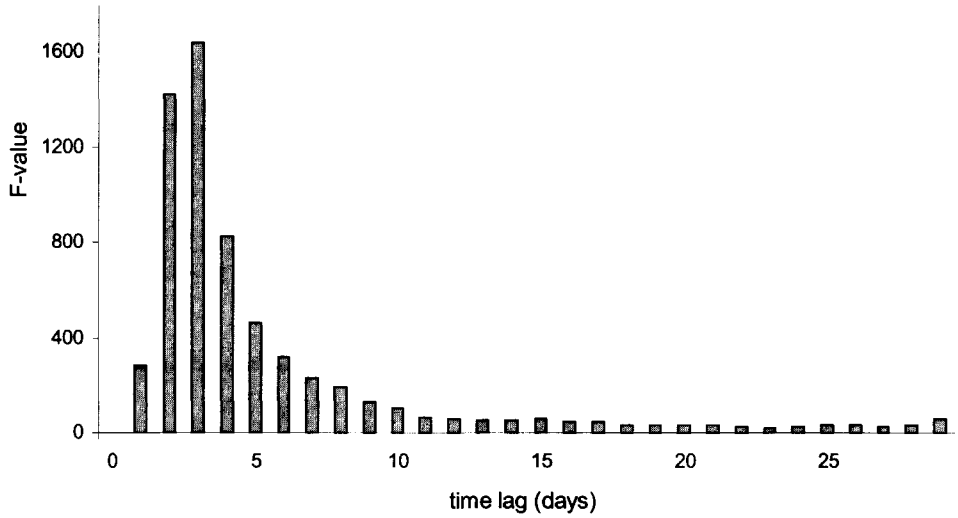

Figure 5.12 Individual F-values for the 30 independent variables

Influence of temporal resolution of precipitation on discharge predictions

The difference between the full line and the dotted line in Figure 5.10 shows that for values of $c<10$, a reasonable approximation of the initial prediction results can be obtained by using the accumulated precipitation of the period under consideration as the single independent variable instead of taking each individual daily precipitation value as one independent value. This means that, in terms of discharge predictions, the knowledge of the temporal distribution of precipitation over the last 10 days in the Mosel basin adds only little information if the accumulated precipitation is known. For values of $c \geq 10$, however, the information on the temporal distribution becomes increasingly important. For instance, if a period of 30 days is considered, it makes a big difference to the resulting discharge whether the majority of the precipitation fell during the first few days or during the last few days. So, for a period of 30 days, information is required on the temporal distribution of precipitation, but not necessarily at the daily time scale. This can be demonstrated by comparing discharge predictions that are based on precipitation series with different temporal resolutions. In order to do so, a period of 30 days is divided into n equally large periods for a number of values of n. Each time, only the accumulated precipitation of these n periods is used. Results are presented in Figure 5.13, where R is shown as a function of the temporal resolution of $30/n$ days.

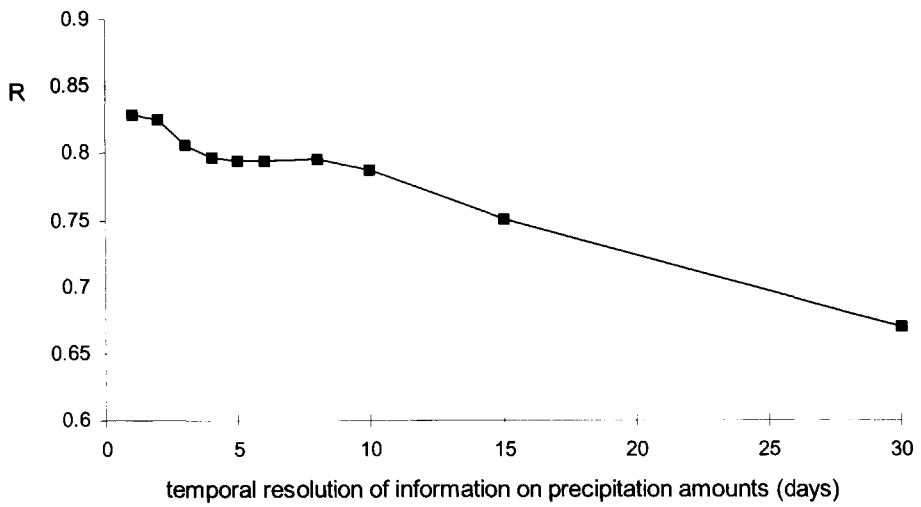

Figure 5.13 Resulting correlation coefficients of discharge predictions as a function of the available temporal resolution of precipitation amounts, on which the predictions have been based.

If the temporal resolution changes from 2 days to 4 days, there is a clear decrease in the value of R. However, between 4 and 8 days the resulting value of R stays more or less constant. As a result, the absolute difference in resulting R-values between a temporal resolution of 1 day and a temporal resolution of 8 days is only small (0.83 and 0.80 respectively). This is relevant information with respect to the required temporal resolution of a rainfall generator, if one is to be set up for the Mosel basin in order to predict probabilities of future flood events. Although prediction errors increase slightly when resolutions of 4-8 days are used instead of a resolution of 1 day, this may be acceptable if this temporal resolution is more adaptable to the temporal resolution of the rainfall generator.

5.3.4 Transfer-function-modelling

As far as the physical interpretation of Figure 5.11 is concerned, there are some misleading elements in the applied method of multiple regression analysis. A regression coefficient λ_i of equation (5.6) is considered as the contribution of the precipitation on day *t-i* to the discharge on day *t*. Although this is true in a purely statistical sense, it is not exactly true in a physical sense, i.e. "contribution" does not literally mean contribution in absolute or even relative quantities of water. This is first of all due to the fact that, as already pointed out in section 5.3.1, the magnitude of the derived contributions partly stems from an indirect influence of today's precipitation on near future discharges through changes in the soil moisture content. This is no problem here, since (again, see section 5.3.1) it is one of the purposes of this chapter to include this effect in the derived statistics.

The other misleading effect is caused by the existing persistence in precipitation amounts, which is not taken into account in regression analysis. The precipitation series contains some significant autocorrelation which influences the values of the derived regression coefficients. This effect can be filtered out through "prewhitening" by using the Box-Jenkins transfer function description (see Appendix C) of the relation between precipitation, D_t, and discharge, P_t:

$$D_t = N_t + v_0 P_t + v_1 P_{t-1} + \ldots = N_t + \sum_{i=0}^{\infty} v_i P_{t-i} \tag{5.7}$$

Coefficients v_0, v_1,.. are referred to as *impulse response weights* since they form the ordinates of the resulting hydrograph if the input series consists of just one unit depth of precipitation. Series N_t is the noise of the model, i.e. the prediction error of the transfer function in one-step-ahead forecasting. In order to go from an infinite number of coefficients to a more practical form with a finite number of coefficients, the transfer function is usually represented as:

$$D_t = \delta_1 D_{t-1} + \delta_2 D_{t-2} + \ldots + \delta_r D_{t-r} + \omega_0 P_{t-b} - \omega_1 P_{t-b-1} - \ldots - \omega_s P_{t-b-s} + N_t \tag{5.8}$$

where δ_1, δ_2,..,δ_r, ω_1, ω_2,.., ω_s are model parameters and b is the "reaction time" of the system. For transfer functions, the noise process N_t is not by definition a white noise model, i.e. the autocorrelation of the noise in these type of systems is mostly observed to be non-zero for values of $k \geq 1$. Therefore, N_t is described by an ARMA-model:

$$N_t = \phi_1' N_{t-1} + \phi_2' N_{t-2} + \ldots + \phi_{p'}' N_{t-p'} + a_t - \theta_1' a_{t-1} - \theta_2' a_{t-2} - \ldots - \theta_{q'}' a_{t-q'} \tag{5.9}$$

where $\phi_1', \phi_2', \ldots, \phi_{p'}', \theta_1', \theta_2', \ldots, \theta_{q'}'$ are model parameters and a_t is a white noise process Furthermore, the precipitation series is also described by an ARMA-model.

$$P_t = \phi_1 P_{t-1} + \phi_2 P_{t-2} + \ldots + \phi_p P_{t-p} + \alpha_t - \theta_1 \alpha_{t-1} - \theta_2 \alpha_{t-2} - \ldots - \theta_q \alpha_{t-q} \tag{5.10}$$

where $\phi_1, \phi_2, \ldots, \phi_p, \theta_1, \theta_2, \ldots, \theta_q$ are model parameters and α_t is a white noise process

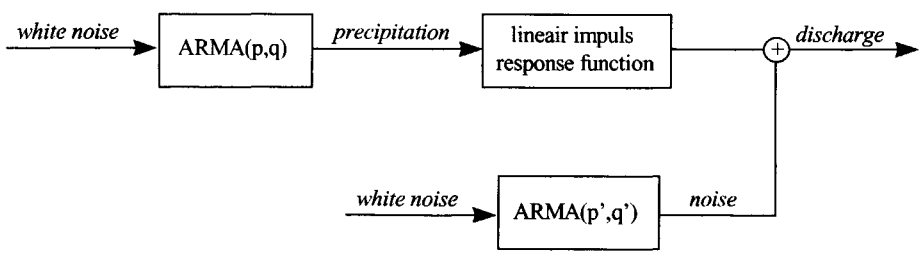

Figure 5.14 Schematical representation of the transfer function

Figure 5.14 shows that discharge D_t is now represented as the output of a linear stochastic system which receives its input from two white noise processes. A first step in the prewhitening procedure is to identify the ARMA(p,q)-model, which means the values of p and q are derived. This is done through observation of both the autocorrelation function and the partial autocorrelation of the observed series of precipitation. Both functions are displayed in Figure 5.15.

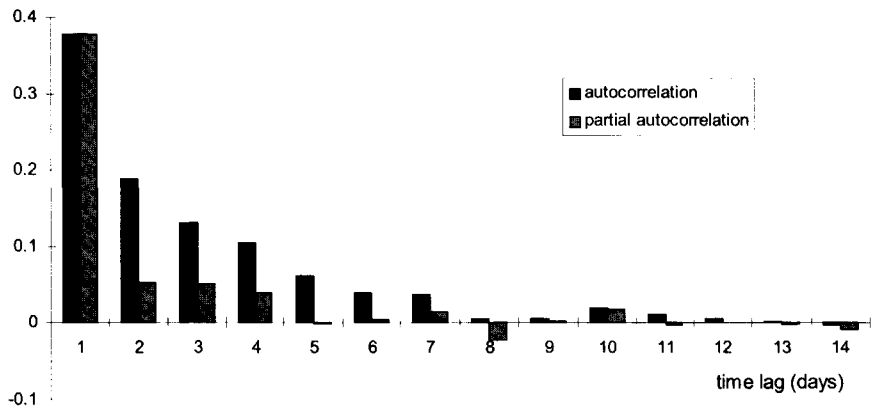

Figure 5.15 Autocorrelation function and partial autocorrelation function of precipitation in the Mosel basin, based on normalised series of the period of 1971-1995.

The *autocorrelation function* decays more or less exponentially to zero, which indicates the precipitation can be described by an AR(p)-model. The value of p should be chosen such, that the coefficients of the *partial autocorrelation* are approximately equal to zero for all time lags>p. Due to the term "approximately equal to zero" the choice of the value of p is not fully objective. In this case, p can be chosen equal to either 1 or 4 (see Figure 5.15). Both options have been tested and it turned out that the choice of 4 parameters leads to an improvement in estimation errors of less than 1% compared to the model with just 1 parameter. Since this gain is only marginal, p was chosen to be equal to 1 in order to limit the dangers of overparameterisation. The resulting AR(p) description of the precipitation series is:

$$P_t = 0.38 P_{t-1} + \alpha_t \tag{5.11}$$

Subsequently, the actual prewhitening procedure can be carried out, which means a linear filter (the inverse of the AR(p)-model of equation (5.11)) is applied to the observed series of precipitation. This operation transforms the precipitation series into a white noise series. Then, the same transformation is applied to the series of discharge, D_t and noise, N_t, since otherwise equation (5.7) would no longer be valid. Since the transformed series of precipitation is now a white noise series, the impulse response weights can be derived directly from the cross covariance of the transformed series of precipitation and discharge (see Appendix C).

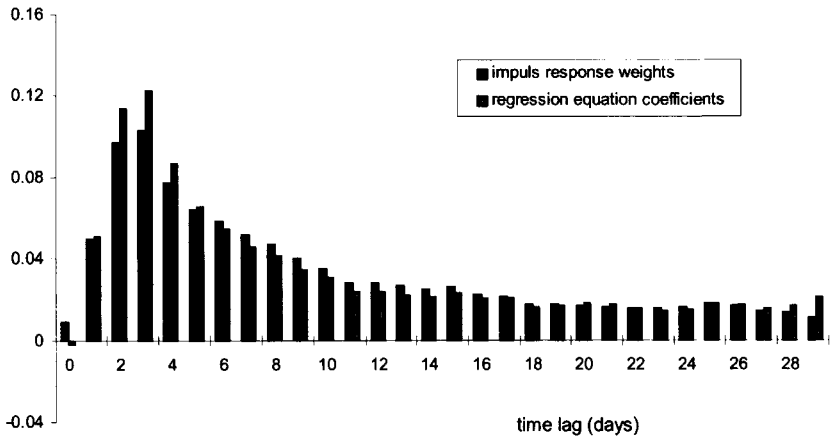

Figure 5.16 Normalised values of impulse response weights and regression equation coefficients for the normalised series of precipitation and discharge in the Mosel basin of 1971-1995.

Figure 5.16 displays the first 30 impulse response weights, $v_0,...v_{29}$, in combination with the regression coefficients of Figure 5.11. Both series of values have been normalised, which means the sums of values of both the impulse response weights and the regression coefficients are equal to 1. Consequently, the values in Figure 5.16 reflect relative contributions instead of absolute contributions. This is done in order to make a fair comparison between the two resulting patterns. In general, differences between the results are only minor. The largest differences are found at time lags 2-4, where the regression coefficients turn out to be somewhat higher than the impulse response weights. This is because contributions are highest for these time lags and this signal is amplified in regression analysis because the precipitation amounts of these three time lags are interrelated. The impulse response weights are freed from this effect as a result of the prewhitening procedure. Therefore, the pattern of the impulse response weights can be considered a more physically realistic representation of the basin response to a unit depth of precipitation. In terms of prediction results, however, the regression coefficients should be preferred, since they generate on average slightly better results (R=0.83) than the impulse response weights (R=0.81)[6]. For time-lags>10 both the impulse response weights and the regression coefficients stay more or less constant, which again shows that almost all direct runoff reaches the basin outlet within 10 days.

6 A major improvement of these prediction results can be obtained through application of the finite transfer function representation of equation (5.8). For instance, if r=1 and s=3, the correlation coefficients of the computed predictions is equal to 0.96 which is significantly closer to 1 than the score of the multiple regression equation (R=0.83). However, this method makes use of observed discharges of previous days for one-day-ahead predictions. Since this chapter is concerned with discharge-predictions based on precipitation amounts only, this application is of no use here.

5.4 Statistical analysis of subsets of the series of precipitation and runoff

So far, only the observed series as a whole have been analysed. The derived statistical quantities (impulse response weights and regression coefficients) represent some sort of "average" response behaviour of the Mosel basin. However, the hydrological response of river basins is known to contain significant temporal variation. The basin response during wet periods, for instance, differs from the response during dry periods, just as the average response during winter months differs from the average response during summer months. In this section these differences are quantified.

5.4.1 Seasonal differences in basin response

In section 0 the seasonal variations in the hydrological response of the Mosel basin have been discussed. In particular the discharge series showed strong quantitative differences between the seasons. In section 5.3.2 some of these differences were filtered out of the observed precipitation and discharge series through a normalisation procedure. As a consequence, expected values and standard deviations were constant throughout the year. Nevertheless, there are still some telling differences between the four seasons, as can be seen from Figure 5.17. For each season, Figure 5.17 shows the correlation coefficient R as a function of the number of independent variables (c+1) in regression equation (5.6).

As can be expected, the extremes of hydrological response behaviour are witnessed during winter and summer, while during spring and fall some sort of intermediate response behaviour occurs. Two clear differences between summer and winter can be detected from Figure 5.17:

1. The correlation between precipitation and discharge is significantly higher during winter months than during summer months. This means the hydrological response of the basin during summer months is less predictable than during winter months. This is mainly caused by the larger variation in soil moisture conditions during summer months. During winter months most soils in the Mosel basin are close to saturation, whereas during summer months both wet and dry conditions occur regularly.
2. For the winter months, the value of the correlation-coefficient is almost constant if more than 10 independent variables are considered whereas for the summer months this value is still visibly increasing up to 30 variables (see Figure 5.17). Only after about 40 variables the correlation for the summer months stays near constant. This implies that the contribution to the discharge in the Mosel of precipitation of more than 10 days ago is negligible during winter months, whereas it plays a significant role during summer

months. Since soil conditions during winter months are generally wet, the percentage of precipitation which runs off directly is relatively high. Consequently, the average flow velocities increase and average residence times decrease. So, compared to the summer months, the percentage of discharge that stems from slow runoff components (base flow) are small during winter months. Accordingly, the relative contribution of time lags ≥ 10 to the regression equation are smaller for winter months than for summer months.

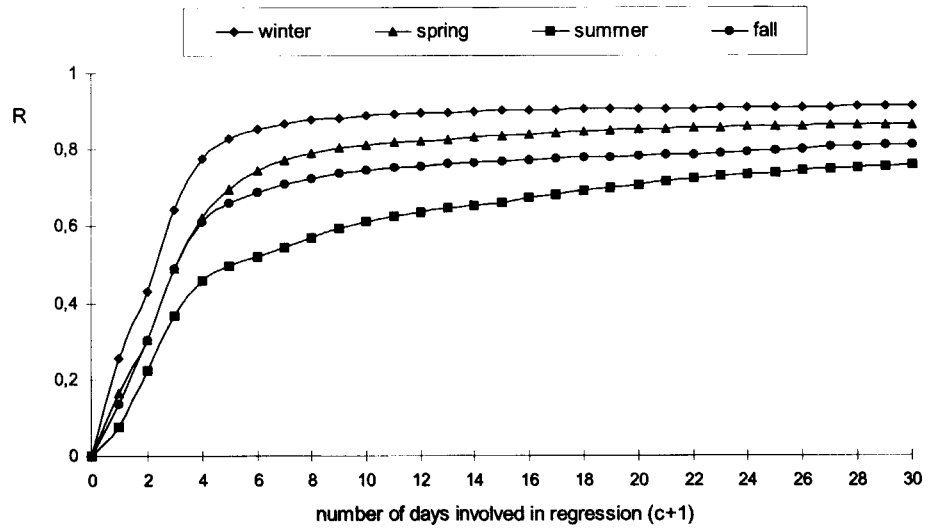

Figure 5.17 Correlation coefficient R as a function of the number of independent variables (daily precipitation amounts) involved in regression equation (5.6) for each of the four seasons. Values of R have been derived from the normalised series of precipitation and discharge in the Mosel basin of 1971-1995.

Figure 5.18 shows impulse response weights of the observed series for both summer and winter. The original series (with both precipitation and discharge expressed in mm/day) have been used instead of the normalised series to show the absolute weights instead of just the pattern of the weights. Differences between summer and winter are negligible for time lags≥15, indicating that base flow contributions at these time scales are constant throughout the year. On the other hand, for time lags<15 differences are substantial. Based on the weights of Figure 5.17, 75% of the winter-precipitation reaches the basin outlet within these 15 days, whereas in summer months only 22% of the precipitation reaches the basin outlet within 15 days. The difference between these two percentages can be mainly put down to differences in evaporation rates.

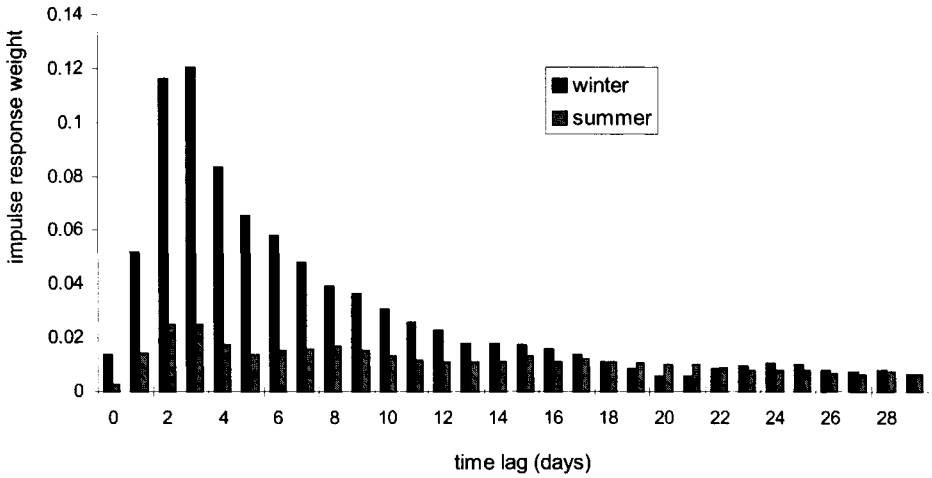

Figure 5.18 Impulse response weights for winter months (Dec.-Feb.) and summer months (Jan.-Aug.) of the observed series of precipitation and discharge in the Mosel basin of 1971-1995

5.4.2 Basin response during high water events.

Based on the results of section 5.4.1, it appears that the relevant information on precipitation amounts consists of daily precipitation values of approximately 10 days for winter events up to 40 days for summer events. However, in deriving these results all types of events were considered, while the hydrological response of the basin during high water events is likely to differ from the derived "average" response. During high water events the quick runoff components are dominant, which means contributions of the impulse response weights and regression coefficients will be increasingly concentrated on the first few time lags.
A practical problem that arises in quantifying these contributions, however, is the lack of data concerning high water events. Standard errors of derived regression coefficients and impulse response weights increase if the number of data on which they are based decreases. One of the consequences is that no ARMA(p,q)-model could be identified to describe the precipitation pattern of the 21 periods during 1971-1995 that were identified as high water events. This makes it impossible to carry out the prewhitening procedure and to derive the impulse response weights. Therefore, no regression and transfer function analysis have been performed for the 21 events. Instead, a more straightforward analysis of the average precipitation pattern of the 21 high water events has been carried out.

Definition of high water events

High water events are defined as periods during which a peak discharge is observed at Cochem, that:

1. Exceeds a threshold of 2000 m^3/s.
2. Is higher than all discharges in a 31-day period which starts at 15 days before its occurrence and ends at 15 days after its occurrence (independence criterion).

During the period of 1971-1995, 21 of these peak discharges have been observed (Table 5.1). During each of the 20 intermediate periods, the discharge has been observed to drop below 500 m^3/s before the next peak occurred. This means it is reasonable to state that the peaks are mutually independent. Figure 5.20 shows that the majority of the high water events occurred during winter months, whereas no peak of over 2000 m^3/s has been observed in the summer.

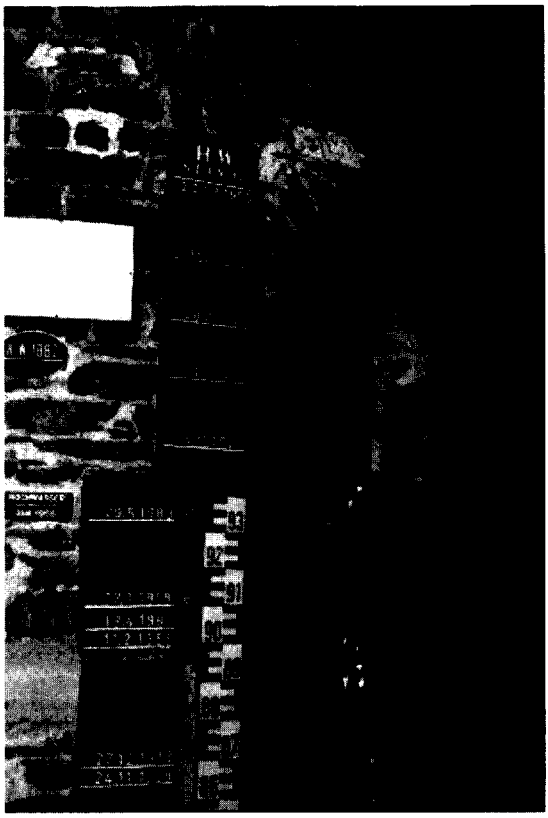

Figure 5.19 Gauge at Cochem with marked maximum water levels of flood events. Photo, courtesy of Linda Groenewegen.

Date	Discharge
22-Feb.-77	2600 m^3/s
27-Feb.-78	2040 m^3/s
02-Jan.-79	2380 m^3/s
14-Feb.-79	2180 m^3/s
07-Feb.-80	2770 m^3/s
18-Oct.-81	2248 m^3/s
01-Jan.-82	2959 m^3/s
01-Feb.-82	2102 m^3/s
21-Dec.-82	2531 m^3/s
13-Apr.-83	3154 m^3/s
29-May.-83	3415 m^3/s
09-Feb.-84	2628 m^3/s
25-Nov.-84	2200 m^3/s
02-Apr.-86	2030 m^3/s
03-Jan.-87	2060 m^3/s
28-Mar.-88	2290 m^3/s
17-Feb.-90	2590 m^3/s
05-Jan.-91	2310 m^3/s
13-Jan.-93	2680 m^3/s
22-Dec.-93	4020 m^3/s
27-Jan.-95	3410 m^3/s

Table 5.1 Peak discharges>2000 m^3/s in the river Mosel at Cochem in the period 1971-1995.

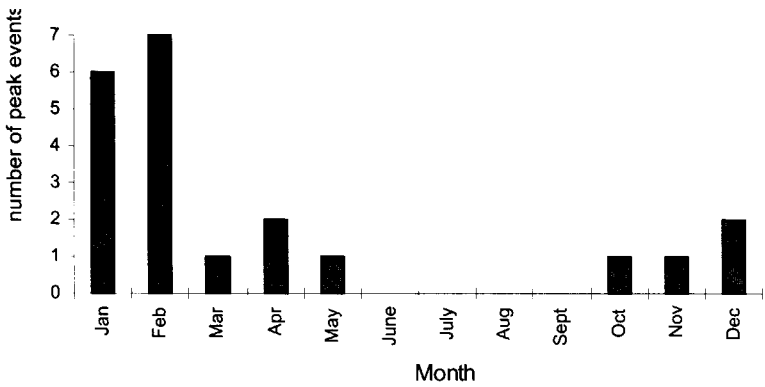

Figure 5.20 Number of observed high water events for each month in the period of 1971-1995

Average precipitation pattern of high water events

The following function has been derived for the 21 peak discharges:

$$\mu_p(a) = \frac{1}{N}\sum_{j=1}^{N} P^n(a,j) \tag{5.12}$$

where N is the total number of peak discharges (21) and P^n(a,j) is the normalised area-average precipitation at a days before peak discharge j; j=1..N. Function μ_P(a), which is depicted in Figure 5.21, represents the average pattern of the normalised precipitation before the occurrence of a peak discharge.

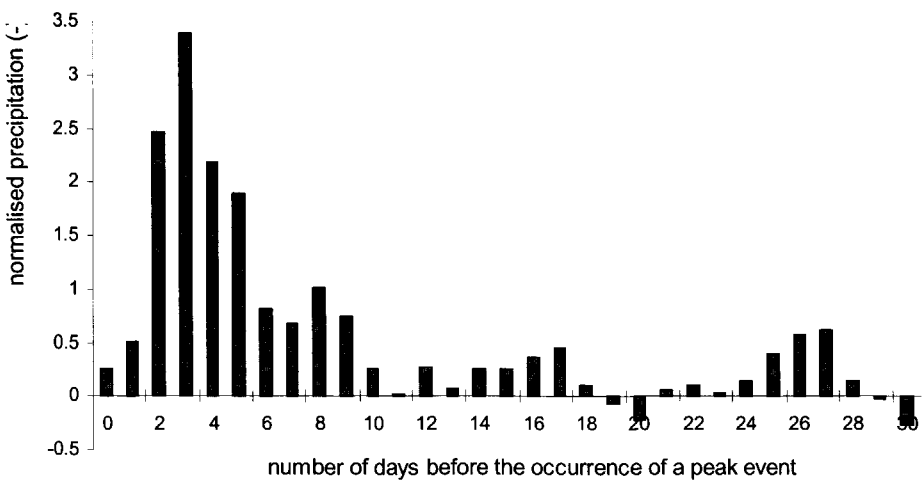

Figure 5.21 Average normalised precipitation in the days before the 21 peak discharges of Table 5.1

The long term daily average value of normalised precipitation is, of course, equal to 0. So Figure 5.21 reveals that "on average" a peak discharge occurs after:

1. A period of approximately 10 days of precipitation that significantly exceeds the long term average daily precipitation.
2. A period of 4 days with of extreme precipitation. This period start at 5 days before the peak discharge and ends at 2 days before the peak discharge.
3. A period of 20 days before the period, mentioned under 1, during which the accumulated precipitation is only slightly above average.

From Figure 5.21 it appears that the build up to a peak discharge does not take longer than 10 days, with maybe some exception to peak discharges that are partly generated by snow melt. This period of 10 days is in line with the length of the period that was considered relevant for the winter season (section 5.4.1). This is probably because the majority of the high water events (15 out of 21) occur during the winter season (Dec.-Feb.). If only high water events of late spring, summer and early fall were considered, the derived length of the relevant period may turn out to be longer than 10 days. Unfortunately, however, during the period of 1971-1995 just one peak event occurred in that time of the year (May 1983), so no confirmation on this hypothesis can be given here.

5.5 Conclusions and discussion

Statistical analyses have been performed to derive relations between the area-average precipitation in the Mosel basin and the resulting discharge in the river Mosel at Cochem. The derived contributions of observed daily precipitation amounts to observed discharges resemble to a large extent the ordinates of a unit hydrograph. The main difference is the fact that a unit hydrograph represents the distribution function of arrival times of the *net* precipitation, whereas in this chapter the *total* precipitation is considered. So, instead of just deriving arrival times, also the influence of infiltrating rainfall water on runoff percentages of near-future precipitation events were considered.

Two statistical techniques have been applied to derive the individual contributions of daily precipitation amounts for different time lags: Correlation analysis and transfer function modelling. It turned out that differences between the resulting contributions of the two methods are only small. The results of both methods showed that contributions are maximum at time lags 2 and 3 days, and that almost all direct runoff reaches the basin outlet within 10 days. The main differences between the two methods are found at time lags of 2-4 days, where the regression coefficients are somewhat higher than the impulse response weights. These contributions are amplified in regression analysis as a result of the existing autocorrelation in precipitation. The impulse response weights of the transfer function are freed from this effect as a result of a prewhitening procedure. Therefore, the pattern of the impulse response weights can be considered a more physically realistic representation of the basin response to a unit depth of precipitation than the regression coefficients. In terms of prediction results, however, the regression coefficients should be preferred, since they generate on average slightly better results (R=0.83) than the impulse response weights (R=0.81).

Correlation analysis also showed the relation between the available information on precipitation depths and the quality of resulting discharge predictions. Two different aspects of information were analysed: The length of the period from which precipitation amounts are known and the available temporal resolution of these values. In both cases it is obvious that if more information on precipitation amounts is available, this will lead to better prediction results. With respect to the length of the period this means that if discharge predictions are based on individual precipitation amounts of c preceding days, then an increase of c will automatically lead to an increase in the correlation coefficient. It is possible to assess the benefit of using c+1 instead of c independent variables through analysis of the gradient of the increasing function R(c). As a result, three different intervals could be distinguished: For values of c between 0 and 5 the gradient of R(c) is steep, for values of c between 5 and 10 the gradient is moderate, while it is close to zero for values of c larger than 10. So, predictions on

the discharge in the river Mosel at Cochem should be mainly based on the observed precipitation of the 5 most recent days, whereas information on precipitation of time lags from 5 to 10 is also still valuable. The use of information on precipitation of more than 10 days ago hardly improve the quality of the predictions. The effect of the temporal resolution of the available information on precipitation has been analysed for a period of 30 days. It turned out that the absolute difference in resulting values of the correlation coefficient between a temporal resolution of 1 day and a temporal resolution of 8 days is only small (0.83 and 0.80 respectively). This is relevant information with respect to the required temporal resolution of a rainfall generator, if one is to be set up for the Mosel basin in order to predict probabilities of future flood events.

Finally, the regression analysis and transfer function models were applied to specific subsets of the period of 1971-1995. During summer months, errors of discharge predictions are significantly larger than during winter months. In general, there is more variation in soil moisture conditions during summer months, which means the hydrological response of the basin shows more variation as well. This complicates predictions of runoff percentages, which is reflected in the relatively low correlation coefficients for summer months. Another clear difference between summer months and winter months is that the relative contribution of time lags $\geq$ 10 days to the discharge in the Mosel at Cochem are still substantial during summer months, whereas for winter months these contributions are negligible. This clearly shows that during winter months, quick runoff components are more dominant than during summer months. If only high water events are concerned, it appears that the build up to a peak discharge does not take longer than 10 days, with maybe some exception to peak discharges that are partly generated by snow melt. Unfortunately, the period of 1971-1995 showed too few of these events to base this conclusion on results with a satisfying statistical significance. For this particular aspect it is recommended to perform an additional analysis for a longer series of measurements.

6. Effects of spatial heterogeneity on the runoff response of a small catchment

6.1 Introduction

In the past three decades increasingly complex mathematical models have been developed to give a detailed representation of the relevant hydrological processes occurring in natural systems. Since spatial and temporal heterogeneity present in natural systems is enormous, there are virtually no limits to the amount of information which can be used to describe characteristics of the system which is modelled. However, due to measurement and modelling errors it is not true that input of more information on system characteristics automatically leads to a better model output. Taking also into account that collecting hydrological data is an expensive and time consuming process, it is obvious that the question of "How to model heterogeneity?" is a relevant one.

Naturally, the answer to this question is strongly related to the purpose for which a hydrological model is built. This chapter concentrates on models built for storm-runoff simulation at the catchment scale. A procedure is developed to analyse the relation between model performance and the scale of the model elements. Application of this procedure provides insight into the scales at which effects of spatial heterogeneity really matter and the scales at which these effects can be neglected. It is anticipated that this type of research, by applying it to a wide range of catchments, will generate useful guidelines on the choice of element size and averaging methods of catchment scale rainfall-runoff models. In this chapter results for the 114 km^2 Zwalm catchment in East-Flanders, Belgium, are presented.

6.2 Literature review

6.2.1 Influence of spatial heterogeneity on the catchment response

Physical characteristics of catchments such as soil depth (Saulnier et al., 1997; Seyfried and Wilcox, 1995) topography (Cerda, 1998; Seyfried and Wilcox, 1995), vegetation cover (Avissar, 1998; Flerchinger et al., 1998; Silberstein and Sivapalan, 1995; Shanholtz et al., 1981) and landuse (Hasmi and Garcia, 1998; Li et al., 1977; Mölders and Raabe, 1996; Shuttleworth, 1988) have been subject of research efforts on heterogeneity effects. By far the most intensively studied catchment characteristics in this type of analysis is the hydraulic

conductivity of the soil layer. Numerous investigations on the effects of spatial heterogeneity of the hydraulic conductivity on various processes, such as surface runoff, infiltration, soil-plant-atmosphere interactions and flow in the soil layer have been reported (e.g. Binley et al. ,1989; Bresler and Dagan, 1983a,b; Dagan and Bresler, 1983; Sharma and Luxmoore, 1979; Sharma et al, 1987; Smith and Hebbert, 1979; Wu et al., 1982; Yeh et al. 1985a,b,c). In these studies heterogeneity effects are often reported to depend strongly on the assumed correlation-length of soil conductivity.

The majority of the above mentioned investigations concentrate on effects at small scales (plot scale, hillslope scale) and do not consider effects at the catchment scale. With respect to heterogeneity effects on runoff generation at the catchment scale, the spatial variability of rainfall intensities have been considered of more interest than catchment characteristics. Extensive research has been performed on this particular issue, mainly motivated by advances in remote sensing techniques, geographical information systems and distributed hydrological modelling. In spite of these research efforts, there appears to be still no clear concept available on the amount of spatial information that is required to generate satisfying model predictions. In some cases, the results of the various studies even seem to contradict each other.

According to Dawdy and Bergman [1969] and Troutman [1983] a lack of information on spatial heterogeneity of rainfall intensities leads to substantial errors in simulation results of hydrological models. Similar conclusions were drawn by Obled et al. [1994], but they emphasised on making a distinction between heterogeneity effects as the cause of modelling errors on one hand and errors in estimating rainfall volumes on the other hand. These authors performed rainfall-runoff simulations for the 71 km^2 Réal Collobrier catchment (South of France) in which 21 raingauges are available. The efficiency of different densities of the network was tested and it was concluded that the use of the full network of 21 rain gauges gave significantly better prediction results than the use of a subset of 5 rainfall stations. On the other hand, if lumped instead of distributed rainfall inputs were used in the model, the results showed no significant differences as long as the catchment average rainfall intensity was preserved. So, a better description of the spatial variability of rainfall patterns does not lead to improved model predictions, even though spatial heterogeneity in this 71 km^2 catchment can be so large that a network of 5 well-distributed raingauges is not sufficient to provide an adequate estimate of the total rainfall input. Therefore, Obled et al. [1994] concluded that "*...the spatial variability of rainfall must be taken into account more because it improves the estimation of the basin-average incoming volume rather than because of some dynamic interactions with flow-generating processes*". Similar conclusions were drawn by Corradini and Singh [1985] and Pessoa et al. [1993] from a number of research projects in different catchments.

However, the findings of the above mentioned authors are contradicted by the results of several other investigations, where it was found that spatial aggregation of rainfall inputs in catchment runoff models can introduce significant modelling errors (Beven and Hornberger, 1982; Finnerty et al.1997; Kouwen and Garland, 1989; Milly and Eagleson, 1988; Ogden and Julien, 1994; Shah et al. [1996]). The contradictions most likely stem from differences in:

[1] The size of the catchments under consideration.
[2] The time scale of interest.
[3] Hydrological characteristics of the catchments.
[4] Meteorological characteristics of the events.
[5] The applied modelling concepts.

Especially the size of the catchment under consideration is often mentioned as a controlling factor on both the nature of the present heterogeneity and its effect on the catchment response. Generally, it is suspected that heterogeneity effects are of more importance in larger catchments (e.g. Krajewski et al. 1991; Milly and Eagleson, 1988; Obled et al., 1994). Hamlin [1983], on the other hand, suggests the exact opposite, stating that "*...for many large catchments the general averaging which takes place balances out any significant variations both in the catchment processes themselves and in the rainfall inputs*".

6.2.2 Techniques for modelling spatial heterogeneity

Models that take into account the spatial heterogeneity of parameters and processes are labelled "distributed models". These type of models have been developed for applications where (a) spatial information on the model output is required (b) the impact of local human interventions need to be assessed or (c) it is anticipated that the spatial variation in hydrological responses results in an integrated response that cannot be reproduced by a fully lumped model. Within the group of distributed models, distinction is made between "semi-distributed models" and "fully distributed models". Semi-distributed models use distribution functions to represent the available spatial variability, while fully distributed models divide the system into a number of elements, each with its own specific characteristics. Well-known semi-distributed modelling concepts are the "Hydrological Response Units", (Leavesly et al., 1983) and the topographic index of TOPMODEL (Beven et al. 1979). Examples of fully distributed models are: SHE (Abbott et al., 1986b), IHDM (Beven et al, 1987), THALES (Grayson et al., 1992a.) and BBSIM (Garote and Bras, 1995).
Although both modelling concepts provide information on the variability of hydrological responses in the system, they are fundamentally different due to the fact that semi-distributed model don't relate the derived responses to locations in the modelled system. The main advantage of using semi-distributed modelling concepts is the relatively low computation time that is required in comparison with fully distributed models. In the research procedure

that is described in this chapter, however, the spatial variability of catchment characteristics needs to be identified, so only fully distributed are considered here.
Various types of model elements have been used to describe spatial variability, such as grids (e.g. SHE, Abbot et al., 1986), Triangular Irregular Networks (e.g. Palacios-Veléz et al., 1998) and flowpath elements (e.g. Grayson et al, 1992a). Generally, the size of the elements are taken to be relatively small compared to the size of the full system, to make sure that [a] model equations that are derived at the laboratory scale are still valid at the catchment scale and [b] sufficient detail of the available spatial variation of the hydrological system is captured in the model. Still, even very detailed models are known to suffer from heterogeneity at scales smaller than the model element scale. This small-scale heterogeneity is often witnessed to effect the hydrological response of the element in ways that cannot properly be reproduced by the model (see the discussion of chapter 3). On the other hand, it has been noted that the nature of heterogeneity is scale-dependent, which leads to the question whether there is a scale at which the effects of small-scale heterogeneity is negligible ("averaged out") and runoff processes can be described by using continuum representations.

In the hope to find such a scale, Wood et al. [1988] introduced the concept of the Representative Elementary Area (REA), which is analogous to the well-known Representative Elementary Volume Concept (REV), used for modelling flow in porous media (Bear, 1972). They defined the REA as "*the critical area at which implicit continuum assumptions can be used without knowledge of patterns of parameter values*". The REA-concept (and analogous the REV-concept) is based on the concept of heterogeneity and spatial correlation as presented in Figure 6.1. Figure 6.1 shows a hypothetical relation between the averaged value of a hydrological entity (e.g. infiltration capacity, soil saturation, specific discharge) and the scale (i.e. volume, area) at which it is averaged. The average infiltration capacity related to the size of the area will be used as an example to clarify this concept. At small scales (<L) the average infiltration capacity as a function of subcatchment size fluctuates heavily due to a number of small-scale heterogeneities. In a forest, for instance, the infiltration capacity of the soil directly underneath a tree may be significantly higher than the infiltration capacity of the surrounding soil due to micro-channel formation by the root system of the tree. If an area of 0.1 m^2 is considered which is situated underneath a tree, the average infiltration capacity is rather high. When the area under consideration increases in size it will also contain soils lying in-between trees which decreases the average infiltration capacity. Further increasing of the subcatchment under consideration may increase the average infiltration capacity again when neighbouring trees are contained in this subcatchment, etc. This small scale fluctuation will be damped at some threshold scale (approximately around L in Figure 6.1) due to averaging effects. When the size of the area of interest increases further, the averaged infiltration capacity remains rather constant up to a point (approximately around U in Figure 6.1) where large scale heterogeneities (e.g. a change in forest characteristics) come into play.

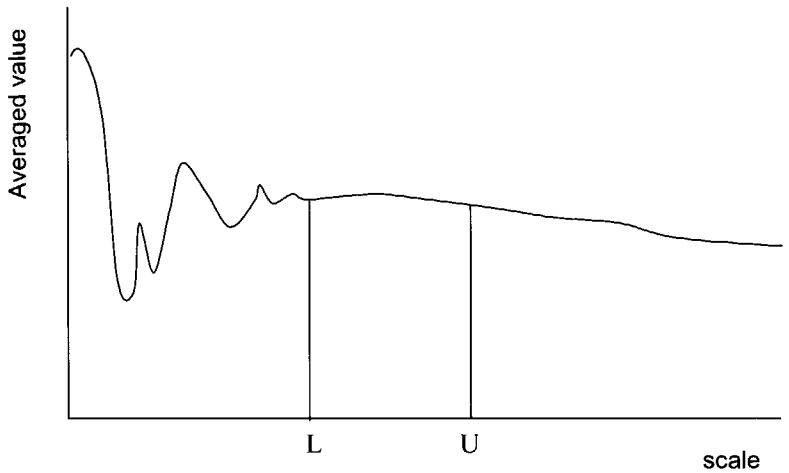

Figure 6.1 Conceptualisation of the relation between the averaged value of a hydrological entity as a function of the scale on which it is averaged (modified after Hassanisadeh and Gray [1979]).

The idea of Wood et al [1988] was to analyse the average specific runoff as a function of subcatchment size, to find the values L and U as in Figure 6.1 and to choose the size of the REA somewhere in between these two values. In this way, the REA-based models would be able to fulfil the need of modelling the effect of large scale heterogeneities and to avoid the impossible deterministic representation of micro-scale heterogeneity.

By analysing specific runoff values of a large number of subcatchments of an experimental catchment in North Carolina, U.S., Wood et al. [1988] found the REA to be approximately 1 km.^{2}, as the specific discharge showed no differences for subcatchments larger than 1 km.^{2}, for a number of experiments. In subsequent studies on this subject, however, (e.g. Blöschl et al., 1995; Woods et al., 1995) other values for the REA were found, which made it clear that the size of the REA, if it exists at all, is catchment-specific. Two reasons for the REA to be catchment-specific are:

1. Hydrological parameters and processes have their own specific nature of heterogeneity. Since the relative influence of parameters and processes on runoff varies between catchments, it can be expected that the size of the REA also varies between catchments.
2. The nature of heterogeneity is dependent on the scale of the catchment under consideration. Seyfried and Wilcox [1995] provided field evidence that different concepts of modelling spatial heterogeneity are required at different scales for the majority of

hydrological processes and parameters. Three different concepts were recognised by these authors: [a] homogeneous representation [b] stochastic representation and [c] deterministic representation. Based on field observations in five different subwatersheds of the Reynolds Creek watershed they came to a definition of the *deterministic length scale*, i.e. the scale (or range of scales) at which the process or parameter of interest has to be modelled in a deterministic manner. At smaller scales the entity can be considered homogeneous, whereas at larger scales a stochastic description suffices.

Furthermore it can be expected that the nature of heterogeneity within one catchment depends on the type of output that is required. Inter-storm runoff, for instance, is dominated by other processes than the runoff of a storm event. Also the length of the time-period that is modelled influences the size of the REA, since periods of considerable length have some averaging effect on the spatial heterogeneity of some hydrological processes. For instance, in small flat catchments, annual precipitation shows no spatial heterogeneity of any significance, whereas convective storm events may generate serious spatial differences in rainfall intensities.

6.2.3 Outline

The sometimes contradicting results reported in literature on effects of spatial heterogeneity and differences in proposed techniques to represent them in hydrological models illustrate there still remains some research to be done on this subject. Relevant questions that remain to be answered are:

I Can physically-based hydrological modelling be improved by adapting the model element size to the nature of heterogeneity of hydrological processes and catchment characteristics that control runoff generation?
II Which kind of heterogeneity should be modelled and which can be neglected?
III If different runoff processes need to be modelled by using elements of different scales, which methods should be used to model the interactions between these processes?
IV To which extent does the nature of heterogeneity vary within one catchment due to the variation of the meteorological inputs?
V Which type of model equations are valid at the defined grid scales?
VI Is it possible to use continuum assumptions within one model element grid or should a stochastic representation be applied?

Each time a distributed model is set up one is confronted with the above stated questions. The lack of proper guidelines increases the danger of choices being made on a purely arbitrary basis. The aim of this research is to contribute to the answering of questions I and II above. A procedure is developed to analyse the relation between model performance and the scale of the model elements. First, this method is applied to a pilot study catchment and subsequently

a sensitivity analysis is performed to find out under what conditions the obtained results are extendible to other catchments.

6.3 Description of the pilot study: The Zwalm catchment

The catchment under consideration is the 114 km^2 Zwalm catchment in East-Flanders, Belgium. The physical and hydrological characteristics of this catchment have been described in chapter 4 where a sensitivity analysis was applied to a catchment-runoff model of the Zwalm. This catchment runoff model (a modified and distributed version of TOPMODEL, Beven and Kirkby, 1979) is also used in the analysis of this chapter. It contains 13 basic parameters of which only 2 parameters (topographic parameters α and β) are represented in a spatially distributed manner.

6.4 Methodology

A procedure has been developed to analyse the relation between model performance and the scale of the model elements. This procedure is similar to the one used in the introductory paper of the representative elementary area (REA) of Wood et al. [1988]. The two main differences are that first, the emphasis is not on the REA-scale, but on an element scale that provides an optimal model output and secondly, that each of the dominant factors (i.e. processes and parameters) are treated separately in order to assess their individual influence on the catchment runoff. This deviation of the approach of Wood et al [1988] is motivated by the fact that, as already pointed out by others (e.g. Fan and Bras, 1995; Seyfried and Wilcox, 1995) the choice of element size should depend on (a) the catchment size (scale), (b) the nature of heterogeneity of dominant factors and (c) the size of the event under consideration. Another advantage of analysing dominant factors separately is that once the optimal element size has been determined, it gives more insight into how an individual process or parameter should be averaged over a model element.

6.4.1 Structure of the research procedure

The procedure that has been applied to analyse the relation between the scale of the model elements and the model performance is shown in Figure 6.2. First, a physically based distributed hydrological model is set up to model the hydrological response of the catchment under consideration. The catchment is then divided into a user defined number of subcatchments, n, where n is substantially smaller than the number of elements of the distributed model. Subsequently, the following two steps are performed:

[I] All model parameters and input variables are "averaged" at the catchment scale, However, for one process or parameter an "average value" (see section 6.4.3 for a

description of the applied averaging procedures) is determined for all the basic elements within one subcatchment.

[II] A model run is performed and the deviation of the computed output in relation to observed output is quantified by the mean square error value (MSE):

$$MSE_1(n) = \frac{1}{T}\sum_{t=1}^{T}\left[d_n(t) - dm(t)\right]^2 \qquad (6.1)$$

where $MSE_1(n)$ is the mean square error as a function of n, T is the number of time steps used in the simulation, $d_n(t)$ is the computed discharge at the catchment outlet at time t and $dm(t)$ is the observed discharge at the catchment outlet at t. Furthermore, also deviations from the output of the fully distributed model are considered:

$$MSE_2(n) = \frac{1}{T}\sum_{t=1}^{T}\left[d_n(t) - dd(t)\right]^2 \qquad (6.2)$$

where $MSE_2(n)$ is the mean square error as a function of n and $dd(t)$ is the discharge at the catchment outlet at time t, derived with the fully distributed model.

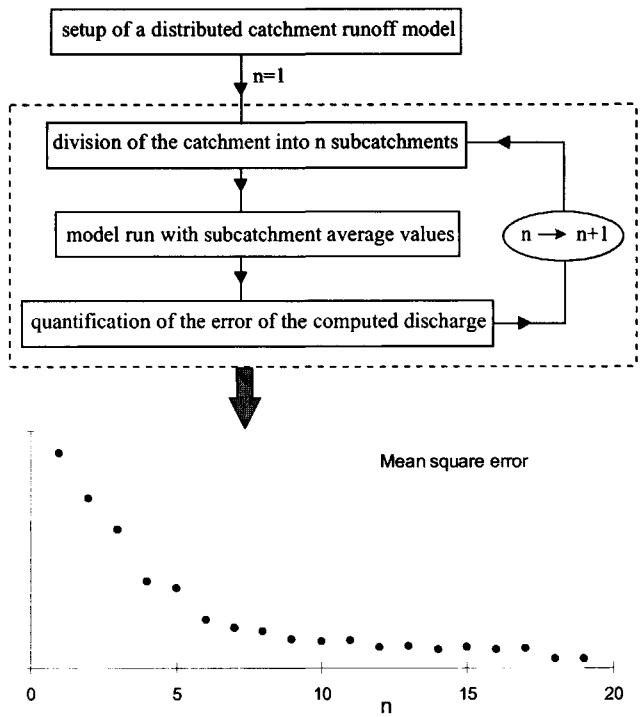

Figure 6.2 Schematical view of the research procedure

These two steps are performed for a number of values of n. Essentially, the value of n represents the amount of spatial information of the process or parameter of interest used in the distributed model. A plot of MSE-values against corresponding values of n, shows the relation between the spatial scale of the model elements and the resulting model performance.

6.4.2 Identification of dominating runoff controls

In chapter 4, two dominant factors were identified that are of influence on the magnitude of a runoff peak in the Zwalm catchment:

[I] Spatial and temporal distribution of rainfall intensities
[II] The percentage of saturated soils at the beginning of the event

So, each parameter or process that is related to factors [I] and [II] is eligible for analysis of effects of heterogeneity. However, in order to prevent redundancy of analysis and results, a selection will be made, as will be explained in the following discussion.

Spatial and temporal distribution of rainfall intensities

Even in a small area like the Zwalm catchment, different rainfall stations sometimes show significant mutual differences in observed rainfall intensities, especially during intense storm events. In chapter 4, a number of simulations were performed, in which the catchment average rainfall input was set equal to the observed values of a single rainfall station. In some cases, the resulting model output showed striking differences between the different model runs. So obviously, a network of rainfall stations in the Zwalm catchment needs to contain more than one rainfall station to capture the effects of spatial heterogeneity of rainfall on the catchment response. However, as already stated by Obled et al. [1994], it is not directly clear whether "*.. the spatial variability of rainfall is important through the dynamic effects of moving rain patterns or through the uncertainty induced on basin average inputs*". This particular issue will be addressed in the remainder of this chapter through application of the procedure of Figure 6.2 to the rainfall input of the catchment runoff model.

The percentage of saturated soils at the beginning of the event

The percentage of saturated soils at the beginning of the event is a major control on runoff amounts in the Zwalm catchment, since storm runoff water is mainly generated on saturated parts of the catchment (Troch et al., 1993). This dominant control on runoff amounts is captured in the catchment runoff model through the following equations:

$$z_i = z_{av} - \frac{1}{f}\left\{\ln\left(\frac{a_i T_e}{T_i \tan\beta_i}\right) - \lambda\right\} \tag{6.3}$$

$$T_i = \frac{K_i}{f} \tag{6.4}$$

$$z_{av} = -\frac{1}{f}\ln\left[\frac{Q(0)}{AT_e \exp(-\lambda)}\right] \tag{6.5}$$

$$S_i = (\theta_s - \theta_r)\left\{\begin{array}{l} z_i - h_c - \frac{1}{f}[(1+(\alpha z_i)^{-n})^{-\frac{1}{n}} \\ \qquad -(1+(\alpha h_c)^{-n})^{-\frac{1}{n}}] \end{array}\right\} \tag{6.6}$$

where:

z_i = depth of the ground water table at location *I*
z_{av} = catchment average ground water table depth
f = exponential decline parameter of hydraulic conductivity with increasing depth
a_i = area of hillslope per unit contour length that drains through location *i*
$\tan\beta_i$ = slope of the ground surface at location *I*
T_i = downslope transmissivity of the soil profile at location *i*
λ = catchment average value of $ln[a_i/tan(\beta_i)]$
K_i = hydraulic conductivity near the ground surface at location *i*
$Q(0)$ = outflow of the Zwalm at the beginning of the event
A = surface area of the catchment.
T_e = catchment average value of T_i
S_i = initial soil moisture deficit at location *I*
θ_s = saturated soil moisture content
θ_r = residual soil moisture content
h_c = capillary fringe
α, n = empirically based soil parameters of the Van Genuchten equation

A soil profile is saturated if the soil moisture deficit, S_i, is less than or equal to zero. Five basic model parameters, h_c, K_i, f, a_i, and β_i are of direct influence on the soil moisture deficit. Three of them, soil parameters h_c, K_i, f, have been subjected to the sensitivity analysis as described in chapter 4. The results showed that the output of the catchment model is highly sensitive to these parameters. The two remaining parameters (topographic parameters a_i, and β_i) were not subjected to the sensitivity analysis since they are modelled in a spatially distributed manner and considered to be well-defined because of the availability of the detailed digital elevation model. For the analysis on effects of heterogeneity on catchment runoff, however, topographic parameters, a_i, and β_i, are more interesting than soil parameters, h_c, K_i, and f. The digital elevation model provides detailed information on the present heterogeneity of a_i, and β_i, whereas no such information is available on h_c, K_i, and f.

Furthermore, the Zwalm catchment is predominantly covered by sandy-loam and loam soils (Troch et al., 1993) which means the soil characteristics are likely to contain only small-scale fluctuations. Therefore, spatial variation of soil characteristics are expected to effect runoff production at the hillslope scale, but not at the catchment scale (Sivapalan et al, 1987).
So, of the five parameters that control the percentage of initially saturated soils, only the topographic parameters, a_i, and β_i, are subjected to the procedure of Figure 6.2.

6.4.3 Averaging methods

A significant aspect of the procedure of Figure 6.2 is the choice of an averaging method for the process or parameter of interest, since this choice can seriously influence the results of the assessment of effects of spatial heterogeneity. Different processes (or parameters) require different averaging techniques because of differences in the way they are of influence on the model output. In this section, the averaging procedures for rainfall and topography will be discussed.

Rainfall

The averaging method of rainfall, makes use of a well-known geostatistical averaging method. A rainfall field at the resolution of the grid cells of the digital elevation model (30 m.) is generated by interpolation of measured rainfall intensities, using the inverse square distance method. According to the inverse square distance method the estimated rainfall intensity, $P_e(i)$ at grid cell i equals:

$$P_e(i) = \frac{\sum_{j=1}^{M} w_j(i) P_O(j)}{\sum_{j=1}^{M} w_j(i)} \quad ; w_j(i) = 1/d^2(i,j) \tag{6.7}$$

where $P_O(j)$ is the observed rainfall intensity at station j and $d(i,j)$ is the distance from grid cell i to station j. Subsequently, the area-average rainfall intensity for each subcatchment is taken to be the arithmetic mean of intensities of all grid cells belonging to this subcatchment.

Topography

For topographical parameters, the choice of an averaging procedure is a less straightforward issue. In general, an averaging method has to be based on the concept of its influence on the system output and a notion of its present heterogeneity. In the catchment runoff model of the Zwalm (chapter 4), three topography-related characteristics are recognised that more or less completely characterise the influence of topography on hillslope runoff:

[1] The lengths of flow paths.
[2] The percentage of soils that are fully saturated at the beginning of the event.
[3] Slope values.

Although the percentage of initially saturated soils (point [2] above) is not directly a topographic characteristic, it is chosen to be treated as such, since it is strongly controlled by the catchment topography (see equations (6.3) and (6.3)). For averaging purposes, three different topographic characteristics are derived:

[a] Surface area as a function of distance to the stream network (see Figure 6.3)
[b] The area of saturated soils as a function of distance to the stream network (see Figure 6.4)
[c] Average slope values as a function of distance to the stream network (see Figure 6.5)

If the spatial and temporal distribution of rainfall intensities are known, the surface distribution function describes how much rain falls at a distance x to the stream network. The time it takes for this water to travel this distance x is inversely proportional to the average flow velocity which, as far as topography is concerned, is related to characteristics [b] (since it controls the overland flow percentages) and [c] (since it controls the flow velocity in Manning's equation). The averaging method used for topographic characteristics is based on this concept of topographic influence on runoff production. For each of the n subcatchments, statistics of topographic characteristics [a]-[c] are derived, resulting in $3 \times n$ functions of distance to the stream network, of which examples are shown in Figure 6.3-Figure 6.5. These functions are derived from the 39.1 m. × 30.9 m. digital elevation model, while function [b] is also based on equations (6.3) - (6.6). Function [b] varies between events, whereas functions [a] and [c] are time-invariant.

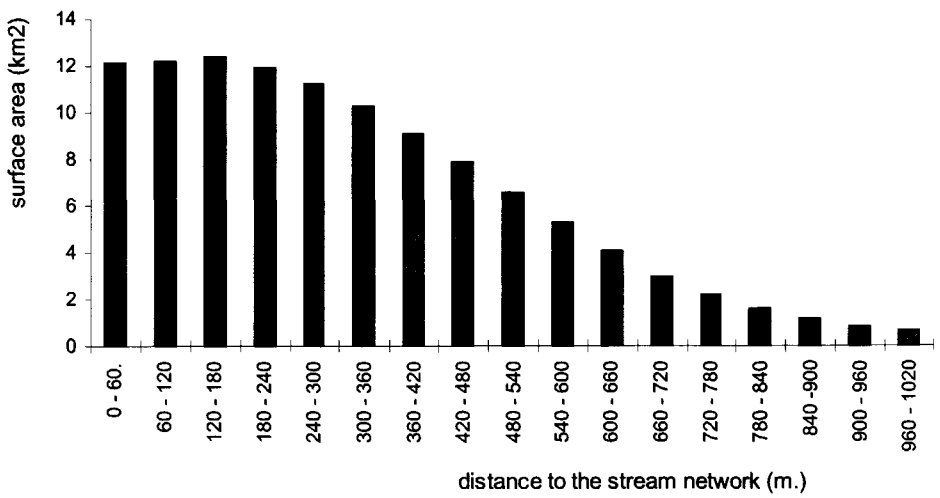

Figure 6.3 Surface distribution as a function of distance to the stream network for the Zwalm catchment.

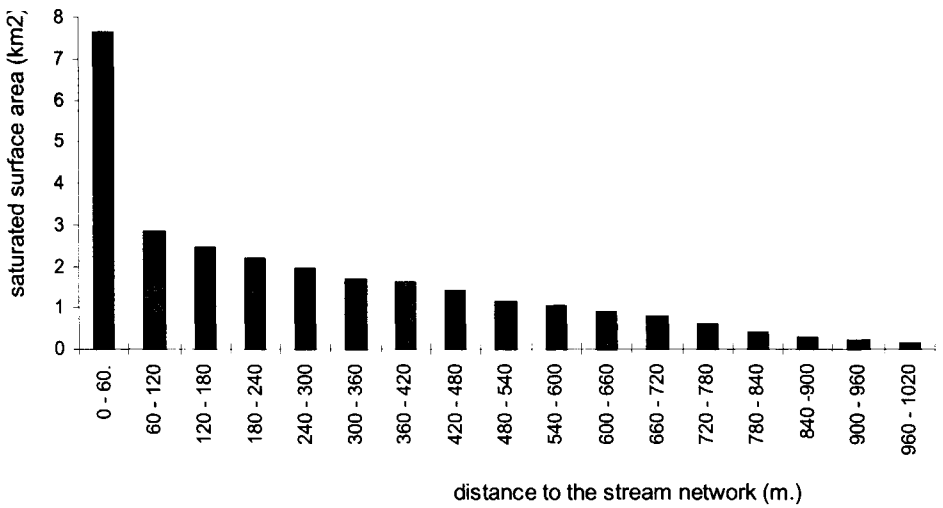

Figure 6.4 Percentage of initially saturated soils in the Zwalm catchment as a function of distance to the stream network; event of 02-06-1992

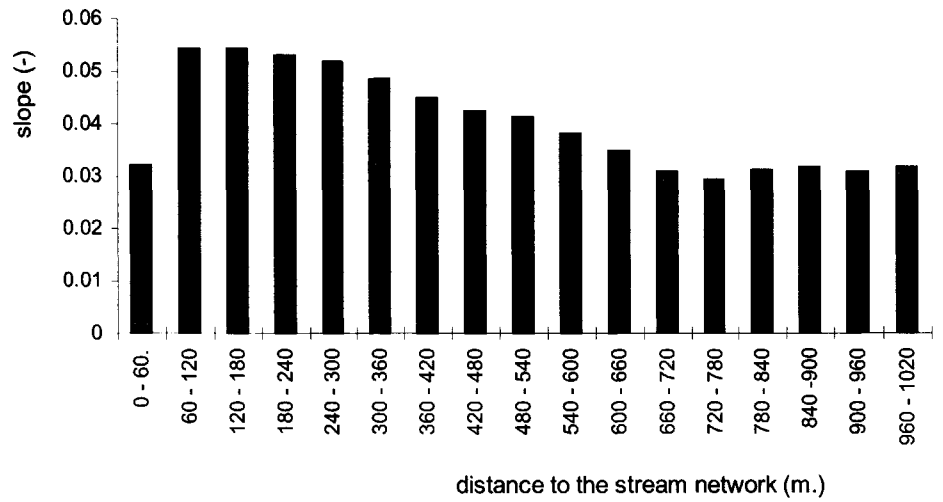

Figure 6.5 Average slope in the Zwalm catchment as a function of distance to the stream network.

This information is used to generate an "average hillslope flow strip", which has the same statistics as functions [a]-[c]. Subsequently, the subcatchments are modelled as a combination of the existing stream network and a number of these average hillslope strips. Naturally, the number of strips is chosen such, that the total surface equals the surface of the subcatchment.

6.5 Results and discussion

Six events have been simulated to assess the influence of spatial heterogeneity of both rainfall and topographic characteristics on catchment runoff. For each of these events, the procedure of Figure 6.2 has been applied to both rainfall and topography. Resulting mean square error values for two events are depicted in Figure 6.6- Figure 6.9. The mean square error values have been derived through application of equation (6.2), which means they quantify the deviation of the various computed hydrographs from the output of the fully distributed model.

Figure 6.6- Figure 6.9 show that for values of $n \geq 4$, the mean square error is approximately constant and only non-zero for reasons of noise production by the model. For topographical characteristics the error is already negligible for values of $n \geq 2$ (Figure 6.7 and Figure 6.9). So, at first sight, it appears that a catchment runoff model of the Zwalm needs to contain at least 4 model elements in order to capture heterogeneity effects of rainfall, while 2 model elements suffice for heterogeneity effects of topographic characteristics. However, even for the fully lumped model ($n=1$) the mean square error is only marginal compared to general modelling errors (i.e. errors in relation to observed discharges, see chapter 4), which means that the distributed model is hardly any better than the lumped model version. Differences between the output of these two model versions are even so small that it's impossible to judge which of the two model versions is likely to generate the most reliable model output. Figure 6.10, for example, shows the output of both model versions for the event of 02-06-1992. Both computed hydrographs are very similar, while they obviously deviate from the observed hydrograph. Differences between the computed hydrographs are only visible for about six hours when the discharge in the Zwalm reaches its peak, but that does not lead to substantial differences in the magnitude of the peak discharge.

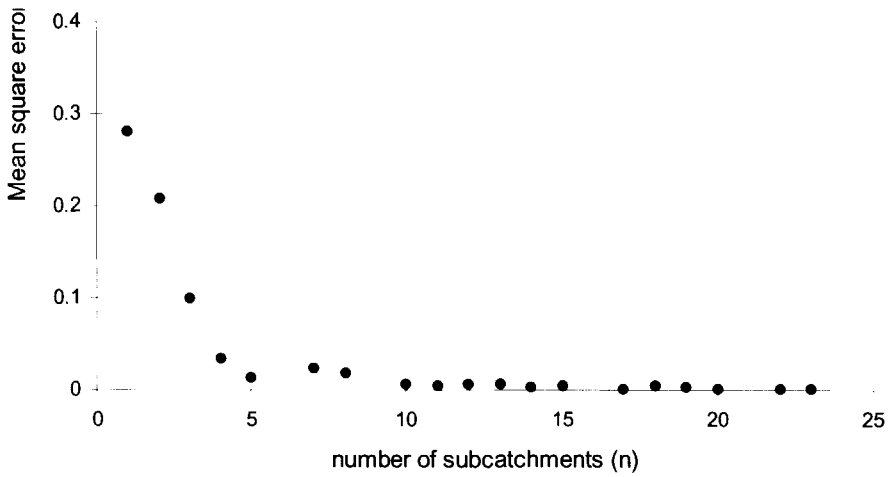

Figure 6.6 Values of $MSE_2(n)$ (equation (6.2)) of the catchment runoff model when the Zwalm catchment is divided into n subcatchments and *rainfall intensities* are averaged over these subcatchments (event of 02-06-1992).

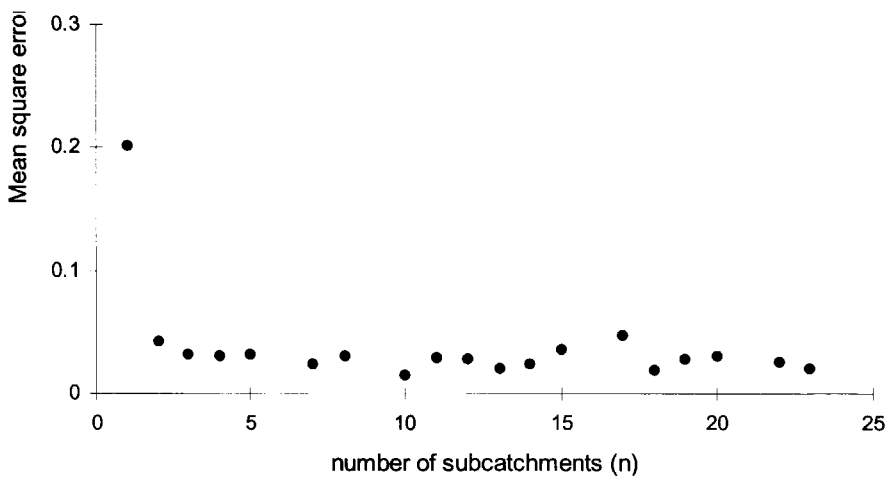

Figure 6.7 Values of $MSE_2(n)$ (equation (6.2)) of the catchment runoff model when the Zwalm catchment is divided into n subcatchments and *topographic characteristics* are averaged over these subcatchments (event of 02-06-1992).

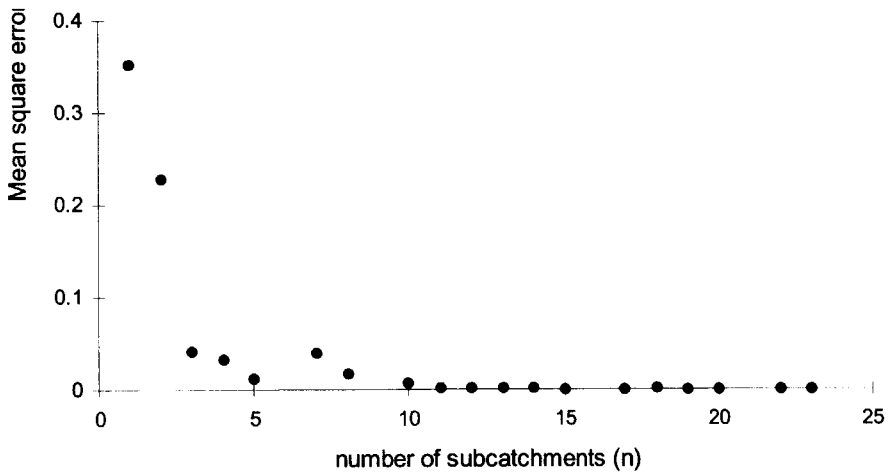

Figure 6.8 Values of $MSE_2(n)$ (equation (6.2)) of the catchment runoff model when the Zwalm catchment is divided into n subcatchments and *rainfall intensities* are averaged over these subcatchments (event of 13-11-1993).

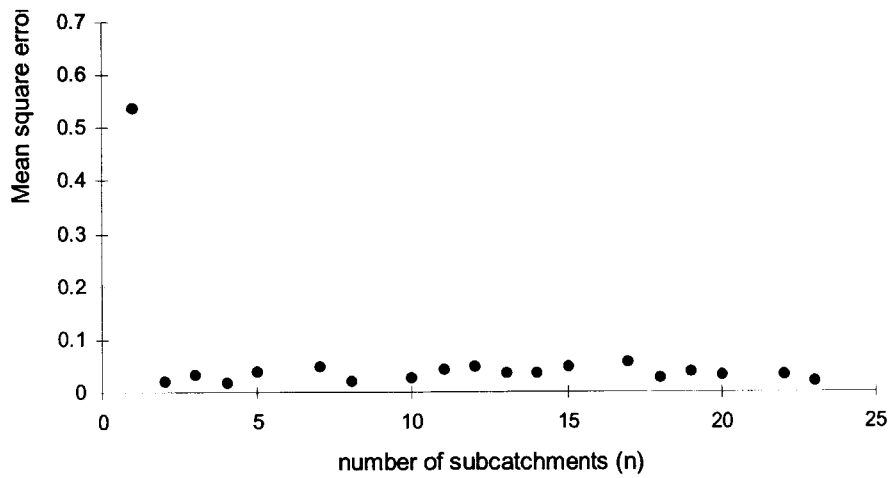

Figure 6.9 Values of $MSE_2(n)$ (equation (6.2)) of the catchment runoff model when the Zwalm catchment is divided into n subcatchments and *topographic characteristics* are averaged over these subcatchments (event of 13-11-1993).

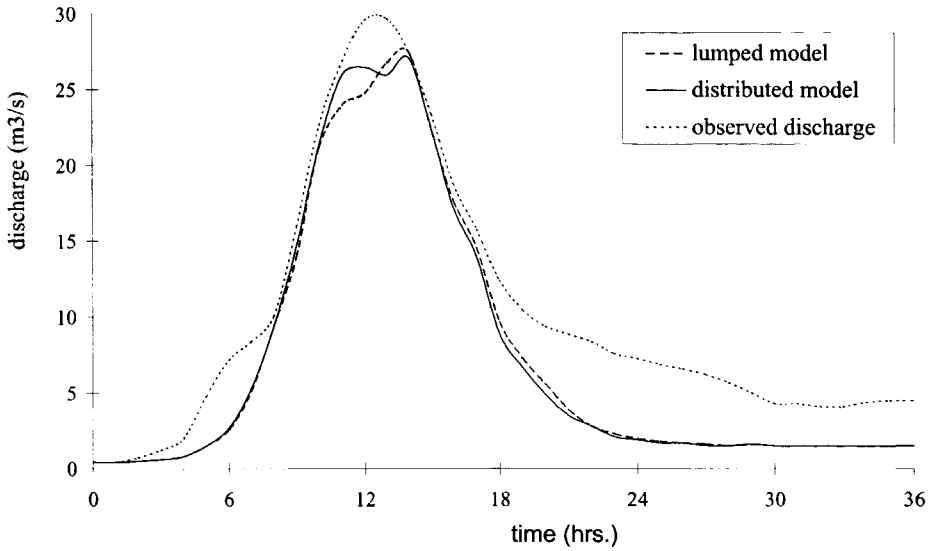

Figure 6.10 Comparison of model performance of a distributed and a lumped catchment runoff model of the Zwalm (event of 02-06-1992).

At first sight, these results seem to contradict the results of chapter 4, where the spatial heterogeneity of rainfall intensities was found to be of serious influence on the runoff hydrograph. In the analysis of chapter 4, a number of simulations were performed, in which each time the observed rainfall of one of the available rainfall stations served as rainfall input for the catchment runoff model. For some events, the resulting hydrographs differed strongly as a result of differences in observed rainfall amounts of different rainfall stations. For the event of Figure 6.10, for instance, the peak discharge resulting from intensities of station Velzeke was even twice as high as the peak discharge resulting from intensities of station Elst. The reason why these differences are not reflected in Figure 6.10, is that in the applied procedure of this chapter (see Figure 6.2) the catchment average rainfall remains the same, regardless whether the distributed or the lumped model version is used. As a consequence, the only difference between the lumped and the distributed model, as far as rainfall is concerned, is the spatial distribution of intensities. In the procedure of chapter 4, on the other hand, the spatial distribution was the same for each simulation (namely spatially invariant intensities) but the magnitude of the intensities were different due to differences in observed rainfall amounts of the available rainfall stations. Consequently, the following two conclusions can be drawn:

1. The use of only one rainfall station is not enough to obtain a reliable estimate of the area-average rainfall in the small, 114 km^2, Zwalm catchment

2. If a reliable estimate of the area-average rainfall in the Zwalm catchment is available, catchment average modelling suffices

The obvious question that arises from the first conclusion is: "How many rainfall stations are needed to guarantee a reliable estimate of the area-average rainfall in the Zwalm catchment?". Unfortunately, the available number of rainfall stations in the Zwalm catchment (5 in total, but most of the time there was at least one station out of order) was too small to provide a direct answer to this question. Therefore, this issue will be treated into further detail in another pilot study (the Mosel basin) in which there are no less than 103 rainfall stations available. The results of the study of the Mosel basin are presented in chapter 7.

The second conclusion also raises a number of questions:

(i) Why does the available information on spatial distribution of rainfall intensities and topographic characteristics hardly add to the model performance?
(ii) Under what conditions is this conclusion applicable on other catchments?

Both these issues will be discussed in the remainder of this chapter.

6.5.1 Present heterogeneity in the Zwalm catchment.

The first step in discussing issues (i) and (ii) above, is to investigate the present heterogeneity in the catchment. There are a number of (geo-)statistical measures (standard deviation, variogram, etc.) available to quantify spatial heterogeneity, but they do not necessarily provide the desired information for each specific case. Consequently, it is essential in this case to select a method of quantification that provides the specific required information. Therefore, in the first place it has to be considered how the spatial heterogeneity of both rainfall intensities and topographic characteristics is represented in the catchment runoff model and in which manner it influences the computed runoff hydrograph.

In the most distributed version of the rainfall-runoff model of the Zwalm, the catchment is divided into 61 subcatchments (see Figure 6.16). For each subcatchment, topographic characteristics and rainfall intensities are "averaged" as described in section 6.4.3. The remaining model parameters (11 in total) are assumed to be equal for all subcatchments. So, even though the topographic characteristics have been derived from a digital elevation model with a 30 m. resolution, its spatial heterogeneity is represented in the model on the resolution of the 61 subcatchments. Therefore, special interest goes to the mutual differences among the 61 subcatchments. For a number of events, runoff hydrographs have been computed for each of the 61 subcatchments. For each event, two simulation runs have been performed:

1. A run with catchment-average topographic characteristics and spatially distributed rainfall intensities
2. A run with a catchment-average rainfall intensity and spatially distributed topographic characteristics.

The resulting statistics of the peak runoff values of the 61 subcatchments are presented in Table 6.1.

	Subcatchment peak-runoff statistics			
	Rainfall intensity distributed		Topographic characteristics distributed	
Date of event	average (mm/hr)	standard deviation	average (mm/hr)	standard deviation
06-02-1992	1.01	0.24	1.02	0.34
22-01-1993	1.24	0.28	1.19	0.30
24-07-1993	2.07	0.40	2.16	0.61
13-11-1993	1.56	0.13	1.55	0.47
12-12-1993	1.43	0.55	1.28	0.27
19-12-1993	0.60	0.06	0.61	0.18

Table 6.1 Peak runoff statistics of the 61 subcatchments for 6 events

This table shows that in general the spatial heterogeneity of topographic characteristics causes more spreading in subcatchment peak discharges than the spatial heterogeneity of rainfall intensities. Generally, the subcatchments that contain banks of the Zwalm river, generate the highest peaks, which is in line with the concept of runoff being mainly generated at saturated near-stream areas. It has to be emphasised that rainfall inputs of the model are smoothed as a result of the applied geostatistical interpolation technique, which means in reality, the spatial heterogeneity of rainfall intensities is likely to cause more variation in subcatchment peak runoff values. Currently, the only event for which rainfall intensities cause more variation in subcatchment peak runoff values than topographic characteristics is the event of 12-12-1993, when a rainfall burst in the northern part of the catchment caused relatively large runoff differences between "northern" subcatchments and "southern" subcatchments.

As an example, Figure 6.11 and Figure 6.12 show scatter plots of the resulting peak values at the subcatchment outlets for the event of 02-06-1992. The variation in peak values in Figure 6.11 is a result of differences in rainfall intensities, whereas the variation in peak values in Figure 6.12 is a result of differences in topographic characteristics. The peak values in Figure 6.11 and Figure 6.12 are presented as specific discharge (unit: mm/hr.) to make a fair comparison between subcatchments of different sizes. Furthermore, for each subcatchment, the (flow-) distance to the catchment outlet is depicted at the x-axis to support the discussion about the role of the flow distance in this analysis, as presented later on in section 6.5.2.

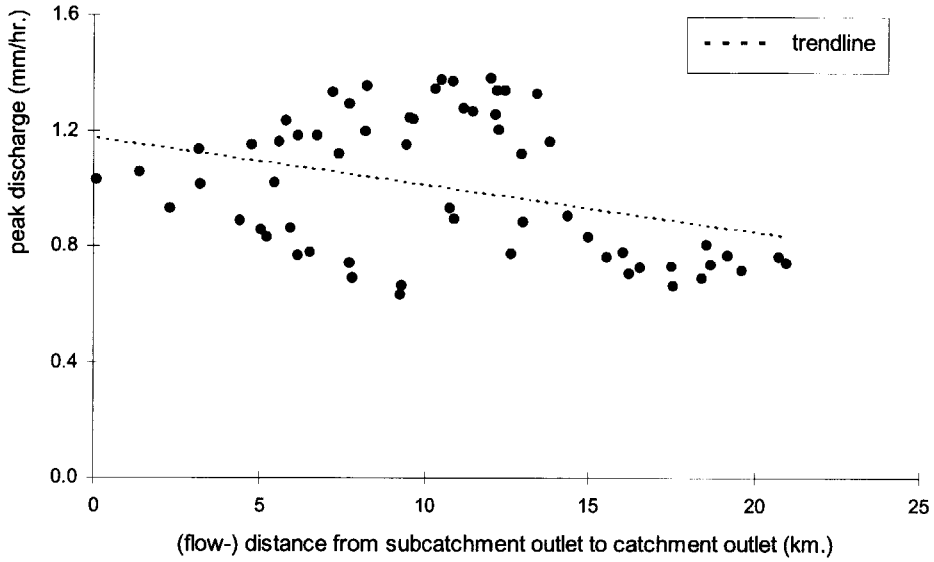

Figure 6.11 Computed peak discharges of 61 subcatchments of the Zwalm catchment, using *variable rainfall inputs* and homogenic topographic characteristics; event of 02-06-1992

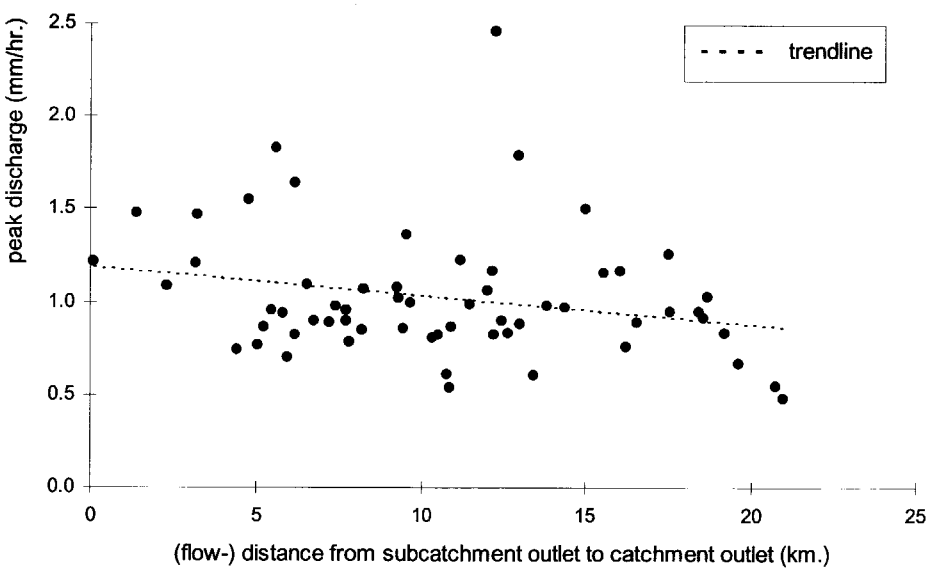

Figure 6.12 Computed peak discharges of 61 subcatchments of the Zwalm catchment, using *variable topographic characteristics* and homogenic rainfall inputs; event of 02-06-1992

Both these Figures show that differences between the various subcatchments can be substantial, which means the negligible effect of the available spatial heterogeneity on catchment runoff is not due to a "lack of heterogeneity". In other words, possible effects of heterogeneity are filtered out to a large extent in the river routing procedure. In the river routing procedure, the outflow, $O_i(t)$, of subcatchment i reaches the catchment outlet after a travel time, L_i. The value of L_i depends on the flow velocity, $v(t)$, in the river and to the flow distance, D_i, from the subcatchment outlet to the catchment outlet. In the catchment runoff model of the Zwalm, the values of $v(t)$, $O_i(t)$ and L_i; i=1..61, are obviously such, that modelling with catchment average values is by no means inferior to distributed modelling. In the next section a sensitivity analysis is performed to find out whether this conclusion is also applicable to other catchments, i.e. to other combinations of $v(t)$, $O_i(t)$ and L_i; i=1..61.

6.5.2 Sensitivity analysis of heterogeneity effects

Spatial trends

One of the possible causes of the negligible effects of spatial heterogeneity on catchment runoff may be that a clear, significant, spatial trend is lacking in the topographic characteristics of the Zwalm catchment and the rainfall inputs of the investigated meteorological events. The presence of a strong spatial trend in hydrological or meteorological characteristics might result in catchment responses which cannot be captured by a model which uses catchment average values. For instance, if during a storm event all subcatchments that generate relatively low peak runoff discharges are situated close to the catchment outlet, the peak of the catchment runoff hydrograph will occur later than would have been the case if these subcatchments are well-distributed over the catchment. If catchment average values are taken (n=1 in the procedure of Figure 6.2) the spatial trend, which is present in "reality", is neglected by the model. As a consequence, the derived peak discharge of the lumped model (n=1) occurs earlier than derived peak discharges of more distributed model versions (n≥2).

Differences between lumped and distributed model versions increase with increasing steepness of the trend lines of which examples are shown in Figure 6.11 and Figure 6.12. A steep trend line indicates there is a strong relation between the peak discharge, M_i, of subcatchment i, and the flow distance, D_i, from the subcatchment outlet to the catchment outlet. The trend lines of Figure 6.11 and Figure 6.12 are obviously not steep enough to cause some serious differences between the model output for different values of n. Only for small values of n, some marginal differences can be distinguished in Figure 6.6 - Figure 6.9. In Figure 6.7-Figure 6.9, deviations from the resulting output of the fully distributed model are even negligible for all values of n≥2. So, even though Figure 6.12 shows there is a spatial trend of topographic characteristics (i.e. the trend line is not horizontal) its effect on the catchment runoff can be fully captured by a model which only uses two model elements.

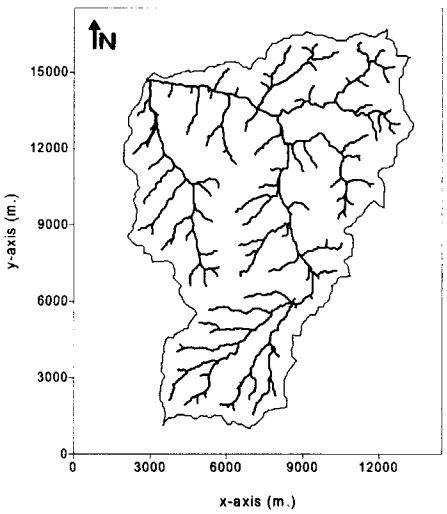

Figure 6.13 The Zwalm catchment

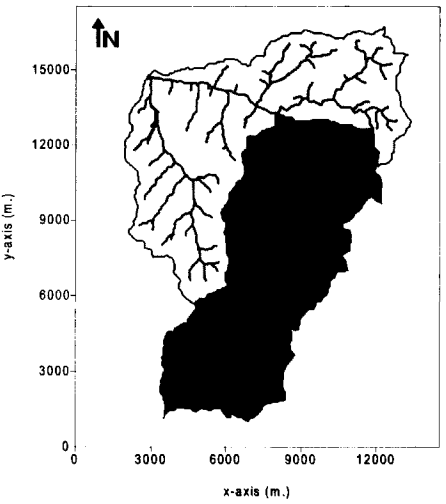

Figure 6.14 The Zwalm catchment, divided into 2 subcatchments

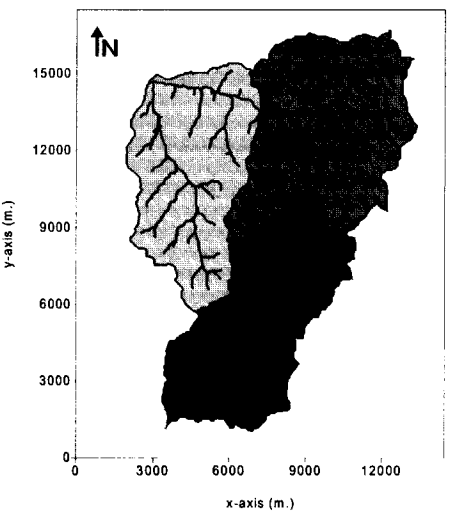

Figure 6.15 The Zwalm catchment, divided into 3 subcatchments

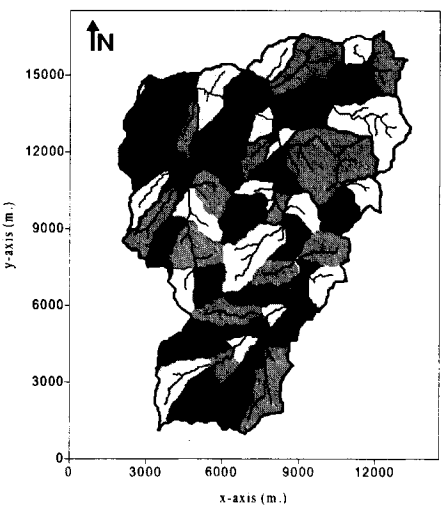

Figure 6.16 The Zwalm catchment, divided into 61 subcatchments

Figure 6.13 - Figure 6.16 show the applied subdivisions of the Zwalm catchment into 1, 2, 3 and 61 subcatchments respectively. From Figure 6.14 it can be seen that the selected subdivision of the catchment into 2 subcatchments more or less splits the catchment into areas that are relatively closely situated to the catchments outlet (The Northern part of the catchment) and areas that are situated relatively far away from the catchment outlet (The Southern part of the catchment). The Northern part of the catchment consists of relatively flat areas in comparison with the areas in the Southern part of the catchment. As a consequence, by clustering these areas into two parts as shown in Figure 6.14, the dominant nature of heterogeneity of topographic characteristics in the Zwalm catchment is captured to a large extent by the catchment runoff model. This is reflected in the relatively large decrease in the mean square error when moving from n=1 to n=2 in Figure 6.7 and Figure 6.9. For rainfall intensities, the main direction of increasing or decreasing trends differ from event to event. For the two events of Figure 6.6 and Figure 6.8, there is also a substantial spatial trend of subcatchment peak in east-west direction, which explains why in these two figures the decrease of the mean square error between n=2 and n=3 is at least as prominent as the decrease between n=1 and n=2.

Obviously, the required number of elements in a catchment runoff model can be decreased by a sensible choice of the subdivision of the catchment into model elements. The problem, however, is that the "optimal" subdivision varies from event to event, due to differences in rainfall patterns. For the Zwalm catchment the choice of an "optimal" subdivision of the catchment does not appear to be too much of an issue, since it has already been demonstrated that for the events under consideration, heterogeneity effects on catchment are negligible. However, in other catchments with more prominent spatial trends in hydrological characteristics, or during events with more prominent spatial trends in meteorological characteristics, these effects may not be negligible. To test this hypothesis, a number of model runs have been executed in which fictive "extreme trends" of spatial heterogeneity have been created through manipulation of the original configuration of the Zwalm catchment. First, the specific runoff during an event is calculated for each of the 61 subcatchments of Figure 6.16. In order to be able to discriminate between heterogeneity effects of both rainfall and runoff, the specific runoff of the subcatchments is computed with [1] a model version in which spatially variable rainfall intensities are used in combination with catchment average topographic characteristics and [2] a model version in which spatially variable topographic characteristics are used in combination with catchment average rainfall intensities. Subsequently, the locations of the subcatchments are switched in such a way that the subcatchments with the highest peak discharges are located furthest away from the catchment outlet. As a result, the "true" representation of the available spatial trend in subcatchment peak runoff generation of, for instance, Figure 6.12 changes into the fictitious spatial trend of Figure 6.17.

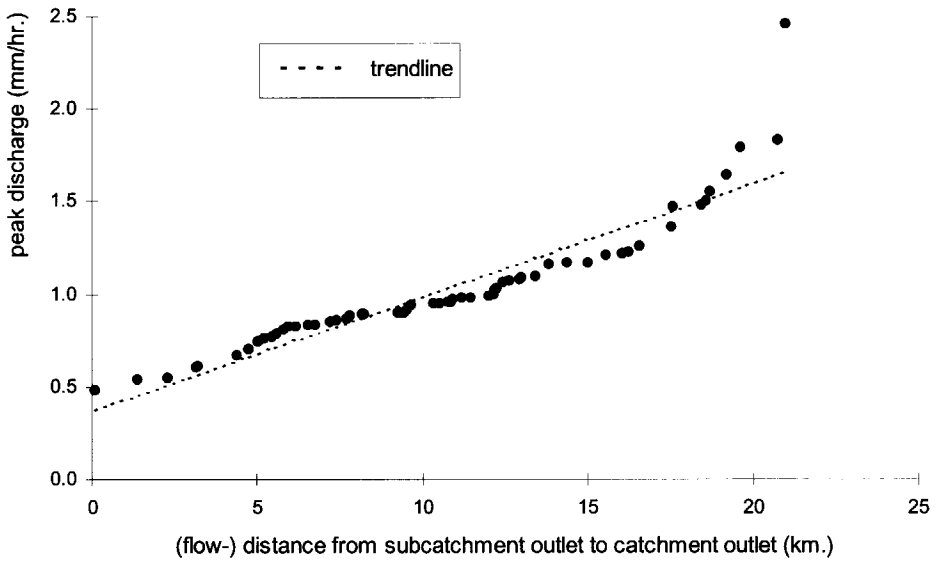

Figure 6.17 Computed peak discharges of 61 subcatchments, using variable topographic characteristics and homogenic rainfall inputs, Zwalm catchment; event of 02-06-1992. The subcatchments have been placed in order of the magnitude of peak discharge

For this fictitious catchment configuration, a run of both the distributed model version as well as the lumped model version have been executed. Differences between the derived hydrographs for these two version are quantified by the mean square error. Results for six events are shown in Table 6.2. and compared with results which already have been derived before for the original configuration of the Zwalm catchment.

Date of event	Mean square error of the fully lumped model			
	Rainfall intensity distributed		Topographic characteristics distributed	
	Original configuration	Fictive configuration	Original configuration	Fictive configuration
06-02-1992	0.28	1.16	0.20	2.67
22-01-1993	0.41	1.29	0.19	2.32
24-07-1993	2.15	5.25	1.51	9.14
13-11-1993	0.35	0.63	0.54	3.23
12-12-1993	0.96	1.37	0.18	0.90
19-12-1993	0.08	0.17	0.16	1.00

Table 6.2 Mean square error values of the fully lumped model (n=1) for the both the original catchment configuration and the fictive catchment configuration in which subcatchments have been placed in order of magnitude of the peak discharge.

As expected, the built-in trend causes an increase in the mean square error values. The amount of the increase varies strongly between events and also between the two entities (rainfall and topography). This can be explained by differences in the mean and standard deviation of the subcatchment peaks (see Table 6.1). Both mean and standard deviation of the subcatchment peaks of the event of 24-07-1993, for instance, are relatively large. Consequently, the trendline is relatively steep for this event, which leads to a relatively large difference in model output between the lumped and the distributed model version. During the event of 19-12-1993 on the other hand, rainfall was almost uniformly distributed over the catchment and caused only small differences in subcatchment peaks, which is reflected in the small standard deviation of 0.06 (see Table 6.1). Consequently, the effect of the built-in trend will also be relatively small.

Catchment size

Another possible cause of the negligible effects of the present spatial heterogeneity on catchment runoff is the fact that flow distances in the river network are relatively short due to the modest river length of approximately 20 km. Consequently, the hydrograph peaks of the subcatchments will always coincide to a large extent, which means effects of spatial differences in hydrological and meteorological characteristics are filtered out at the catchment outlet. In larger river systems, on the other hand, differences in travel times between different subcatchments are more substantial. Furthermore, the extent of the available spatial heterogeneity is likely to be more eminent in larger catchments. Since catchment average modelling of hydrological and meteorological characteristics always results to some extent in relocation of runoff amounts, it is expected that representation of spatial heterogeneity in catchment runoff models becomes increasingly important with increasing catchment size.

In order to investigate the relation of travel distances in the river network on one hand and heterogeneity effects on catchment runoff on the other hand, again the configuration of the Zwalm catchment is manipulated. This time, for a number of values of k, the Zwalm catchment is equally "stretched" in two directions. As a result, a hypothetical catchment is created that has a surface area which is k^2 times the size of the surface area of the Zwalm catchment (i.e. k^2*114 km^2) while the length of its river is k times as long as the Zwalm river (i.e. $\pm k$*20 km). The fictive events that are simulated for this hypothetical catchment are based on the characteristics of the real events that have been simulated before. The specific runoff hydrographs that have been computed for each of the subcatchments are used again as the input of the river routing procedure. Differences are that absolute runoff values of the subcatchments are larger (since the surface areas of the subcatchments have been increased by a factor k^2) and that travel distances are k times larger than before.

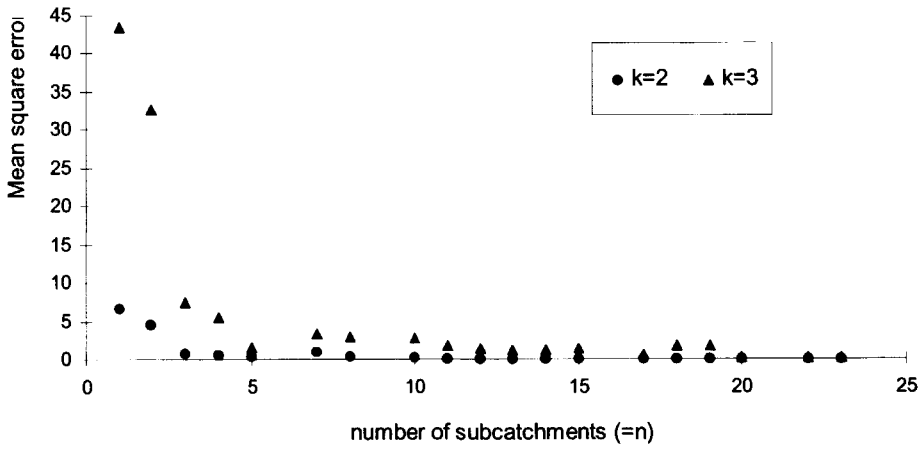

Figure 6.18 Comparison between MSE-values for two manipulated versions of the Zwalm catchment, in which the river length is k times the original length and the surface is k^2 times the original surface. MSE-values are calculated by dividing a catchment into n subcatchments with *varying rainfall intensities* and comparing the model output with the model output of the case when n=61; (rainfall intensities are taken from the event of 02-06-1992

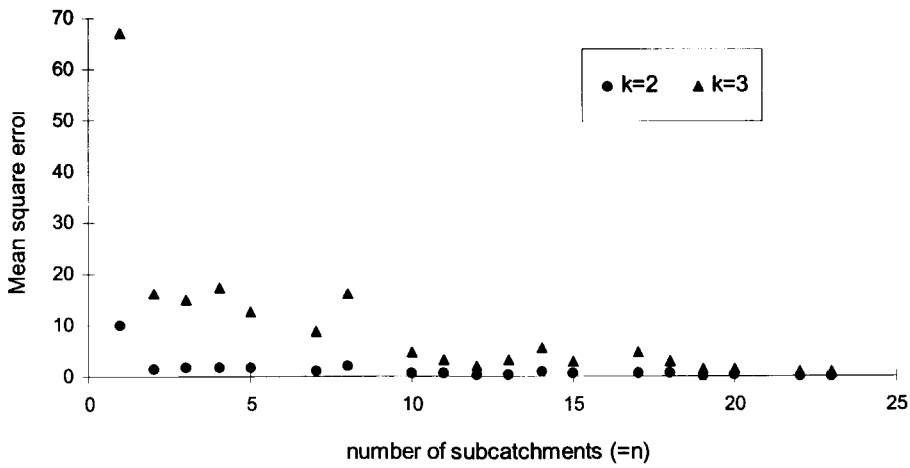

Figure 6.19 Comparison between MSE-values for two enlarged versions of the Zwalm catchment, in which the river length is k times the original length and the surface is k^2 times the original surface. MSE-values are calculated by dividing a catchment into n subcatchments with *varying topographic characteristics* and comparing the model output with the model output of the case when n=61; rainfall intensities are taken from the event of 02-06-1992

For two different versions of this fictive catchment (corresponding to k=2 and k=3) mean square errors have been computed through application of the procedure of Figure 6.2. Figure 6.18 and Figure 6.19 show the results for the event of 02-06-1992. The results of the original configuration (i.e. k=1) have been added to these Figures. The first thing to notice from these two Figures is that MSE-values increase significantly with increasing value of k, which, of course, is largely due to the fact that these fictive catchments are larger and, consequently, generate higher discharges. The second aspect to notice from Figure 6.18 and Figure 6.19 is the fact that, again, the smallest values of n (n=1, n=2 in Figure 6.18 and n=1 in Figure 6.19) show significantly larger MSE-values than the remaining n-values. The difference is that for values of n>2 there is, especially in case of k=3, a more clear decreasing trend with increasing value of n is visible. Obviously, the increasing river length causes a slower convergence of the output of a model, using n subcatchments as basic elements towards the output of the distributed model. It is interesting to find out whether this effect is either amplified or damped when real patters of present heterogeneity in larger catchments (river basins) are used instead of the fictive patterns of this section. Therefore, the research procedure of Figure 6.2 has also been applied to the 28152 km^2 Mosel basin. Results are presented in chapter 7.

6.6 Conclusions

A methodology has been presented which serves to analyse the influence of the spatial heterogeneity of parameters and processes on runoff generation. Application of this methodology to a wide range of catchments will generate useful guidelines on the amount of information on spatial heterogeneity present in hydrological systems which is needed in order to obtain the best possible output of a rainfall-runoff model. The 114 km^2 Zwalm catchment in East-Flanders served as a pilot study. In chapter 4 it was already demonstrated that the heterogeneity of rainfall intensities in this catchment are far from negligible. Differences between observed intensities in different rainfall stations showed that the use of only one rainfall station is not enough to obtain a reliable estimate of the area-average rainfall during storm events in this small catchment. Furthermore it was shown in this chapter that spatial heterogeneity of rainfall intensities and topographic characteristics in the Zwalm may cause substantial differences in peak rates of specific runoff between the 61 defined subcatchments of the Zwalm catchment. However, in spite of the substantial spatial variability in the Zwalm catchment, it was found that a lumped catchment-runoff model performs equally well as more distributed versions. In other words, as long as a reliable estimate of the spatially averaged properties of rainfall intensities and catchment characteristics is available, spatially distributed modelling is not required for the Zwalm catchment.

Possible effects of spatial heterogeneity on runoff generation are averaged out to a large extent in the river routing procedure of the catchment response model. This is mainly due to the relatively short flow distances in the river network (approximately 20 km at maximum). Hydrograph peaks of the subcatchments therefore coincide to a large extent, which means that effects of spatial differences in hydrological and meteorological characteristics are filtered out at the catchment outlet. Heterogeneity effects on the integrated response are therefore expected to be of greater importance in larger catchments. In order to validate this hypothesis, a sensitivity analysis was performed in which the procedure of Figure 6.2 was applied to a (synthetic) larger version of the Zwalm catchment. In this sensitivity analysis, heterogeneity patterns were taken to be equal to original patterns, which gave the opportunity to filter out the influence of the river length on heterogeneity effects. Results showed that an increasing river length indeed leads to increasing effects of the present heterogeneity on the catchment response.

7. Effects of spatial heterogeneity on the runoff response of a large river basin

7.1 Introduction

The influence of the available spatial heterogeneity in river catchments (basins) on runoff generation depends strongly on the physical characteristics of the catchment under consideration. In this respect the size of the catchment is often mentioned as one of the main controlling factors. (e.g. Krajewski et al. 1991; Milly and Eagleson, 1988; Obled et al., 1994). In the previous chapter, heterogeneity effects have been analysed for the small, 114 km^2, Zwalm catchment. It was concluded that taking spatial variability into consideration is of crucial importance in estimating the area-average rainfall volumes. On the other hand, it was also found that the performance of a rainfall-runoff model of the Zwalm catchment hardly suffers from the use of a spatially average representation of rainfall intensities, as long as the area-average rainfall is preserved. However, a sensitivity analysis showed that the latter conclusion may not hold for larger catchments (basins). It was demonstrated that an increase of the catchment size entails more prominent effects of spatial heterogeneity on the model performance due to an increase of flow distances in the river network. Furthermore, as discussed earlier in chapter 3, also the nature of heterogeneity is strongly related to the size of the river catchment. Therefore, in order to investigate the combined effect of increased flow distances and large scale heterogeneity on the integrated runoff response, the 28152 km^2 Mosel basin is also subjected to the research procedure as described in section 6.4.1.

Furthermore, the availability of an extensive network of 103 raingauges in this basin enables an investigation on the required spatial coverage of the raingauge network to guarantee a satisfying estimation of the areal precipitation. For this purpose the efficiency of different subsets of the existing raingauge network in the Mosel basin with regard to the resulting model performance of a rainfall-runoff model is investigated.

7.2 Description of the pilot study: The Mosel basin

The basin under consideration is the 28152 km^2 Mosel basin, which covers parts of France, Germany and Luxembourg. The physical and hydrological characteristics of this basin have been described in chapter 5 where a statistical analysis on rainfall-runoff relations was performed. Again, as in chapter 5, the water level gauge at Cochem is considered to be the basin outlet in the analysis of this chapter, since no discharge measurements of the actual outlet of the Mosel in Koblenz are available. As a consequence, the size of the basin under consideration is 27030 km^2 instead of 28152 km^2.

Figure 7.1 - Figure 7.4 show locations in the Mosel basin where discharge, rainfall, evaporation and temperature measurements have been performed. Almost all series consist of daily average values. The data set concerns the period of 1960-1997, but only a few series cover this whole period. Therefore, only events which occurred in the period of 1971-1995 have been considered in this analysis.

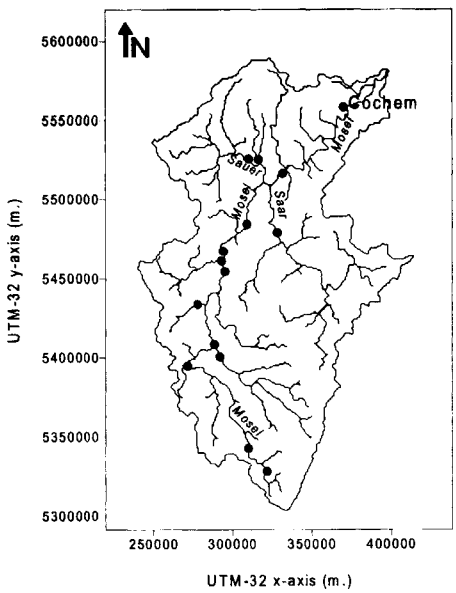

Figure 7.1 The Mosel river basin with 15 discharge measurement stations

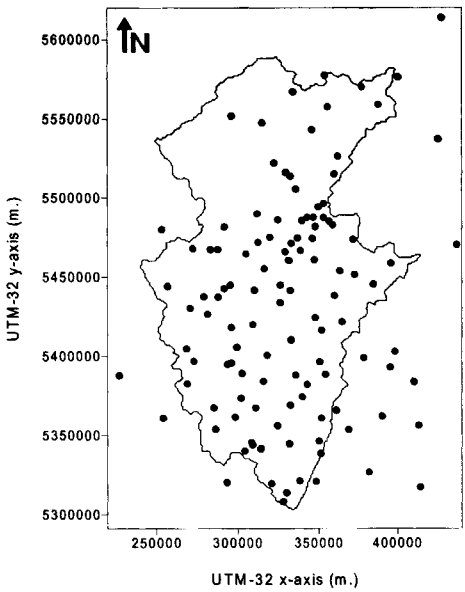

Figure 7.2 The Mosel river basin with 103 raingauges.

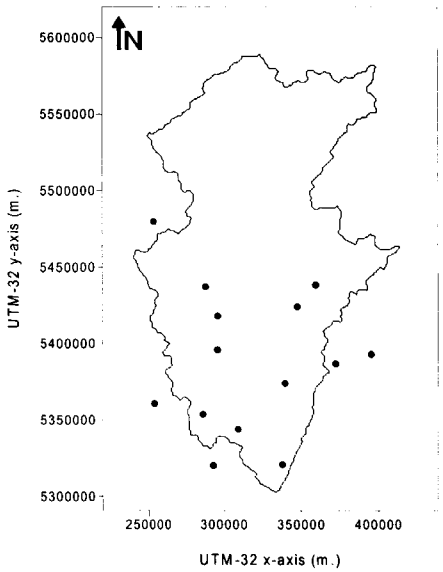

Figure 7.3 The Mosel river basin with 14 temperature stations

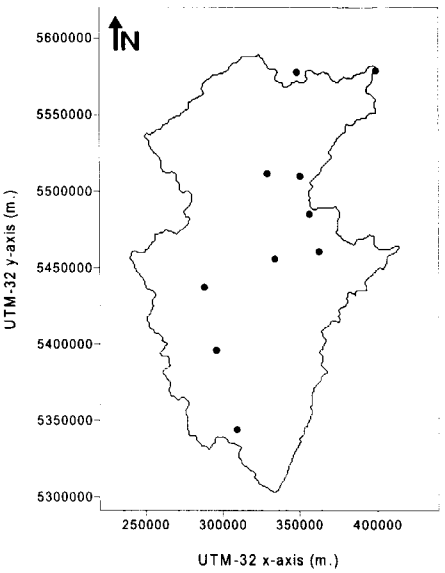

Figure 7.4 The Mosel river basin with 10 evaporation stations

7.3 Methodology

Again, as in the previous chapter for the Zwalm catchment, the effects of spatial heterogeneity on the integrated runoff response of the Mosel basin are investigated by performing a number of model runs with an increasing use of the available information on spatial heterogeneity. In this case, however, two different procedures, instead of just one, are applied to quantify heterogeneity effects of precipitation (see Figure 7.5):

I. The first procedure is similar to the one used for the Zwalm catchment in chapter 6. First, a distributed hydrological model is set up to simulate the hydrological response of the Mosel basin. For each simulated event, a rainfall field at the resolution of the grid cells of the model (1 km^2) is generated through geostatistical interpolation ("Kriging", see Deutsch and Journel [1992]) of measured precipitation depths. The basin is then divided into a user defined number of subbasins, n, where n is substantially smaller than the number of elements of the distributed model. The precipitation depth for each model cell is taken to be equal to the arithmetic mean of all cells belonging to the same subbasin and subsequently a model run is performed. This averaging procedure and the model run are both repeated for a number of values of n. Essentially, the value of n represents the amount of spatial information of precipitation used in the distributed model.

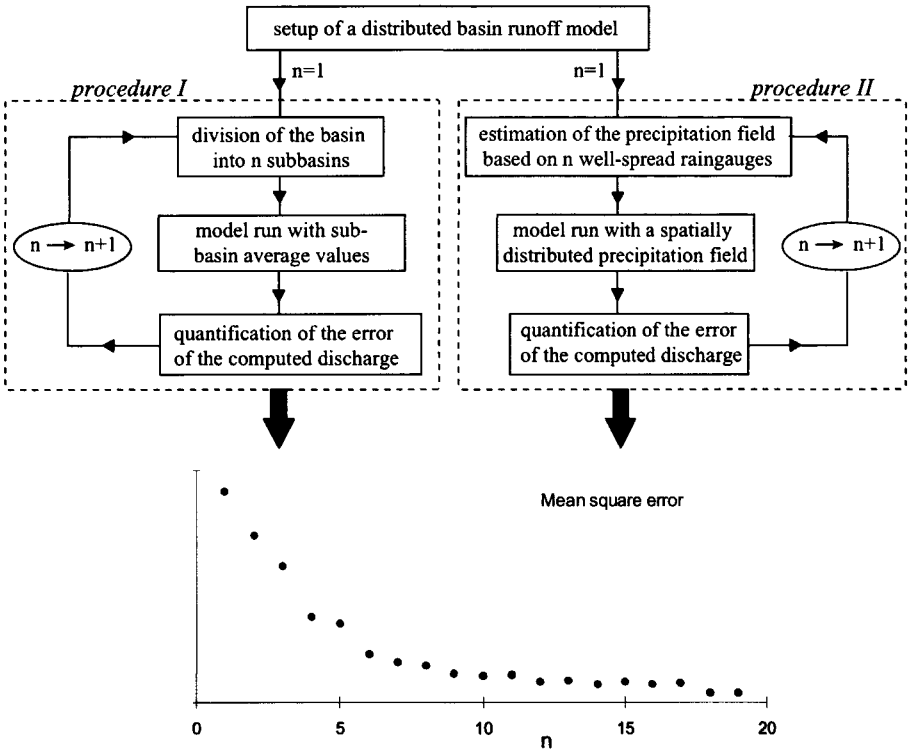

Figure 7.5 Schematical view of the two procedures which are applied to quantify effects of spatial heterogeneity of precipitation intensities on runoff predictions at the basin scale.

II. The second procedure assesses the influence of spatial variability on the accuracy of the estimation of incoming precipitation volumes. The precipitation pattern of the entire basin is estimated through spatial interpolation of measured volumes of *n* raingauges, selected from the available 103 raingauges. An additional procedure has been developed to guarantee optimal spreading of the gauges for each value of *n*. Subsequently, the derived precipitation field is used as input for a simulation with the same distributed model as used in procedure I. Again, these steps are repeated for a number of values of *n*. Deviations from the observed hydrograph show the efficiency of different densities of the raingauge network.

The motivation for the application of these two different procedures stems from the findings of chapter 6, where it was emphasised to make a distinction between heterogeneity effects being the cause of modelling errors on one hand and errors in estimating rainfall volumes on the other hand. For the 114 km^2 Zwalm catchment it was found that ignoring spatial heterogeneity during the measurement process may lead to significant modelling errors, since

reliable estimates of the catchment average precipitation cannot be guaranteed. On the other hand, the use of lumped precipitation volumes in a catchment runoff model of the Zwalm only lead to negligible changes in the derived output, as long as the catchment average value were preserved. In a significantly larger river basin the relative importance of these two forms of heterogeneity effects may change. A comparison of results of the two procedures of Figure 7.5 will show whether or not this is the case.

Besides precipitation, also spatial heterogeneity of initial soil moisture conditions and its effects on model predictions are analysed. For this particular purpose a procedure which is analogue to procedure I above, is performed.

7.4 Hydrological modelling of the Mosel river basin

7.4.1 Introduction

In order to make fair comparisons between the quantification of heterogeneity effects for the Zwalm river on one hand and the Mosel river on the other hand the same concepts of hydrological modelling should be applied. The size of the Mosel basin is approximately 250 times the size of the Zwalm catchment (28152 km^2 for the Mosel and 114 km^2 for the Zwalm). Ideally, the Mosel basin is split up into 250 subbasins on which the same modelling concept is applied as the one used to simulate the runoff response of the Zwalm catchment (see chapter 4). Unfortunately, this approach could not be used for a number of reasons:

1. The rainfall-runoff model of the Zwalm catchment is based on the TOPMODEL-concept. The developers of TOPMODEL suggest that topographic index values should be derived from digital elevation models with a resolution of 50 m. or better (Beven et al., 1995). For the Mosel basin, the resolution of the digital elevation model is 1 km^2.
2. In the rainfall-runoff model of the Zwalm catchment the antecedent soil moisture conditions are related to the observed base flow at the beginning of an event through application of the method of Sivapalan et al. [1987]. In the Mosel basin, the density of the network of available discharge measurement stations (in terms of number of stations per km^2) is not as high as in the Zwalm catchment. Consequently, in some areas of the Mosel basin the distance to the first downstream measurement station is so large that the application of this method of deriving initial moisture conditions cannot be used.
3. A number of measurements were specifically performed during field campaigns in the Zwalm catchment to derive values of parameters of TOPMODEL (and the Van Genuchten equation). For the Mosel river basin such measurements are not available.

Even if initially another modelling concept would have been selected to simulate the hydrological response of the Zwalm catchment, one would still be confronted with these

scale-related problems. In order to model spatial heterogeneity within the Zwalm catchment a resolution is required which in this case is too high for the Mosel basin (in terms of available data and computer power). Consequently, physics have to be described at different resolutions for the two studied areas, which automatically means different modelling concepts are required. Still, for comparative reasons the two models should contain as much similarities as possible. Rainfall-runoff modelling of the Zwalm catchment, according to the model of chapter 4, essentially comes down to the determination of the following aspects:

I. The soil moisture conditions at the beginning of an event
II. The decrease of the remaining capacity of the soil layer for absorption of incoming rainfall during an event
III. The percentage of rainfall that runs off (which is strongly related to I and II)
IV. Runoff velocities

Consequently, the response model of the Mosel basin also needs to focus essentially on these four aspects, albeit on a different scale. Fortunately, the hydrological characteristics of the Mosel basin are such, that this requirement does not conflict with the concept of runoff generation in the basin.

The HBV-model of the Swedish Meteorological and Hydrological Institute (Bergström, 1995; Killingtveit and Sælthun, 1995) has been selected to model the land-phase of the basin, while a modified version of the Muskingum-Cunge model is used to simulate river flow dynamics. Since the original HBV-model is almost fully lumped, a fully distributed version has been developed in order for the model to be applicable in the research procedure as depicted in Figure 7.5. For this purpose, the GIS-software package "PCRaster" (PCRaster, 1996) was used, as it has already proven its usefulness for making a distributed version of lumped modelling concepts (see Van Deursen and Kwadijk, 1990,1993).

Figure 7.6 presents a schematic view of a simulation run of the hydrological response model of the Mosel basin during a meteorological event. It shows that the HBV-model is also used to estimate the initial conditions in the Mosel basin. Information on initial conditions is of crucial importance for discharge predictions. Therefore, a period of 180 days before the beginning of the actual event is simulated. The selection of a period of this length is based on the experience that in the model, the hydrological state of the basin at the end of this period is insensitive to the conditions at the beginning of this period.

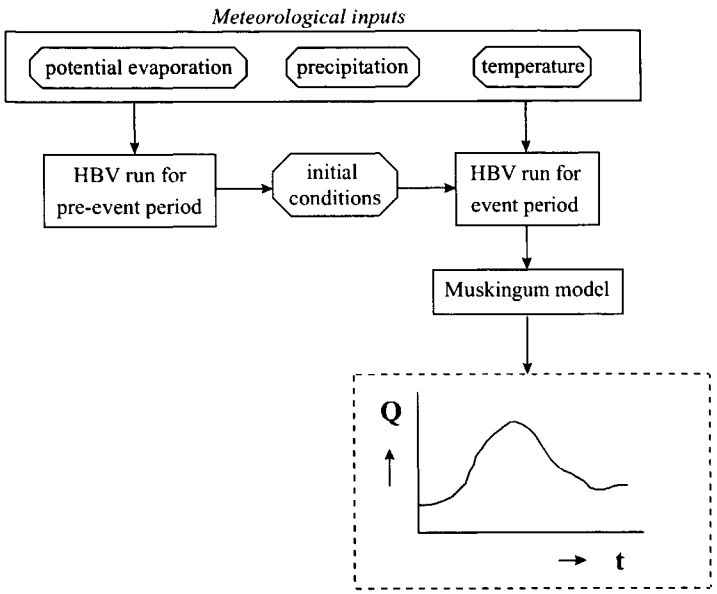

Figure 7.6 Flowchart of the hydrological response model of the Mosel basin

Sections 7.4.3 and 7.4.4 describe the model components and equations in detail. First, section 7.4.2 describes the required topographic analysis of the Mosel basin.

7.4.2 Topographic analysis

A digital elevation model (DEM) of an area of approximately 35000 km^2 containing the Mosel basin is used to derive topographic characteristics like basin boundaries, flowpaths and the location of the river network. The resolution of the original DEM is 100 m. × 100 m, i.e. the area is divided into cells of 100 m. × 100 m, and for each cell the average elevation is known. For this studies, however, an aggregated version of the DEM of 1 km^2 by 1 km^2 is used for computational purposes. Topographic characteristics have been derived through application of the same procedure as used for topographic analysis of the Zwalm catchment (see chapter 4). It consists of the following five stages:

1. Derivation of flow directions of each grid cell based on elevation differences with neighbouring cells.
2. Removal of unnatural pits from the DEM.
3. Derivation of the number of upstream contributing cells for each grid cell.
4. Identification of the location of the river network. All cells with more than N (N is a user defined number) contributing cells are marked as a river cell.

5. Derivation of basin boundaries by marking all contributing cells of the basin outlet as basin cells.

Subsequently, the accuracy of the derived locations of the river network and subbasin boundaries was evaluated through visual comparison with their true locations on topographic maps (from: CHR, 1977). In general, results were very good, except for two locations, where the model derived a completely different route for two of the tributaries of the Mosel (the Saar and the Nied-Francaise). In both cases these rivers pass through a relatively narrow, steep valley. The average elevation of the grid cells containing this valley is too high for the model to recognise the river valley. As a result, the model automatically looks for another route, which does not exist in reality. Therefore, the elevation of a number of grid cells had to be adjusted manually to create a river valley at these locations into the DEM. Subsequently, the entire procedure of deriving topographic characteristics was performed again. This time, the accuracy of the derived locations of the river network and subbasin boundaries turned out to be satisfactorily.

7.4.3 Rainfall-runoff modelling: The HBV-model

The Mosel basin is divided into a number of grid cells (27030 in total) of 1 km^2. For each of the cells individually, daily runoff is computed through application of the standard version of the HBV model, as described by Killingtveit and Sælthun [1995]. The use of the grid cells offers the possibility to turn the HBV modelling concept, which is originally lumped, into a distributed model.

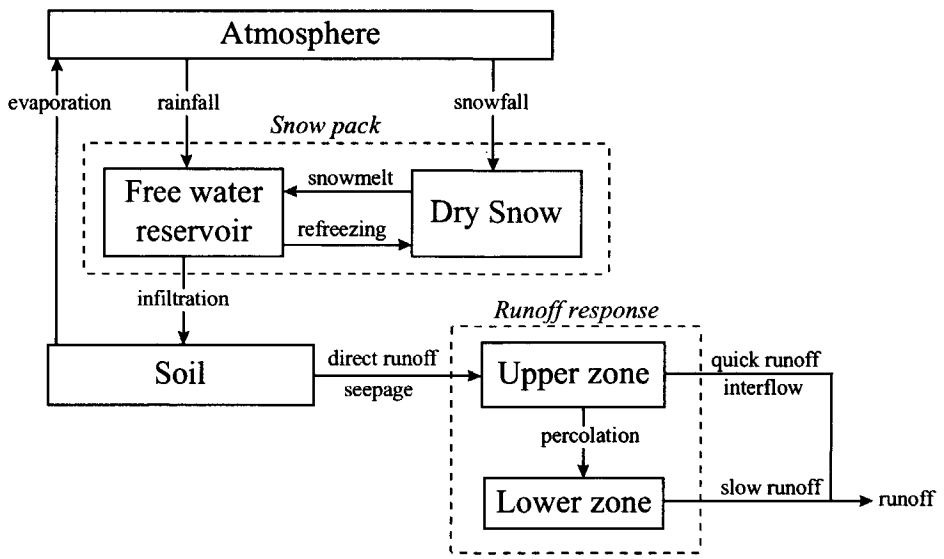

Figure 7.7 Schematic view of the relevant components of the HBV model.

Figure 7.7 shows a schematic view of hydrological response simulation with the HBV-modelling concept. The land-phase of the hydrological cycle is represented by three different components: a snow routine, a soil routine and a runoff response routine. Each component is discussed separately.

The snow routine

Precipitation enters the model via the snow routine. If the air temperature, T_a, is below a user-defined threshold T_x (≈ 0 °C) precipitation occurs as snowfall, whereas it occurs as rainfall if $T_a \geq T_x$. If precipitation occurs as snowfall, it is added to the dry snow component within the snow pack. Otherwise it ends up in the free water reservoir, which represents the liquid water content of the snow pack. Between the two components of the snow pack, interactions take place, either through snow melt (if temperatures are above a threshold T_s) or through snow refreezing (if temperatures are below threshold T_s). The respective rates of snow melt and refreezing are:

$$F_m = C_x(T_a - T_s) \quad ; T_a > T_s$$

$$F_r = C_x C_r (T_s - T_a) \quad ; T_a < T_s \tag{7.1}$$

where F_m is the rate of snow melt, F_r is the rate of snow refreezing, and C_x and C_r are user defined model parameters. The air temperature, T_a, is related to measured daily average temperatures, with additional compensation for vertical gradients (a constant temperature decrease of T_L °C per 1000 m. is assumed to exist). In the original HBV-concept, elevation differences within the catchment are represented through a distribution function (i.e. a hypsographic curve) which makes the snow module semi-distributed. In the modified version that is applied here, the temperature, T_a, is represented in a fully distributed manner, which means for each grid cell the temperature is related to the grid elevation.

The fraction of liquid water in the snow pack (free water) is at most equal to a user defined fraction, C_p, of the water equivalent of the dry snow content. If the liquid water concentration exceeds C_p, either through snow melt or incoming rainfall, the abundant water becomes available for infiltration into the soil:

$$S_{in} = \max\{(SW - C_P * SD), 0\} \tag{7.2}$$

where S_{in} is the volume of water added to the soil module, SW is the free water content of the snow pack and SD is the dry snow content of the snow pack.

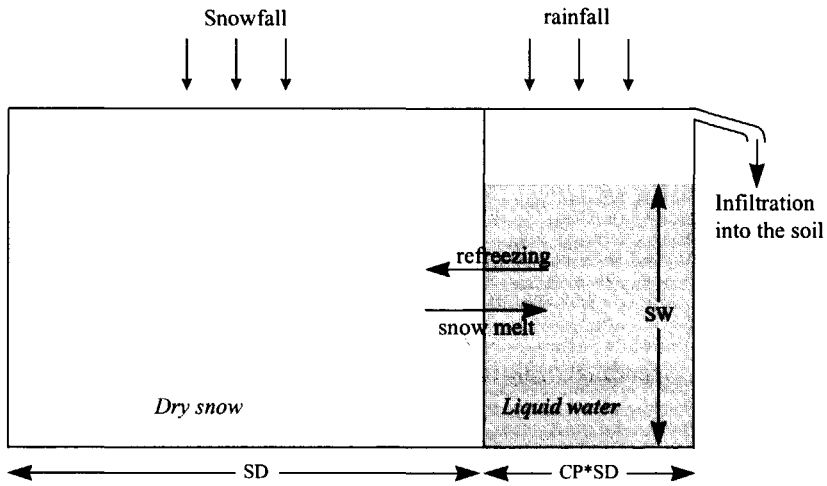

Figure 7.8 Schematic view of the snow routine

The soil routine

The incoming water from the snow routine, S_{in}, is available for infiltration in the soil routine. The soil layer has a limited capacity, F_c, to hold soil water, which means if F_c is exceeded the abundant water cannot infiltrate and, consequently, becomes directly available for runoff.

$$S_{dr} = \max\left\{(SM + S_{in} - F_c), 0\right\} \tag{7.3}$$

where S_{dr} is the abundant soil water (also referred to as direct runoff) and SM is the soil moisture content. Consequently, the net amount of water that infiltrates into the soil, I_{net}, equals:

$$I_{net} = S_{in} - S_{dr} \tag{7.4}$$

Part of the infiltrating water, I_{net}, will runoff through the soil layer (seepage). This runoff volume, SP, is related to the soil moisture content, SM, through the following power relation:

$$SP = \left(\frac{SM}{F_c}\right)^{\beta} I_{net} \tag{7.5}$$

where β is an empirically based parameter. Application of equation (7.5) implies that the amount of seepage water increases with increasing soil moisture content. The fraction of the infiltrating water which doesn't runoff, I_{net} - SP, is added to the available amount of soil moisture, SM.

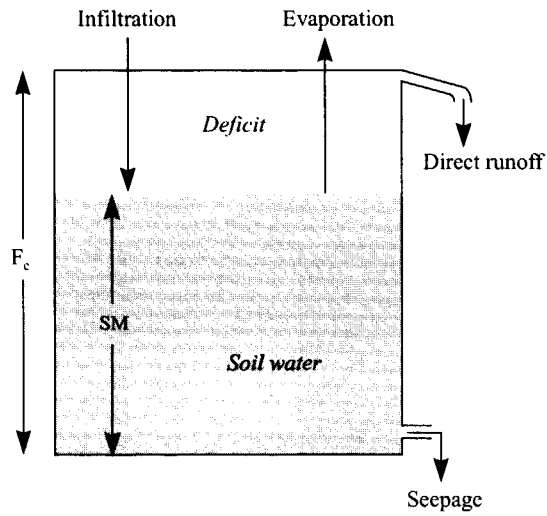

Figure 7.9 Schematic view of the soil moisture routine

A percentage of the soil moisture will evaporate. This percentage is related to the measured potential evaporation and the available amount of soil moisture:

$$E_a = \frac{SM}{T_m} E_p \quad ; SM < T_m$$

$$E_a = E_p \quad ; SM \geq T_m \tag{7.6}$$

where E_a is the actual evaporation, E_p is the potential evaporation and T_m ($\leq F_c$) is a user defined threshold, above which the actual evaporation equals the potential evaporation.

The runoff response routine

The volume of water which becomes available for runoff, $S_{dr} + SP$, is transferred to the runoff response routine. In this routine the runoff delay is simulated through the use of a number of linear reservoirs. Three types of runoff are distinguished:

1. Quick runoff
2. Interflow
3. Slow runoff (baseflow)

Two linear reservoir are defined to simulate these three different processes: the *upper zone* (generating quick runoff and interflow) and the *lower zone* (generating slow runoff). The available runoff water from the soil routine (i.e. direct runoff, S_{dr}, and seepage, SP) in

principle ends up in the lower zone, unless the percolation threshold, P_m, is exceeded, in which case the redundant water ends up in the upper zone:

$$\Delta V_{LZ} = \min\{P_m, (S_{dr} + SP)\}$$

$$\Delta V_{UZ} = \max\{0, (S_{dr} + SP - P_m)\} \tag{7.7}$$

where V_{UZ} is the content of the upper zone, V_{LZ} is the content of the lower zone and Δ means "increase of".

The lower zone is a linear reservoir, which means the rate of slow runoff, Q_{LZ}, which leaves this zone during one time step equals:

$$Q_{LZ} = K_{LZ} * V_{LZ} \tag{7.8}$$

where K_{LZ} is the reservoir constant.

The upper zone is also a linear reservoir, but it is slightly more complicated than the lower zone because it is divided into two zones: A lower part in which interflow is generated and an upper part in which quick flow is generated (see Figure 7.10).

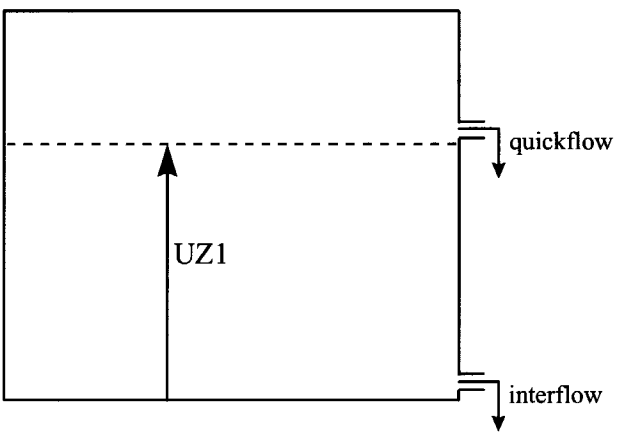

Figure 7.10 Schematic view of the Upper zone

If the total water content of the upper zone, V_{UZ}, is lower than a threshold *UZ1*, the upper zone only generates interflow. On the other hand, if V_{UZ} exceeds *UZ1*, part of the upper zone water will runoff as quick flow:

$$Q_i = K_i * \min\{UZ1, V_{UZ}\}$$

$$Q_q = K_q * \max\{(V_{UZ} - UZ1), 0\} \tag{7.9}$$

Where Q_i is the amount of generated interflow in one time step, Q_q is the amount of generated quick flow in one time step and K_i and K_q are reservoir constants for interflow and quick flow respectively.

The total runoff rate, Q, is equal to the sum of the three different runoff components:

$$Q = Q_{LZ} + Q_i + Q_q \tag{7.10}$$

The runoff behaviour in the runoff response routine is controlled by two threshold values P_m and UZ1 in combination with three reservoir parameters, K_{LZ}, K_i and K_q. In order to represent the differences in delay times between the three runoff components, the reservoir constants have to meet the following requirement:

$$K_{LZ} < K_i < K_q \tag{7.11}$$

7.4.4 River routing: The Muskingum-Cunge model

The available runoff (equation (7.10)) as derived by the distributed HBV-model serves as input of the river routing module. River routing is simulated with the Muskingum-Cunge method (Cunge, 1969), which is a modified version of the well-known Muskingum method.

Basic equations of the Muskingum model

De Muskingum-model for flow routing in rivers has been developed in the 1930's (McCarthy, 1938) and is still widely applied. The basic assumption of the model is the existence of a linear relation between the storage, S, of a river segment on one hand and the inflow, I, and outflow, O, of the segment on the other hand:

$$S_t = K[\theta I_t + (1-\theta)O_t] \tag{7.12}$$

where K and θ are parameters that represent the physical characteristics of the river segment, and t is the time index. Besides the storage-discharge equation the mass conservation law is used:

$$\frac{dS}{dt} = I_t - O_t \tag{7.13}$$

Substitution of equation (7.12) into equation (7.13) gives:

$$I_t - O_t = K\left[\theta\frac{dI_t}{dt} + (1-\theta)\frac{dO_t}{dt}\right] \tag{7.14}$$

which, after discretisation, gives:

$O_t = c_1 I_{t-1} + c_2 I_t + c_3 O_{t-1}$,with:

$$c_1 = \frac{0.5\Delta t + \theta K}{0.5\Delta t + (1-\theta)K} \quad ; c_2 = \frac{0.5\Delta t - \theta K}{0.5\Delta t + (1-\theta)K} \quad ; c_3 = \frac{-0.5\Delta t + (1-\theta)K}{0.5\Delta t + (1-\theta)K} \tag{7.15}$$

where Δt is the length of the time step of discretisation. If no lateral flow is added, the outflow, O_t, of the segment is equal to the inflow, I_t, of the segment which is situated directly downstream. Consequently, for a river branch that is made up of a number of segments which do not receive any lateral flow, flow routing can be performed through application of (7.15), if the following information is available:

- The initial state in the branch, i.e. the value of I_0 and O_0 for each segment.
- The upstream boundary condition: The value of I_t at the upstream end of the branch.

Lateral flow

In most cases, we cannot assume that no lateral flow reaches the modelled river branch. In the Muskingum model, a number of methods are available to add the lateral flow to the river system. A first, and most simple, method is to assume that all lateral flow is added at the beginning of a river segment, implying that the rate of lateral flow can be added directly to the derived incoming discharge I_t. If the assumption of concentrated lateral flow is invalid, equation (7.15) needs to be adapted. In that case it may be acceptable to assume a uniformly distributed addition of lateral flow to a river segment, which means equation (7.15) changes into:

$$O_t = c_1 I_{t-1} + c_2 I_t + c_3 O_{t-1} + c_4 \bar{q}$$

$$c_1 = \frac{0.5\Delta t + \theta K}{0.5\Delta t + (1-\theta)K} \quad ; c_2 = \frac{0.5\Delta t - \theta K}{0.5\Delta t + (1-\theta)K}$$

$$c_3 = \frac{-0.5\Delta t + (1-\theta)K}{0.5\Delta t + (1-\theta)K} \quad ; c_4 = \frac{\Delta t \Delta x}{0.5\Delta t + (1-\theta)K} \tag{7.16}$$

where $\bar{q}$ is the lateral flow per unit length. For a description and analysis of more complex methods of lateral flow modelling, the interested reader is referred to Hassanuzzaman Khan [1993].

Parameter estimation according to Cunge

In the original approach of the Muskingum method (McCarthy, 1938), parameters K and θ were estimated through calibration, based on observed inflow and outflow hydrographs. Approximately 30 years later, Cunge [1969] showed that the Muskingum method is actually a finite difference approximation of the diffusion wave equation. As a result, he was able to directly relate K en θ to physical characteristics of the river system. Since then, a number of modified versions of the Cunge's method have been developed. In this chapter, the model of Perumal [1992] is applied.

The following relation has been derived for routing parameter θ through discretisation of the diffusion wave equation:

$$\theta = \frac{1}{2} - \frac{Q_0}{2S_l Bc\Delta x} \tag{7.17}$$

where S_l is the bed slope of the segment, B is the width of the channel, c is the wave celerity, Δx is the length of the segment and Q_0 is the reference discharge. In principle, this reference discharge Q_0 is equal to the outflow of the segment, O_t, but in some cases Q_0 is taken as a constant in order to avoid having a time-dependent routing parameter θ. Instead of the diffusion wave equation, also the full St. Venants equations can be simplified to relate θ with a number of physical parameters after discretisation (Perumal, 1992):

$$\theta = \frac{1}{2} - \frac{Q_0}{2S_l Bc\Delta x}\left(1 - \frac{4}{9}F_0^{\,2}\right) \tag{7.18}$$

where F_0 is the Froude number:

$$F_0 = \frac{v}{\sqrt{gy}} \tag{7.19}$$

where v is the average flow velocity, y is the water depth and g is the gravity acceleration constant. Flow velocity v is derived through application of the Manning equation for rectangular channels:

$$v = \left(\frac{Q_0}{B}\right)^{0.4} S_l^{\,0.3} N^{-0.6} \tag{7.20}$$

where N is Manning's friction constant. From this relation it is also possible to relate the wave celerity to the flow velocity:

$$c = \frac{5}{3}v \tag{7.21}$$

The wave celerity is directly related to parameter K of the Muskingum model:

$$K = \frac{\Delta x}{c} \tag{7.22}$$

So, if the physical parameters B, S_l, N, and Δx are known for a river segment, K en θ can be derived through application of equations (7.19) t/m (7.22) in combination with either equation (7.17) or equation (7.18).

7.4.5 Differences between the applied models of the Zwalm catchment and the Mosel basin

In section 7.4.1 it was emphasised that the response models for the Zwalm and the Mosel need to contain as much similarities as possible in order to make a fair comparison possible between the derived results of the research on heterogeneity effects. For both models, rainfall-runoff simulation essentially comes down to the determination of the following aspects:

I. The soil moisture conditions at the beginning of an event
II. The decrease of the remaining capacity of the soil layer for absorption of incoming rainfall during an event
III. The percentage of rainfall that runs off (which is strongly related to I and II)
IV. Runoff velocities

Due to scale differences , it was not possible to use the same modelling concept for the Mosel basin as for the Zwalm catchment. In this section, differences between the two models are highlighted for each of the above mentioned four aspects.

Estimation of Initial soil moisture conditions

In the catchment runoff model of the Zwalm, the method of Sivapalan et al. [1987] is used to relate initial soil moisture conditions to the discharge at the catchment outlet and to local soil and topographic characteristics. Since this concept could not be applied to the Mosel basin (due to scale differences) the HBV-model is used to simulate the hydrological state of the Mosel basin during the period of 180 days which ends when the actual (high water) event of interest begins. The computed hydrological state of the basin after 180 days is used as starting condition for the simulation of the event.

Simulation of soil moisture dynamics during an event

In both models the soil is represented at the element scale as a reservoir with a given maximal capacity for soil moisture. Water is added through infiltration and leaves the soil through seepage. The main difference between the models is the fact that soil moisture loss through evaporation is simulated for the Mosel basin whereas it is neglected in the model for the Zwalm catchment. Evaporation is a strong control on initial soil moisture conditions of the event, so indirectly it can be of significant influence on the magnitude peak discharges. Since

initial soil moisture conditions for the Mosel basin are based on model simulations, the evaporation from the soil had to be considered in the response model of the Mosel basin. During high water events, however, evaporation plays a negligible role.

Estimation of runoff percentages

Although infiltration excess overland flow can occur in the model of the Zwalm, surface runoff is mainly generated on saturated parts of the catchment. Therefore, it is essential to obtain information on the percentage of fully saturated soil profiles in the catchment. This percentage is strongly related to the topographic index, ln[*a/tan(β)*], of Beven en Kirkby (Beven and Kirkby, 1979). In the model, a soil profile is fully saturated at the beginning of the event if:

$$\ln\left[\frac{a}{\tan(\beta)}\right] \geq f(z_{av} - h_c) + \lambda \tag{7.23}$$

Where a is the contributing area per unit contour length, $tan(\beta)$ is the slope of the ground surface, z_{av} is the catchment-average ground water depth, h_c is the capillary fringe, λ is the catchment-average value of ln[a/tan(β)] and f is the exponential decline parameter of hydraulic conductivity with increasing depth. Topographic index values are derived at the resolution of the cells of the DEM. For the Zwalm, the resolution of the applied DEM is 30 m, whereas for the Mosel this resolution is 1 km. Differences between these two scales with regard to the simulation of soil moisture dynamics are considerable. With the relatively fine resolution which is used for the Zwalm catchment it is possible, for example, to give a proper impression of the internal heterogeneity of an area of 1 km^2 (i.e. an area as large as one cell of the DEM of the Mosel). This is illustrated in Figure 7.11, where the spatial variability of topographic index values within an area of 1 km^2 is represented with grid cells of 30 m. × 30 m.

An area of 1 km^2 contains approximately 1000 grid cells of 30 m × 30 m, each with their own degree of saturation. In the Zwalm model, all rain falling on a fully saturated grid cell directly becomes available for runoff, whereas on an unsaturated cells most rainfall will infiltrate as long this cell is not fully saturated. The integrated response of the 1000 cells during a period of rainfall will show a gradual decrease of the remaining soil capacity and a gradual increase of the runoff percentage. Consequently, the concept of a sudden change in response behaviour of a single cell of 30 m × 30 m, which occurs in the model when it gets fully saturated, should not be applied for a grid cell of 1 km^2. Therefore the following equation, which is used for determination of the runoff percentage of a single cell in the runoff model of the Mosel basin, is more appropriate:

$$SP = \left(\frac{SM}{F_c}\right)^{\beta} I_{net} \tag{7.24}$$

where I_{net} is the rate of infiltrating water, SP is seepage, SM is the soil moisture content, F_c is the maximum soil moisture storage in the soil layer and β is an empirically based parameter.

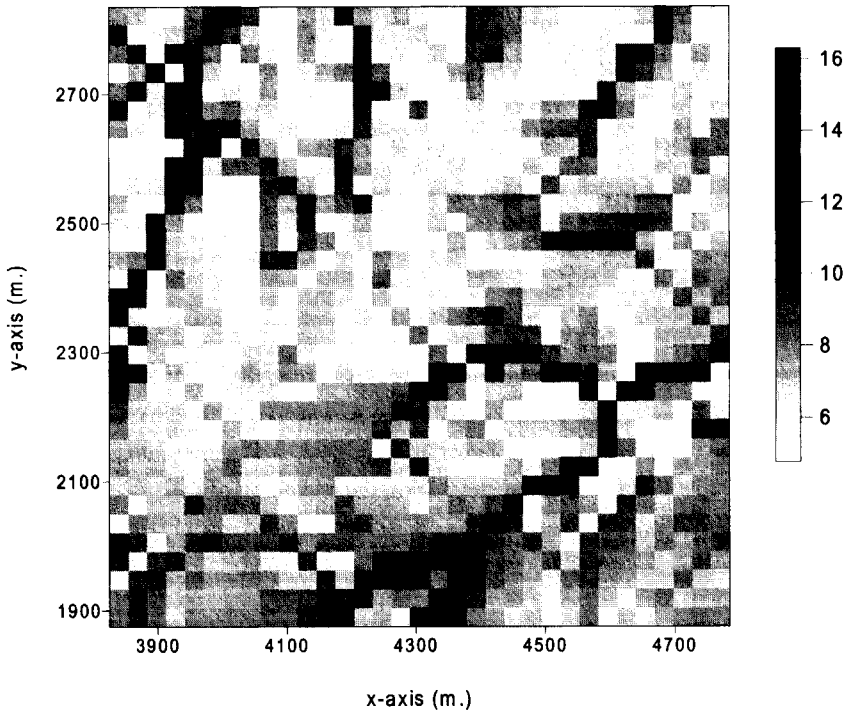

Figure 7.11 Topographic index values (ln[a/tan(β)]) for an area of 1 km^2 in the Zwalm catchment.

Routing

The Manning equation is applied for surface runoff routing in the Zwalm catchment. Furthermore, flow routing through the Zwalm river is realised with a simple power relation between flow velocity and discharge. During intense storm events, the time difference in the peak of the rainfall and the discharge peak at the catchment outlet is in the order of magnitude of 3 to 4 hours. Since the response model of the Mosel basin uses daily time steps, a complete peak event can occur during one time step in a subcatchment of the Mosel basin with the size of the Zwalm catchment. As a consequence, these small scale peak events cannot be reproduced within the response model of the Mosel basin. Therefore, no detailed hillslope runoff routing module has been applied for the Mosel basin. Instead, hillslope runoff routing is simulated with a reservoir (the upper zone), which is divided in two compartments: One for interflow generation and one for quick flow generation. In this way, the dynamic,

non-linear behaviour of hillslope runoff can be reproduced to a large extent. Furthermore a different river routing models have been applied for the Zwalm river and the Mosel river because of the obvious differences in river dimensions.

7.5 Calibration and validation

7.5.1 Parameters of the HBV-model

Killingtveit and Sælthun [1995] present default values and ranges of the parameters of the HBV-model, based on calibrated values from other applications of the model (see Table 7.1).

		From: Killingtveit and Sælthun, 1995		
Name	Unit	Range	Default	Mosel basin
T_x	°C	-1.0-2.0	1.0	0
T_s	°C	-1.0-2.0	0.0	0
T_L	°C km^{-1}	4-10	6	6
C_x	mm day^{-1} °C^{-1}	3.0-6.0	4.0	4
C_r	-	0.0-0.01	0.005	0.005
F_c	mm	75-300	150	0-580
T_m	mm	70%-100% of F_c	100% of F_c	80% of F_c
β	-	1.0-4.0	2.0	3.0
P_m	mm day^{-1}	0.5-1.0	0.6	0.6
UZ1	mm	10-40	20	20
K_{LZ}	day^{-1}	0.0005-0.002	0.001	0.01
K_i	day^{-1}	0.05-0.15	0.1	0.1
K_q	day^{-1}	0.1-0.5	0.3	0.3

Table 7.1 Parameter values of the HBV-model.

These default values serve as a basis for the parameters in this research. However three parameters have been calibrated: F_c (Field capacity), β (the parameter controlling runoff percentages) and K_{LZ} (the base flow recession constant). Parameters F_c and β were selected because the sensitivity of the model to changes in parameter values is highest for these two parameters and K_{LZ} was selected because it can be easily derived from the shape of hydrograph recession curves. The resulting parameter values are presented in the last column of Table 7.1. In case of parameter F_c, a range is given instead of a single selected value. This means this parameter is actually represented in a spatially distributed manner. Soil maps with a resolution of 1 km are available for the Mosel basin and for all present soil types the water holding capacity *per meter depth* is known. So, in order to know the water holding capacity of the whole layer, the depth of the layer, D_L has to be known. Therefore, the value of D_L has been used as the calibration parameter for field capacity F_c.

7.5.2 River routing

Results of the river routing module showed some major inconsistencies with the observed hydrographs. The computed wave celerity turned out to be too high during high water events and too low during periods of low flow. In the river routing component the flow velocity and the wave celerity are derived as follows (see equations (7.20) and (7.21)):

$$v = \left(\frac{Q_0}{B}\right)^{0.4} S_l^{\,0.3} N^{-0.6} \tag{7.25}$$

$$c = \frac{5}{3} v \tag{7.26}$$

where v is the flow velocity, Q_0 is the reference discharge, B is the width of the channel, S_l is the bed slope of the segment, N is Manning's friction constant and c is the wave celerity. The power function of equation (7.25) causes a variation in the computed flow velocities that is substantially larger than the variation in observed velocities. This is due to the assumption of a rectangular channel (on which equation (7.25) is based) since this is too much a violation of reality. Especially during high water events, differences between computed and measured velocities are found. During high water events the flood plains are inundated, which causes a significant decrease of average flow velocities, especially in the French part of the Mosel basin where the river valley is relatively wide. In the model, however, an increase of the discharge (see equation (7.25)) only leads to a further increase of flow velocities. The geometry of the river network and its floodplains should therefore preferably be modelled in a more detailed manner. In that case, however, a much more complicated hydrodynamic model is required to be able to reproduce the effects of the inundation of the flood plains on the wave celerity in the river system. Since there was insufficient information on the geometry available to carry out such an approach, a much simper approach has been applied, in which the wave celerity, c, is related to the specific discharge as follows:

$$c = \begin{cases} 1 + 0.25q & ; q \le 4 \\ 2 & ; 4 < q \le 8 \\ 2 - 0.25(q-8) & ; 8 < q \le 12 \\ 1 & ; q > 12 \end{cases} \tag{7.27}$$

where q is the specific runoff (in: mm/day) in the river segment. This function, graphically shown in Figure 7.12, is selected after extensive analysis of the wave propagation in the river system. Since the only purpose of the routing model is only to simulate wave propagation, equation (7.27) is considered to be applicable here. However, one should not put a high value on its physical significance.

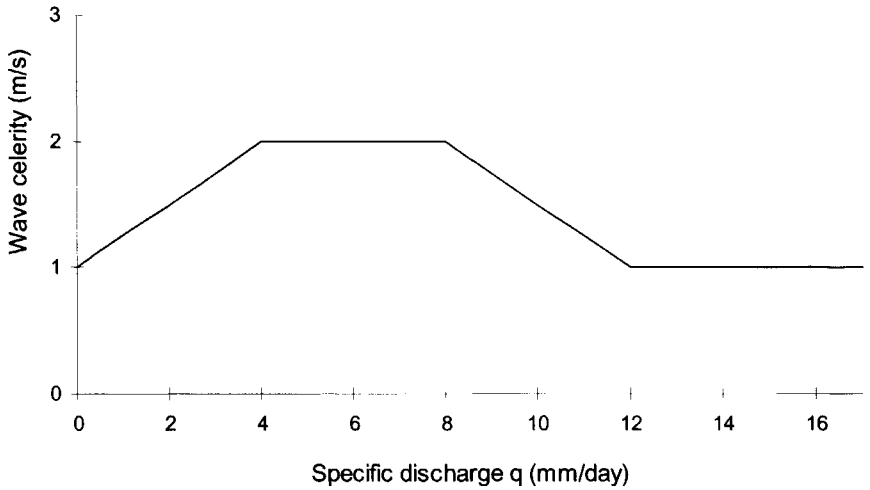

Figure 7.12 Wave celerity as a function of specific discharge

Model performance

The combined land-phase runoff and river routing model has been applied to a number of high water events. Furthermore, for every event the model also has been applied to a period of 180 days preceding the event. This period of 180 days is modelled for two reasons:

1. To derive initial soil moisture conditions of the high water event
2. To check the validity of the model under conditions, other than the (extremely) wet conditions of the high water events

Figure 7.13-Figure 7.20 display observed and computed hydrographs for four high water events (December 1993, May 1983, January 1995 and December 1981/January 1982) and their preceding periods. The simulated periods contain the five highest observed runoff peaks at Cochem in the period of 1971-1995 (The fourth highest peak discharge, which occurred in April 1983, is shown in Figure 7.15 where the pre-event period of the high water event of May 1983 is displayed). The peak of December 1993 is even the highest observed since the beginning of measurements at Cochem in 1817 (Engel, 1998). Figure 7.13-Figure 7.20 show that results of the model are good. In general, the computed hydrograph follows the pattern of the observed hydrograph. The main notable difference is the smoothness of the computed hydrograph in comparison with the observed hydrograph, i.e. the small scale peaks could not be simulated into detail. The main cause for this difference is the fact that daily average precipitation values form the model input, which cause the output to be smoother than would have been the case for hourly precipitation values.

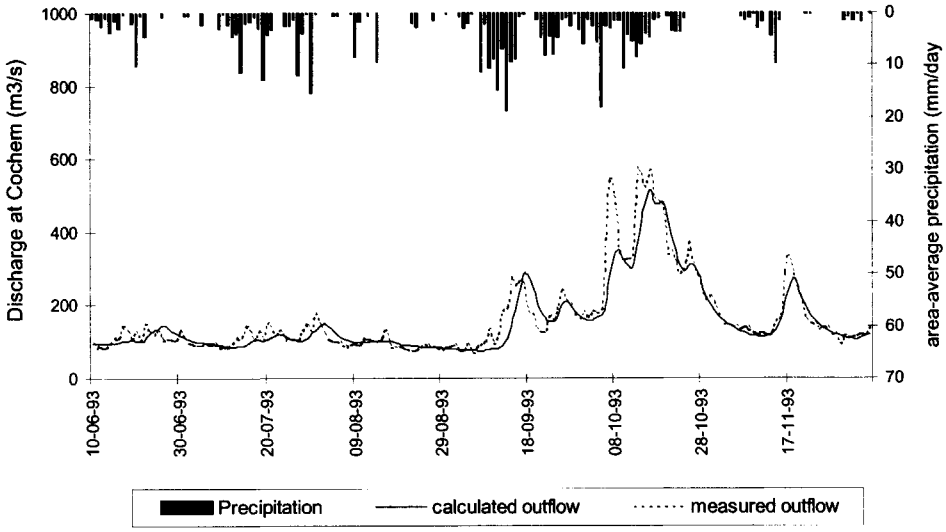

Figure 7.13 Observed and computed discharge in the river Mosel at Cochem from 10-06-1993 until 06-12-1993.

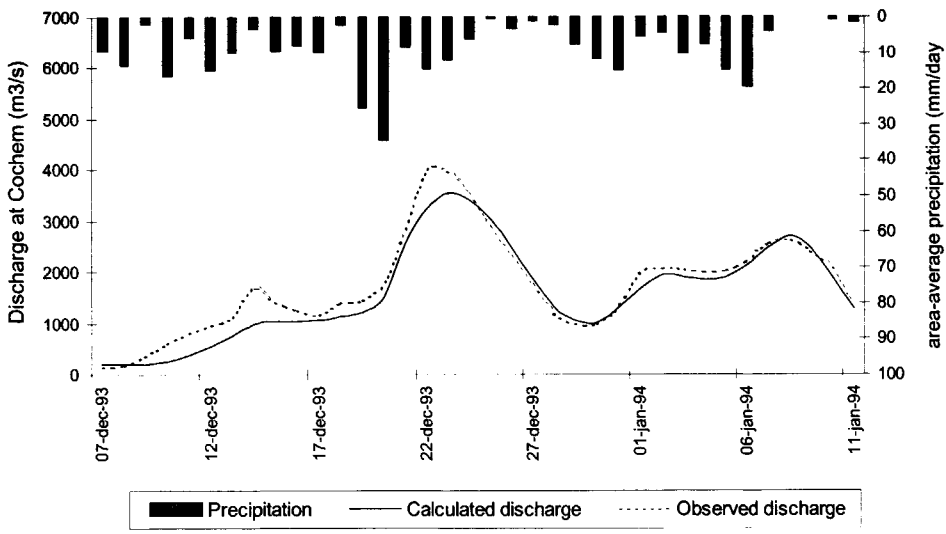

Figure 7.14 Observed and computed discharge in the river Mosel at Cochem during the high water event of Dec. 1993

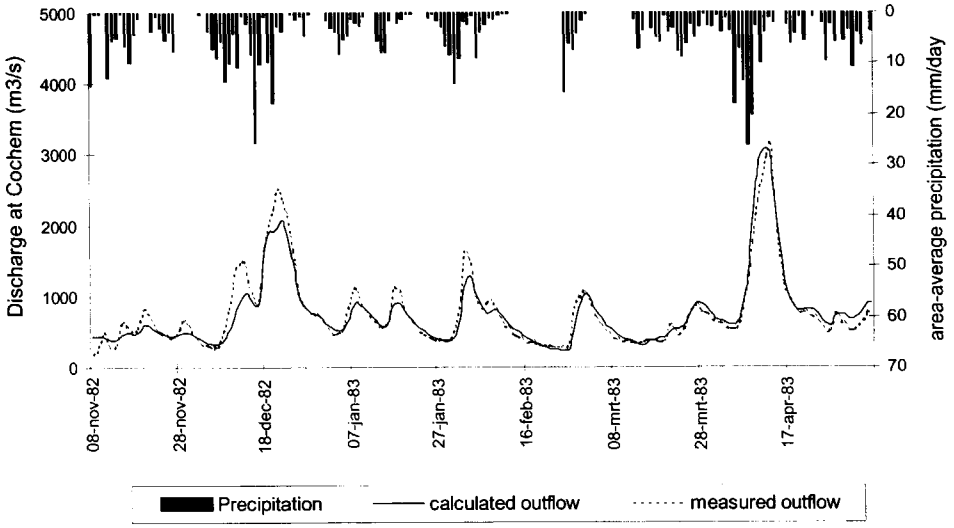

Figure 7.15 Observed and computed discharge in the river Mosel at Cochem from 08-11-1982 until 06-05-1983

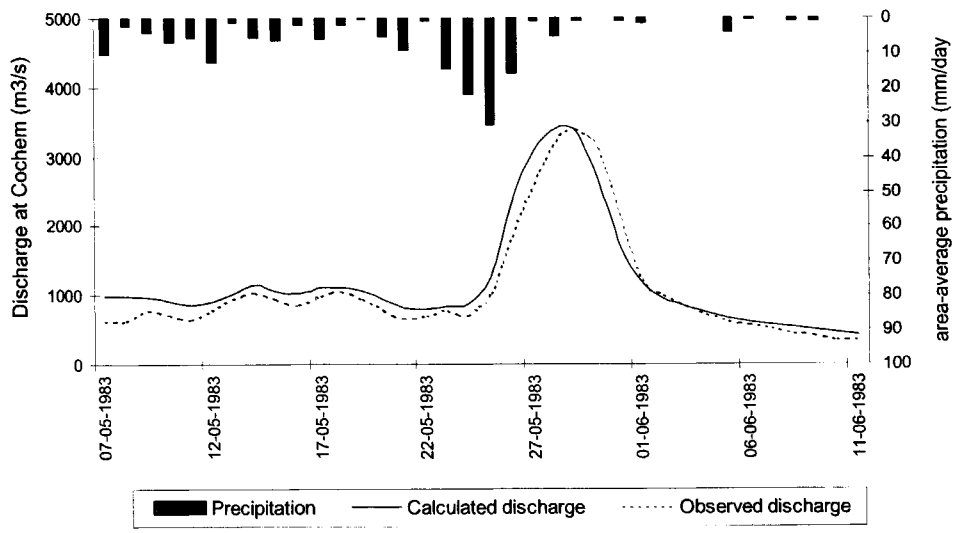

Figure 7.16 Observed and computed discharge in the river Mosel at Cochem during the high water event of May 1983

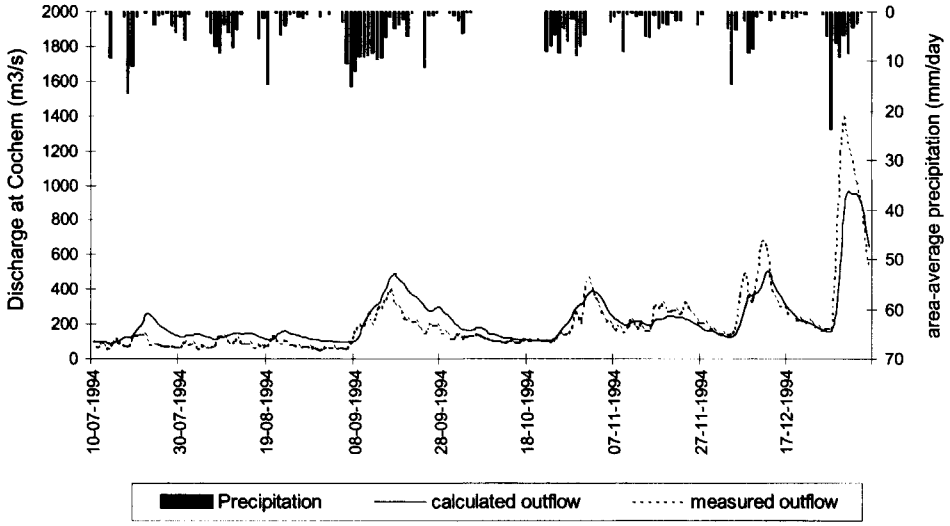

Figure 7.17 Observed and computed discharge in the river Mosel at Cochem from 10-07-1994 until 05-01-1995

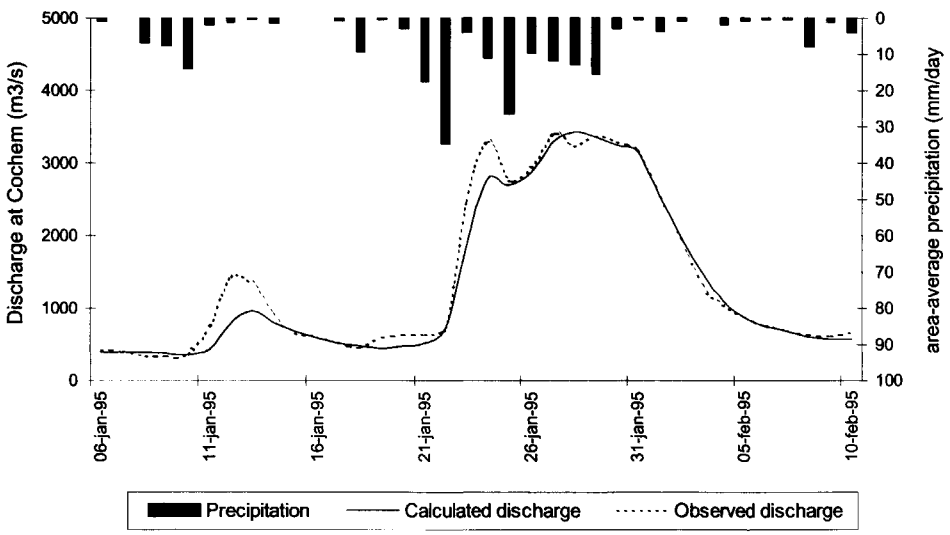

Figure 7.18 Observed and computed discharge in the river Mosel at Cochem during the high water event of Jan. 1995

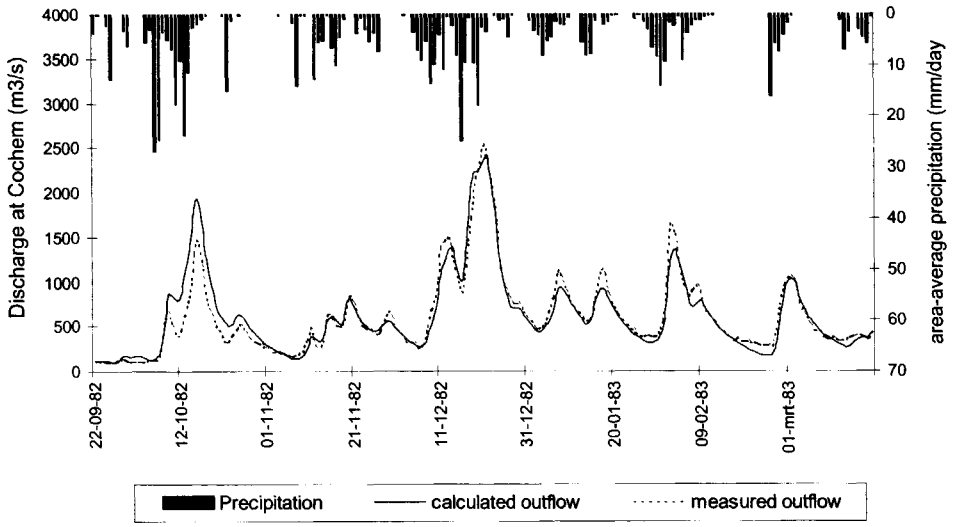

Figure 7.19 Observed and computed discharge in the river Mosel at Cochem from 25-06-1981 until 21-12-1981

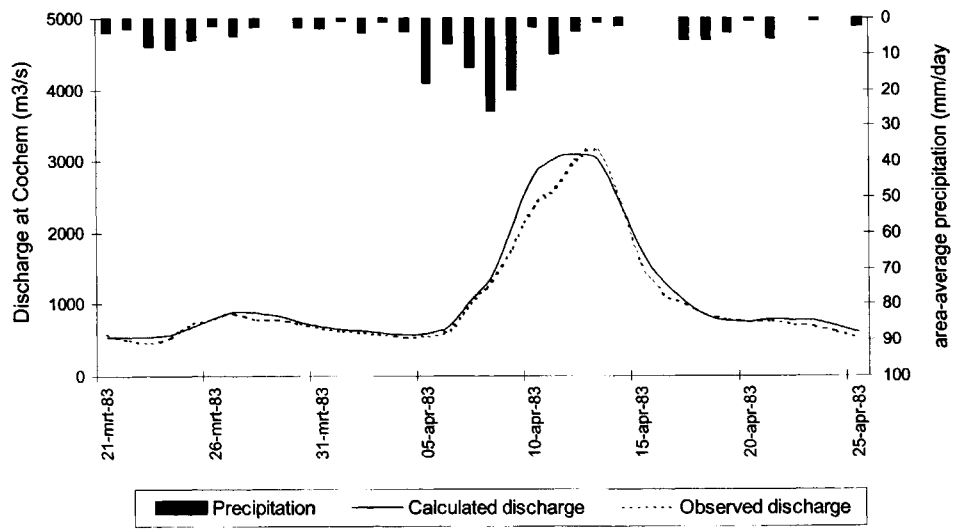

Figure 7.20 Observed and computed discharge in the river Mosel at Cochem during the high water event of Dec. 1981/Jan. 1982

7.6 Quantification of heterogeneity effects

7.6.1 Precipitation

Nine events have been simulated to assess the effects of spatial heterogeneity of precipitation on the response of the Mosel basin. As explained in section 7.2 and schematically depicted in Figure 7.5, two different procedures have been applied in order to make a distinction between heterogeneity effects being the cause of modelling errors on one hand and errors in estimating rainfall volumes on the other hand. Two measures are used to quantify the model performance as a function of the used number of model elements:

$$MSE_1(n) = \frac{1}{T}\sum_{t=1}^{T}\left[d_n(t) - dm(t)\right]^2 \tag{7.28}$$

$$MSE_2(n) = \frac{1}{T}\sum_{t=1}^{T}\left[d_n(t) - dd(t)\right]^2 \tag{7.29}$$

where both $MSE_1(n)$ and MSE_2(n) reflect the mean square error as a function of the number of model elements (n), T is the number of time steps used in the simulation, d_n(t) is the computed discharge at time t of the model as a function of the number of model elements (n), dm(t) is the observed discharge at t and dd(t) is the discharge at time t, derived with the fully distributed model. Consequently, $MSE_1(n)$ quantifies deviations from the observed hydrograph whereas MSE_2(n) quantifies deviations from the resulting hydrograph of the fully distributed model.

Results of procedure I

Procedure I compares the performance of a lumped version of the model of section 7.4 with more distributed model versions. In this case the words "lumped" and "distributed" refer to the extent in which spatial information of *precipitation* is represented in the model. Naturally, effects of heterogeneity of precipitation on the basin response depend strongly on the characteristics of the event under consideration. As a consequence, the results of the procedure vary from event to event. Still, it turned out that for all investigated events the distributed model version generated closer approximations to the observed hydrograph than the lumped model version. Figure 7.21, for instance, shows that for the event of April 1983 the mean square error (more specifically: $MSE_1(n)$ of equation (7.28)) clearly decreases with increasing value of n, especially for small values of n. For values of $n \geq 4$, the mean square error stays more or less constant, suggesting that the spatial variability of precipitation during this event can be properly represented by using only 4 model elements. Figure 7.22 shows that $MSE_2(4)$ is relatively close to zero which means that the computed hydrograph for n=4 is indeed almost completely converged to the hydrograph, derived with the fully distributed

model. Differences between these two computed hydrographs are relatively small compared to their respective deviations from the measured hydrograph (i.e.: $MSE_2(4)$ is small compared to $MSE_1(4)$). If less than 4 model elements are used, relevant information on spatial patterns is lost during the averaging procedure. Figure 7.23 depicts the observed hydrograph in combination with the computed hydrographs of both the fully lumped model version and the fully distributed model version. It shows that the resulting peak of the lumped model is too high and occurs too early. This is due to the fact that during the event of April 1983, the majority of the rain fell relatively far away from the basin outlet, which means the average travel distance in the river network was relatively long. In the lumped model version this aspect is not considered as a result of the averaging procedure, which means both the time-to-peak and the flood wave attenuation are underestimated.

Not for all events the results of the distributed model were clearly better than those of the lumped model. Figure 7.24 for instance, shows that for the event of December 1981/January 1982, the model performance is almost completely insensitive to the amount of spatial information which is used in the model. For this event the precipitation is more evenly spread over the basin in comparison with the event of April 1983. Consequently, changes in computed hydrographs due to alterations of the applied number of model elements (n) are only small (see the difference in magnitude of the mean square error values between Figure 7.22 and Figure 7.25). Furthermore, the model performance for this event was not as good as for other events (compare Figure 7.26 with Figure 7.14, Figure 7.16, Figure 7.18 and Figure 7.20) which also contributes to the fact that the gain of using a distributed model instead of a lumped model is negligible for this event.

For the five highest peak runoff events of the period 1971-1995, the use of about 4 elements seems to be sufficient to represent the present heterogeneity of precipitation depths. The mean square error of the model version with 4 elements is at most 20 % larger than the mean square error of the fully distributed model. Simulation results for two moderate peak events, however, show that this is not generally the case. For the event of November 1972, for instance, the 20 %-"criterion" is only met if the model is divided into 12 or more elements. The event of November 1972 was selected for simulation because of its extreme spatial variability in generated runoff volumes. In the upstream part of the Mosel river basin discharges have been observed which belong to the highest of the 25-year series considered. However, runoff contributions from downstream parts of the basin were such that the peak discharge in Cochem was just about 1500 m^3/s, which is only 37% of the peak discharge of December 22nd 1993. Particularly for events with these large spatial differences, a catchment runoff model benefits from a more spatially distributed representation of precipitation amounts. For the most extreme high water events, however, it can be expected that significant contributions come from all parts of the basin. Consequently, the spatial variation of these events is such that its main aspects can be captured to a large extent by using in the order of 4 model elements.

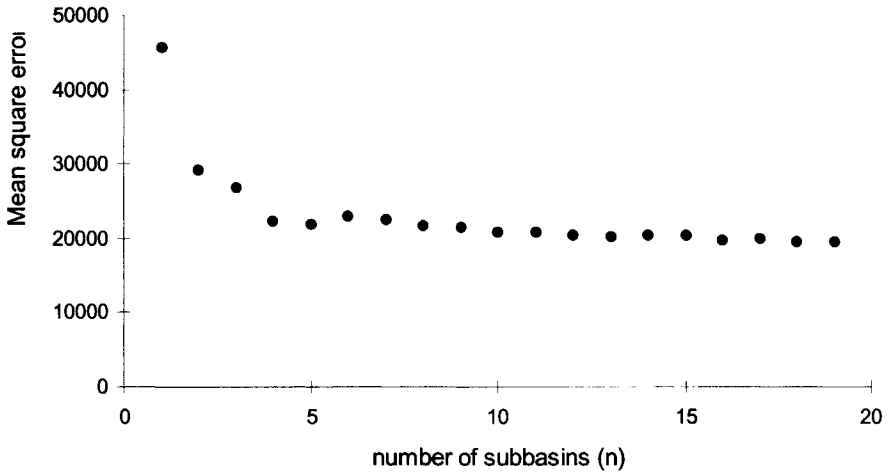

Figure 7.21 Mean square error values (related to the *observed discharge*, see equation (7.28)), of the Mosel runoff simulation model when the Mosel basin is divided into *n* subbasins and precipitation is averaged on these subbasins; High water event of April 1983.

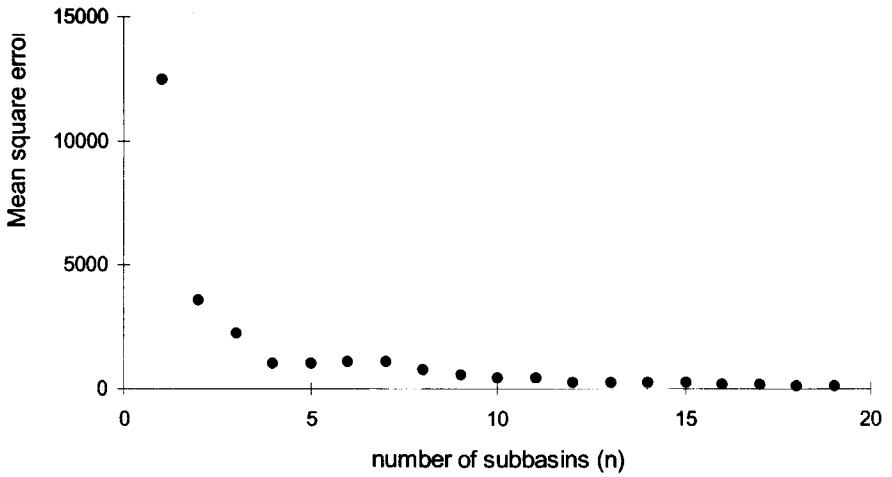

Figure 7.22 Mean square error values (related to the *resulting hydrograph of the fully distributed model*, see equation (7.29)), of the Mosel runoff simulation model when the Mosel basin is divided into *n* subbasins and precipitation is averaged on these subbasins; High water event of April 1983.

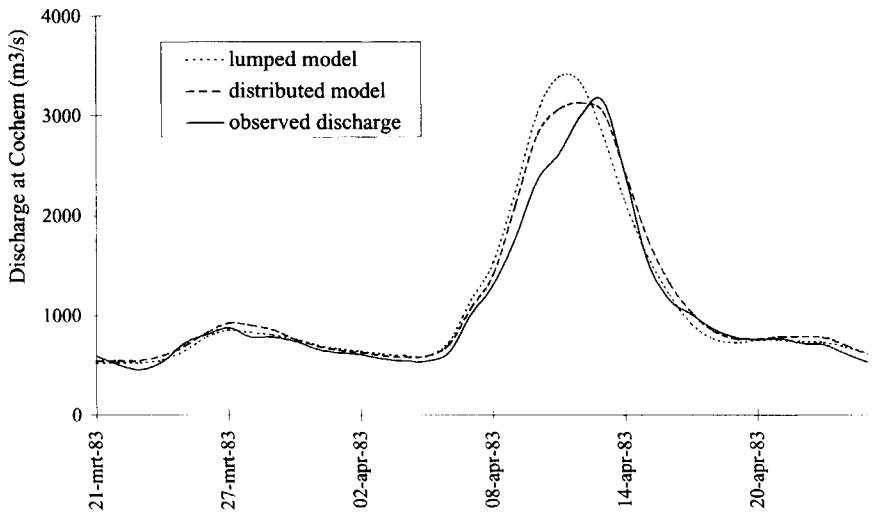

Figure 7.23 Comparison of model performance of a distributed and a lumped runoff simulation model of the Mosel; High water event of April 1983.

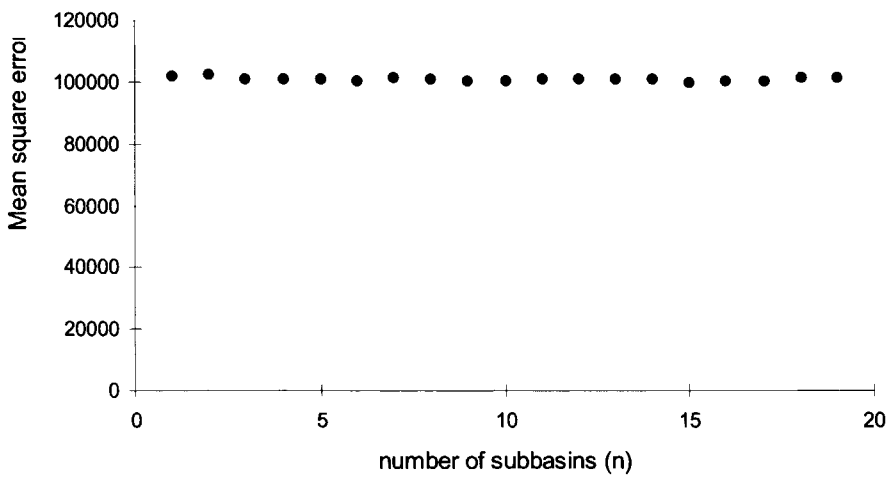

Figure 7.24 Mean square error values (related to the *observed discharge*, see equation (7.28)), of the Mosel runoff simulation model when the Mosel basin is divided into n subbasins and precipitation is averaged on these subbasins; High water event of Dec. 1981/ Jan. 1982.

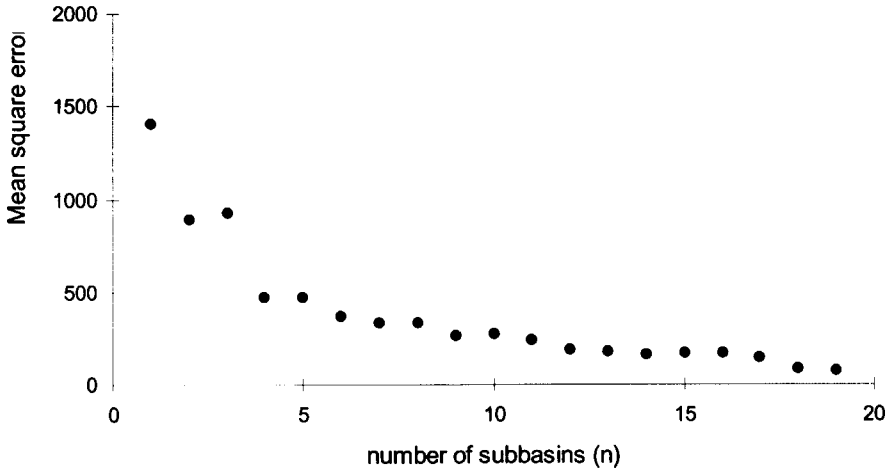

Figure 7.25 Mean square error values (related to the *output of the fully distributed model*), of the Mosel runoff simulation model when the Mosel basin is divided into *n* subbasins and precipitation is averaged on these subbasins; High water event of Dec. 1981/ Jan. 1982.

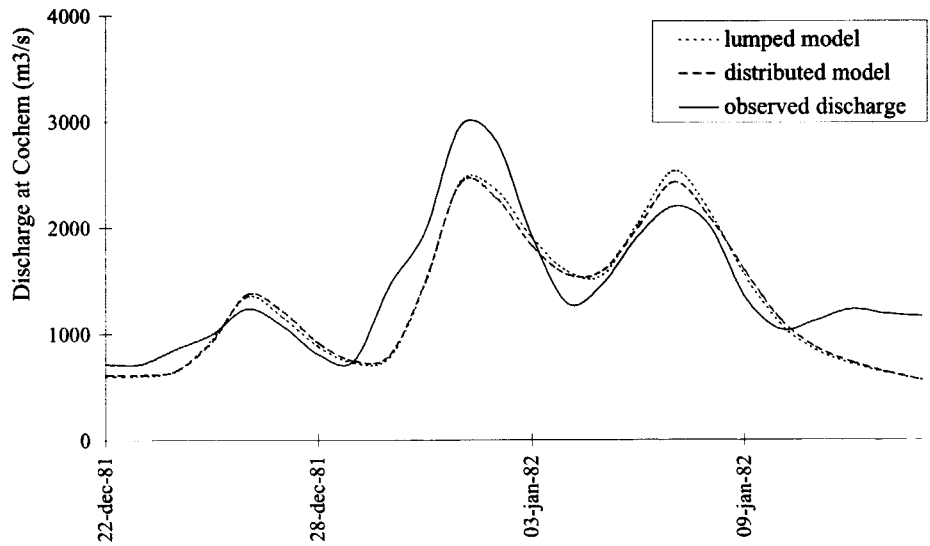

Figure 7.26 Comparison of model performance of a distributed and a lumped runoff simulation model of the Mosel; High water event of Dec. 1981/ Jan. 1982).

Results of procedure II

Procedure II assesses the efficiency of different densities of the raingauge network in the Mosel basin. For a number of values of n, the precipitation pattern of the entire basin is estimated through spatial interpolation of measured volumes of n well-spread raingauges. This gives an idea of the minimum amount of raingauges needed to be able to generate satisfying predictions of the discharge in the Mosel river basin during high water events. Again, as with procedure I, results vary from event to event. The main noticeable difference with procedure I is that for small values of n the mean square error values are often substantially larger. This is in agreement with the findings of chapter 6 for the Zwalm catchment, where it was found that taking spatial variability of rainfall intensities into account is of more importance in the measuring process than in the modelling process.

A good example that shows the influence of the density of the raingauge network is presented in Figure 7.27, where the measured hydrograph of the high water event of January 1995 is compared with computed hydrographs resulting from the use of [a] 1 raingauge [b] 2 raingauges [c] 10 raingauges and [d] the available 81 raingauges. Figure 7.27 shows that, as confirmed by results of other events, the use of one or two raingauges is not enough to obtain reliable estimates of the incoming precipitation in the Mosel basin. If only one raingauge is used the model predicts a peak discharge which is only 40% of the actual peak discharge. The raingauge that is used is the most centrally located raingauge in the Mosel basin, while during this event extreme precipitation amounts mainly occur in the Northern and Southern part of the basin. As a consequence, the model generates a poor prediction of the observed peak discharge. If two raingauges are used instead of just one, the performance of the model already improves significantly. In that case, one raingauge is located near the centre of the Northern half of the basin while the other station is located near the centre of the Southern half of the basin. As a consequence, both stations are located in the areas where the extreme precipitation takes place. Still, though, the resulting predictions are inferior to predictions that result from a precipitation input which is based on observations from the available 81 raingauges. Naturally, the quality of predictions improves if the number of raingauges increases. From Figure 7.27 it can be seen that for this event a close approximation of the predicted hydrograph which results from the use of the available 81 raingauges is already realised by using a set of only 10 well-spread raingauges.

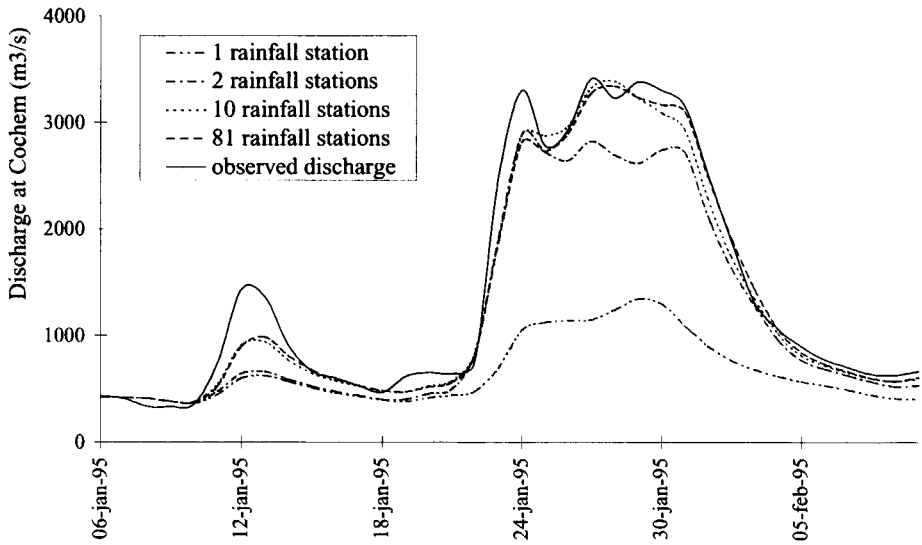

Figure 7.27 Comparison of the observed hydrograph with computed hydrographs, resulting from the use of [a] 1 raingauge [b] 2 raingauges [c] 10 raingauges and [d] the available 81 raingauges; High water event of January 1995.

Another noticeable difference between the results of procedure I and procedure II is the manner of decrease of prediction errors with increasing value of n. The results of procedure I showed a more or less monotone decrease of prediction error with increasing value of n. In other words, the model performance improves if more information on spatial patterns of precipitation are represented in the model. For procedure II, there is also a trend of decreasing prediction errors with increasing value of n, but this decrease is far from monotone. So, although an increase of the number of raingauges generally leads to an improvement of the model performance, it is by no means a guarantee for it. Obviously, a factor of coincidence plays a more significant role in procedure II than in procedure I. Due to the choice of locations of rain gauges it may be that, for instance, a set of 6 raingauges offers a more accurate estimation of the actual basin average precipitation than a set of 8 raingauges. To eliminate this effect as much as possible, mean square errors have been averaged over the nine simulated high water events. Results are shown in Figure 7.28. For small values of n, this Figure shows a sharp decrease of the average prediction error with increasing value of n. For values of $n \geq \pm 10$, on the other hand, the mean square error is more or less constant. So, for the Mosel, a network of 10 well-spread raingauges suffices to obtain reliable estimates of the basin-average rainfall. Compared to the use of the full set of available raingauges (85 in function on average) the use of 10 well-spread raingauges will lead to an increase of the mean square error of only 2%.

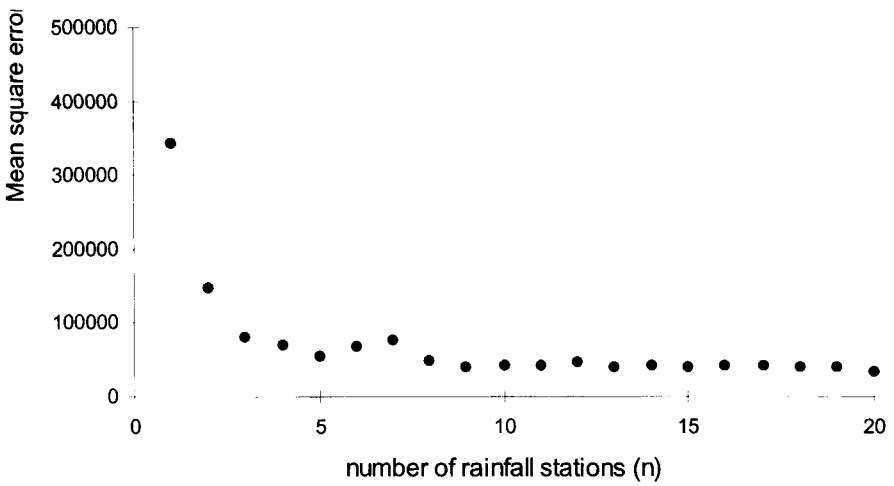

Figure 7.28 MSE-values (related to the output of the fully distributed model), of the runoff model when the precipitation input is obtained from only n raingauges; Combined result from nine high water events.

7.6.2 Initial conditions

Effects of spatial heterogeneity of initial soil moisture conditions on the resulting basin response during high water events have been analysed through application of procedure I (see Figure 7.6). The only difference in comparison with the analysis of heterogeneity effects of precipitation is, of course, the averaging procedure. For this particular purpose the spatial average value of the following 6 entities are derived for each subbasin:

- The water content of the five model reservoirs (i.e. dry snow, free water, soil moisture, upper zone and lower zone)
- The capacity, F_c, of the soil layer to hold soil water.

Subsequently, all concerning parameters and variables of all grid cells within a subbasin are set equal to the derived subbasin-average values. As a result of the averaging procedure, spatial differences of initial conditions within the subbasin no longer exist, while conditions for the subbasin as a whole haven't changed.

For each of the nine investigated events it turned out that the possible gain of representing spatial heterogeneity of the antecedent conditions in modelling peak discharge events is only marginal. For some events, the lumped model version even generated slightly better results than the distributed model version.

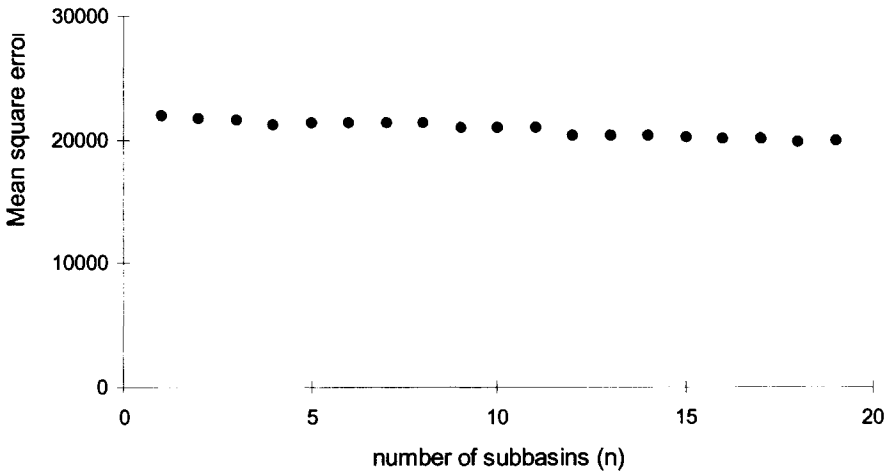

Figure 7.29 Mean square error values (related to the *observed discharge*, see equation (7.28)), of the Mosel runoff simulation model when the Mosel basin is divided into n subbasins and antecedent soil moisture conditions are averaged on these subbasins; High water event of April 1983.

Figure 7.29 shows result for the event of April 1983, which are representative for all investigated events. It demonstrates that the model performance is almost completely insensitive to the amount of spatial information on initial soil moisture conditions which is used in the model. It has to be stated that this is partly due to the applied definition of the beginning of the simulated high water events. Meteorological events which cause peak discharges to occur in the Mosel river are generally made up of a period of about 1-2 weeks of above-average precipitation, followed by a few days of extreme precipitation. (see chapter 5). For each simulated peak discharge, the complete meteorological events had to be considered. This implies that the time lag between the occurrence of conditions which were labelled as initial conditions and the actual peak discharge was always in the order of magnitude of 15-20 days. If the definition of the beginning of the high water events is changed in such a way that this time-lag decreases, the gain of modelling spatial heterogeneity of initial conditions can be expected to increase.

7.7 Conclusions

A combined rainfall-runoff and river routing model has been developed for the 28152 km^2 Mosel basin, which covers parts of France, Germany and Luxembourg. The model performance in terms of simulation results were satisfactorily. Subsequently, the effects of spatial heterogeneity on the integrated runoff response of the Mosel basin were investigated by performing a number of model runs in which the available information on spatial heterogeneity is represented to different extents. It turned out that, in contrast to the results for the 114 km^2 Zwalm catchment, it does pay off to take the spatial heterogeneity of precipitation into account in the rainfall-runoff model of the Mosel basin. For each investigated event, the distributed model version generated closer approximations to the observed hydrograph than the lumped model version. Among the simulated events were the five highest observed peak runoff events at Cochem in the period of 1971-1995. For these events the use of 4 model elements, each with its own spatially averaged precipitation, was sufficient to capture the main aspects of the spatial heterogeneity of precipitation to a large extent. However, simulations of the event of November 1972 (a moderate peak event, mainly generated in the Southern part of the basin) showed that this is not always the case. Still, for the most extreme high water events it can be expected that significant contributions come from all parts of the basin. Consequently, the spatial variation of these events is such that its main aspects can be captured to a large extent by using in the order of 4 model elements.

Furthermore, it has been investigated which spatial coverage of the raingauge network is required in order to provide a satisfying model predictions. For a number of values of n, the precipitation pattern of the entire basin is estimated through spatial interpolation of measured volumes of n well-spread raingauges. If only 1 or 2 rainfall stations were used, the deviations of the predicted hydrographs from the observed hydrographs were usually substantially larger than deviations caused by lumping of precipitation in the model. This is in agreement with the findings of chapter 6 for the Zwalm catchment, where it was found that taking spatial variability of rainfall intensities into account is of more importance in the measuring process than in the modelling process. As expected, an increase of the number of raingauges generally leads to an improvement of the model predictions, but it is by no means a guarantee for it. It may occur that, for instance, a set of 6 raingauges by coincidence offers a more accurate estimation of the actual basin average precipitation than a set of 8 raingauges even when in both cases an optimal spreading of raingauges is realised. Still, in spite of the coincidence-factor, it could be shown that for the Mosel basin, a network of 10 well-spread raingauges suffices to obtain reliable estimates of the areal precipitation. Compared to the use of the full set of available raingauges (±85 on average) the use of 10 well-spread raingauges lead to an increase of the mean square error of only 2% in the model predictions.

Finally, the possible gain of representing spatial heterogeneity of the antecedent conditions in modelling peak discharge events has been analysed. It turned out that this gain was only marginal, although it has to be stated that this is partly due to the applied definition of the beginning of the simulated high water events.

8. Conclusions and recommendations

This PhD. research project was set up to investigate the possibilities of a physically based approach towards flood frequency analysis. The research mainly focuses on the hydrological aspects of physically based flood frequency analysis, i.e. the meteorological aspects were only a side issue. The two central issues of the thesis are:

1. Which processes and parameters are dominant under (extremely) wet conditions and should therefore be represented on a physically meaningful way in a rainfall-runoff model?
2. What model complexity is required to represent the spatial heterogeneity of these parameters and processes?

The 114 km^2 Zwalm catchment (Belgium) and the 28152 km^2 Mosel basin (covering parts of France, Germany and Luxembourg) served as pilot area throughout this thesis.

Dominant processes and parameters

In general, three types of mechanisms are recognised to be responsible for the relatively fast transport of rainfall water towards the stream network during storm events:

1. Infiltration excess overland flow.
2. Saturation overland flow.
3. Subsurface storm flow.

For each storm flow process, a number of factors are known to enhance the occurrence of the process during storm events:

1. *Infiltration excess overland flow*: Impermeable soils, no vegetation, high rainfall intensities.
2. *Saturation overland flow*: Shallow, moderately permeable soils, concave-shaped hills, wide valley bottoms.
3. *Subsurface storm flow*: Steep straight slopes, deep permeable soils, forests, narrow valley bottoms.

Consequently, the processes and parameters which are dominant under (extremely) wet conditions are strongly catchment specific. Still, it is widely recognised that in vegetated catchments with humid climatic conditions (which cover a major part of Western Europe) a large proportion of stream runoff originates from the saturated areas of the catchment, mainly

to be found adjacent to the stream network. Consequently, the percentage of saturated soil profiles is a dominant control of the runoff percentages during a storm event, as demonstrated by a sensitivity analysis of the TOPMODEL concept, applied on the Zwalm catchment. For these type of catchments, it is therefore recommended against the use of models that do not explicitly take into account the varying size of these saturated source areas.

For the Zwalm catchment, four parameters were identified to which the model is most sensitive. Three of them are controls on the percentage of saturated soils, while the fourth one is the dominant control on flow velocities in the river network. Consequently, model calibrations or measurement campaigns should mainly focus on these particular parameters. A problem that arises with calibration, however, is that some parameters are interdependent with regard to the resulting model output. This means a change in the value of one parameter can be largely compensated for by a change in another parameter with regard to the model output. As a result, simultaneous calibration of interdependent parameters is a delicate matter and should be advised against if calibration is only based on the observed runoff at the catchment outlet. A bivariate sensitivity analysis showed that the model parameters can be divided in two groups with regard to existing interdependence. Between two parameters of the same group relevant interdependence with regard to the integrated catchment response exists, while this is not the case for two parameters from the opposite groups. The reason why this strict subdivision is possible stems from the fact that the first group consists of parameters which are (mainly) involved in relating the initial soil moisture conditions to the observed base flow at t=0, while the second group consist of parameters that are only involved in controlling flow velocities during storm events. The possibility of a subdivision of parameters into these two groups confirms that rainfall-runoff modelling during storm events essentially comes down to the derivation of [I] the percentage of rainfall which becomes available for runoff and [II] the time which is required for the available runoff water to reach the catchment outlet. Therefore, the following four aspects should be explicitly captured by a rainfall-runoff model of the Zwalm catchment (or, indeed, each catchment where runoff is mainly generated on variable saturated source areas):

I. The soil moisture conditions at the beginning of an event
II. The remaining capacity of the soil layer for absorption of incoming rainfall during an event
III. The percentage of rainfall that runs off (which is strongly related to I and II)
IV. Runoff velocities

With respect to the first aspect, a concept of the "memory" of the system is required in physically based flood frequency analysis, since direct measurements of the initial state cannot be performed for hypothetically occurring future meteorological events. In other words

a notion of the number of days, *b*, for which the hydrological state of the catchment at day *t-b* is of negligible influence on the observed (peak) discharge at day *t*. In order to obtain such a concept, statistical analyses have been performed on a 25-years series of precipitation and discharge of the Mosel basin. Two techniques have been applied: Regression/correlation analysis and transfer function modelling. It was shown that almost all direct runoff reaches the basin outlet within 10 days. Relative contributions of daily precipitation values to observed discharges of time lags>10 days were found to be small, except during summer months, when quick runoff components are less dominant than during the rest of the year. For high water events, it also appeared that the build up to a peak discharge does not take longer than 10 days, with maybe some exception to peak discharges that are partly generated by snow melt. Moreover, it was shown that predictions on the discharge in the river Mosel at Cochem should be mainly based on the observed precipitation of the 5 most recent days, whereas information on precipitation for time lags from 5 to 10 is also still valuable. The use of information on precipitation of more than 10 days ago hardly improved the quality of predictions.

Representing spatial heterogeneity in rainfall-runoff models

Due to measurement and modelling errors the use of additional information on spatial heterogeneity of precipitation and catchment characteristics in rainfall-runoff models does not automatically lead to a better model output. The relative complexity of distributed models enhances negative effects of overparameterisation, which is why these models often "work right for the wrong reasons". Furthermore, lack of detailed information and exact process knowledge cause the simulation of the hydrological response at the element scale of a distributed model to be a "mission impossible". Therefore, if one is only interested in simulating the runoff at the catchment outlet, it is recommended to decrease the complexity of distributed models to the extent that they are just able to capture the dominant aspects of spatial heterogeneity in river catchments. Consequently, rainfall-runoff modelling can benefit from a concept of representing spatial variability which is based on a notion of the nature of heterogeneity of dominating parameters and processes. Therefore, a procedure has been developed to analyse the relation between model performance and the scale of the model elements. Application of this procedure provides insight into the scales at which effects of spatial heterogeneity really matter and the scales at which these effects can be neglected.

The procedure was applied to the 114 km^2 Zwalm catchment. It was found that a lumped catchment-runoff model performed equally well as more distributed versions. In other words, as long as a reliable estimate of the spatially averaged properties of rainfall intensities and catchment characteristics is available, spatially distributed modelling is not required for the Zwalm catchment. Possible effects of spatial heterogeneity on runoff generation are averaged out to a large extent in the river routing procedure of the catchment-runoff model, which is mainly due to the relatively short flow distances in the river network (approximately 20 km at maximum). Hydrograph peaks of the subcatchments will therefore always coincide to a large

extent, which means effects of spatial differences in hydrological and meteorological characteristics are filtered out at the catchment outlet. Heterogeneity effects on the integrated response are therefore expected to be of greater importance in larger catchments (basins). In order to validate this hypothesis, a similar analysis has been performed for the 28152 km^2 Mosel basin. For this basin it turned out that it does pay off to take the spatial heterogeneity of precipitation into account in a rainfall-runoff model. For the five highest observed peak runoff events in the period of 1971-1995, the main aspects of the spatial heterogeneity of precipitation could be captured to a large extent by using only 4 model elements. Results for a number of moderate peak discharge events showed this is not always the case. However, for extreme high water events it can be expected that significant contributions come from all parts of the basin. Consequently, the spatial variation of these events is such that its main aspects can be captured to a large extent by using in the order of 4 model elements.

Differences in results between the two pilot study areas (Zwalm and Mosel) show there is no generally valid concept of an optimal representation of spatial heterogeneity in rainfall-runoff models. The same conclusion is drawn from a literature research on this particular subject, where results in some cases even seem to contradict each other. These contradictions most likely stem from differences in:

[1] The size of the catchments under consideration.
[2] The time scale of interest.
[3] Hydrological characteristics of the catchments.
[4] Meteorological characteristics of the events.
[5] The applied concept of the models that have been used to asses heterogeneity effects.

Especially the size of the catchment under consideration is often mentioned as a controlling factor on both the nature of the present heterogeneity and its effect on the catchment response.
The results off a sensitivity analysis showed that this is the main reason why effects are negligible for the 114 km^2 Zwalm catchment, while they are not negligible for the 28152 km^2 Mosel basin. In other words, heterogeneity effects on the integrated response are generally of greater importance in larger catchments (basins). However, as found from the literature research, there is by no means a one to one relationship between catchment size and heterogeneity effects, which can be put down to the influence of the above mentioned aspects [2]-[5]. Therefore, it is recommended to further explore the relation between the above stated four aspects and resulting heterogeneity effects, in order to come to useful guidelines on representing spatial heterogeneity in rainfall-runoff models.

Data requirements to capture spatial variability

Even though spatially distributed modelling is not required for the Zwalm catchment, it does not mean that a single raingauge suffices to estimate the area-average rainfall. It was

demonstrated that spatial heterogeneity in this catchment during a storm event is often far from negligible. Differences between observed intensities in different rainfall stations showed that the use of only one rainfall station can introduce significant errors in the model output. Furthermore, it was shown that spatial heterogeneity of rainfall depths and topographic characteristics (a dominant control on the spatial variability of initial soil moisture conditions) in the Zwalm can cause substantial differences in peak rates of specific runoff between the 61 defined subcatchments of the Zwalm catchment. In other words, taking spatial variability of rainfall intensities into account is of more importance in the measuring process than in the modelling process. Since collecting hydrological data is an expensive and time consuming process, there is a need for a notion on the required spatial resolution of measurements to guarantee reliable estimates of spatially averaged values.

Unfortunately, the available number of rainfall stations in the Zwalm catchment (5 in total, but most of the time there was at least one station out of order) was too small to provide an idea of the amount of raingauges which is required to guarantee a reliable estimate of the area-average rainfall. For the Mosel basin, on the other hand an extensive network of 103 raingauges enabled an analysis of the required spatial coverage of the raingauge network in order to provide satisfying model predictions. A procedure was developed in which, for a number of values of n, the precipitation input of a rainfall-runoff model was estimated through spatial interpolation of measured volumes of n raingauges. It was shown that a network of 10 well-spread raingauges suffices to obtain reliable estimates of the areal precipitation. Compared to the use of the full set of available raingauges (±85 on average) the use of 10 raingauges lead to an increase of the mean square error of only 2% in the model predictions.

Application of the above described procedure may help reducing costs by reducing the number of raingauges if some of them appear to be redundant. Furthermore, it can also be applied to test the suitability of the existing raingauge network. For instance, the rainfall input of a rainfall-runoff model can be estimated from n-1 instead of the available n raingauges. If it turns out that this hardly influences the modelling results (regardless from which particular station is left out of the estimation procedure) one can be confident on the suitability of the network. On the other hand if significant errors are introduced in the model results, it may be profitable to increase the number of raingauges.

Summary

This PhD. research project is a result of a collaboration between Delft Hydraulics and the section Hydrology and Ecology of Delft University of Technology. The project was set up with the aim to investigate the possibilities of a physically based approach towards flood frequency analysis. A physically based approach implies that information is required on both the meteorological events which can be expected in the future and the hydrological response of river catchments to these events. In modelling terms this means a catchment-runoff model is combined with a meteorological model which generates characteristics of future flood generating events and their probability of occurrence.

The research as described in this thesis focused on the hydrological aspects of physically based flood frequency analysis, i.e. the meteorological aspects were only a side issue. First, a review was performed on a large amount of field studies that were dedicated to monitor the occurrence and characteristics of rainfall-runoff processes. Subsequently, the various concepts that are available to model these processes have been studied. It is concluded that physically based rainfall-runoff models can benefit from a concept of representing spatial variability, based on a notion of the nature of heterogeneity of dominating parameters and processes. This lead to the formation of the two central issues of the thesis:

1. Which processes and parameters are dominant under (extremely) wet conditions and should therefore be represented on a physically meaningful way in a catchment-runoff model?
2. What model complexity is required to represent the spatial heterogeneity of these parameters and processes?

Since the answers to these questions are catchment-specific, the emphasis was more on the development and application of procedures and techniques than to provide some generally valid answer. The 114 km^2 Zwalm catchment (Belgium) and the 28152 km^2 Mosel basin (covering parts of France, Germany and Luxembourg) served as pilot area throughout this thesis.

First, a univariate sensitivity analysis has been applied to a well known rainfall-runoff modelling concept (TOPMODEL) to investigate relative importance of occurring runoff generating processes and related characteristics in the Zwalm catchment. Four parameters were identified to which the model is most sensitive. Particularly the values of these parameters need to be accurately determined, either through measurements, or through calibration. A problem that arises with calibration, however, is that some parameters are

interdependent with regard to the resulting model output. This means a change in the value of one parameter can be largely compensated for by a change in another parameter with regard to the model output. As a result, simultaneous calibration of interdependent parameters is a delicate matter and should be advised against if calibration is only based on the observed runoff at the catchment outlet.

A bivariate sensitivity analysis showed that the model parameters can be divided into two groups with regard to existing interdependence. Between two parameters of the same group relevant interdependence with regard to the integrated catchment response exists, while this is not the case for two parameters, taken from the opposite groups. The reason why this strict subdivision is possible stems from the fact that the first group consists of parameters which are (mainly) involved in relating the initial soil moisture conditions to the observed base flow at t=0, while the second group consist of parameters that are only involved in controlling flow velocities during storm events. The possibility of a subdivision of parameters into these two groups confirms that rainfall-runoff modelling during storm events essentially comes down to the derivation of [I] the percentage of rainfall which becomes available for runoff (which is strongly related to initial soil moisture conditions) and [II] the time which is required for the available runoff water to reach the catchment outlet.

Both the univariate sensitivity analysis and the bivariate sensitivity analysis demonstrated the dominant influence of initial soil moisture conditions on peak runoff rates. So, in order to obtain reliable model predictions of peak runoff rates, the hydrological state of the catchment at the beginning of the high water event should be known to a certain extent. In real-time forecasting, this type of information may be obtained through direct measurements of ground water tables, soil moisture contents, discharges, etc. However, in physically based flood frequency analysis, direct measurements of the initial state cannot be performed, since hypothetically occurring future meteorological events are involved. Therefore, either the initial state condition or the meteorological conditions that occur prior to the event have to be considered as an extra stochastic input of an event (besides the precipitation amount of the event itself). For both options, a concept of the "memory" of the system is required, i.e. a notion of the number of days, b, for which the hydrological state of the catchment at day t-b is of negligible influence on the observed (peak) discharge at day t. In order to obtain such a concept, statistical analyses have been performed on a 25-years series of precipitation and discharge of the Mosel basin. Two techniques have been applied: Regression/correlation analysis and transfer function modelling. It was shown that almost all direct runoff reaches the basin outlet within 10 days. Relative contributions of daily precipitation values to observed discharges of time lags>10 days were found to be small, except during summer months, when quick runoff components are less dominant than during the rest of the year. For high water events, it also appeared that the build up to a peak discharge does not take longer than 10 days, with maybe some exception to peak discharges that are partly generated by snow melt. Moreover, it was shown that predictions on the discharge in the river Mosel at

Cochem should be mainly based on the observed precipitation of the 5 most recent days, whereas information on precipitation for time lags from 5 to 10 is also still valuable. The use of information on precipitation of more than 10 days ago hardly improved the quality of predictions.

In order to find out what model complexity is required to represent the spatial heterogeneity of precipitation depths and the dominant catchment characteristics, a procedure was developed to investigate the relation between the performance of a distributed rainfall-runoff model and the scale of its elements. The procedure was applied to the 114 km^2 Zwalm catchment. With regard to measured rainfall depths, it was demonstrated that spatial heterogeneity in this catchment during a storm event is often far from negligible (i.e. a single raingauge is not enough to relay on for obtaining estimates of the area-average rainfall in this catchment). Furthermore, it was shown that spatial heterogeneity of rainfall intensities and topographic characteristics in the Zwalm can cause substantial differences in peak rates of specific runoff between the 61 defined subcatchments of the Zwalm catchment. Still, it was found that a lumped catchment-runoff model performed equally well as more distributed versions. In other words, as long as a reliable estimate of the spatially averaged properties of rainfall intensities and catchment characteristics is available, spatially distributed modelling is not required for the Zwalm catchment. Possible effects of spatial heterogeneity on runoff generation are averaged out to a large extent in the river routing procedure of the catchment-runoff model. This is mainly due to the relatively short flow distances in the river network (approximately 20 km at maximum). Hydrograph peaks of the subcatchments will therefore always coincide to a large extent, which means effects of spatial differences in hydrological and meteorological characteristics are filtered out at the catchment outlet.

Heterogeneity effects on the integrated response are therefore expected to be of greater importance in larger catchments (basins). In order to validate this hypothesis, a similar analysis has been performed for the 28152 km^2 Mosel basin. Furthermore, it has been investigated which spatial coverage of the raingauge network is required in order to provide satisfying model predictions. It turned out that, in contrast to the results for the Zwalm catchment, it does pay off to take the spatial heterogeneity of precipitation into account in a rainfall-runoff model of the Mosel basin. For the five highest observed peak runoff events in the period of 1971-1995, the main aspects of the spatial heterogeneity of precipitation could be captured to a large extent by using only 4 model elements. Results for a number of moderate peak discharge event showed this is not always the case. However, for extreme high water events it can be expected that significant contributions come from all parts of the basin. Consequently, the spatial variation of these events is such that its main aspects can be captured to a large extent by using in the order of 4 model elements. Furthermore, it was shown that for the Mosel basin, a network of 10 well-spread raingauges suffices to obtain reliable estimates of the areal precipitation. Compared to the use of the full set of available

raingauges (±85 on average) the use of 10 well-spread raingauges lead to a negligible increase of the error in the model predictions.

Samenvatting

Dit promotie-onderzoek is het resultaat van een samenwerking tussen WL Delft Hydraulics en de sectie Hydologie&Ecologie van de Technische Universiteit Delft. Het onderzoek komt voort uit ontevredenheid over een aantal tekortkomingen van de gangbare statistische frequentieanalyse van hoogwaters. Er is behoefte aan een meer fysisch gebaseerde methoden, hetgeen impliceert dat een neerslag-afvoer model gecombineerd wordt met een model waarmee van toekomstige neerslaggebeurtenissen zowel de meteorologische karakteristieken als de kansen van optreden gegenereerd worden.

Het onderzoek is met name gericht op de hydrologische aspecten van de fysisch gebaseerde frequentieanalyse, d.w.z. de meteorologische aspecten worden slechts zijdelings behandeld. Allereerst is een literatuurstudie verricht naar de bevindingen van een groot aantal veldcampagnes, waarin het monitoren van neerslag-afvoer processen centraal stond. Vervolgens is een overzicht gegeven van de beschikbare modelconcepten om deze processen te simuleren. Eén van de bevindingen van deze literatuurstudie is dat er behoefte is aan meer gefundeerde methoden om de aanwezige ruimtelijke variabiliteit in een stroomgebied te modelleren. Hieruit werden twee onderzoeksvragen afgeleid:

1. Welke processen en parameters zijn dominant tijdens perioden van (extreem) hoogwater en dienen derhalve op fysisch gebaseerde wijze gerepresenteerd te worden in een neerslag-afvoer model?
2. In welke mate dient de ruimtelijke variabiliteit van deze processen en parameters gemodelleerd te worden?

Aangezien de antwoorden op deze vragen afhankelijk zijn van het te modelleren stroomgebied, lag de nadruk meer op het ontwikkelen en toepassen van methodieken dan op het geven van een algemeen antwoord. Het 114 km^2 grote stroomgebied van de Zwalm (België) en het 28152 km^2 grote stroomgebied van de Moezel (Dat zich op Frans, Duits Luxemburgs en Belgisch grondgebied bevind) hebben in dit onderzoek als testgebied gefungeerd.

Ter beantwoording van de eerste onderzoeksvraag is een univariate gevoeligheidsanalyse toegepast op een bekend onderzoeksmodel (TOPMODEL) waarmee de Zwalm gemodelleerd is. Vier parameters werden geïdentificeerd, waarvoor het model relatief gevoelig is. Met name de waarden van deze parameters dienen nauwkeurig bepaald te worden, hetzij door metingen, hetzij door calibratie. Het probleem in geval van calibratie is echter dat een aantal parameters sterk onderling afhankelijk zijn met betrekking tot de berekende afvoer. Dit betekent dat,

voor wat betreft de resulterende model uitvoer, een wijziging in de waarde van een parameter voor een groot deel gecompenseerd kan worden door een wijziging in de waarde van een andere parameter. Het gevolg is dat een simultane calibratie van twee afhankelijke parameters op basis van afvoermetingen zeer lastig is en eigenlijk af te raden.

Met een bivariate gevoeligheidsanalyse is aangetoond dat de model parameters in twee groepen onderverdeeld kunnen worden op basis van onderlinge afhankelijkheid, d.w.z. tussen twee parameters uit dezelfde groep bestaat een duidelijke onderlinge afhankelijkheid, terwijl dit niet het geval is voor twee parameters uit de verschillende groepen. De oorzaak voor het bestaan van deze strikte onderverdeling is het gegeven dat parameters uit de eerste groep (voornamelijk) in modelvergelijkingen voorkomen waarin de initiële bodemvocht condities worden bepaald, terwijl de tweede groep parameters in modelvergelijkingen voorkomen waarin de snelheid van afstroming bepaald wordt. De strikte verdeling in twee parameter groepen geeft aan dat neerslag-afvoer modellering in periodes van intensieve neerslag in essentie neerkomt op het bepalen van [I] het percentage neerslag dat tot afvoer komt (hetgeen sterk gerelateerd is aan initiële bodemcondities) en [II] de snelheid waarmee de neerslag tot afvoer komt.

Uit zowel de univariate als de bivariate gevoeligheidsanalyse kwam naar voren dat de initiële condities in het stroomgebied van grote invloed zijn op de hoogte van de afvoerpieken. Om betrouwbare afvoervoorspellingen te doen dient derhalve enige kennis van deze condities beschikbaar te zijn. Voor "real-time" voorspellingen kan de toestand in het stroomgebied bepaald worden op basis van metingen van grondwaterspiegels, bodemvocht, debieten, etc. Echter, bij een fysisch gebaseerde frequentieanalyse van hoogwaters zijn deze metingen niet beschikbaar aangezien in een dergelijke analyse met mogelijk optredende toekomstige hoogwaters gewerkt wordt. Daarom dienen ofwel de initiële condities in het stroomgebied ofwel de meteorologische condities voorafgaande aan hoogwaters als extra stochast in beschouwing genomen te worden (naast de meteorologische condities die tijdens het hoogwater optreden) in een dergelijke frequentieanalyse. In beide gevallen dient er een beeld te bestaan van het "geheugen" van het stroomgebied, m.a.w. een idee van het aantal dagen b, waarvoor de toestand in het stroomgebied op dag t-b van verwaarloosbare invloed is op de afvoer van dag t. Voor dit doel is een statistische analyse uitgevoerd op een 25-jarige reeks van neerslag- en afvoerwaarden in het Moezelgebied. Twee verschillende technieken zijn toegepast: Een regressie/correlatie analyse en transfer-functie modellering. Resultaten gaven aan dat de afvoerbare neerslag vrijwel volledig binnen 10 dagen uit het stroomgebied verdwenen is. Bijdragen aan gemeten afvoeren van neerslag van meer dan 10 dagen geleden zijn relatief klein, behalve gedurende de zomermaanden wanneer de snelle afvoer-componenten minder dominant zijn dan gedurende de rest van het jaar. Ook voor extreme hoogwaters bleek dat de opbouw naar de piekafvoer niet langer dan 10 dagen in beslag neemt, met uitzondering van hoogwaters waarbij sneeuwsmelt een rol van betekenis speelt. Verder kwam naar voren dat afvoer-voorspellingen op basis van neerslaggegevens

voornamelijk gebaseerd kunnen worden op de neerslag van de afgelopen vijf dagen. De neerslag van de periode van vijf tot 10 dagen levert ook nog bruikbare informatie op, maar kennis van de neerslag van meer dan 10 dagen geleden leidt nauwelijks tot betere voorspellingen.

De benodigde complexiteit van een neerslag-afvoer model om de aanwezige ruimtelijke variatie in het stroomgebied te modelleren is onderzocht middels een procedure waarmee de relatie bepaald wordt tussen de kwaliteit van modelvoorspellingen en het aantal elementen in het model. Allereerst is deze procedure toegepast voor de Zwalm. Hoewel dit stroomgebied relatief klein is (114 km^2), is de ruimtelijke variatie van bijvoorbeeld de neerslag-intensiteit soms aanzienlijk. Het gebruik van slechts 1 neerslagstation kan leiden tot grote fouten in de schatting van de gebiedsgemiddelde neerslag en als gevolg daarvan in de afvoervoorspelling. Verder is aangetoond dat ruimtelijke verschillen in topografische karakteristieken leiden tot significante verschillen in afvoerkarakteristieken van verschillende deelstroomgebieden. Desondanks bleek dat afvoervoorspellingen van gedistribueerde modellen niet beter zijn dan afvoervoorspellingen van gelumpte modellen. Met andere woorden, zolang men de beschikking heeft over betrouwbare metingen van gebiedsgemiddelde waarden van neerslag-intensiteiten en gebiedskarakteristieken, is het niet nodig om een gedistribueerd model van het gebied te ontwikkelen indien men alleen in de afvoer bij het uitstroompunt geïnteresseerd is. Mogelijke effecten van ruimtelijke variatie worden voor een groot gedeelte uitgemiddeld in de module waarin stroming door het rivierennetwerk gesimuleerd wordt. Dit wordt met name veroorzaakt door de relatief korte af te leggen afstanden in de rivier (hooguit 20 km). Afvoerpieken van deelstroomgebieden vallen daardoor voor een groot gedeelte samen, zodat de gevolgen van ruimtelijke verschillen uitgefilterd zijn bij het uitstroompunt.

In grote stroomgebieden zijn effecten van ruimtelijke variabiliteit daarom naar verwachting groter. Om deze hypothese te toetsen is dezelfde procedure eveneens toegepast voor de Moezel. Verder is voor dit gebied nagegaan hoeveel neerslagstations benodigd zijn om een betrouwbare schatting van de gebiedsneerslag te geven. Het bleek dat, in tegenstelling tot de bevindingen voor de Zwalm, betere voorspellingen gedaan kunnen worden door de aanwezige ruimtelijke variabiliteit op te nemen in het model. Voor de vijf meest extreme hoogwaters uit de periode 1971-1995 konden de belangrijkste aspecten van de ruimtelijke verschillen in de neerslag echter al voor een groot gedeelte gemodelleerd worden door gebruik van slechts vier model elementen. Voor een middelmatig hoogwater met extreme ruimtelijke verschillen werd daarentegen aangetoond dat het gebruik van vier elementen niet altijd afdoende is. Voor extreme hoogwaters kan echter verwacht worden dat alle delen van het stroomgebied significante bijdragen leveren aan de hoge afvoer. De ruimtelijke variatie bij extreme hoogwaters zal dus naar verwachting zodanig zijn dat de belangrijkste aspecten al met vier model elementen gemodelleerd kunnen worden. Tenslotte is aangetoond dat een netwerk van 10 goed gespreide neerslagstations volstaat om een betrouwbaar beeld van de gebiedsneerslag te geven. In vergelijking met het gebruik van het volledige aanwezige netwerk (±85 stations

gemiddeld) leidde het gebruik van 10 stations tot een verwaarloosbare stijging in de voorspellingsfout voor alle onderzochte gebeurtenissen.

Dankwoord

Hoewel het doen van promotie-onderzoek nog wel eens gekenschetst wordt als een eenzame bezigheid, heb ik in de ruim vier jaar dat ik mij er mee bezig gehouden heb toch een groot aantal mensen leren kennen dat een bedankje mijnerzijds meer dan waard is. Allereerst wil ik mijn promotor en hoofd van de sectie Hydrologie & Ecologie, Cees van den Akker, bedanken voor het feit dat hij mij in staat gesteld heeft om het promotie-onderzoek te verrichten. Verder ben ik erkentelijk voor zijn begeleiding en de grote onderzoeksvrijheid die hij mij vanaf het begin toevertrouwde. Tenslotte bedank ik hem voor de verlenging van mijn contract halverwege het jaar 2000, hetgeen mij in staat stelde het proefschrift af te ronden.
Naast de sectie Hydrologie & Ecologie heeft ook het Waterloopkundig Laboratorium een deel van de financiering van het onderzoek voor haar rekening genomen, waarvoor ik met name Roelof Moll en Eelco van Beek wil bedanken. Verder ben ik erkentelijk voor het feit dat het Waterloopkundig Laboratorium een kamer met computer beschikbaar stelde zodat ik de luxe beschikking had over twee werkplekken.
Voor de genoten begeleiding wil ik in het bijzonder Albert van Mazijk en Jaap Kwadijk bedanken. De vele inhoudelijke gesprekken hebben een wezenlijke bijdrage aan het onderzoek geleverd. Verder heb ik veel profijt gehad van de adviezen van de leden van mijn begeleidingscommissie, waarvoor ik, naast eerder genoemden, mijn dank betuig aan Ron Passchier, Karel Heynert, Tom Rientjes, Paul Torfs, Bart Parmet en Huub Savenije.
Ook niet onvermeld mag blijven mijn verblijf aan de Universiteit van Gent bij het Laboratorium voor Hydrologie en Watermanagement. Allereerst ben ik hiervoor dank verschuldigd aan Francois de Troch en Peter Troch die mijn bezoek aan Gent mogelijk hebben gemaakt. Verder bedank ik Nico Verhoest, Yves Van Herpe, Luc Debruyckere, Freek Vandersteene en Rudi Hoeben voor hun behulpzaamheid en voor het feit dat ik mijn verblijf in Gent als zeer plezant heb ervaren.
Tenslotte wil ik alle collega's van de sectie Hydrologie & Ecologie en van het W.L. danken voor het grote aantal leuke herinneringen dat ik aan deze periode heb overgehouden. Vooral tussen promovendi onderling blijken bijzondere banden c.q. vriendschappen te kunnen ontstaan. Op het gevaar af anderen tekort te doen, wil ik hierbij vooral de namen vermelden van Lennart Weltje, Paul Verlaan, Marlies Schuttelaar, Nicolette Bouman, Birgitte Putters, Frank van Weert, Julius Ndambuki en Paolo Reggiani. Tevens bedank ik het trio Margreet, Betty en Eva voor hun luisterend oor dat vaak nodig was als ik weer eens mijn ei kwijt moest.

Curriculum Vitae

Nederlandse versie

De auteur van dit proefschrift, Ferdinand Diermanse, is in Den Haag geboren op 3 Juni 1971. In April 1973 verhuisde hij naar 's Gravenzande, alwaar hij in 1989 zijn Atheneum diploma behaalde aan het Zandevelt College. Vervolgens heeft hij een studie Technische Wiskunde gevolgd aan de Technische Universiteit Delft. In Januari 1995 heeft hij zijn ingenieursdiploma (Ir.) ontvangen. Gedurende zijn afstudeerproject, uitgevoerd bij het Waterloopkundig Laboratorium, kwam hij voor het eerst met hydrologie in aanraking. Het project was een haalbaarheidsstudie van een operationeel beheerssyteem voor een systeem van reservoirs in het Nederlandse deel van het stroomgebied van de Geul (Limburg). In 1995 verruilde hij de boeken voor de wapenen om zijn militaire dienstplicht te vervullen. In Februari 1996 keerde hij terug aan de universiteit van Delft om een promotie-onderzoek te doen naar het gebruik van fysisch gebaseerde neerslag-afvoer modellen bij het bepalen van overschrijdingskansen van rivier-afvoeren. Het onderzoek werd uitgevoerd bij de sectie Hydrologie & Ecologie, Faculteit Civiele Techniek en werd deels gefinancierd door het Waterloopkundig Laboratorium. Gedurende het onderzoek heeft hij tevens geparticipeerd in een project van het Waterloopkundig Laboratorium ter bepaling van de nieuwe maatgevende afvoer voor de Rijn bij Lobith. Sinds 1 September 2000 is hij onder contract bij het Waterloopkundig Laboratorium, inmiddels WL | Delft Hydraulics geheten.

English version

The author of this thesis, Ferdinand Diermanse, was born in Den Haag on the third of June, 1971. In April 1973 he moved to 's Gravenzande where he, in 1989, graduated from secondary school at the Zandevelt College. After that he studied Technical at Delft University of Technology. He received his engineer degree (Ir.) in January 1995. During his graduation project, which was performed at Delft Hydraulics, he got involved with hydrology for the first time. The project was an inventory studies of an operational management system for a system of detention reservoirs in the Dutch part of the Geul catchment (Limburg, The Netherlands). The year of 1995 was spent in the army, as he had to fulfil his military service. In February 1996, he returned to Delft University to start a PhD. research on the application of physically based rainfall-runoff models in flood frequency analysis. The research project was performed at the section of Hydrology & Ecology, Faculty of Civil engineering of Delft University and partly funded by Delft Hydraulics. During his time as a PhD. student he also participated in a project at Delft Hydraulics in which the new design discharge for the river Rhine at the German-Dutch border was determined. Since September 1st he started a new job at Delft Hydraulics.

References

Abbott, M.B., Bathurst, J.C., Cunge, J.A., Connel, P.E. and Rasmussen, J., 1986a: An introduction to the European Hydrological system - 1. History and philosophy of a physically-based, distributed modelling system, *J. Hydrol*, 87, 45-59.

Abbott, M.B., Bathurst, J.C., Cunge, J.A., Connel, P.E. and Rasmussen, J., 1986b: An introduction to the European hydrological system - Système Hydrologique Européen, "SHE" - 2. Structure of a physically-based, distributed modelling system, *J. Hydrol.* 87, 61-77.

Anderson, M.G. and Burt, T.P., 1990: Subsurface runoff, In: M.G. Anderson and T.P. Burt (eds.), *Process studies in hillslope hydrology*, John Wiley, 365-400.

Avissar, R., 1998: Which type of soil-vegetation-atmosphere transfer scheme is needed for general circulation models: a proposal for a higher order scheme, *J. Hydrol.*, 212-213, 136-154.

Bárdossy, A. and Plate, E.J., 1991: Modelling daily rainfall using a semi-Markov representation of circulation pattern occurrence, *J. Hydrol.*, 122, 33-47.

Bathurst, J.C., 1986: Physically-based distributed modelling of an upland catchment using the Système Hydrologique Européen, *J.Hydrol.*, 87, 79-102.

Bear, J., 1972: *Dynamics of fluids in porous media*, Elsevier, Amsterdam.

Bergström, S., 1995: The HBV model, In: V.P. Singh (ed.): *Computer models of watershed hydrology*, Water Resourses Publications, Colorado, 443-476.

Betson, R. P., 1964: What is watershed runoff? *J. Geophys. Res.*, 69, 1541-1552.

Betson, R.P. and Marius, J.B., 1969: Source areas of storm runoff, *Water Resour. Res.*, 5(3), 574-582.

Beven, K., 1982, On subsurface stormflow: An analysis of response times, *Hydr. Sci. J.*, 4(12), 1982.

Beven, K., 1986: Runoff productions and flood frequency in catchments of order n: An alternative approach, In: *Scale problems in hydrology*, Gupta, V.K., Rodriguez-Iturbe, I. and Wood, E.F. (eds.), D. Reidel, Dordrecht, 1-17.

Beven, K., 1989: Changing ideas in hydrology - The case of physically based models, *J. Hydrol*, 105, 157-172.

Beven, K. J. and Hornberger, G.M., 1982: Assessing the effect of spatial pattern of precipitation in modelling stream flow hydrographs, *Water Resour. Bull.*, 18(5), 823-829.

Beven, K.J. and Kirkby, M.J., 1979: A physically based, variable contributing area model of basin hydrology, *Hydr. Sci. Bull.*, 24, 43-69.

Beven, K. and Germann, P., 1982: Macropores and water flow in soils, *Water Resour. Res.*, 18(5), 1311-1325.

Beven,-K., Calver,-A., Morris,-E.M., 1987: *The Institute of Hydrology Distributed Model*, Institute of Hydrology, Wallingford.

Beven, K., Lamb, R., Quinn, P., Romanowicz, R. and Freer, J., 1995: TOPMODEL, In: V.P. Singh, *Computer models of watershed hydrology*, Water resources publications, Highlands Ranch., 627-668.

Binley, A., Elgy, J. and Beven, K., 1989: A physically based model of heterogeneous hillslopes. 1. Runoff production, *Water Resour. Res.*, 25(6), 1219-1226.

Biswas, A. K., 1972: *History of hydrology*, North Holland publishing company, Amsterdam.

Blöschl, G. and Sivapalan, M., 1995: Scale issues in hydrological modelling: A Review, *Hydrol. Process.*, 9, 251-290.

Blöschl, G. and Sivapalan, M., 1997: Process controls on regional flood frequency: Coefficient of variation and basin scale, *Water Resour Res.*, 33(12), 2967-2980.

Blöschl G., Grayson R.B. and Sivapalan, M., 1995: On the representative elementary area (REA) concept and its utillity for distributed rainfall runoff modelling, *Hydrol. Process.*, 9, 313-330.

Boertien I (Ministerie van verkeer en waterstaat), 1993: *Toetsing uitgangspunten rivierdijkversterkingen, deelrapport 1: Veiligheid tegen overstromingen* (in Dutch).

Box, G. E. P. and Jenkins, G. M., 1976: *Time series analysis: Forecasting and control*, Holden-Day, San Francisco.

Brandsma, T. and Buishand, T.A., 1998: Simulation of extreme precipitation in the Rhine basin by nearest-neighbour resampling. *Hydrol. Earth Sys. Sci.*, 2, 195-209.

Bresler, E. and Dagan, G., 1983a: Variability of yield of and irrigated crop and its causes, 1. Statement of the problem and methodology, *Water resour. Res.*, 24(3), 381-387

Bresler, E. and Dagan, G., 1983b: Variability of yield of and irrigated crop and its causes, 2. Input data and illustration of results, *Water resour. Res.*, 24(3), 389-394

Bronstert, A. and Plate, E., 1996: Ein physikalisch begründetes hydrologisches modell für hänge und kleine einzugsgebiete, *Wasserwirtschaft*, 86(6), 1996 (in German).

Burnash, R. J. C., Ferrel, R. L. and McGuire, R. A., 1973: A general streamflow simulation system - Conceptual modelling for digital computers, *Report by the joint federal state river forecasting center,* Sacramento, California.

Busch, N., Engel, H. and Zimmer, K.-H., 1996: Untersuchungen zur wirkung denkbarer rückhaltemaßnahmen an der Französischen Obermosel auf den hochwasserablauf in der Mosel (analysis of effects of potential flood retention facilities on the French upper Moselle river on floodflow in river Moselle), *Deutsche Gewässerkundlkiche Mitteilungen*, 40, 58-69 (in German).

Caroni, E., Singh, V. P. and Ubertini, L., 1984: Rainfall-runoff-sediment yield relation by stochastic modelling, *Hydr. Sci. J.*, 29(2), 203-218.

Cerda, A., 1998: The influence of aspect and vegetation on seasonal changes in erosion under rainfall simulation on a clay soil in Spain, *Can. J. Soil Sci.*, 78(2), 321-330

Chorley, R.J., 1978: The hillslope hydrological cycle, In: M.J. Kirkby (ed.), *Hillslope hydrology*, John Wiley, 1-42.

Chow, K.C.A., Watt, W.E. and Watts, D.G., 1983: A stochastic-dynamic model for real-time flood forecasting, *Water Resour. Res.*, 19(3), 746-752.

CHR, 1977 (Commission Hydrologique du Rhin): Le Bassin du Rhin.

Clark, C.O., 1945: Storage and the unit hydrograph, *Transactions of the american society of civil engineers*, 110, 1419-1446.

Clarke, R.T., 1972: A review of some mathematical models used in hydrology, with observations on their calibration and use, *J. Hydrol.*, 19, 1-20.

Commissie rivierdijken, 1977: *Rapport Commissie rivierdijken*, Min. Verkeer en Waterstaat, 's Gravenhage (in Dutch)

Commissie watersnood Maas (commissie Boertien), 1994: *Onderzoek watersnood Maas, deelrapport 4: Hydrologische aspecten.*, Delft Hydraulics (in Dutch).

Corbett, E.S., Sopper, W.E. and Lynch, J.A., 1975: Watershed response to partial area applications of simulated rainfall, in *Hydrological caracteristics of river basins and the effects on these caracteristics of better water management*, IAHS publ. 117, 63-73.

Corradini, C. and Singh, V.P., 1985: Effect of spatial variability of effective rainfall on direct runoff by a geomorphologic approach, *J. Hydr.*, 81, 27-43.

Crawford, N. H. and Linsley, R. K., 1962. The synthesis of continuous streamflow hydrographs on a digital computer. *Technical report 12*, Department of Civil Engineering, Stanford University California.

Crawford, N. H. and Linsley, R. S., 1966: Digital simulation in hydrology: The Stanford watershed model IV. *Technical report No 39*, Department of Civil Engineering, Stanford University, Palo Alto, California.

Cunge, J. A., 1969: On the subject of a flood propagation computation method (Muskingum method), *J. Hydraul. Res.*, 7(2).

Dagan, G. and Bresler, E., 1983: Variability of yield of and irrigated crop and its causes, 3. numerical simulation and field results, *Water resour. Res.*, 24(3), 395-401

Dawdy, D. R. and Bergmann, J. M., 1969: Effect of rainfall variability on streamflow simulation, *Water Resour. Res.*, 5(5), 958-966.

Deutsch, C.V. and Journel, A.G., 1992: *GSLIB: geostatistical software library and users guide*, Oxford University Press, New York, 335 pp.

Diaz-Granados, M. A., Valdes, J. B. and Bras, R. L., 1984: A physically based flood frequency distribution, *Water Resour. Res.*, 20(7) 995-1002.

Diermanse, F., 1994: *Onderzoek naar besturingssystemen voor reservoirs in het stroomgebied van de Geul*, masters thesis, WL | delft hydraulics (in Dutch).

Diermanse, F., 1999: *Onderzoek 1/1250 jaar afvoer bij Lobith*, deelrapport I, WL | delft hydraulics (in Dutch).

Duan, Q., Sorooshian, S. And Gupta, V., 1992: Effective and efficient global optimazation for conceptual rainfall runoff models, *Water Resour. Res.*, 28(4), 1015-1031.

Dunne, T., 1978: Field studies of hillslope processes, In: M.J. Kirkby (ed.), *Hillslope hydrology*, John Wiley, 227-293.

Dunne, T., 1983: Relation of field studies and modelling in the prediction of storm runoff, *J. Hydrol.*, 65, 25-48.

Dunne, T., and Black, R.D., 1970a: An experimental investigation of runoff production in permeable soils, *Water Resour. Res.*, 6(2), 478-490.

Dunne, T., and Black, R.D., 1970b: Partial area contributions to storm runoff in a small new England watershed, *Water Resour. Res.*, 6(5) 1296-1311.

Eagleson, P.S., 1972: Dynamics of flood frequency, *Water Resour. Res.*, 8(4), 878-898.

Edwards, A.L., 1984: *An introduction to lineair regression and correlation*, W.H. Freeman and Company, New York.

Engel, H., 1998: The flood events 1993/1994 and 1995 in the Rhine river basin; Causes and Developments, In: R. Casale, G.B. Pedroli and P. Samuels, *Ribamod; River basin modeling, management and flood mitigation, concerted action*, Office for official publications of the European communities, 23-36.

Engman, E.T., 1986: Roughness coefficients for routing surface runoff, J. *Irr. Drain. Eng.*, 112(1) 39-53.

Epstein, D. and Ramirez, J.A., 1994: Spatial dissaggregation for studies of climatic hydrologic sensitivity, *J. Hydraul. Eng.*, 120(12), 1449-1467.

Fan, Y and Bras, R.L., 1995: On the concept of a representative elementary area in catchment runoff, *Hydrol. Process.*, 9, 821-832.

Finnerty, B. D., Smith, M. B., Seo, D-J., Koren, V. and Moglen, G. E., 1997: Space-time scale sensitivity of the Sacramento model to radar-gage precipitation inputs, *J. Hydrol.*, 203, 21-38.

Flerchinger, G. N., Cooley, K. R., Hanson, C. L. And Seyfried, M. S., 1998: A uniform versus an aggregated water balance of a semi-arid watershed, *Hydrol. Process.*, 12(2), 331-342.

Flury, M., Flühler, H., Jury, W.A. and Leuenberger, J., 1994: Susceptibility of soils to preferential flow of water: A field study, *Water Resour. Res.*, 30(7), 1945-1954.

Ford, P.M.,1959: *Multiple correlation in forecasting seasonal runoff*, United States departement of the interior bureau of reclamation.

Freeze, R.A. and Harlan, R.L., 1969: Blueprint for a physically based digitally simulated hydrologic responce model, *J. Hydrol.*, 9, 237-258.

Garrote, L. and Bras, R.L., 1995: A distributed model for real-time flood forecasting using digital elevation models, *J Hydrol.*, 167, 279-306.

Gerits, J.J.P., de Lima, J.L.M.P., and van den Broek, T.M.W., 1990: Overland flow and erosion, In: M.G. Anderson and T.P. Burt (eds.), *Process studies in hillslope hydrology*, John Wiley, 173-214.

Germann, P.F. and Beven, K.J., 1986: A distribution function approach to water flow in soil macropores based on kinematic wave theory, *J. Hydrol.*, 83, 173-183.

Gnedenko, B.V., 1943: On the limiting distribution of the maximum term in a random series, In S. Kotz. and N.L. Johnson (eds.), *Breakthroughs in statistics, vol. I, Foundations and basic theory*, 1992, Springer-Verlag, New-York.

Goel, N. K., Kurothe, R. S., Mathur, B. S. And Vogel, R. M., 2000: A derived flood frequency distribution for correlated rainfall intensity and duration, *J. Hydrol.*, 228, 56-67.

Gozzini, B., Marachi, G., Meneguzzo, F. and Nicolai, M., 1998: The catastrophic flood occurred in Versalia basin, Tuscany, on 19th June 1996: A way to predictability, In: R. Casale, G.B. Pedroli and P. Samuels, *Ribamod; River basin modeling, management and flood mitigation, concerted action*, Office for official publications of the European communities, 211-228.

Grayson, R.B., Moore, I.D. and McMahon, T.A., 1992a: Physically based hydrologic modelling. 1. A terrain-based model for investigative purposes, *Water Resour. Res.*, 28(10), 2639-2658.

Grayson, R.B., Moore, I.D. and McMahon, T.A., 1992b: Physically based hydrologic modelling. 2. Is the concept realistic?, *Water Resour. Res.*, 28(10), 2659-2666.

Gyasi-Ayei, Y, de Troch, F.P. and Troch, P.A., 1996: Adynamic hillslope response model in a geomorphology based rainfall-runoff model, *J. Hydrol.*, 178, 1-18.

Hall, F. J., 1987: Contributions of Robert E. Horton, In: E.R. Landa and S. Ince (eds.), *History of geophysics*, American Geophysical Union.

Hamlin, M. J., 1983: The significance of rainfall in the study of hydrological processes at basin scale, *J. Hydrol.*, 65, 73-94.

Harr, R.D., 1977: Water flux in soil and subsoil on a steep forested slope, *J. Hydrol.*, 33.

Harris, D., McDonnell, J.J. and Rohde, A., 1995: Hydrograph separation using continuous open system isotope mixing, *Water Resour. Res.*, 31(1), 157-171.

Hasmi, M. A. and Garcia, L. A., 1998: Spatial and temporal errors in estimating regional evapotranspiration, *J. Irr. and Drain. Eng.*, 124(2), 108-114.

Hassanisadeh, M. and Gray, W.G., 1979: General conservation equations for multiphase systems: 1. Averaging procedure, *Advances in water resources*, 2, 131-144.

Hassanisadeh, M. and Gray, W.G., 1980: General conservation equations for multiphase systems: 3. Constitutive theory for porous media flow, *Adv. water resour.*, 3, 25-40.

Hassanuzzaman Khan, M., 1993: Muskingum flood routing model for multiple tributuaries, *Water Resour Res.*, 29(4), 1057-1062.

Hebson, C. and Wood, E.F., 1982: A derived flood frequency distribution using horton order ratios, *Water Resour. Res.*, 18(5), 1509-1518.

Hess, G.W. and Inman, E.J., 1994: Effects of urban flood-detention reservoirs on peak discharges and flood frequencies, and simulation of flood-detention reservoir outflow hydrographs in two watersheds in Albany, Georgia, *Open file reports section, box 25286, MS 517, Denver, Co, 80225 (USA), USGS, Earth science information center*, 31 pp.

Hewlett, J. D., 1961: Watershed management. *Annu. rep. U.S. Dep. Of Agric. For. Serv. Southeast. For. Exp. Stn. Asheville, N.C. Journal of hydrology*, 61-66.

Hewlett, J.D. and Hibbert, A.R.,1967: Factors affecting the response of small watersheds to precipitation in humid areas, In: W.E. Sopper and H.W. Lull (editors), *Forest hydrology*, Pergamon, Oxford, 275-290.

Hornberger, G.M., Beven, K. J., Cosby, B. J. and Sappington, D. E., 1985: Shenandoah watershed study: Calibration of a topography-based, variable contributing area hydrological model to a small forested catchment, *Water Resour. Res.*, 21(12), 1841-1850.

Hornberger, G.M., Germann, P.F. and Beven, K.J., 1991: Throughflow and solute transport in an isolated sloping soil blok in a forested catchment, *J. Hydrol.*, 124, 81-99.

Iacobellis, V. and Fiorentino, M., 2000: Derived distribution of floods based on the concept of partial area coverage with a climatic model, *Water Resour. Res.*, 36(2), 469-482.

Jones, A., 1971: Soil piping and stream channel initiation, *Water Resour. Res.*, 7(3), 602-610.

Kendall, D. R. and Dracup, J. A., 1991: A comparison of index-sequential and AR(1) generated hydrologic sequences, *J. Hydrol.*, 122, 335-352.

Killingtveit, Å and Sælthun, N. R., 1995: *Hydropower development: Hydrology*, Norwegian institute of Technology.

Kite, G. W., 1995: Scaling of input data for macroscale hydrologic modeling, *Water Resour. Res.*, 31(1), 2769-2781.

Klemeš, V., 1986: Dillettantism in hydrology: Transition or destiny?, *Water Resour. Res.*, 22(9) 177-188.

Klemeš, V., 1988: A hydrological perspective, *J. Hydrol.*, 100, 3-28.

Klemeš, V., 1993: Probability of extreme hydrometeorological events- a different approach, In: Z.W Kundzewics, D. Rosbjerg and S.P. Simonovic (eds.), *Extreme hydrological events: Precipitation, floods and droughts* (Proceedings of the Yokohama symposium, july 1993), IAHS Publ. 213, 167-176.

Klemeš, V., 1994: Statistics and probability: Wrong remedies for a confused hydrologic modeler, In: V. Barnett and K.F. Turkman, *Statistics for the environment 2: water related issues*, John Wiley & Sons Ltd., Chisester, England, 345-370.

Kouwen, N. and Garland, G., 1989: Resolution considerations in using radar rainfall data for flood forecasting, *Can J. Civ. Eng.*, 16, 279-289.

Krajewski, W. F., Lakshmi, V., Georgakakos, K. P. and Jain, S. C., 1991: A Monte Carlo study of rainfall sampling effect on a distributed catchment model, *Water Resour. Res.*, 27(1), 119-128.

Kubota, J. and Sivapalan, M., 1995: Towards a catchment-scale model of subsurface runoff generation based on synthesis of small-scale process-based modelling and field-studies, *Hydrol. Process.*, 9, 541-554.

Kuchment, L.S., Demidov, V.N., Motovilov, Yu.G., Mazarov, N.A. and Smakhtin, V.Yu., 1993: Estimation of disastrous floods risk via physically based models of river runoff generation, In: Z.W Kundzewics, D. Rosbjerg and S.P. Simonovic (eds.), *Extreme hydrological events: Precipitation, floods and droughts* (Proceedings of the Yokohama symposium, july 1993), IAHS Publ. 213, 177-182.

Kunkel, K. E., 1994, A climatic perspective on the 1993 flooding rains in the upper Mississippi river basin, *Water Int.*, 19(4), 186-189.

Lall, U. and Sharma, A., 1996: A nearest neighbor bootstrap for resampling hydrologic time series, 32(3), 679-693.

Leavesly, G.H., Lichty, R.W., Troutman, B.M. and Saindon, L.G., 1983: Preciptation-runoff modeling system, users manual, *USGS Water-Resources investigations report*, 83-4238, Denver, Colorado.

Lemke, K. A., 1991: Transfer function of suspended sediment concentration, *Water Resour. Res.*, 27(3), 293-305.

Li, E. A., Shanholtz, V. O., Contractor, D. N. and Carr, J. C., 1977: Generating rainfall excess based on readily determinable soil and landuse characteristics, *Trans. Am. Soc. Of Agr. Eng.*, 20(6), 1070-1078

Lorenz and Kwadijk, 1999: *Onderzoek 1/1250 jaar afvoer bij Borgharen*, concept deelrapport 3, WL | delft hydraulics (in Dutch).

Loukas, A., Quick, M.C. and Russel, S.O., 1996: A physically based stochastic-deterministic procedure for the estimation of flood frequency, *Water Resour. Man.*, 10(6), 415-437.

Mantoglou, A. and Gelhar, L.W., 1987: Effective hydraulic conductivities of transient unsaturated flow in stratified soils, *Water Resour. Res.*, 23(1), 57-67.

McCarthy, G.T., 1938: The Unit Hydrograph and flood routing, *Conf. North Atlantic Division,* US Army Corps of Engineers.

McDonnell, J.J., 1990: A rationale for old water discharge through macropores in a steep, humid catchment, *Water Resour. Res.*, 26(11), 2821-2832.

Mein, R.G. and Brown, B.M., 1978: Sensitivity of optimized parameters in watershed models, *Water Resour. Res.*, 14(2).

Melcher, N. B. and Parrett, C., 1993: Upper Mississippi river floods, *Geotimes*, 38(12), 15-17.

Melching, C. S. and Marquardt, J. S., 1996: Equations for estimating synthetic unit hydrograph parameter values for small watersheds in lake county Illinois, *USGS open file report, branch of information series, Box 25286, Federal center, Denver, 80225-0046 (USA).*

Merkl, G., 1973: *Korrelationen zwischen mittlerer wasserführung und hydro-meteorologischen faktoren im hinblick auf mittelfristige abflußprognosen*, Institut für hydraulik und gewässerkunde, Technische universität München (In German).

Middelkoop, H. (red.), 1998: *Twee rivieren, Rijn en Maas in Nederland*, RIZA rapport 98041 Arnhem: RIZA. (in Dutch).

Mikovari, A., Peter, C. and Leibundgut, Ch., 1995: Investigation of preferential flow using tracer techniques, In: Ch. Leibundgut (ed.), *Tracer Technologies for hydrological systems* (Proceedings of a boulder symposium, july 1995), IAHS Publ. 229, 87-97.

Milly, P.C.D. and Eagleson, P.S., 1988: Effect of storm scale on surface runoff volume, *Water Resour. Res.*, 24(4), 620-624.

Mölders, N, and Raabe, 1996: Numerical investigations on the influence of subgrid-scale surface heterogeneity on evapotranspiration and cloud processess, *J. Appl. Metteor*, 35, 782-795.

Montgomery, D.R. and Dietrich, W.E., 1995: Hydrologic processes in a low-gradient source area, *Water Resour. Res.*, 31(1), 1-10.

Mosley, M.P., 1979: Streamflow generation in a forested watershed, New Zealand, *Water Resour. Res.*, 15(4), 795-806.

Mosley, M.P., 1982: Subsurface flow velocities through selected forest soils, South Island, New Zealand, *J. Hydrol.*, 55, 65-92.

Naden, P. S., 1992: Spatial variability in flood estimation for large catchments: The exploitation of channel network structure, *Hydr. Sc. J.*, 37(1), 53-71.

Naghettini, M., Potter, K.W. and Illangasekaze, T., 1996: Estimating the upper tail of flood-peak frequency distributions using hydrometeorological information, *Water Resour. Res.*, 32(6) 1729-1740.

Nash, J. E. and Sutcliffe, J. V., 1970: River flow forecasting through conceptual models. Part I: a discussion of principles, *J. Hydrol.*, 10, 282-290.

Novotny, V. and Zheng, S., 1989: Rainfall-runoff transfer function by ARMA modeling, *J. Hydraul. Eng.*, 115(10), 1386-1400.

Obled, Ch., Wending, J. and Beven K., 1994: The sensitivity of hydrological models to spatial rainfall patterns: an evaluation using observed data, *J. Hydrol.*, 159, 305-333.

Ogden, F.L. and Julien, P.Y., 1994: Runoff model sensitivity to radar rainfall resolution, *J. Hydrol.*, 158, 1-18.

Onodera, S. and Kobayashi, M., 1995: Evaluation of seasonal variation in bypass flow and matrix flow in a forest soil layer using bromide ion, In: Ch. Leibundgut (ed.), *Tracer Technologies for hydrological systems* (Proceedings of a boulder symposium, july 1995), IAHS Publ. 229, 99-107.

Overall, J.E. and Klett, C., 1972: *Applied multivariate analysis*, McGraw-Hill.

Palacios-Vélez, O., Gandoy-Bernasconi, W. and Cuevas-Renaud, B., 1998: Geometric analysis of surface runoff and the computation order of unit elements in distributed hydrological models, *J. Hydrol.*, 211, 266-274.

Parmet, B., Buishand, T. A., Brandsma, T. and Mülders, R., 1999: Design discharge of the large rivers in The Netherlands- towards a new methodology, In *Hydrological extremes: Understanding, Predicting, Mitigating*, IAHS Publ., 255, 269-272.

PCRaster, 1996, *PCRaster manual*, version 2, Utrecht University, department of Physical Geography, 384 pp.

Pearce, A.J., Stewart, M.K. and Sklash, M.G., 1986: Storm runoff generation in humid headwater catchments. 1. Where does the water come from?, *Water Resour. Res.*, 22(8) 1263-1272.

Perumal, M., 1992: Multilinear Muskingum flood routing method, *J. Hydrol.*, 133, 259-272.

Pessoa, M. L., Bras, R. L. and Williams, E. R.,1993: Use of weather radar for flood forecasting in the Sieve River basin: A senstivity analysis, *J. appl. Meteor.*, 32(3), 462-475.

Peters, D.L., Butte, J.M., Taylor, C.H. and LaZerte, B.D., 1995: Runoff production in a forested, shallow soil, Canadian shield basin, *Water Resour. Res.*, 31(5), 1291-1304.

Pierce, R.S.,1967: Evidence of overland flow on forest watersheds, In: W.E. Sopper and H.W. Lull (editors), *Forest hydrology*, Pergamon, Oxford, 247-253.

Pilgrim, D.H., 1983: Some problems in transferring hydrological relationships between small and large drainage basins and between regions, *J. Hydrol.*, 65, 49-72.

Pilgrim, D.H. and Cordery, I., 1993: Flood runoff, In: D.R. Maidment (ed.), *Handboook of hydrology*, McGraw-Hill.

Raines, T. H., and Valdés, J. B., 1992: Estimation of flood frequencies for ungauged catchments, *J. Hydraul. Eng.*, 119(10), 1138-1154.

Rawitz, E., Engman, E.T. and Cline, G.D., 1970: Use of the mass balance method for examinating the role of soils in controling watershed performance, *Water Resour. Res.*, 6(4), 1115-1123.

Refsgaard, J.C., 1996: Terminology, modelling protocol and classification of hydrological models, In: M.B. Abbot and J.C. Refsgaard (eds.), *Distributed hydrological modelling*, , Kluwer academic publishers, 17-39.

Robinson, M., 1993: Changing ideas regarding storm runoff processes in small basins, In *Inventory of streamflow generation studies*, Flow regimes from international experimental and netwerk data (FRIEND), Vol III, Robinson, M. (ed.), ISBN 094854056 7, 3-16.

Rodriguez-Iturbe, I. and Valdés, J.B., 1979: The geomorphologic structure of hydrologic responce, *Water Resour. Res.*, 15(6), 1409-1420.

Rodriguez-Iturbe, I., Febrez De Power, B., Sharifi, M.B. and Georgakakos, K.P., 1989: Chaos in rainfall, *Water Resour. Res.*, 25(7), 1667-1675.

Sánchez-Villa, X., Girardi, J.P. and Carrera, J., 1995: A synthesis of approaches to upscaling of hydraulic conductivities, *Water Resour. Res.*, 31(4), 867-882.

Sánchez-Villa, X., Carrera, J. and Girardi, J.P., 1996: Scale effects in transmissivity, *J. Hydrol.*, 183, 1-22.

Saulnier, G.-M., Beven, K. And Obled, C., 1997: Including spatial variable effective soil depths in TOPMODEL, *J. Hydrol.*, 202, 158-172.

Seibert, J., 1997: Estimation of parameter uncertainty in the HBV-model, *Nordic Hydrol.*, 28(4/5), 247-262.

Seo, D. and Smith, J.A., 1996: On the relationship between catchment scale and climatological variability of surface-runoff volume, *Water Resour. Res.*, 32(3), 633-643.

Seyfried, M.S. and Wilcox, B.P., 1995: Scale and the nature of spatial variabillity: Field examples having implications for hydrologic modelling, *Water Resour. Res.*, 31(1), 173-184.

Shah, S.M.S., O' Connell and Hosking, J.R.M., 1996: Modelling the effects of spatial variability in rainfall on catchment response; 2. Experiments with distributed and lumped models, *J. Hydrol.*, 175, 89-111.

Shanholtz, V. O. Ross, B. B. and Carr, J. C., 1981: Effect of spatial variability on the simulation of overland and channel flow, *Transactions of the ASAE*, 24(1), 124-138.

Sharma, M.L. and Luxmoore, R.J., 1979: Soil spatial variability and its consequences on simulated water balance, *Water Resour. Res.*, 15(6), 1567-1573.

Sharma, M.L., Luxmoore, R.J., DeAngelis, R., Ward, R.C. and Yeh,G.T., 1987: Subsurface water flow simulated for hillslopes with spatially dependent soil hydraulic characteristics, *Water Resour. Res.*, 23(8), 1523-1530.

Shaw, E. M., 1988: *Hydrology in practice, second edition*, Chapman and Hall.

Shen, H.W. and Julien, P. Y., 1993: Erosion and sediment transport, In: Maidment, D. (Ed.), *Handbook of hydrology*, McGraw-Hill.

Sherman, L. K., 1932: Streamflow from rainfall by the unit hydrograph method, *Eng. news record,* 108, 501-505.

Shuttleworth, W. J., 1988: Macrohydrology: The new challenge for process hydrology, *J. Hydrol.*, 100, 31-56, 1988.

Silberstein, R.P. and Sivapalan, M., 1995: Estimation of terrestrial water and energy balances over heterogeneous catchments, *Hydrol. Process.*, 9, 613-630.

Silva, W. and Dijkman, J. P. M., 2000: Maatregelen in het stroomgebied van de Rijn, *RIZA report*, Institute for Inland Water Management and Waste Water Treatment (RIZA) (in Dutch).

Singh, V. P., 1995: Watershed modeling, In: V.P. Singh (ed.), *Computer models of watershed hydrology*, Water resources publications, Highlands Ranch.

Sivapalan, M., 1993: Linking hydrologic parameterizations across a range of scales: hillslope to catchment to region, In: H.J. Bolle, R.A. Feddes and J.D. Kalma (eds.), *Exchange processes for a range of space and time scales* (Proceedings of the Yokohama symposium, july 1993), IAHS Publ. 212, 115-123.

Sivapalan and Blöschl, 1998: Transformation of point rainfall to areal rainfall: Intensity-duration-frequency curves, *J. Hydrol.*, 204, 150-167.

Sivapalan, M., Beven, K.J. and Wood, E.F., 1987: On hydrologic similarity. 2. A scaled model of storm runoff production, *Water Resour. Res.* 23(12), 2266-2278.

Sivapalan, M., Wood, E.F., and Beven, K.J., 1990: On hydrologic similarity. 3. A dimensionless flood frequency model using a generalised geomorfologic unit hydrograph and partial area runoff generation, *Water Resour. Res.* 26(1), 43-58.

Sklash, M.G., 1990: Environmental isotope studies of storm and snowmelt runoff generation, In: M.G. Anderson and T.P. Burt (eds.), *Process studies in hillslope hydrology*, John Wiley, 401-435.

Smith, R.L., 1992: Introduction to Gnedenko (1943): On the limiting distribution of the maximum term in a random series, In S. Kotz and N.L. Johnson (eds.), *Breakthroughs in statistics, Foundations and basic theory*, 1992, Springer-Verlag, New-York.

Smith, R.E. and Hebbert, R.H.B., 1979: A Monte Carlo analysis of the hydrologic effects of spatial variability of infiltration, *Water Resour. Res.*, 15(2), 419-429.

Storm, B. and Refsgaard, A., 1996: Distributed physically-based modelling of the entire land phase of the hydrological cycle, In: M.B. Abbot and J.C. Refsgaard (eds.), *Distributed hydrological modelling*, Kluwer academic publishers, 55-67.

Strang, G., 1988: *Lineair algebra and its applications*, third edition, Harcourt Brace Jovanovich publisher, San Diego.

Subramanya, K., 1994: *Engineering hydrology*, McGraw-Hill, New Delhi.

TAW (Technical advisory committee on water retaining structures), 1995: *Under pressure, 1995*, TAW Delft.

Thorndike, R. M., 1978: *Correlational procedures for research*, Gardner Press.

Troch, P.A., de Troch, F.P., and Brutsaert, W., 1993, Effective water table depth to describe initial conditions prior to storm rainfall in humid regions, *Water Resour. Res.*, 29(2), 427-434.

Troutman, B. M., 1983: Runoff prediction errors and bias in parameter estimation induced by spatial variability of precipitation, *Water Resour. Res.*, 19(3), 791-810.

Uhlenbrook, S., Seibert, J., Leibundgut, C. and Rohde, A., 1999: Prediction uncertainty of conceptual rainfall-runoff models caused by problems in identifying model parameters and structure, *Hydrol. Sci. J.*, 44(5), 779-797.

Van Deursen, W.P.A. and Kwadijk, J.C.J. 1990: Using the watershed tools for modelling the Rhine catchment, In: *Proceedings on the first European Conference on G.I.S.*., Utrecht, faculty of Geographical Sciences EGIS foundation, 254-263.

Van Deursen, W.P.A. and Kwadijk, J.C.J. 1993: RHINEFLOW: an integrated GIS water balance model for the River Rhine. In: K. Kovar and Nachtnebel (eds.), *Application of Geographical Information systems in hydrology and water resources management*, Proceedings of the conference on HYDROGIS. IAHS publication 211, Wallingford, 507-519.

Van Genuchten, M. T., 1980: A closed-form equation for predicting the hydraulic conductivity of unsaturated soils, *Soil Sci. Soc. A. J.*, 44, 892-898.

Wen, X.H. and Gómez-Hernández, 1996: Upscaling hydraulic conductivities in heterogeneous media: an overview, *J. Hydrol.*, 183.

Whipkey, R.Z.,1967: Theory and mechanics of subsurface stormflow, In: W.E. Sopper and H.W. Lull (editors), *Forest hydrology*, Pergamon, Oxford, 255-260.

Wilby, R., Greenfield, B. and Glenny, C., 1994: A coupled synoptic-hydrological model for climate change impact assessment, *J. Hydrol.*, 153, 265-290.

Wilcox, P. W., Seyfried, M. S., Cooley, K. R. and Hanson, C. L., 1991: Runoff characteristics of sagebrush rangelands: modeling implications, *J. soil water cons.*, 46(2), 153-158.

Wood, E.F. and Hebson, C.S., 1986: On hydrologic similarity. 1. Derivation of the dimensionless flood frequency curve, *Water Resour. Res.*, 22(11), 1549-1554.

Wood, E.F., Sivapalan, M., Beven, K. and Band, L., 1988: Effects of spatial variabillity and scale with implications to hydrologic modelling, *J. Hydrol*, 102, 29-47.

Woods, R., Sivapalan, M. and Duncan, M., 1995: Investigating the representative elementary area concept: An approach based on field data, *Hydrol. Process.*, 9, 291-312.

Woolhiser, D.A., 1996: Search for physically based runoff models- a hydrologic El Dorado?, *J. Hydr. Eng.*, 122(3), 122-129.

Wu, Y.-H., Woolhiser, D.A. and Yevjevich, V., 1982: Effects of spatial variability of hydraulic resistance of runoff hydrographs, *J. of Hydrol.*, 59, 231-248.

Yeh, T. -C., Gelhar, L.W. and Gutjahr, A.L., 1985a: Stochastic analysis of unsaturated flow in heterogeneous soils, 1. Statistically isotropic media, *Water Resour. Res.*, 21(4), 447-456

Yeh, T. -C., Gelhar, L.W. and Gutjahr, A.L., 1985b: Stochastic analysis of unsaturated flow in heterogeneous soils, 2. Statistically anisotropic media with variable α, *Water Resour. Res.*, 21(4), 457-464

Yeh, T. -C., Gelhar, L.W. and Gutjahr, A.L., 1985c: Stochastic analysis of unsaturated flow in heterogeneous soils, *Water Resour. Res.*, 21(4), 465-471

Appendix A: Additional figures of chapter 4

Univariate parameter sensitivity analysis

This section presents graphical presentations (Figures A1-A8) of the computed hydrographs of section 4.4. In section 4.4, a univariate sensitivity analysis was presented to which eleven parameters (described in Table 4.1) of a rainfall-runoff model of the Zwalm catchment have been subjected. Since the rainfall-runoff model turned out to be completely insensitive to changes in the value of three parameters (n, α and m) the resulting hydrographs of the sensitivity analysis of these parameters have been left out of this appendix. Furthermore, for the sake of clarity, only 5 hydrographs have been displayed in each figure, instead of the 7 computed hydrographs.

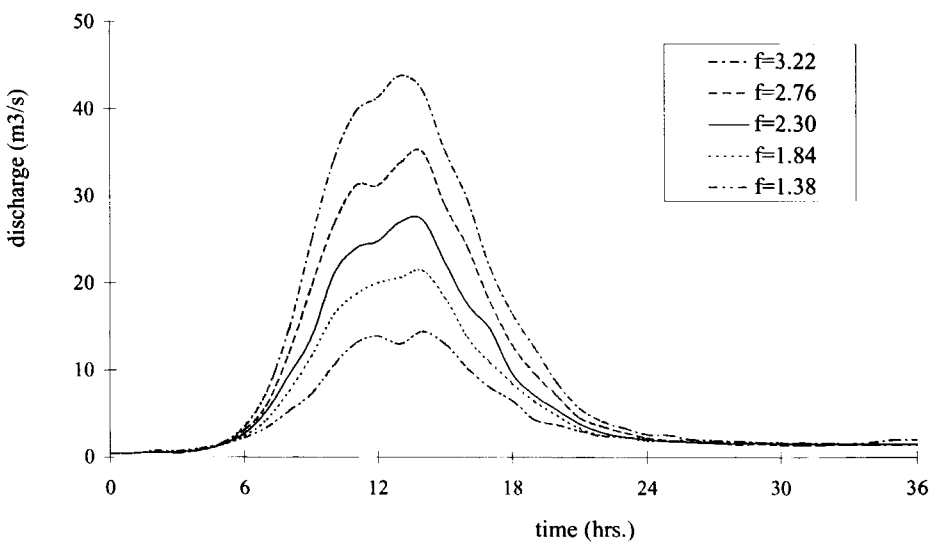

Figure A1 Sensitivity of the model output to parameter *f*

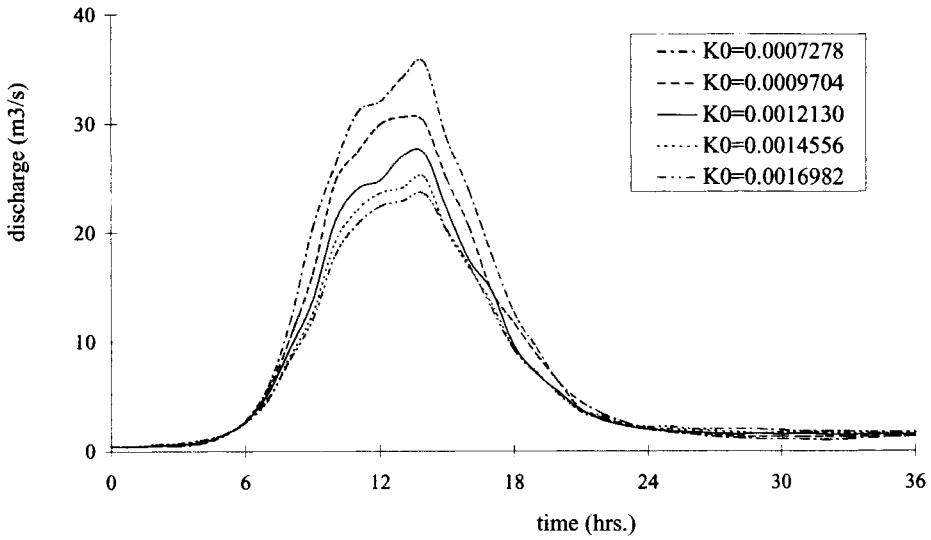

Figure A2 Sensitivity of the model output to parameter K_0

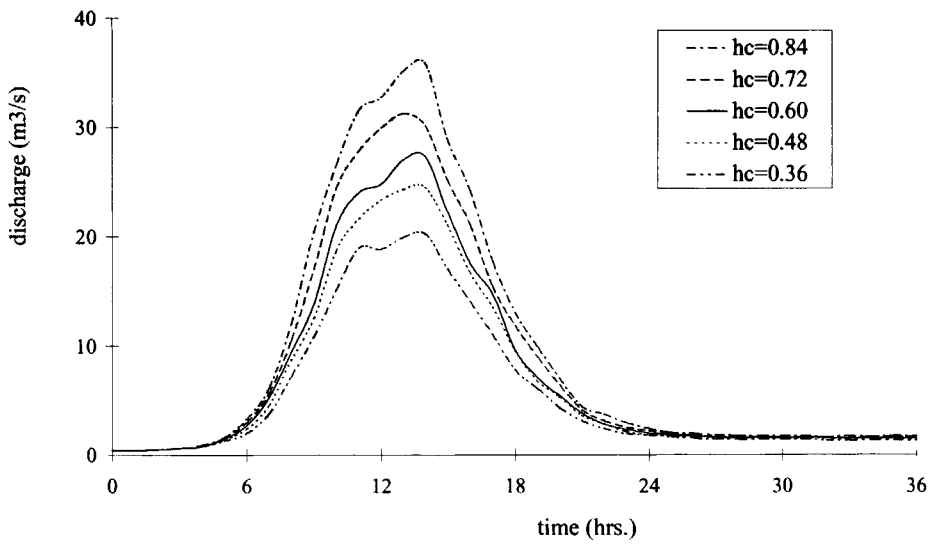

Figure A3 Sensitivity of the model output to parameter h_c

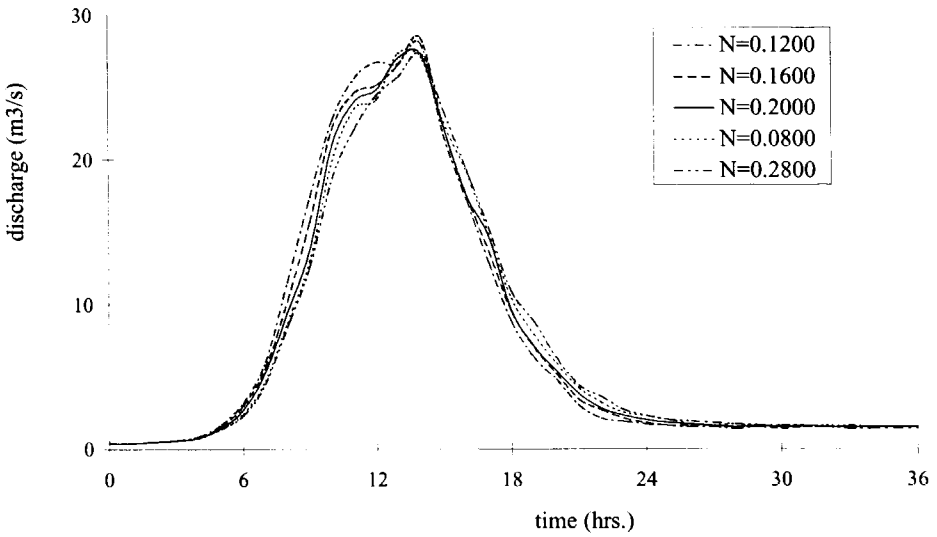

Figure A4 Sensitivity of the model output to parameter N

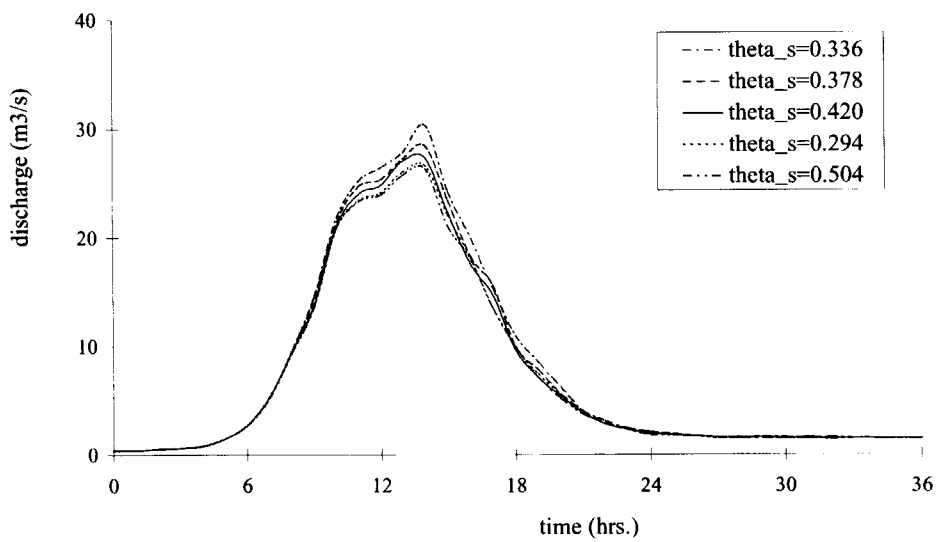

Figure A5 Sensitivity of the model output to parameter θ_s

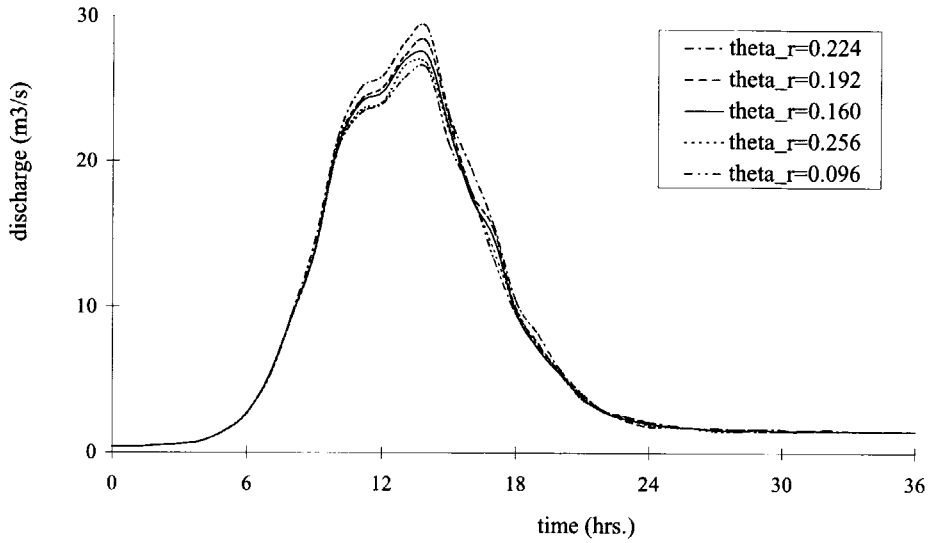

Figure A6 Sensitivity of the model output to parameter θ_r

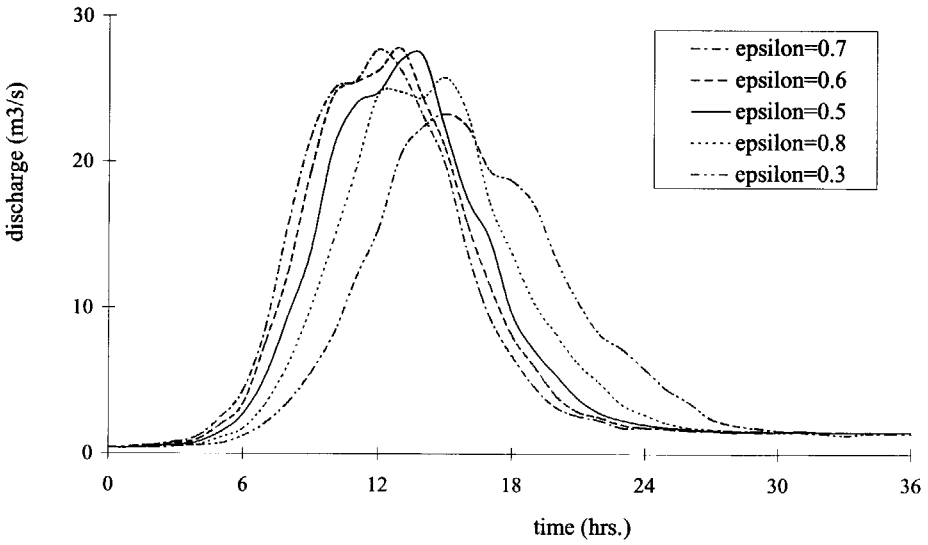

Figure A7 Sensitivity of the model output to parameter ε

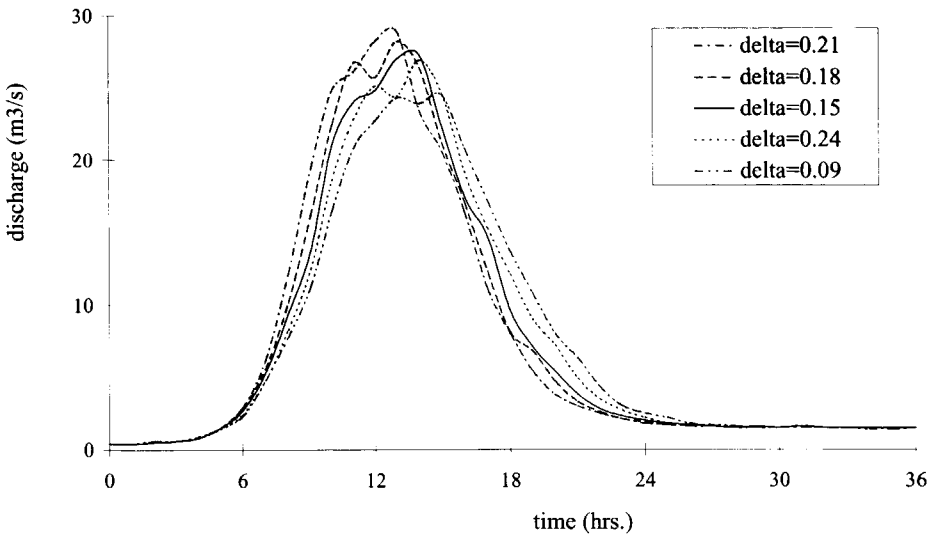

Figure A8 Sensitivity of the model output to parameter δ

Bivariate parameter sensitivity analysis

This section presents resulting hydrographs of the bivariate sensitivity analysis of section 4.5. The purpose of these figures is both to confirm the hypothesises, based on contour plots of MSE* values and to provide information which could not be distracted from the contour plots.

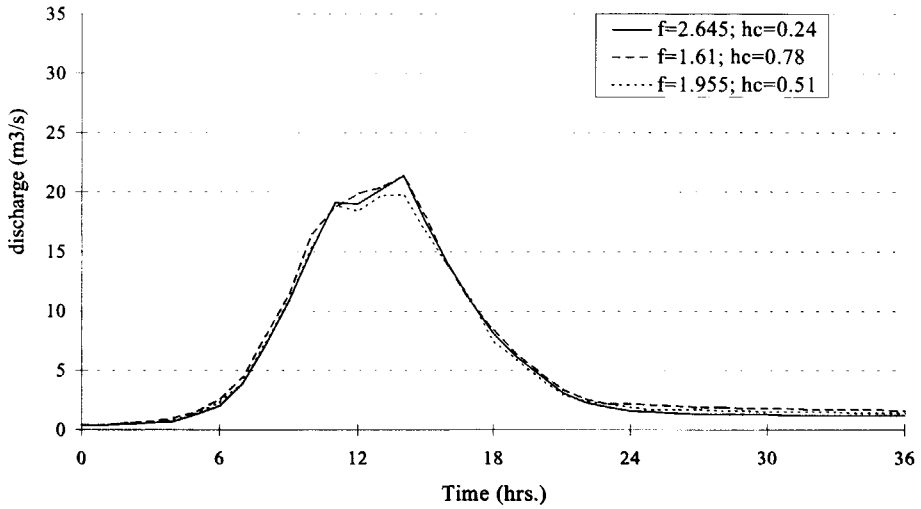

Figure A9 Model output of parameters f and h_c with MSE*≈2.0, connected by the contour line in the lower left part of 4.27

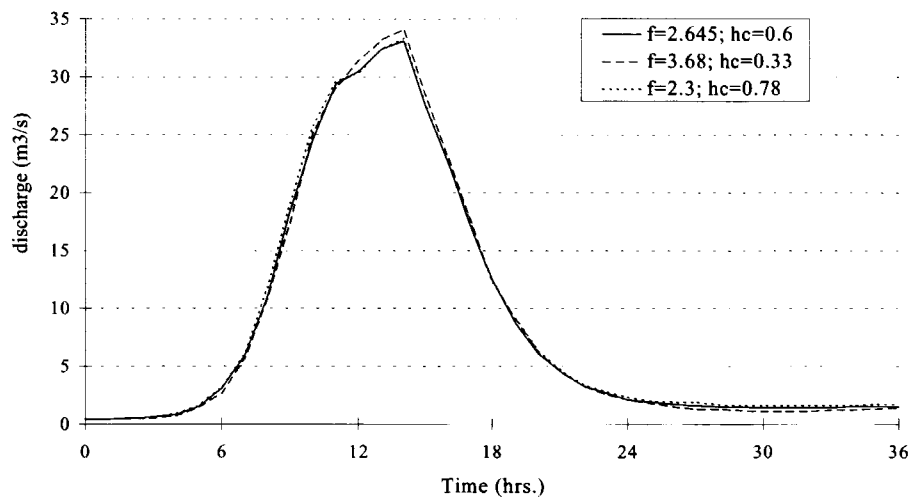

Figure A10 Model output of parameters f and h_c with MSE*≈2.0, connected by the contour line in the upper right part of Figure 4.27

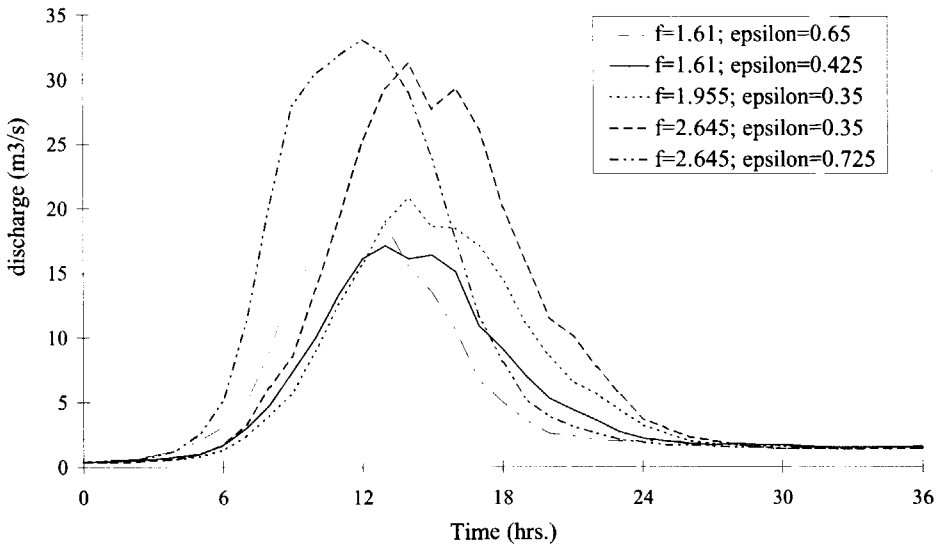

Figure A11 Model output of parameters f and ε with MSE*≈3.0

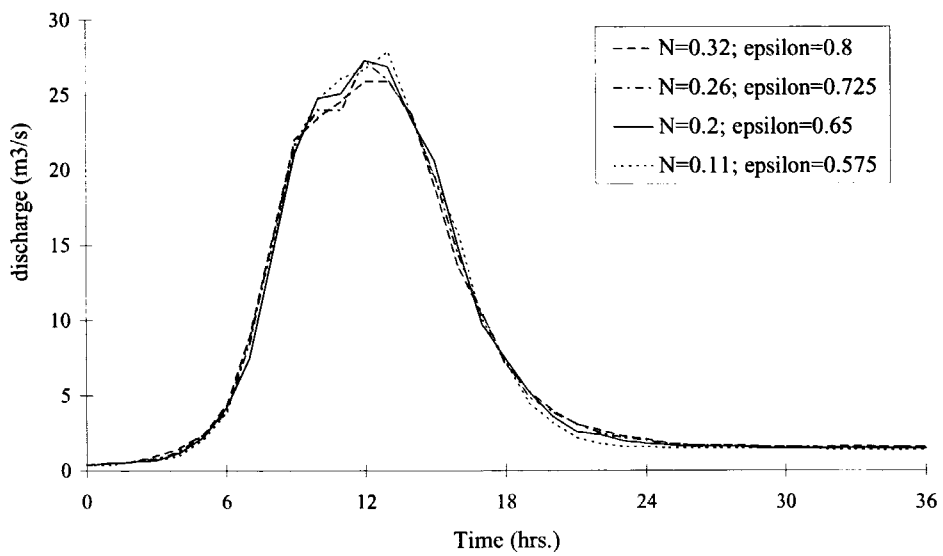

Figure A12 Model output of parameters N and ε with MSE*≈1.8

Appendix B: Multiple regression and correlation analysis

Multiple regression and correlation techniques serve to study the relationship between a single dependent variable on one hand and a number of independent variables on the other hand. Based on a series of observations of the variables involved, a regression equation is derived which can be used for future predictions of the independent variable. Prediction models that are based on regression analysis, have been developed in a variety of hydrological disciplines (e.g. Ford, P.M., 1959, Melching and Marquardt, 1996; Merkl, G., 1973). The correlation-coefficient is a measure of the ability of the regression equation to predict the observed values of the dependent variable. An extensive overview on the theory and applications of regression and correlation techniques can be found in Edwards [1984], Overall and Klett [1972] and Thorndike [1978]. This appendix presents a short review on the theory behind these techniques.

Linear regression analysis

In linear regression analysis, predictions on the value of a dependent variable are generated with the following equation:

$$\tilde{y} = \beta_0 + \beta_1 x_1 + \beta_2 x_2 + ... + \beta_p x_p \qquad \text{(B.1)}$$

where:

$\tilde{y}$ = predicted value of dependent variable y

$x_1, x_2, .., x_p$ = observed values of the p independent variables

$\beta_0, \beta_1, .., \beta_p$ = weighting coefficients of the regression equation

First, the p+1 weighting coefficients, $\beta_0, \beta_1, .., \beta_p$, need to be derived. Suppose there are n combined observations $(y; x_1, .., x_p)_i$; $i=1..n$ available, then $\beta_0, \beta_1, .., \beta_p$ are estimated from:

$$\begin{aligned} y_1 &= \beta_0 + \beta_1 x_{11} + \beta_2 x_{12} + .. + \beta_p x_{1p} \\ y_2 &= \beta_0 + \beta_1 x_{21} + \beta_2 x_{22} + .. + \beta_p x_{2p} \\ &\vdots \\ y_n &= \beta_0 + \beta_1 x_{n1} + \beta_2 x_{n2} + .. + \beta_p x_{np} \end{aligned} \qquad \text{(B.2)}$$

where:

y_i = observed value of dependent variable y at time i

x_{ij} = observed value of independent variable x_j at time i

In matrix notation this means:

$$\begin{pmatrix} 1 & x_{11} & x_{12} & \cdots & x_{1p} \\ 1 & x_{21} & x_{22} & \cdots & x_{2p} \\ 1 & x_{31} & x_{32} & \cdots & x_{2p} \\ \vdots & \vdots & \vdots & \ddots & \vdots \\ 1 & x_{n1} & x_{n2} & \cdots & x_{np} \end{pmatrix} \begin{pmatrix} \beta_0 \\ \beta_1 \\ \beta_2 \\ \vdots \\ \beta_p \end{pmatrix} = \begin{pmatrix} y_1 \\ y_2 \\ y_3 \\ \vdots \\ y_n \end{pmatrix} \Rightarrow X \bullet \beta = Y \tag{B.3}$$

where X (n×[p+1]), β (1×[p+1]) and Y (1×n) are in matrix-notation. If the number of observations of Y-values is less than or equal to the number of β-coefficients (i.e. if $n \leq p+1$) then an exact solution of (B.3) can be found in general. Usually, however, the number of available observations exceeds the number of variables, so no exact solution is expected to exist. Therefore, $\beta_0, \beta_1, .., \beta_p$ should be chosen such, that the average error of a prediction is minimised:

$$\min_{\beta_0, \beta_1, \ldots, \beta_p} \frac{1}{n} \sum_{i=1}^{n} (y_i - \tilde{y}_i)^2 \tag{B.4}$$

This criterion is known as the *least-squares criterion*. According to Strang [1988], (B.4) reaches its minimum value, if β equals:

$$\beta = (X^T X)^{-1} (X^T Y) = \begin{pmatrix} n & \sum_{i=1}^{n} x_{i1} & \sum_{i=1}^{n} x_{i2} & \cdots & \sum_{i=1}^{n} x_{ip} \\ \sum_{i=1}^{n} x_{i1} & \sum_{i=1}^{n} (x_{i1})^2 & \sum_{i=1}^{n} x_{i1} x_{i2} & \cdots & \sum_{i=1}^{n} x_{i1} x_{ip} \\ \sum_{i=1}^{n} x_{i2} & \sum_{i=1}^{n} x_{i1} x_{i2} & \sum_{i=1}^{n} (x_{i2})^2 & \cdots & \sum_{i=1}^{n} x_{i2} x_{ip} \\ \vdots & \vdots & \vdots & \ddots & \vdots \\ \sum_{i=1}^{n} x_{ip} & \sum_{i=1}^{n} x_{i1} x_{ip} & \sum_{i=1}^{n} x_{i2} x_{ip} & \cdots & \sum_{i=1}^{n} (x_{ip})^2 \end{pmatrix}^{-1} \begin{pmatrix} \sum_{i=1}^{n} y_i \\ \sum_{i=1}^{n} x_{i1} y_i \\ \sum_{i=1}^{n} x_{i2} y_i \\ \vdots \\ \sum_{i=1}^{n} x_{ip} y_i \end{pmatrix} \tag{B.5}$$

The correlation coefficient

The correlation coefficient, R, serves as a measure of how well the observed y-values can be predicted through linear regression. It is based on a normalised version of the least squares criterion (B.4):

$$R^2 = 1 - \frac{\frac{1}{n} \sum_{i=1}^{n} (y_i - \tilde{y}_i)^2}{\frac{1}{n} \sum_{i=1}^{n} (y_i - \bar{y}_i)^2} \tag{B.6}$$

where $\bar{y}$ is the average value of dependent variable y. The numerator in (B.6) is equal to the average squared value of the prediction error, while the denominator is equal to the variance

of y. Coefficient R can take on values, ranging from 0 to 1 (although sometimes the negative square root of R^2 is also considered, which means the value of R ranges from -1 to 1). If $R \approx 1$, the average squared value of the prediction errors is small compared to the variance of y, while if $R \approx 0$, the value of the squared average value is approximately equal to the variance of y. So, if $R \approx 1$, regression equation (B.1) can be considered a good predictor for variable y, whereas if $R \approx 0$, there exists no linear relation between y and $(x_1,..,x_p)$ which approximately fits the observed values.

Tests of significance of the derived correlation

The n combined observations $(y; x_1,..,x_p)_i$, $i=1..n$ of the involved variables are considered as realisations of a stochastic process. Accordingly, if the stochastic process is repeated, the observed values will be different and consequently the derived coefficients $\beta_0,\beta_1,..,\beta_p$ and correlation coefficient R will change. Therefore, derived statistics of observed series always contain a certain degree of uncertainty. This uncertainty is quantified by the standard error, SE_i, of a derived regression coefficient β_i, which equals:

$$SE_i = \sqrt{\frac{SS_{res}}{n-p-1} c_{ii}} \quad ; SS_{res} = \sum_{j=1}^{n} (\tilde{y} - \bar{y})^2 \tag{B.7}$$

where c_{ii} is the i^{th} diagonal element of matrix $(X^tX)^{-1}$. If the dependent variable, y, is uncorrelated with independent variable x_i, then the statistic

$$t = \frac{\beta_i}{SE_i} \tag{B.8}$$

is distributed as Student's t with n-p-1 degrees of freedom:

$$\int_{-\infty}^{t} \frac{\Gamma(0.5(u+1))}{\sqrt{\pi u}\ \Gamma(0.5u)} \left(1 + \frac{h^2}{u}\right)^{-0.5(u+1)} dh \quad ; u = \text{degrees of freedom} \tag{B.9}$$

where $\Gamma[.]$ is the gamma-function. Suppose there exists no linear relationship between the dependent variable, y, and independent variable x_{i*} and the outcome of t (equation (B.9)), resulting from the n observations, equals t^*. Since there is no linear relationship between y and x_{i*}, $|t^*|$ is expected to be relatively close to 0, especially when the number of observations is large. With distribution function (B.9) the exceedance probability of $|t^*|$, i.e. $P(|t| \geq |t^*|)$, can be derived. If $P(|t| \geq |t^*|)$ is small (i.e. smaller than a user defined level, usually taken to be 0.05 or 0.01) the assumption of absence of a linear relationship between y and x_{i*} is not likely to hold. In that case the correlation between y and x_{i*} is said to be statistically significant.

Closely related to the Student's t-test is the F-test of Fisher, which assesses the statistical significance of the derived correlation between y and $(x_1,..,x_p)$. If the dependent variable y is uncorrelated with the set of independent variables, $x_1,..,x_p$, then the statistic

$$F = \frac{R^2(n-p-1)}{(1-R^2)p} \tag{B.10}$$

is F-distributed, with p and n-p-1 degrees of freedom. This distribution function is equal to:

$$\int_0^F \frac{\Gamma[(u+v)/2]}{\Gamma[u/2]\Gamma[v/2]}\left(\frac{u}{v}\right)^{u/2} h^{(u-2)/2}\left(1+\frac{u}{v}h\right)^{-(u+v)/2} dh \quad ;u,v = \text{degrees of freedom} \tag{B.11}$$

Again, exceedence probabilities can be derived with the distribution function, in order to judge whether the correlation between y and $(x_1,..,x_p)$ is statistically significant.

Finally, the additional contribution of a single variable to the full multiple regression equation can be tested. Again, the F-test of Fisher is used. The appropriate F-ratio equals:

$$F_i = \frac{\left(R^2 - R_{-i}^{\ 2}\right)(n-p-1)}{1-R^2} \tag{B.12}$$

where R_{-i} is the multiple correlation coefficient of variable y and all x-variables *except* x_i. If for a certain variable x_{i*} the value of F_{i*} turns out to be relatively close to zero, then x_{i*} can be left out of the multiple correlation analysis without significantly increasing the errors of the predictions.

Some remarks on the linearity assumption

The regression and correlation techniques as presented in this appendix assume approximate linear relations exists between the variables of interest. In some cases, the relation of the variables may be better described by non-linear functions, such as the power function:

$$\tilde{y} = \beta_0 + \beta_1 x_1^{\lambda_1} + \beta_2 x_2^{\lambda_2} + ... + \beta_p x_p^{\lambda p} \tag{B.13}$$

In that case linear regression equation will provide a far from optimal fit (see Figure B1) and resulting R-values indicate a weaker dependence between the variables than exists in reality.

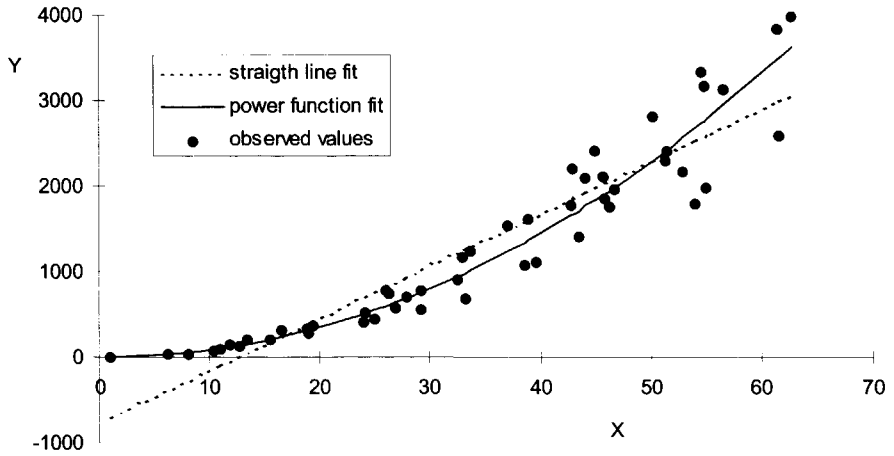

Figure B1 Straight line fit and power function fit of a fictional (x,y) data-set, where x and y are approximately related through a power function.

However, as long as the relation between the variables is linear with respect to the β-coefficients this serves no problem. In case of equation (B.13) one should simply take $x_i^{\lambda_i}$ as the independent variable instead of x_i. In the example of Figure B1 this leads to an increase in R from 0.935 to 0.992, which is a large relative difference if deviations from full correlation (R=1) are considered.

Appendix C: ARMA models and linear transfer functions

Autoregressive-moving average (ARMA)-models and transfer functions are statistically based descriptors of stationary time series. ARMA- models and transfer functions are often used for predictional purposes (Caroni et al., 1984; Chow et al., 1983; Lemke, 1991; Novotny and Zheng, 1989). Besides serving as predictive tools, they also obtain an insight in the behaviour of the underlying processes that are involved in generating the observed time series. ARMA-modelling is used for analysis of single time series, while transfer functions are used for bivariate modelling of stochastic processes where quantities of one process (output) are dependent on the other process (input). The ARMA-models are derived from the auto-correlation functions of the observed time series, whereas transfer functions are based on both the autocorrelation functions and the cross-correlation function of the different series.

The models described here are Box-Jenkins type models (Box and Jenkins, 1976) This appendix presents a short review on the theory behind these techniques.

ARMA-modelling

A discrete stationair time series z_1, z_2,...z_t,..., is considered. It is assumed the expected value, μ_z, of this series is equal to 0 (if this is not the case, the series $z_t^* = z_t - \mu_z$ will be considered). Successive values of z are usually correlated ("persistent"), i.e. if z_t is significantly above average, then z_{t+1} is expected to be above average as well. This structure of mutual dependence between successive observed values is the main focus in time series analysis. In statistics, it is quantified either with the autocorrelation function or with the autocovariance function:

$$\text{autocovariance: } c_z(k) = E[(z_t - E(z_t))(z_{t+k} - E(z_{t+k}))] \quad ;k = 0,1,2,... \tag{C.1}$$

$$\text{autocorrelation: } \rho_Z(k) = \frac{c_Z(k)}{Var(z)} \quad ;k = 0,1,2,... \tag{C.2}$$

The time series of interest will be represented through stochastic models. This means the observed values are treated as if they are generated from a stochastic generator which fulfils the derived statistics of the observed series. Two well-known stochastic models are the autoregressive (AR) model and the moving average (MA) model:

AR model: $z_t = \phi_1 z_{t-1} + \phi_2 z_{t-2} + .. + \phi_p z_{t-p} + a_t$ (C.3)

MA model: $z_t = a_t - \theta_1 a_{t-1} - \theta_2 a_{t-2} - ... - \theta_q a_{t-q}$ (C.4)

where $\phi_1,..,\phi_p$ and $\theta_1,..,\theta_q$ are parameters of the autoregressive model and the moving average model respectively. Time series $\{a_t\}$ is a white noise process, i.e. a time series with expected value equal to 0 and autocorrelation $\rho_z(k)=0$ for $k \geq 0$

In some cases, the structure of the observed time series is such that a mixed autoregressive-moving average (ARMA) model is required:

ARMA-model: $z_t = \phi_1 z_{t-1} + \phi_2 z_{t-2} + ... + \phi_p z_{t-p} + a_t - \theta_1 a_{t-1} - \theta_2 a_{t-2} - ... - \theta_q a_{t-q}$ (C.5)

Identification procedure

The process of deriving a proper ARMA-model starts of with the identification of p and q. First, an estimation of the autocorrelation function is derived:

$$r_k = \frac{c_k}{c_0}, k = 1,2,.. \quad ; c_k = \frac{1}{n}\sum_{t=1}^{n-k}(z_t - \bar{z})(z_{t+k} - \bar{z}) \tag{C.6}$$

where r_k is the estimated value of $\rho(k)$ (equation (C.2)), c_k is the estimated value of $c_z(k)$ (equation (C.1)), $\bar{z}$ is the average of the series and n is the number of observations. Subsequently, an estimation of the partial autocorrelation function, $\nu(k)$ is derived. For each value of $k \geq 1$, $\nu(k)$ is equal to ϕ_{kk} in the following matrix-vector equation:

$$\begin{pmatrix} 1 & \rho(1) & \rho(2) & \cdots & \rho(k-1) \\ \rho(1) & 1 & \rho(1) & \cdots & \rho(k-2) \\ \rho(2) & \rho(1) & 1 & \cdots & \rho(k-3) \\ \vdots & \vdots & \vdots & \ddots & \vdots \\ \rho(k-1) & \rho(k-2) & \rho(k-3) & \cdots & 1 \end{pmatrix} \begin{pmatrix} \phi_{k1} \\ \phi_{k2} \\ \phi_{k3} \\ \vdots \\ \phi_{kk} \end{pmatrix} = \begin{pmatrix} \rho(1) \\ \rho(2) \\ \rho(3) \\ \vdots \\ \rho(k) \end{pmatrix} \tag{C.7}$$

Of course, the real auto-correlation function $\rho(k)$ is not known, so instead the estimated values r_1, r_2,... are used. Then, an estimation of p and q can be obtained from a plot of both $\rho(k)$ and $\nu(k)$, based on the information of Table C.1.

	AR(p)	MA(q)
$\rho(k)$	asymptotic decrease of absolute value	=0, k>q
$\nu(k)$	=0, k>p	asymptotic decrease of absolute value

Table C.1 Behaviour of the autocorrelation function, $\rho(k)$, and the partial autocorrelation function, $\nu(k)$, for both the autoregressive model and the moving average model.

Estimation procedure

The next step is to derive the values of model parameters $\phi_1,..,\phi_p,\theta_1,..,\theta_q$. The likelihood criterion is applied to find an optimal solution. This criterion can be rewritten into:

$$\min_{\phi_1,..,\phi_p,\theta_1,..,\theta_q} = \sum_{t=1}^{n} a_t^2 \qquad \text{(C.8)}$$

where, from (C.5), a_t is equal to:

$$a_t = z_t - \phi_1 z_{t-1} - \phi_2 z_{t-2} - ... - \phi_p z_{t-p} + \theta_1 a_{t-1} + \theta_2 a_{t-2} + ... + \theta_q a_{t-q} \qquad \text{(C.9)}$$

A number of iterative procedures are available to find the solution of (C.8). These procedures will not be discussed here. The interested reader is referred to Box and Jenkins [1976].

Linear transfer functions

Transfer functions are used to describe the dynamic behaviour of paired observations (X_t, Y_t) where the X-values are the input and Y-values are the output of a system (e.g. precipitation and discharge). The general description of a linear transfer function is:

$$Y_t = N_t + v_0 X_t + v_1 X_{t-1} + ... = N_t + \sum_{i=0}^{\infty} v_i X_{t-i} \qquad \text{(C.10)}$$

where coefficients v_0, v_1,.. are the ordinates of the impulse response function and N_t is noise. In order to go from an infinite number of coefficients to a finite number of coefficients the transfer function is usually represented as:

$$Y_t = \delta_1 Y_{t-1} + \delta_2 Y_{t-2} + ... + \delta_r Y_{t-r} + \omega_0 X_{t-b} - \omega_1 X_{t-b-1} - ... - \omega_s X_{t-b-s} + N_t \qquad \text{(C.11)}$$

where δ_1, δ_2,..,δ_r, ω_1, ω_2,.., ω_s are parameters of the model and b is the "reaction time" of the system.

For transfer functions, the noise process N_t is not by definition a white noise model since the autocorrelation of the noise in these type of systems is often observed to be non-zero for values of $k \geq 1$. Therefore, N_t is often described through an ARMA-model:

$$N_t = \phi_1' N_{t-1} + \phi_2' N_{t-2} + ... + \phi_{p'}' N_{t-p'} + a_t - \theta_1' a_{t-1} - \theta_2' a_{t-2} - ... - \theta_{q'}' a_{t-q'} \qquad \text{(C.12)}$$

where $\phi_1', \phi_2', .., \phi_{p'}', \theta_1', \theta_2', .., \theta_{q'}'$ are model parameters and a_t is a white noise process

Identification procedure

In identifying model parameters the cross-covariance function between X and Y plays an important role:

$$\gamma_{xy}(k) = E\left[\left(X_t - \mu_x\right)\left(Y_{t+k} - \mu_y\right)\right] \tag{C.13}$$

where μ_x and μ_y are expected values for the two series. An estimation of this function, based on the available observations, is obtained through:

$$c_{xy}(k) = \frac{1}{n}\sum_{t=1}^{n-k}\left(x_t - \bar{x}\right)\left(y_{t+k} - \bar{y}\right) \tag{C.14}$$

where n is the amount of paired observations and $\bar{x}$ and $\bar{y}$ are the averages of the two series. The idea of the identification procedure is to estimate the v-coefficients of equation (C.10) from the estimated cross-correlation function and subsequently to estimate the values of b, s and r of equation (C.11) from the v-coefficients.

The v-coefficients can be derived in two ways: with or without prewhitening. If no prewhitening is applied, it has to be assumed that there is an integer value K for which v_k-values are effectively zero if k≥K. Then, the v-coefficients are derived from:

$$\begin{pmatrix} \gamma_{xy}(0) & \gamma_{xy}(1) & \gamma_{xy}(2) & \cdots & \gamma_{xy}(K) \\ \gamma_{xy}(1) & \gamma_{xy}(0) & \gamma_{xy}(1) & \cdots & \gamma_{xy}(K-1) \\ \gamma_{xy}(2) & \gamma_{xy}(1) & \gamma_{xy}(0) & \cdots & \gamma_{xy}(K-2) \\ \vdots & \vdots & \vdots & \ddots & \vdots \\ \gamma_{xy}(K) & \gamma_{xy}(K-1) & \gamma_{xy}(K-2) & \cdots & \gamma_{xy}(0) \end{pmatrix} \begin{pmatrix} v_0 \\ v_1 \\ v_2 \\ \vdots \\ v_K \end{pmatrix} = \begin{pmatrix} \gamma_{xy}(0) \\ \gamma_{xy}(1) \\ \gamma_{xy}(2) \\ \vdots \\ \gamma_{xy}(K) \end{pmatrix} \tag{C.15}$$

On the other hand, if prewhitening is applied it is assumed that the X-series can be described through an ARMA-model:

$$X_t = \phi_1 X_{t-1} + \phi_2 X_{t-2} + \ldots + \phi_p X_{t-p} + \alpha_t - \theta_1\alpha_{t-1} - \theta_2\alpha_{t-2} - \ldots - \theta_q\alpha_{t-q} \tag{C.16}$$

where $\phi_1, \phi_2, \ldots, \phi_p, \theta_1, \theta_2, \ldots, \theta_q$ are model parameters and α_t is a white noise process

From observed values of X_t, the α_t-values can be derived recursively. Then, the α-values will be used as input of the system instead of the X-values. In other words, the original input is transformed into a white noise process. Consequently, this same transformation has to be applied to Y_t and N_t as well:

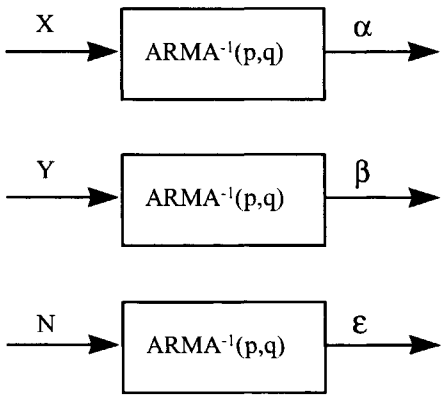

Figure C.1 Performed transformations of the prewhitening procedure

These transformations change equation (C.10) into:

$$\beta_t = \varepsilon_t + v_0\alpha_t + v_1\alpha_{t-1} + \ldots = \varepsilon_t + \sum_{i=0}^{\infty} v_i\alpha_{t-i} \qquad \text{(C.17)}$$

Now, the *v*-coefficients can easily be derived from:

$$v_k = \frac{\gamma_{\alpha\beta}(k)}{\sigma_\alpha^2} \quad ,k = 0,1,\ldots \qquad \text{(C.18)}$$

where σ_α is the standard deviation of α_t and $\gamma_{\alpha\beta}$ is the cross-covariance function of α_t and β_t.

The second step in the identification procedure is to estimate the values of *b*, *s* and *r* of equation (C.11) from the *v*-coefficients. For a model as described in equation (C.11), the *v*-values of equation (C.10) consist of:

I. k=0..*b*-1: v_k=0
II. k=*b*..*b*+*s*-*r*: v_k-values follow no fixed pattern
III. k≥*b*+*s*+*r*+1: v_k-values follow the pattern of the following difference equation:

$$v_k = \delta_1 v_{k-1} + \delta_2 v_{k-2} + \ldots + \delta_r v_{k-r} \qquad \text{(C.19)}$$

Taking in mind the information of I-III, the values of *b*, *r* and *s* can be identified from a plot of *v*-values.

Estimation procedure

The criterion for deriving "optimal" parameter values of a transfer function is similar to the one for ARMA-models:

$$\min_{\delta_1,..,\delta_r,\omega_1,..,\omega_s,\phi_1,..,\phi_p,\theta_1,..,\theta_q} \sum_{t=1}^{n} a_t^2 \tag{C.20}$$

where, according to equations (C.11) and (C.12), a_t is equal to:

$$\begin{aligned} a_t = {} & Y_t - \delta_1 Y_{t-1} - \ldots - \delta_r Y_{t-r} \phi_1 - \omega_0 X_{t-b} + \omega_1 X_{t-b-1} + \ldots + \omega_s X_{t-b-s} \\ & - \phi_1 N_{t-1} - \ldots - \phi_p N_{t-p} - \theta_1 a_{t-1} + \ldots + \theta_q a_{t-q} \end{aligned} \tag{C.21}$$

A number of iterative procedures are available to find the solution of (C.20). These procedures will not be discussed here. The interested reader is referred to Box and Jenkins [1976].

ISBN: 90-407-2154-8

DUP Science